2012

Soil and Slope Stability Study of Geomorphic Landform Profiles versus Approximate Original Contour for Valley Fill Designs

Harold Russell
West Virginia University

Soil and Slope Stability Study of Geomorphic Landform Profiles versus Approximate Original Contour for Valley Fill Designs

Harold Russell, EIT

Thesis submitted to the
Benjamin M. Statler College of Engineering and Mineral Resources
at West Virginia University
in partial fulfillment of the requirements
for the degree of

Master of Science
in
Civil and Environmental Engineering

John D. Quaranta, Ph.D., P.E., Chair
Hema Siriwardane, Ph.D., P.E.
Vladislav Kecojevic, Ph.D

Department of Civil and Environmental Engineering

Morgantown, West Virginia
2012

KEYWORDS: Approximate original contour, geomorphic landform design, valley fill, slope stability analysis, soil testing

ABSTRACT

Soil and Slope Stability Study of Geomorphic Landform Profiles versus Approximate Original Contour for Valley Fill Designs

Harold B. Russell

This report presents the findings of geotechnical testing on two material types retrieved from a surface mine site in Logan County, West Virginia, and investigates geomorphic landform design as an alternative in lieu of typical valley fill design and approximate original contour (AOC) surface mine reclamation design. Laboratory testing was carried out according to ASTM standard test methods. The scope of the testing performed involved grain size distribution analysis, hydrometer analysis, saturated shear strength testing under an *insitu* consolidation load, Atterberg limits including plastic and liquid limits, compaction at three predetermined compaction energies, and rigid wall permeameter hydraulic conductivity testing. Data was evaluated and analyzed to find to what degree the material particles moved under certain hydraulic gradients and if the particle movement affected the shear strength of the samples. The objectives of the testing were to understand the movement and behavior of small diameter soil particles at a valley fill and use the strength values as input parameters into several modules of GeoStudio™ for numerical slope stability modeling.

The numerical modeling involved geomorphic design for a proposed valley fill in southern West Virginia using commercial software following the Geofluv® method. A comprehensive seepage and slope stability analysis was then developed using the SEEP/W, SIGMA/W, and SLOPE/W modules of GeoStudio2007™ for assessing the groundwater flow characteristics of the blasted, unweathered sandstone fill, an *insitu* load calculation, and the resultant limit equilibrium analysis of slope stability (static factor of safety). These analyses were performed for both the AOC and geomorphic fill designs.

The cumulative analysis for the geomorphic valley fill alternative design yielded the highest factors of safety. Most cases produced factors of safety over 2.0. The failure locations were sought out to produce the lowest factors of safety for the structure. None of the factors of safety modeled yielded factors of safety under 1.0 for the geomorphic design. The results imply that the geomorphic design can remain very stable when a range of hydrologic conditions and geometries are applied.

Regulations require that reclaimed slope factors of safety must remain above 1.5. The analyses performed showed that the AOC valley fill design could withstand *insitu* loads and produced slope angles under most hydrologic conditions analyzed. Elevated pore pressures tended to result at the toe of the slope, and decreased the factor of safety. The most critical scenario was a fully saturated toe which yielded a factor of safety of 0.50.

If particle transport can occur and alter toe pore pressures, it is possible that some small slope failure may occur. The gradations that were found for the unweathered well graded sand with silt fill material showed that particle transport would not be a significant concern. The gradations that were found for the range of cases analyzed for the unweathered well graded sand with silt showed aggregation phenomena which could have implications on the long term stability of the earthen structures.

ACKNOWLEDGEMENTS

I would like to gratefully acknowledge the enthusiastic supervision of Dr. John D. Quaranta, a great teacher and advisor who was abundantly helpful and offered invaluable assistance, support and guidance to accomplish this research project. His technical insight was of priceless value.
I wish to thank Dr. Hema J. Siriwardane and Dr. Vlad Kecojevic for being in my advisory Committee.
I wish to thank Mr. Jeremi Stawovy, Mr. Nathan DePriest, and Ms. Allison Sears for assistance in laboratory testing and computer modeling.
I also wish to thank the engineers and staff members from Coal-Mac, Incorporated who provided support for the program.
I would like to dedicate this thesis to my wonderful grandparents, parents, brother, and my closest friends for the love, support and encouragement they have provided throughout my academic career. Additionally, I would like to recognize the contribution of the events, good and bad, over the course of my life thus far which have shaped me to take on a challenging career in civil engineering.

TABLE OF CONTENTS

LIST OF TABLES

LIST OF FIGURES

1. Introduction

1.1 Introduction & Background

Coal mining has long been a significant aspect of the state economies in the Appalachian region. Shallow coal seams can be retrieved by implementing a method of mining called surface mining. Surface mining involves removing overburden, extracting coal, and reclaiming the disturbed area. Federal law requires that all surface mine sites be reclaimed according to approximate original contour (AOC) design. In West Virginia, Kentucky, Tennessee, and south-western Virginia, pre-SMCRA state laws did not require elimination of high walls by complete backfilling. SMCRA was adopted into law in 1977 and since then much of central Appalachian surface mine land has been returned to AOC. Approximate original contour design and excess spoil disposal on surface mining sites in West Virginia are regulated by the state of West Virginia and the United States Federal Government. The Surface Mining Control and Reclamation Act of 1977 (SMCRA) establishes that surface mining sites must be returned to "approximate original contour," (AOC) and requires surface mining equipment operators to "…grade in order to restore the approximate original contour of the land with all high walls, spoil piles, and depressions eliminated…" [Sec. 515(b)3]. West Virginia has its own version of SMCRA called WVSCMRA which has primacy over SMCRA due to its unique steep sloped terrain. WVSCMRA has similar requirements when compared to SMCRA.

Since the terrain in Appalachia is unique to surface mining, it is thought that AOC may not always be an appropriate method of landform design (Superfesky, 2007). Fluvial geomorphic landform design is an alternative landform design method to AOC design. Fluvial geomorphology utilizes concepts that attempt to establish a nature-emulated landforms where erosive forces are in equilibrium with the land surface. This alternative earthwork design method has a great potential to increase the durability of reclamation earthwork designs and decrease the critical nature of some of the issues involved with AOC. One drawback about fluvial geomorphic design is that the software used to generate the design models do not incorporate slope stability analysis. In steep sloped Appalachian terrain, slope stability analysis can be a critical element of the design process. Slope stability analysis can be run quickly and effectively by many different versions of computer software. By integrating fluvial geomorphic design into surface mine reclamation, landform designers have the potential to create a more natural, less erosive, and more stable landform as opposed to AOC.

1.2 Research Purpose & Objectives

The objective of this research was to sample and identify a surface mine spoil in southern West Virginia, characterize its associated physical properties as well as the strength aspects for appropriate input parameter key in into a slope stability software analysis tool to compare stability results of an AOC valley fill and a geomorphic landform design with regard to a factor of safety computed by the general limit equilibrium method. Laboratory values were used along with the surface mine permit documentation of the proposed slope geometry to validate, assess, and calibrate the models. A deterministic analysis method was then used along with the general limit equilibrium computational method in order to perform a risk assessment with regard to a factor of safety. The factor of safety output data was addressed to develop insights into risk assessment of the generated landform model compared to the AOC valley fill design.

The unweathered sandstone overburden is a blasted rock material. Blasted rock material properties vary from naturally occurring soil particle properties. A blasted rock particle may be very small and may share the relative size or diameter of a weathered particle, but the two are significantly dissimilar. A blasted rock particle's affinity to retain water as well as its strength properties vary significantly. A naturally occurring particle whose location provided it to be exposed to weathering and chemical processes over time changes its characteristics, strength behavior, and geotechnical properties. A blasted rock particle has not participated in these processes. Geotechnical laboratory testing is necessary to establish design limitations.
The blasted rock material plays a significant role in the unique design of valley fills. It is important to understand the grading envelopes that occur under varying compaction efforts. Small particles can be carried by water and create internal erosion or suffosion phenomena. In order for a valley fill to be durable, internal erosion processes must be slowed as much as possible. This can be done by constructing the valley fill at compaction efforts that reach a desired density condition without creating a significant volume of fine particles. Void spaces are created by internal erosion in the upper regions of the valley fill, and are filled in the lower regions. Lower regions that begin to hold large volumes of fine particles can result in increased pore pressures, and decrease the stability of the valley fill.

2. Literature Review

State and Federal regulations directing mine reclamation using the Approximate Original Contour approach have resulted in geotechnically stable designs of valley fills constructed using waste rock overburden. Environmental concerns at mountain top mining sites abound because of the loss of headwater stream length and increased flooding risk. One promising technique to lessen the impacts involves fluvial geomorphic landform design applied to the waste rock fill and slope profiles. Geomorphic designs have proven successful in semi-arid regions; however, this approach has not been adapted to eastern surface mining reclamation. Research results are presented using fluvial geomorphic design principles which show alternative valley fill design approaches for a mountain top mine site under construction in southern West Virginia. Features of the design are the channelizing of surface water from the rock fill flats and sloped faces, and directing the runoff to engineered perimeter channels.

Introduction

Concerns of detrimental environmental impacts originating from surface mining and valley fill construction are of constant debate, resulting in numerous lawsuits (e.g. Hasselman, 2002, Davis and Duffy, 2009) and scientific studies throughout Central Appalachia (Hartman et al., 2005; Pond et al., 2008; Ferrari et al, 2009). State and Federal regulations have been promulgated to control environmental impacts associated with surface mining and valley fill construction through the Surface Mining Control and Reclamation Act (SMCRA) and the Clean Water Act (CWA). West Virginia has primacy of the State's regulatory enforcement and thus must meet stringent regulatory standards for valley fill construction.

These regulations have resulted in geotechnically stable designs of valley fills with runoff management; however, major environmental concerns have resulted, specifically the loss of headwater stream length, increased flooding risk, and degraded water quality in downstream communities. The predicted headwater stream loss in WV is approximately 3,200 km by 2012, thus impacting the ability of West Virginia to support high quality and unique aquatic species

(USEPA, 2005). Studies have shown that streams below valley fills often have elevated conductivity levels, resulting from water contact with the overburden (Hartman et al., 2005, Pond et al., 2008). Additionally, changes in downstream thermal regime, chemistry, and sedimentation are potential impacts (USEPA, 2005). One promising innovative technique used to lessen impacts involves fluvial geomorphic landform design that incorporates mature landform shapes into the designs. These landform designs add variability and aid in establishing a site with a long-term hydrologic balance.

The objective of the research performed was to investigate alternative geomorphic design and reclamation approaches applied to surface mining methods in West Virginia. First, an overview of geomorphic landform design and associated regulations are presented, noting challenges associated with the application of the technique in West Virginia. Then, a conceptual geomorphic landform design of a valley-fill currently under construction is discussed.

Regulatory Drivers Affecting Geomorphic Landform Design

Challenges associated with implementing the landforming approach in the WV Central Appalachia Region extend beyond the complexity of designing and constructing mature landforms in steep terrain. Current, civil engineering based regulations for meeting Approximate Original Contour (AOC) and Surface Water Runoff Analysis (SWROA) do not readily support this nontraditional design approach, and perceived initial construction costs are greater than traditional designs (Michael et al., 2010).

Reclamation by approximate original contour (AOC) design is a practiced in the central Appalachian region of the United States. These promulgated design requirements were needed to provide standards and controls. Prior to the Surface Mining Control and Reclamation Act (SMCRA), adopted into law in 1977, non-designed earth moving practices resulted in spoil materials being deposited into valleys, hillsides, and over ephemeral streams without consideration of erosion, geotechnical stability, seepage, and hydrology. Generically termed "shoot-and-shove", the end results included slope washes, loss of topsoil, and stream siltation.

The approximate original contour design and excess spoil disposal on surface mining sites in West Virginia are regulated by the state of West Virginia and by the US Office of Surface Mining, Reclamation, and Enforcement (OSM) (WVDEP, 1999).

In West Virginia the AOC guidelines are promulgated by WVSMRR, CSR §38 which require slope profile configurations constructed by backfilling and grading of disturbed areas have a final profile which in effect closely resemble the general surface configuration of the land prior to mining (WVDEP, 1999). The post mining configuration is intended to ensure slope stability, control drainage, complement the drainage pattern of the surrounding terrain, and prevent stream sedimentation. These requirements are comprehensive covering the drainage pattern of the surrounding terrain, high walls, and spoil piles. The State does consider special circumstances and permits variances. In addition, the West Virginia Department of Environmental Protection (WVDEP) and the US Environmental Protection Agency (EPA) implement the Clean Water Act of 1972 through the National Pollution Discharge and Elimination System (NPDES) in order to provide requirements for drainage and sediment control requirements for the quality of the discharged runoff.

The AOC requirements result in the typically profiled slope shapes exhibiting uniform benches, planar slopes having unvarying contours with perimeter or center surface water ditches. The

AOC guidelines have performed well and as intended, the reduction in environmental degradation of mountain streams and the stability of slopes have been the benefit. In West Virginia the revegetation efforts using select grasses and hardwoods have proven very effective in concealing the planar slope profiles and surface drainage structures. The effectiveness of post mine land use implemented by the mining industry has, to a large extent, been so successful that when the tree canopy matures the slopes appear natural.

The aesthetic and geotechnical safety benefits of the AOC requirements although are not able to balance trade-offs with the loss of streams and changes in watershed sizes. Under natural conditions, landforms develop a balance between erosive and resistance forces, resulting in a system in equilibrium with low erosion rates. The fluvial geomorphic landform design approach attempts to design landforms in this steady-state condition, considering long-term climatic conditions, soil types, slopes, and vegetation types (Toy and Chuse, 2005; Bugosh, 2009). The need to balance valley fill construction stability with surface hydrologic reclamation needs has opened the opportunity to introduce geomorphic design.

Geomorphic Landform Design

Compared to traditional designs, landforming appears natural, reduces long-term maintenance, requires fewer artificial elements, and supports long-term stability (Martin-Duque et al., 2009).

While this innovative design approach has been used with success in semi-arid regions of the U.S. (e.g. Toy and Chuse, 2005; Measles and Bugosh, 2007; Bugosh, 2009; Robson et al., 2009) and outside of the U.S. (e.g. Marin-Duque et al., 2009; Martin-Moreno et al., 2008), the approach has not been utilized in West Virginia surface mining design or reclamation.

The geomorphic landform design procedure builds a drainage network using a reference landform approach; a reference watershed must be identified and characterized. The following information is necessary to inform successful design (Toy and Chuse, 2005; Eckels and Bugosh, 2010): i) main channel slope and landform profile shape; ii) drainage density and area; and, iii) channel characteristics. Each of these design requirements is discussed separately below.

> i) Main channel slope represents the watershed slope. As the main channel slope increases, the stream power and erosion potential increase (Toy and Chuse, 2005). Landform longitudinal profile shapes must also be considered as the concave shape differs among headwater and downstream locations. In mountainous terrain the nature of slope profiles develop into compound surface profiles. These profiles exhibit steep convex slopes at the head of the valley then progressively transition into a concave form gradually tapering to a uniform profile. The fluvial influence stream cutting and surfical erosion and the rill to gulley erosion all couple to effect the development of natural stream design. Valley fills end up as unique landforms, they do exhibit geotechnical stability; however, they are not suited, as currently regulated, to incorporate surface hydrologic features to enable stream replacement or development.
>
> ii) Drainage density is measure of the average stream channel spacing and results from flow interactions with sediment and soil, topography, weather variables, and vegetation (Bugosh, 2004; Toy and Chuse, 2005). For a given reference landform, the drainage density describes the drainage network that can be supported without significant aggradation or erosion (Bugosh, 2004). The fluvial geomorphic design approach

assumes a dendritic pattern, a configuration common for unconsolidated materials (Toy and Chuse, 2005; Eckels and Bugosh, 2010).

iii) Natural channels vary in characteristics with location in the watershed. Headwater streams are often steep (>4% slope) and relatively straight (sinuosity = 1.0-1.2), and down-stream channels have a lower gradient (<4% slope) and increased sinuosity (>1.2; Rosgen, 1996). Stream characteristics must be considered to designs systems that will properly manage both flow and sediment discharge: bankfull width, width to depth ratio, sinuosity, meander belt width, "A" channel reach length (the distance of one-half of a meander length in steep channels), and sinuosity (Eckels and Bugosh, 2010). Ridge to head of channel distance defines the length required to form concentrated flow, advising the channel head location in reference to the watershed boundary.

Geomorphic Landform Design of a Valley Fill Under Construction

The design tool Carlson Natural Regrade with GeoFluv® was used to apply the geomorphic landform design approach to a specific valley fill site currently under construction. The study site is in the southern WV coalfield region. The area is characterized by a system of steep-sloped ridges and valleys (Figure 1.1).

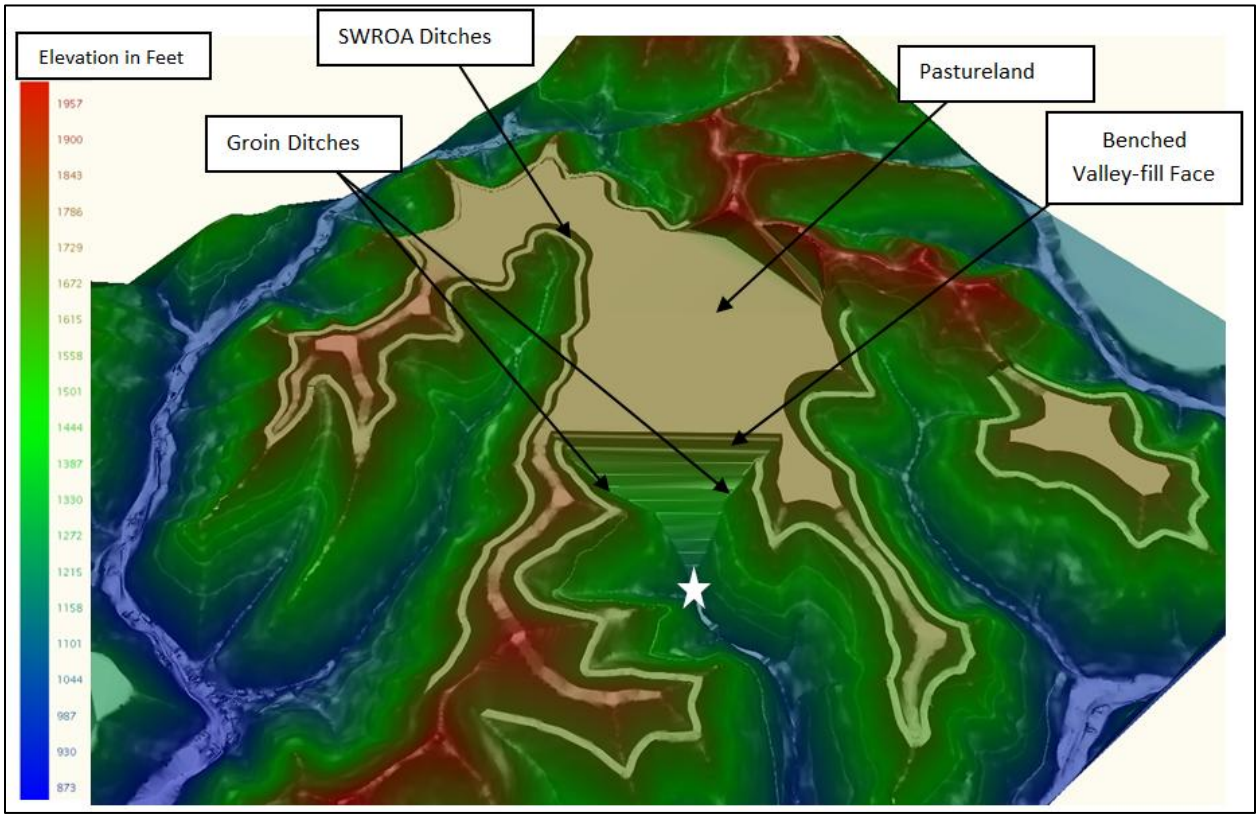

Figure 1.1 Valley fill under construction with labeled design features

Slope Stability

GeoFluv® generated geomorphic landform designs do not analyze the stability of the slopes. It is critical that slope structures remain durable and do not fail when constructed with surface mine overburden for several reasons. If toxic mineralogy exist within the overburden, slope stability becomes an especially critical analysis that should be performed before construction begins. Slope structures have the capacity to encapsulate and contain ecologically destructive mineralogy. In steep sloped Appalachia, it is also especially critical to perform slope stability analysis to ensure the durability of the structure. In some cases, AOC or GeoFluv® designs may not be adequate for the stability of slopes. As slope angles increase, the factor of safety of a slope structure decreases, and the probability of failure increases. In Appalachia, it is not uncommon to find mountainous terrain with shear rock cliffs which cannot be reconstructed to AOC. Exceedingly steep slopes should not be built. Safety concerns may also arise when constructing steep slopes.

If adequate slope stability analysis is performed on GeoFluv® generated slopes which are associated with specified design limitation criteria, then the environmental, and societal benefit could result. Inevitably, all surface mined areas are contributors to large watersheds. Slope failure has the potential in many cases to introduce ecologically destructive mineralogy into the watershed, as well as sediment pollution. Sediment accumulation can alter stream beds and have great potential to result in a legion of significant erosion impacts, and can cause flooding. When taking these very realistic scenarios into account, it can easy be understood that slope failure can have a significant impact on the health and safety of downstream communities as well as the operators constructing the structures.

3. Approach

The approach taken for this study involved considering the design limitations of two types of soil retrieved from a surface mine site in southern West Virginia. The shear strength of the unweathered sandstone overburden material was determined via direct shear testing in order to have a better understanding of its geotechnical properties. During the course of the research effort, it was decided that only the unweathered sandstone material would be examined thoroughly for strength. The geotechnical values that were found via testing were input into GeoSlope software for modeling analysis.

Step#1: Acquire physical and engineering properties of a cover material and a blasted fill material.

Step#2: Assess the strength characteristics of the field soil as the primary material in the slope structures to be modeled.

Step#3: Consider the grain size distribution of as received and pre-permeability specimens prepared at predetermined compaction energies in order to develop grading envelopes to better understand how the materials may degrade and create fine particles with transport potential when compacted in the field during slope construction.

Step#4: Evaluate the pre-and-post-permeability grain size distributions to determine particle movement behavior

Step #5: Utilize GeoSlope® software modules SIGMA/W, SEEP/W, and SLOPE/W to model the valley fill under inspection and determine the stability of the structure using general limit

equilibrium and sensitivity analysis as well as insitu stress calculations involving hydraulic parameters generated with a 10 years of infiltration with a set hydraulic conductivity.

4. Materials and Methods

The materials selected for this research included a blasted, weathered sandstone material and a blasted, unweathered sandstone material retrieved from a surface mine site in Logan County, West Virginia on the hot, dry day of June 7th 2011. The materials will be simply referred to as "weathered sandstone," and "unweathered sandstone." The samples were obtained from the disturbed area at an active surface mine reclamation site where piles of end dumped material were allotted some time to be exposed to surface conditions. The samples were obtained prior to any leveling or compaction effort. The geotechnical material physical and engineering property tests were performed according the ASTM standard test methods and included: Moisture content (D-2216), Sieve/hydrometer (D-422), Specific Gravity (D-854), Atterberg Limits (D-4318), Standard Proctor (D-698), Soil Classification–USCS (D-2487), Direct Shear (D-3080), and Hydraulic Conductivity (D-5856). Many of the specimen labels incorporate the terms "brown" and "gray," but will be referred to in the text as "weathered sandstone" and "unweathered sandstone," respectively. The results of the experimental testing are reported in the following sections. The laboratory tests included duplicate and triplicate specimen testing for precision. Most test data is presented in the appendices. The results are reported in Chapter 5 through Chapter 12.

5. Material Properties and Results: Weathered Sandstone

The objective of the testing performed is to discover the geotechnical properties and gradations of a weathered sandstone sampled at a nearby site to the unweathered sandstone overburden material discussed in other sections. The results of this laboratory testing will be compared to the unweathered sandstone overburden to determine whether or not their properties vary significantly enough to be included as input parameters in the numerical slope stability modeling. The test methods and associated results are shown in the following text. The material under inspection in this section was classified using the United Soil Classification System (USCS) – ASTM D 2487. After assessment, the weathered sandstone material was classified to be a well graded gravel (GW).

5.1 Moisture Content

Testing was performed according to ASTM standard test method D 2216-05. The sampling was performed on a hot, dry day; however, the moisture content was measured in the laboratory after the specimens acclimated to the indoor climate. The coefficient of variation was found to be 0.017, which implies little variability in the results of the testing. The average moisture content was found to be 8.07%. Table 5.1, Table 5.2, and Table 5.3 present the results for the triplicate specimen testing.

Table 5.1 Moisture Content Data

Test Number	1	2	3
Empty Container, $M_{c,}$ (g)	17.41	17.3	18.77
Container + Wet Sample, M_{cms}, (g)	73.92	80.97	80.85
Container + Dry Sample, M_{cds}, (g)	69.63	76.29	76.22
Moisture content w (%)	**8.22**	**7.93**	**8.06**

Table 5.2 Average Moisture Content and Statistics

Average Moisture Content (%):	**8.070**
Sample Standard Deviation (s)	0.141
Coefficient of Variation (COV)	0.017

Table 5.3 Equations Used

M_w = mass of water = M_{cms} - M_{cds}
M_s = mass of dry sample = M_{cds} - M_c
w% = (M_w/M_s) x 100

5.2 As Received Grain Size Distribution and Hydrometer Analysis

Sieve analysis was performed according to ASTM D 422-63. A duplicate test was performed to ensure accuracy in the data. The objective of this testing was to obtain appropriate data in order to classify the material, and understand its original as received grain size distribution. The as received grain size distribution results were a critical element in the understanding of material changes that can occur during construction under different compaction energies. A hydrometer test was run for the particles passing the #200 sieve. For the first test the critical indices were D_{90} = 24, D_{60} = 9, D_{50} = 6.3, D_{30} = 2.00, D_{25} = 1.3, D_{10} = .22(mm). The uniformity coefficient (C_u) was 40.91 and the coefficient of gradation (C_c) was 2.02. For the second test the critical indices were D_{90} = 33, D_{60} = 6.9, D_{50} = 6.2, D_{30} = 1.7, D_{25} = 1.3, D_{10} = 0.29(mm). The uniformity coefficient (C_u) was 23.79 and the coefficient of gradation (C_c) was 1.44. Some variability occurred in the data as represented by the coefficient of variation at 0.374 for the uniformity coefficient and 0.235 for the coefficient of gradation. The variation is likely the result of clodding of the particles due to the presence of moisture. The data does follow the same trend approximately. The hydrometer analysis illustrated the presence of few fine particles relative to the sample size. The results are shown in Table 5.4 through Table 5.9, Figure 5.1 and Figure 5.2. Table 5.8 shows data according to ASTM D-422 tables and associated values.

Table 5.4 Mass Loss of Sample

As Received	**Test 1**	**Test 2**
Mass of Sample	500	500
Mass Loss(%)	0.28	0.23

Table 5.5 Critical Index Values and Coefficients

Results		
Critical Indices	Test 1	Test 2
D_{90}	24.00	33.00
D_{60}	9.00	6.90
D_{50}	6.30	6.20
D_{30}	2.00	1.70
D_{25}	1.30	1.30
D_{10}	0.22	0.29
Uniformity Coefficient, C_u	**40.91**	**23.79**
Coefficient of Gradation, C_c	**2.02**	**1.44**

Table 5.6 Uniformity coefficient statistics

Uniformity Coefficient, C_u	
Average Uniformity Coefficient	32.351
Sample Standard Deviation (s)	12.103
Coefficient of Variation (COV)	0.374

Table 5.7 Coefficient of gradation statistics

Coefficient of Gradation, C_c	
Average Coefficient of Gradation	1.732
Sample Standard Deviation (s)	0.407
Coefficient of Variation (COV)	0.235

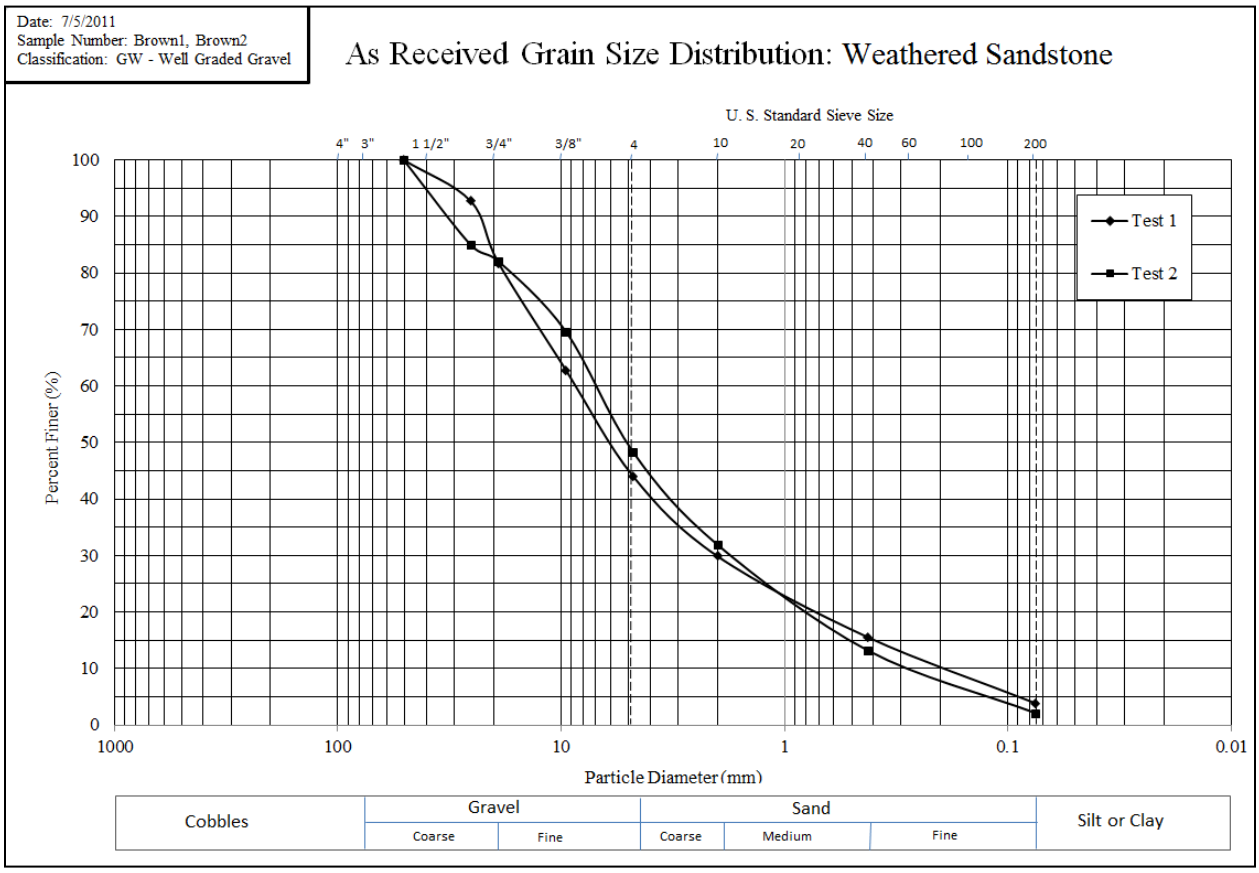

Figure 5.1 Grain Size Distribution of two as received samples

Table 5.8 Weathered Sandstone GW sample hydrometer data.

Hydrometer No.:		Sample Moist Mass, g	Moisture Content , w%		Sample Dry Mass, g		G_s	
152H		100	8.07		91.93		2.75	
Elapsed Time, (T) min	Hydrometer Reading	Actual Hydrometer Reading, R	Temp, °C	K (Table3)	a (Table1)	% Finer, P	Effective Depth, (L) cm (Table 2)	Particle Diameter, (D) mm
2	63	63	22	0.01249	0.98	67.2	8.1	0.0251
5	60	60	22	0.01249	0.98	64	8.9	0.0167
15	52	52	22	0.01249	0.98	55.4	9.9	0.0101
30	46	46	22	0.01249	0.98	49	10.6	0.0074
60	41	41	22	0.01249	0.98	43.7	11.1	0.0054
250	29	29	22	0.01249	0.98	30.9	12.2	0.0028
1440	20	20	22	0.01249	0.98	21.3	13.3	0.0012

Table 5.9 Hydrometer equations and definitions

151H:	$P=[(100{,}000/W)x(G/(G-G_1)])(R-G_1)$
152H:	P=(Ra/W)x100
a	Correction factor to be applied to the reading of hydrometer 152H.
P	Percentage of soil remaining in suspension at the level at which the hydrometer measures the density of the suspension.
R	Hydrometer reading with composite correction applied
W	Oven-dry mass of soil in a total test sample represented by mass of soil dispersed (g)
G	Specific gravity of the soil particles
G_1	Specific gravity of the liquid in which soil particles are suspended.
K	Constant depending on the temperature of the suspension and the specific gravity of the soil particles
L	Distance from the surface of the suspension to the level at which the density of the suspension is being measured
T	Interval of time from beginning of sedimentation to the taking of the reading, min.
D	Diameter of particle, mm.
Note:	Meniscus correction is the difference between the hydrometer reading and zero for 152H hydrometer (7.3)
$D = K\sqrt{\frac{L}{T}}$	

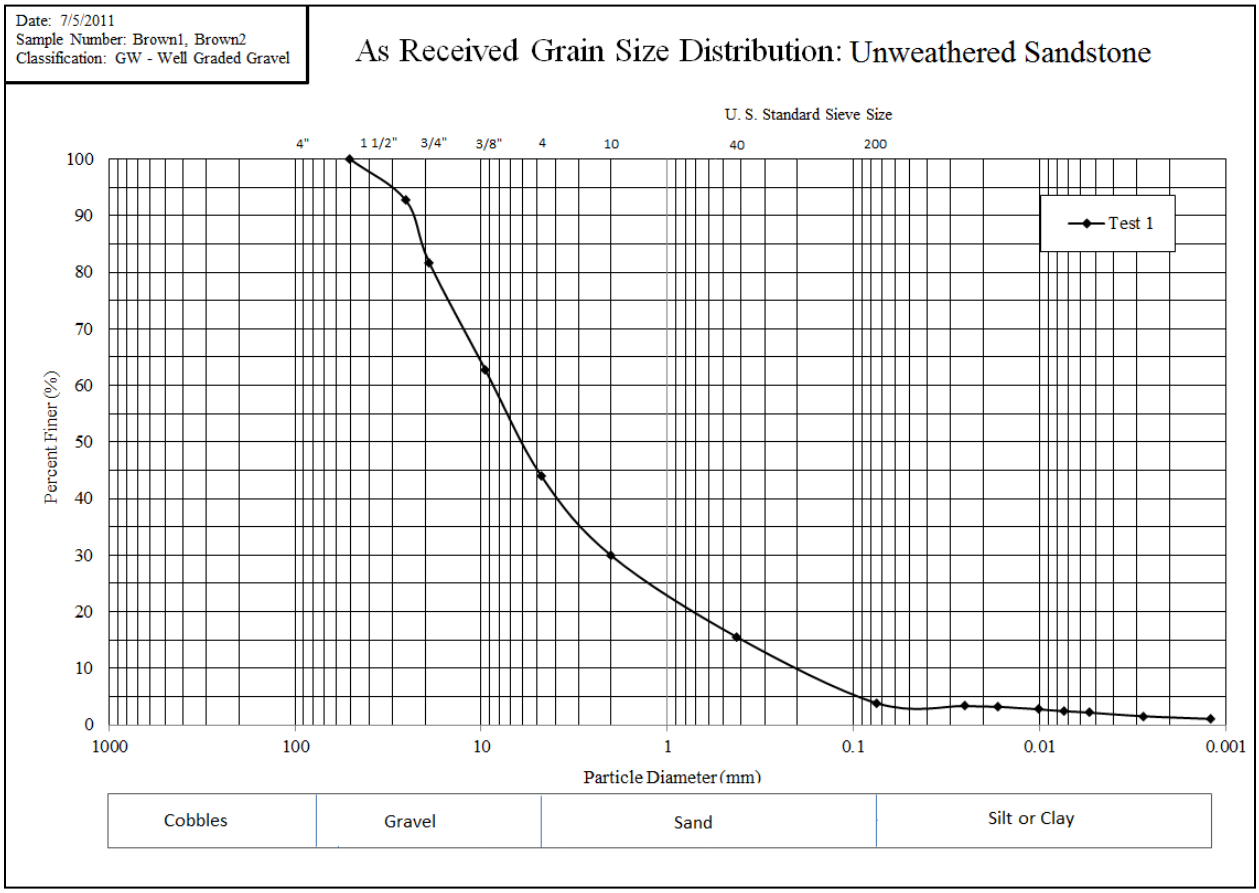

Figure 5.2 Grain size distribution graph including hydrometer data.

5.3 Specific Gravity – Test 1

Specific gravity testing was performed according to ASTM standard test method D 854. Three tests were run in order to ensure the accuracy of the data. The objective of the specific gravity testing was to obtain knowledge about the physical characteristics of the material. For the first test, the specific gravity was found to be 2.81. For the duplicate test, the specific gravity was found to be 2.75. The high precision of the tests is represented by the coefficient of variation of 0.014. The results for the first test are shown in Table 5.10 through Table 5.12 . Table 5.12 shows the equations used and the associated definitions. The data for this test are presented in appendix IV.

Table 5.10 Test statistics for specific gravity of soil solids.

Average Specific Gravity, G_t:	**2.810**
Sample Standard Deviation for G_t (s)	0.041
Coefficient of Variation for G_t (COV)	0.014

Table 5.11 Test statistics for specific gravity at the test temperature.

Avg. Specific Gravity at Test Temp, G_{tt}:	**2.810**
Sample Standard Deviation for $G_{tt,}$ (s)	0.041
Coefficient of Variation for G_{tt} (COV)	0.014

Table 5.12 Specific gravity equations and definitions

M_p = the mass of the dry pycnometer, g
V_p = the volume of the pycnometer, mL
$\rho_{w,t}$ = the density of water at the test temperature (T_t), g/mL
ρ_s = the density of the soil solids (Mg/m^3) or (g/cm^3)
$w = (M_w/M_s) \times 100$ (%)
$M_{pws,t}$ = the mass of pycnometer, water, and soil solids at the test temperature, (T_t), (g)
K = temperature coefficient
M_w = mass of water = $M_{cms} - M_{cds}$ (g)
M_s = mass of dry sample = $M_{cds} - M_c$ (g)
$M_{pw,t}$ = mass of the pycnometer and water at the test temperature (T_t), g
Note: K and ρ_w values acquired in Table 1 of ASTM D 854 -06
$M_{pw,t} = M_p + (V_p * \rho_{w,t})$
$G_T{}^oC = K * G_t$
$G_t = \rho_s/\rho_{w,t} = M_s/(M_{\rho w,t}-(M_{\rho ws,t}-M_s))$

5.4 Specific Gravity – Test 2

Specific gravity testing was performed according to ASTM standard test method D 854. Three tests were run in order to ensure the accuracy of the data. The objective of the specific gravity testing was to obtain knowledge about the physical characteristics of the material. This duplicate test was performed to achieve high precision for the specific gravity testing of the weathered sandstone. The coefficient of variation of the data was found to be 0.002; implying little variation in the results. The average specific gravity was found to be 2.75. The data is located in appendix IV. The results for the duplicate specific gravity test are shown in Table 5.13 and Table 5.14.

Table 5.13 Test statistics for specific gravity of soil solids.

Average Specific Gravity, G_t:	**2.75**
Sample Standard Deviation for G_t, s	0.004
Coefficient of Variation for G_t (COV)	0.002

Table 5.14 Test statistics for specific gravity at the test temperature.

Avg. Specific Gravity at Test Temp, G_{tt}:	**2.75**
Sample Standard Deviation for $G_{tt,}$ (s)	0.004
Coefficient of Variation for G_{tt} (COV)	0.002

5.5 Atterberg Limits

Atterberg limit tests including the plastic limit and liquid limit tests were performed on the weathered sandstone material according to ASTM standard test method D 4318. The objective of the testing was to determine the liquid limit, plastic limit, and plasticity index of the material. The liquid limit of the material was found to be 26.2. The plastic limit was found to be 22.4 with a plasticity index of 3.8. The test results are presented in the following Table 5.15 and Figure 5.3.

Table 5.15 Determination of plastic limit, liquid limit and plasticity index

Plastic Limit:	**22.4**
Liquid Limit:	**26.2**
Plasticity Index:	**3.8**

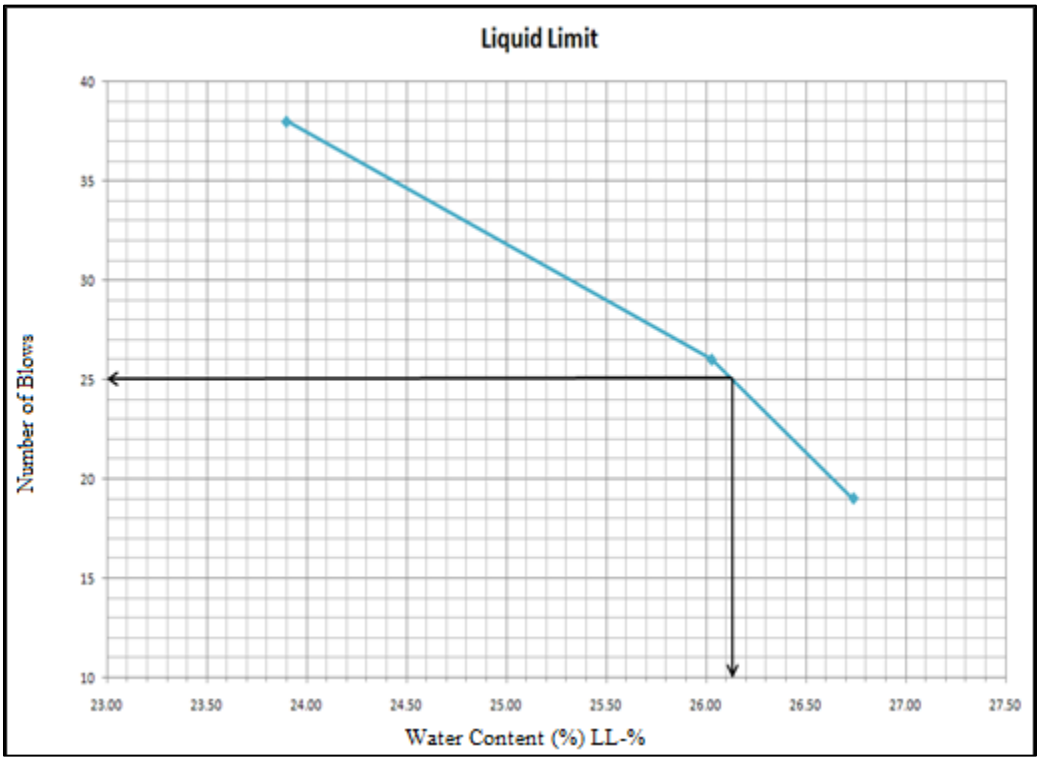

Figure 5.3 Liquid limit graph for the weathered sandstone material

6. Material Properties: Unweathered Sandstone Overburden

The unweathered sandstone overburden was sampled at a surface mine site in southern West Virginia. The sampling site was the same as for the weathered sandstone material. The unweathered sandstone overburden was a blasted sandstone material. The material was classified using the United Soil Classification System (USCS) – ASTM D 2487. After assessment, the unweathered sandstone material was classified to be a well graded sand (SW). In accordance with ASTM test methods, the material was sieved between the #4 and #200 sieves. The sieved gradation was classified as a SW-SM material or a well graded sand with silt.

6.1 Moisture Content

Testing was performed according to ASTM standard test method D 2216-05. The sampling was performed on a hot, dry day; however, the moisture content was measured in the laboratory after the specimens acclimated to the indoor climate. There was little variation in the results. The coefficient of variation was found to be 0.052, implying high precision in the data. Table 6.1and Table 6.2 present the results for the triplicate specimen testing. Table 6.3 shows the equations used for the calculations.

Table 6.1 Moisture Content Data

Test Number	1	2	3
Empty Container, $M_{c,}$ (g)	16.89	21.79	30.03
Container + Wet Sample, M_{cms}, (g)	70.86	74.82	100.21
Container + Dry Sample, M_{cds}, (g)	69.37	73.33	98.42
Moisture content w (%)	**2.84**	**2.89**	**2.62**

Table 6.2 Average Moisture Content and Statistics

Average Moisture Content (%):	**2.78**
Sample Standard Deviation (s)	0.145
Coefficient of Variation (COV)	0.052

Table 6.3 Equations Used

M_w = mass of water = M_{cms} - M_{cds}
M_s = mass of dry sample = M_{cds} - M_c
$w = (M_w/M_s) \times 100$

6.2 As Received Grain Size Distribution

Sieve analysis was performed according to ASTM D 422-63. A duplicate test was performed to ensure accuracy in the data. The objective of this testing was to obtain appropriate data in order to classify the material, and understand its original as received grain size distribution. The as received grain size distribution results were a critical element in the understanding of material changes that can occur during construction under different compaction energies. For the first test the critical indices were D_{90} = 12, D_{60} = 2.7, D_{50} = 1.6, D_{30} = 0.55, D_{25} = 0.40, D_{10} = 0.13(mm). The uniformity coefficient (C_u) was 20.77 and the coefficient of gradation (C_c) was 0.86. For the second test the critical indices were D_{90} = 10.7, D_{60} = 3.0, D_{50} = 1.6, D_{30} = 0.55, D_{25} = 0.39, D_{10} = 0.12(mm). The uniformity coefficient (C_u) was 25.00 and the coefficient of gradation (C_c) was 0.84. The data approximately followed the same trend along their curves. The precision of the data is shown by a coefficient of variation for the uniformity coefficient of 0.131, and a coefficient of variation for the coefficient of gradation of 0.018. The hydrometere analysis illustrated that there are few fines in the sample relative to the sample size. The results are shown in Table 6.4 through Table 6.7, Figure 6.1and Figure 6.2.

Table 6.4 Critical Index-Values and Coefficients

Results		
Critical Indices	Test 1	Test 2
D_{90}	12	10.7
D_{60}	2.7	3
D_{50}	1.6	1.6
D_{30}	0.55	0.55
D_{25}	0.4	0.39
D_{10}	0.13	0.12
Uniformity Coefficient, C_u	**20.77**	**25**
Coefficient of Gradation, C_c	**0.86**	**0.84**

Table 6.5 Uniformity coefficient statistics

Uniformity Coefficient, C_u	
Average Uniformity Coefficient	22.885
Sample Standard Deviation (s)	2.992
Coefficient of Variation (COV)	0.131

Table 6.6 Coefficient of gradation statistics

Coefficient of Gradation, C_c	
Average Coefficient of Gradation (%)	0.851
Sample Standard Deviation (s)	0.015
Coefficient of Variation (COV)	0.018

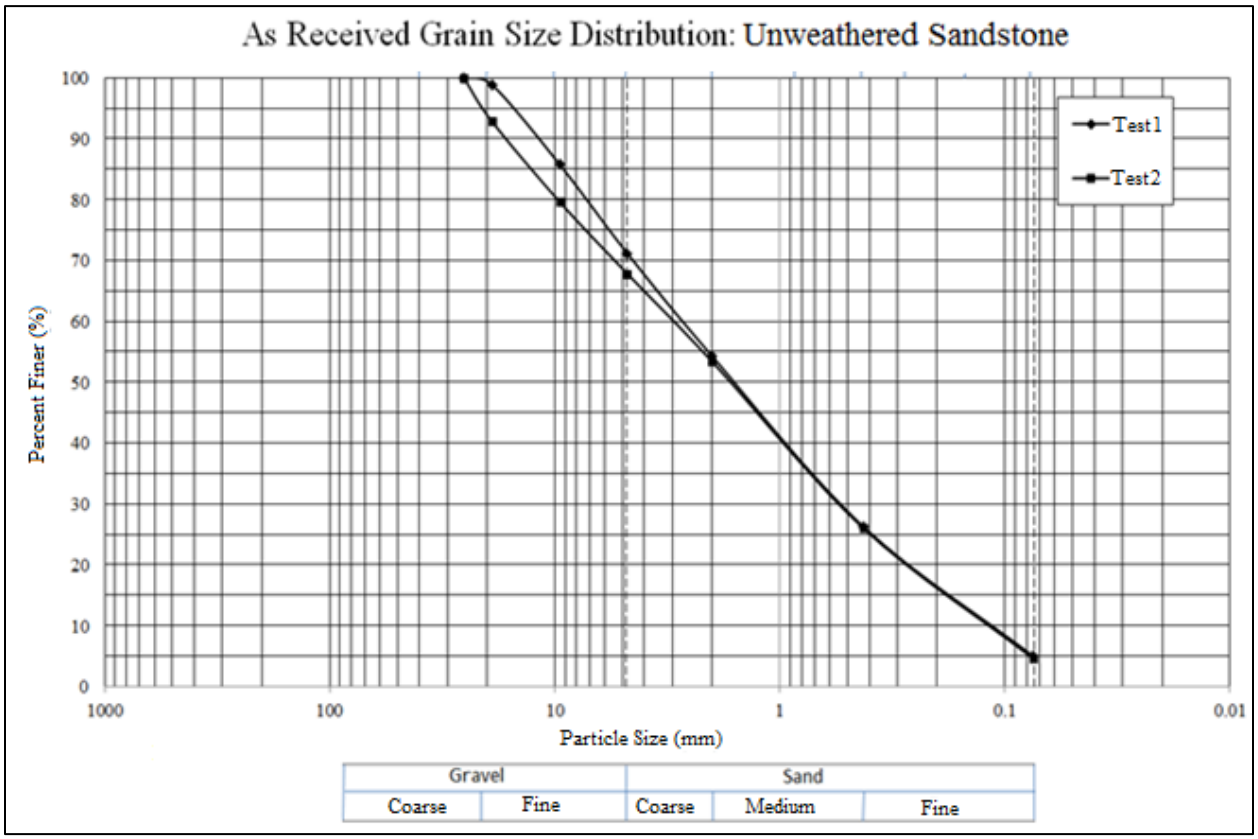

Figure 6.1 Grain Size Distribution of two samples of unweathered sandstone overburden SW.

Table 6.7 Unweathered Sandstone SW-SM sample hydrometer data.

Hydrometer No.:		G_s		Sample Moist Mass, g		Moisture Content , w%	Sample Dry Mass, g	
152H		2.75		100		2.78	97.22	
Elapsed Time, (T) min	Hydrometer Reading	Actual Hydrometer Reading, R	Temp, °C	K (Table3)	a (Table1)	% Finer, P	Effective Depth, (L) cm (Table 2)	Particle Diameter, (D) mm
2	60	60	22	0.01294	0.98	60.5	6.5	0.0233
5	56	56	22	0.01294	0.98	56.4	7.1	0.0154
15	46	46	22	0.01294	0.98	46.4	8.8	0.0099
30	40	40	22	0.01294	0.98	40.3	9.7	0.0074
60	36	36	22	0.01294	0.98	36.3	10.4	0.0054
250	26	26	22	0.01294	0.98	26.2	12	0.0028
1440	18	18	22	0.01294	0.98	18.1	13.3	0.0012

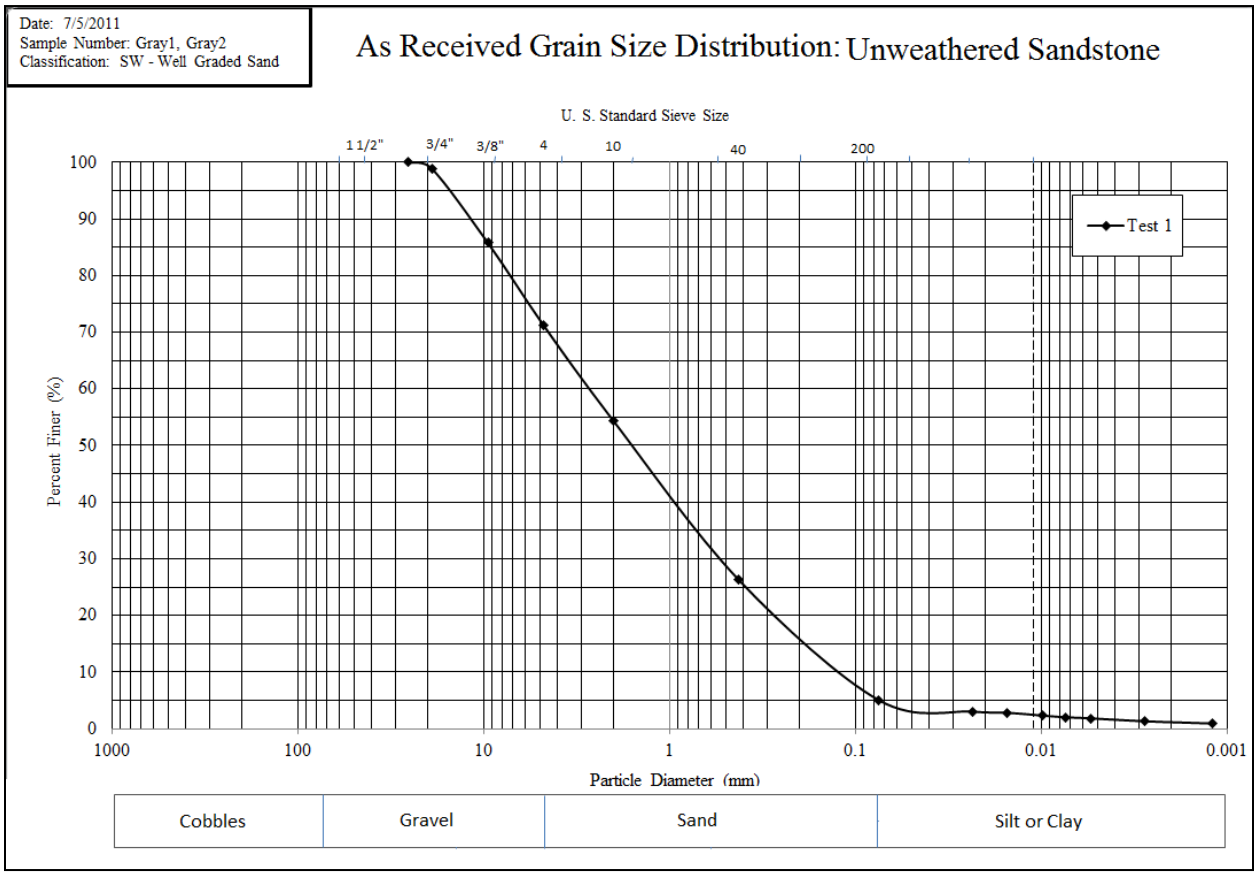

Figure 6.2 Grain size distribution including hydrometer data.

6.3 Specific Gravity

Specific gravity testing was performed according to ASTM standard test method D 854. The objective of the specific gravity testing was to obtain knowledge about the physical characteristics of the material. The specific gravity was found to be 2.69. The precision of the testing was reflected by the coefficient of variation. The coefficient of variation was found for the specific gravity and the specific gravity at the test temperature to be 0.029. The test data are shown in Table 6.8 and Table 6.9.

Table 6.8 Test statistics for specific gravity of soil solids.

Average Specific Gravity, G_t	2.690
Sample Standard Deviation for G_t, s	0.078
Coefficient of Variation for G_t (COV)	0.029

Table 6.9 Test statistics for specific gravity at the test temperature.

Avg. Specific Gravity at Test Temp, G_{tt}:	2.690
Sample Standard Deviation for G_{tt}, s	0.078
Coefficient of Variation for G_{tt} (COV)	0.029

6.4 Atterberg Limits – Test 1

Atterberg limit tests included the plastic limit and liquid limit test. The tests were performed on the unweathered sandstone material according to ASTM standard test method D 4318. A duplicate test was performed in order to ensure accuracy in the data. The objective of the testing was to determine the liquid limit, plastic limit, and plasticity index of the material. For the first test the liquid limit of the material was found to be 19.3. The plastic limit was found to be 16.3 with a plasticity index of 3.1 which indicates that the material is slightly plastic (PL 1-5) (Das, 2006). For the second test the liquid limit of the material was found to be 19.1. The plastic limit was found to be 16.5 with a plasticity index of 2.6. The test results are presented in Table 6.10 and Figure 6.3. The data is presented in Appendix IV

Table 6.10 Determination of plastic limit, liquid limit and plasticity index

Plastic Limit:	**16.3**
Liquid Limit:	**19.3**
Plasticity Index:	**3.1**

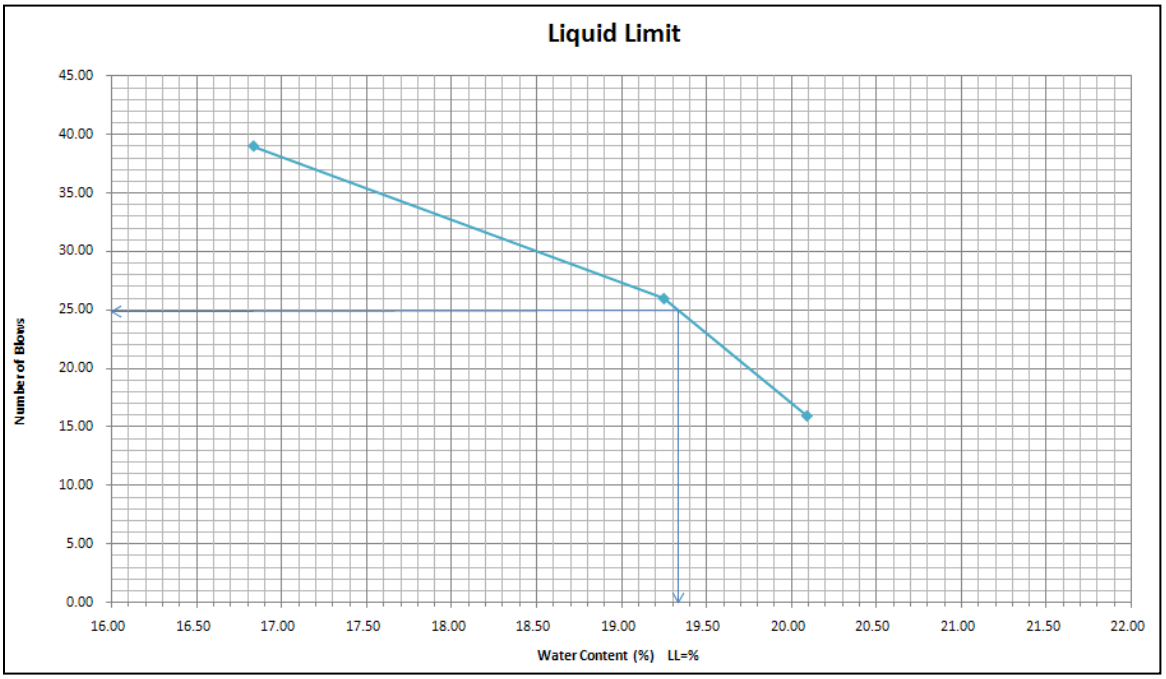

Figure 6.3 Liquid Limit graph for test 1

6.5 Atterberg Limits – Test 2

Atterberg limit tests included the plastic limit and liquid limit test. The tests were performed on the unweathered sandstone material according to ASTM standard test method D 4318. This duplicate test was performed in order to ensure accuracy in the data. The objective of the testing was to determine the liquid limit, plastic limit, and plasticity index of the material. For this duplicate test, the liquid limit of the material was found to be 19.1. The plastic limit was found to be 16.5 with a plasticity index of 2.6 which indicates that the soil is slightly plastic (PL 1-5) (Das, 2006). The test results for the Atterberg Limits are shown in Table 6.11 and Figure 6.4. The data is presented in Appendix IV.

Table 6.11 Determination of plastic limit, liquid limit and plasticity index

Plastic Limit:	**16.5**
Liquid Limit:	**19.1**
Plasticity Index:	**2.6**

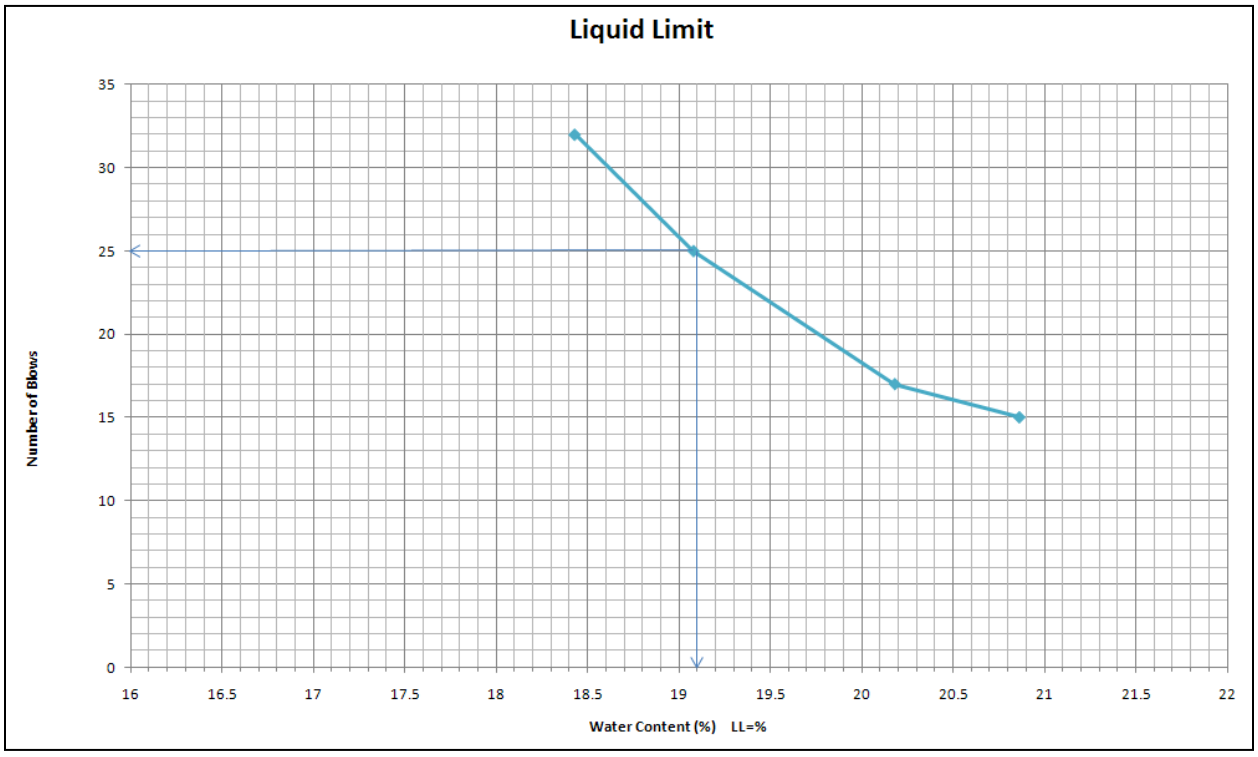

Figure 6.4 Liquid limit graph for test 2

6.6 Weathered and Unweathered Sandstone Comparison

The two materials "unweathered sandstone" and "weathered sandstone" were tested for their individual geotechnical material properties and as received grain size distributions. The results show that the materials are somewhat different. The weathered and the unweathered sandstone are both slightly plastic soils (Das, 2006). The grain size analysis illustrates that the gradations do vary. No strength testing was performed for the weathered material, and it was not included in the numerical modeling of the slopes. Since most of the volume of a landform design typically consists of overburden material, only the weathered sandstone was used for input into the numerical models. A summary of the material properties and as received grain size distributions are shown in Table 6.12 and Figure 6.5. It is important to note that the Atterberg limits test method was for the material passing a #40 sieve. The unweathered material was reclassified as a well graded sand with silt or SW-SM, as the more coarse particles were separated for the laboratory testing.

Table 6.12 Soil Property summary table for unweathered and weathered sandstone

Soil Property Summary	**Unweathered Sandstone**	**Weathered Sandstone**
Soil Classification	SW	GW
As Received Moisture Content, w (%)	2.78	8.07
As Received GSD		
Test 1		
C_u (mm)	20.77	40.91
C_c (mm)	0.86	2.02
Test 2		
C_u (mm)	25	23.79
C_c (mm)	0.84	1.44
Specific Gravity, G_s	2.69	2.81
Atterberg Limits – Passing #40 Sieve		
LL	19.3	22.4
PL	16.3	26.2
PI	3.1	3.8

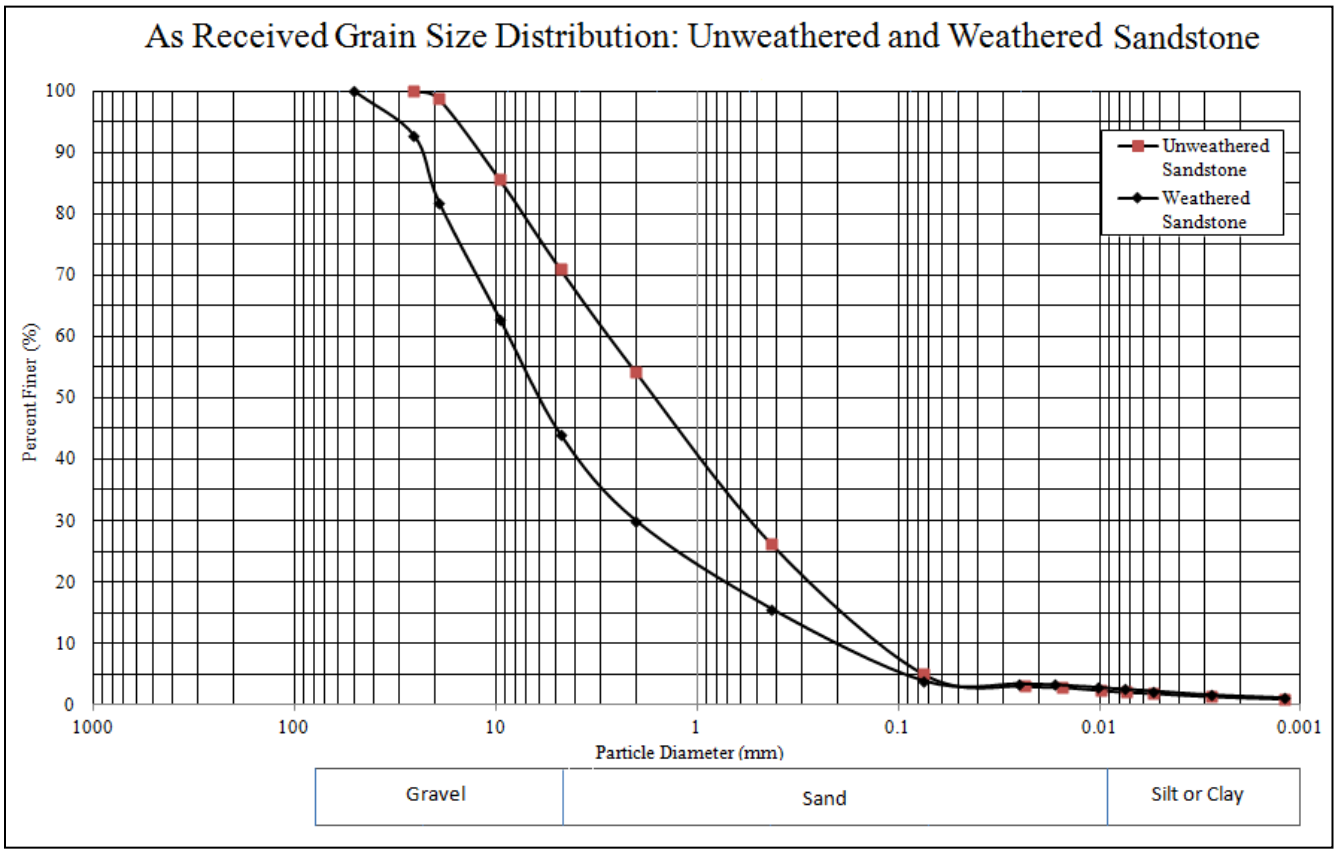

Figure 6.5 As received grain size distributions of weathered and unweathered sandstone

7. Compaction

Compaction testing was performed to find the maximum dry density of the unweathered sandstone overburden material at three predetermined compaction energies. The tests were run at a standard proctor compaction effort (energy applied = 592.5 kJ/m^3), at a 34% Proctor effort (energy applied = 203.6 kJ/m^3), and at an 11% Proctor compaction effort (67.85 kJ/m^3). Multiple water contents were used for the testing for the optimization of each test. The objective of the compaction testing was to find the optimum and minimum dry density of the material at the compaction energies listed above. The compaction testing data are presented in this chapter.

7.1 Standard Proctor (592.5 kJ/m^3)

The testing described in this section were run at a standard proctor compaction effort (energy applied = 592.5 kJ/m^3). Four water contents were tested. The water contents were calculated to be 4.12%, 9.94%, 11.54%, and 12.86%. The optimum dry density of the material was found to be 18.75 kN/m^3 at a water content of 10.75%. The data are shown in Table 7.1 and Figure 7.1.

Table 7.1 Compaction test results

Test Calculations	**Test 1**	**Test 2**	**Test 3**	**Test 4**
Specific Gravity of Soil, G_s	2.69	2.69	2.69	2.69
Dry Unit Weight of Compacted Specimen(KN/m^3), γ_d	16.65	18.51	18.54	13.92
Dry Unit Weight at S=1.0 (KN/m^3),γ_d	19.57	20.09	20.78	23.71
Dry Unit Weight at S=0.9 (KN/m^3),γ_d	19.03	19.58	20.3	23.45
Degree of Saturation (%), $S=G_s*w/e$	0.59	0.73	0.64	0.12
Saturated Water Content, w_{sat}(%)	21.62	15.71	15.64	33.14
Water Content, w=(Mw/Ms)x100(%)	12.86	11.54	9.94	4.12

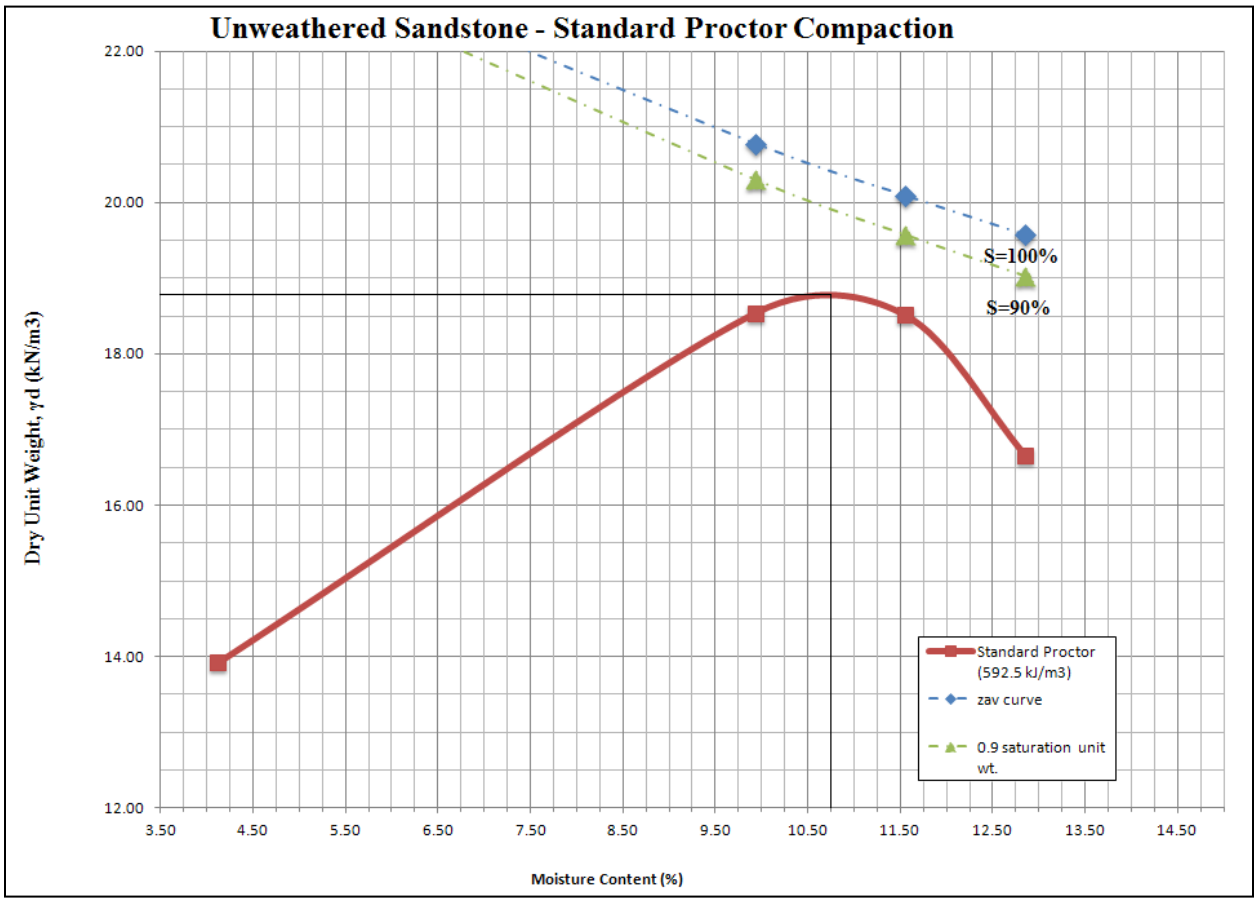

Figure 7.1 Standard proctor curve with lines at 100% and 90% saturation.

7.2 Proctor Compaction Energy at 34%: 12 Blows/Layer, 2 Layers (203.6 kJ/m^3)

The testing described in this section were run at 34% Proctor compaction effort (energy applied = 203.6 kJ/m^3). The test applied 12 blows of a 5 pound compaction hammer to 2 layers of material in a typical compaction mold. The volume of the compaction mold is given in the data below. Seven water contents were tested. The water contents were calculated to be 7.45%, 9.57%, 11.20%, 12.73%, 12.85%, 15.73%, and 17.97%. The optimum dry density of the material was found to be 18.1 kN/m^3 at a water content of 14.5%. The data are shown in Table 7.2 and Figure 7.2.

Table 7.2 Compaction Test Results

Test Calculations	**Test 1**	**Test 2**	**Test 3**	**Test 4**	**Test 5**	**Test 6**	**Test 7**
Specific Gravity of Soil, G_s	2.69	2.69	2.69	2.69	2.69	2.69	2.69
Dry Unit Weight of Compacted Specimen (KN/m^3), γ_d	16.11	16.21	16.48	17.98	17.94	17.8	14.37
Dry Unit Weight at S=1.0 (KN/m^3),γ_d	21.94	20.95	20.24	19.57	19.62	18.51	17.75
Dry Unit Weight at S=0.9 (KN/m^3),γ_d	21.54	20.48	19.73	19.03	19.08	17.91	17.13
Degree of Saturation (%), $S=G_s*w/e$	0.32	0.41	0.5	0.74	0.73	0.88	0.58
Saturated Water Content, w_{sat} (%)	23.58	23.22	22.22	17.28	17.39	17.84	30.96
Water Content, (%) $W= (M_w/M_s)x100$	7.45	9.57	11.2	12.85	12.73	15.73	17.97

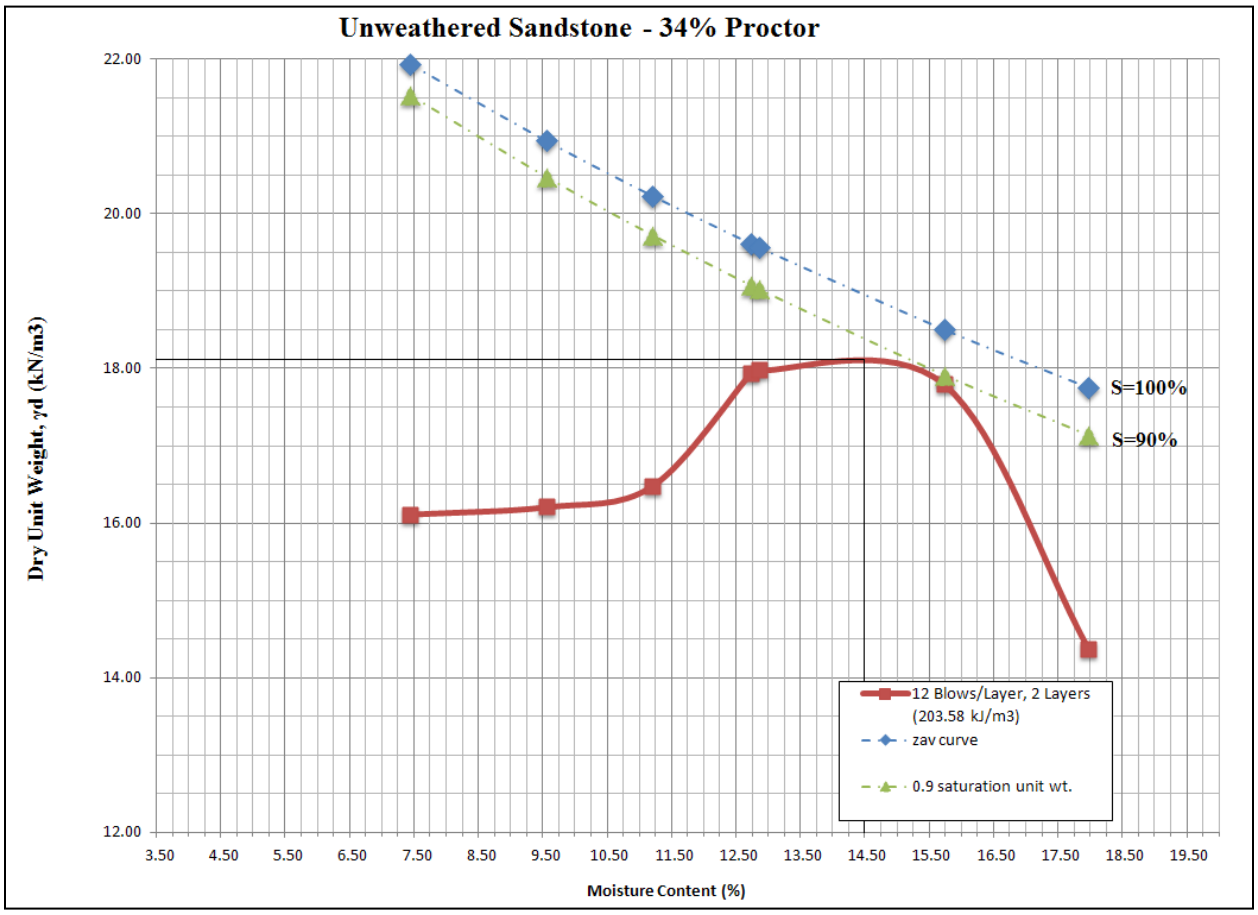

Figure 7.2 34% Proctor curve with lines at 100% and 90% saturation.

7.3 Proctor Compaction Energy at 11%: 4 Blows/Layer, 2 Layers (67.85 kJ/m^3)

The testing described in this section were run at an 11% Proctor compaction effort (energy applied = 67.85 kJ/m^3). The test applied 4 blows of a 5 pound compaction hammer to 2 layers of material in a typical compaction mold. The volume of the compaction mold is given in the data below. Seven water contents were tested. The water contents were calculated to be 4.36%, 9.78%, 11.60%, 11.65%, 15.47%, 16.89%, and 17.45%. The optimum dry density of the material was found to be 17.6 kN/m^3 at a water content of 16.89%. The minimum dry density was found to be 14.9 kN/m^3 at a corresponding water content of 9.75%. The minimum dry density was used to find design limitations in hydraulic conductivity. The hydraulic conductivity testing that was performed is described later in this document. The data for the 11% Proctor compaction effort tests are shown in Table 7.3 and Figure 7.3.

Table 7.3 Compaction Test Results

Test Calculations	Test 1	Test 2	Test 3	Test 4	Test 5	Test 6	Test 7
Specific Gravity of Soil, G_s	2.69	2.69	2.69	2.69	2.69	2.69	2.69
Dry Unit Weight of Compacted Specimen (KN/m^3), γ_d	15.39	16.9	15.2	14.93	15.07	17.6	16.55
Dry Unit Weight at S=1.0 (KN/m^3),γ_d	23.57	18.6	20.07	20.85	20.05	18.11	17.92
Dry Unit Weight at S=0.9 (KN/m^3),γ_d	23.3	18.01	19.55	20.38	19.53	17.5	17.31
Degree of Saturation (%), $S=G_s*w/e$	0.16	0.75	0.43	0.34	0.42	0.92	0.79
Saturated Water Content, w_{sat} (%)	26.45	20.74	27.22	28.41	27.79	18.46	21.97
Water Content, (%) $W= (M_w/M_s)x100$	4.36	15.47	11.6	9.78	11.65	16.89	17.45

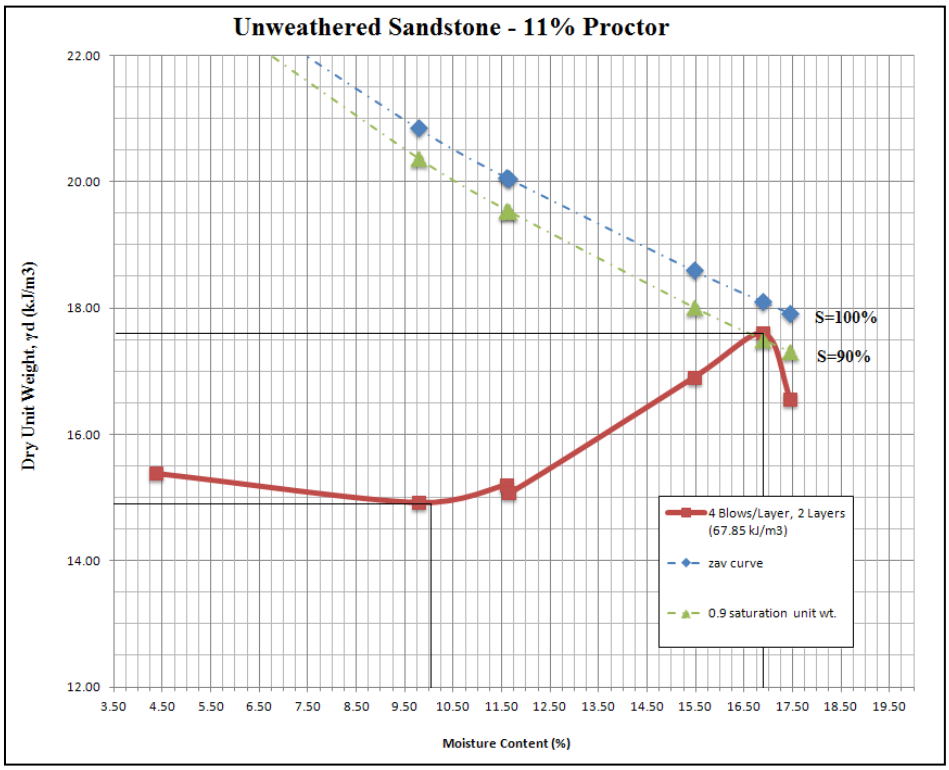

Figure 7.3 11% Proctor compaction curve with lines at 100% and 90% saturation.

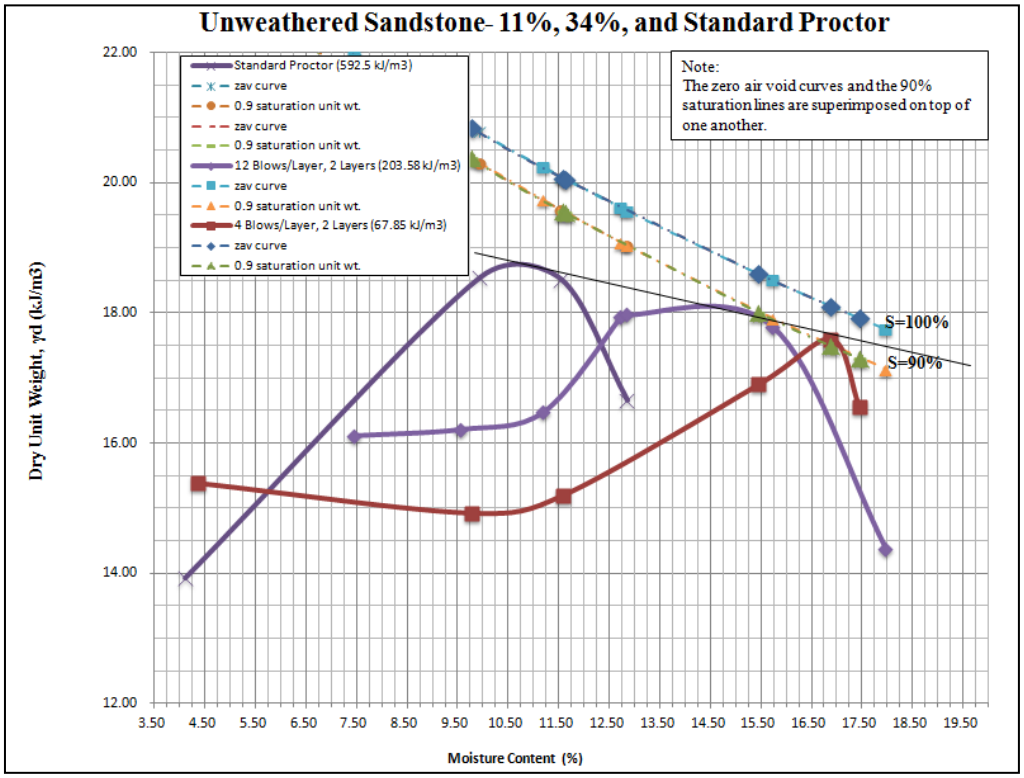

Figure 7.4 Compaction curve compilation

Discussion

The compaction curves in Figure 7.4 show different behavior. The standard proctor curve is a typical bell shaped curve with an optimum dry unit weight of 18.75 kN/m^3 at a moisture content of approximately 10.75%. The 34% proctor curve resembles a transition between standard proctor and 11% proctor curves. The optimum dry density of the 34% proctor curve was 18.1 kN/m^3 at a moisture content of 14.50%. The 11% proctor curve shows a compaction curve resembling a standard behavior for a well graded sand. The optimum dry density of the 11% proctor was at 17.6 kN/m^3 with a moisture content of approximately 17.00%. The minimum dry density of the 11% curve was at 10.50% moisture content at a value of 14.90 kN/m^3. The compaction energy applied in these three scenarios varied from 592.5 kJ/m^3 (standard proctor), 203.6 kJ/m^3(34% proctor), and 67.85 kJ/m^3 (11% proctor). The optimum dry densities did not increase by much, only a difference of 1.15 kN/m^3 between standard proctor and 11% proctor compaction. The corresponding moisture contents for these maximums varied from 10.75% (standard proctor) to 17.00% (11% proctor) at a difference of 6.25%. The material does not need a significant amount of compaction in order to achieve a high dry density, but it does need the accompanying moisture content to achieve it.

7.4 Variability in Compaction

After reducing the compaction data, it was found that some significant variability occurred for the 34% and 11% Proctor compaction effort testing. The variability is a result of a thick first lift in the compaction mold. At a low energy, some of the specimen could not experience the full effect of the compaction effort. The points lying off of the curve are the compaction points for 34% Proctor compaction effort permeability triplicate specimen testing and a direct shear specimen. The variability effects are shown in Figure 7.5 and Figure 7.6.

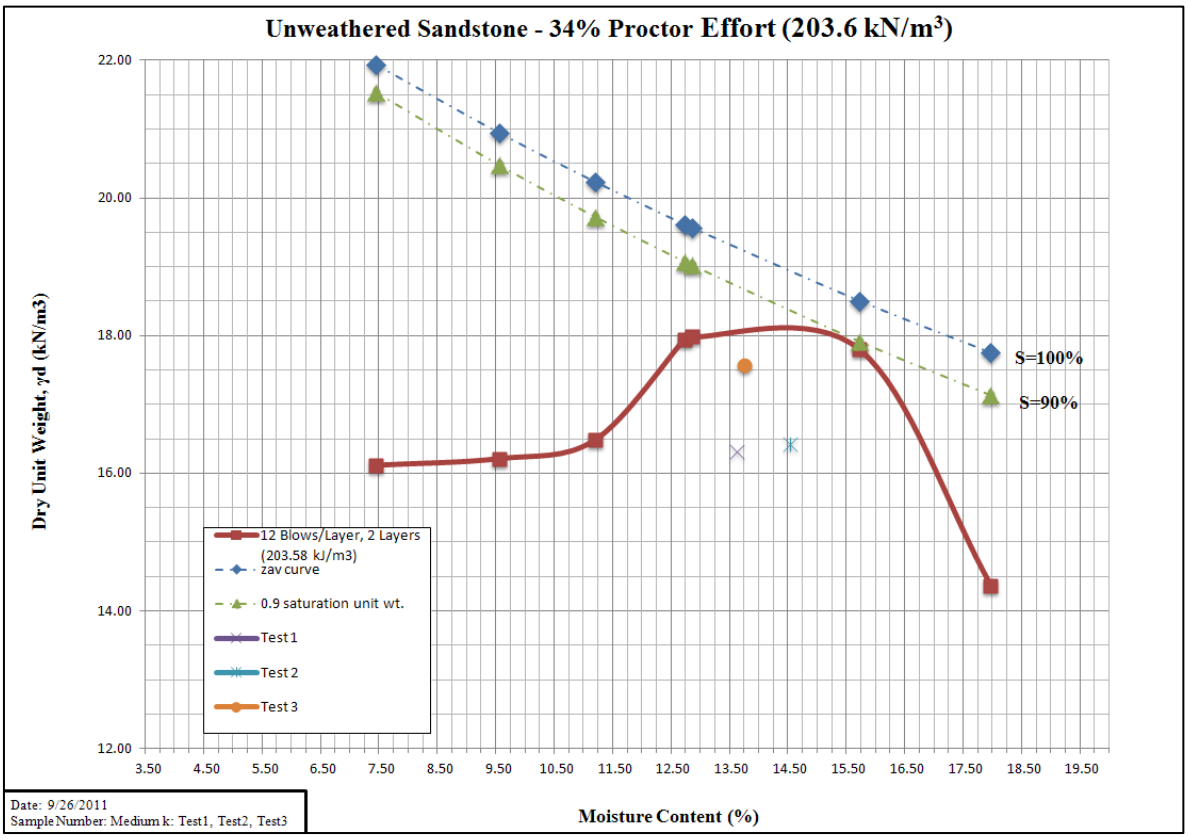

Figure 7.5 34% Proctor compaction energy (203.6 kJ/m^3): Variability in dry density

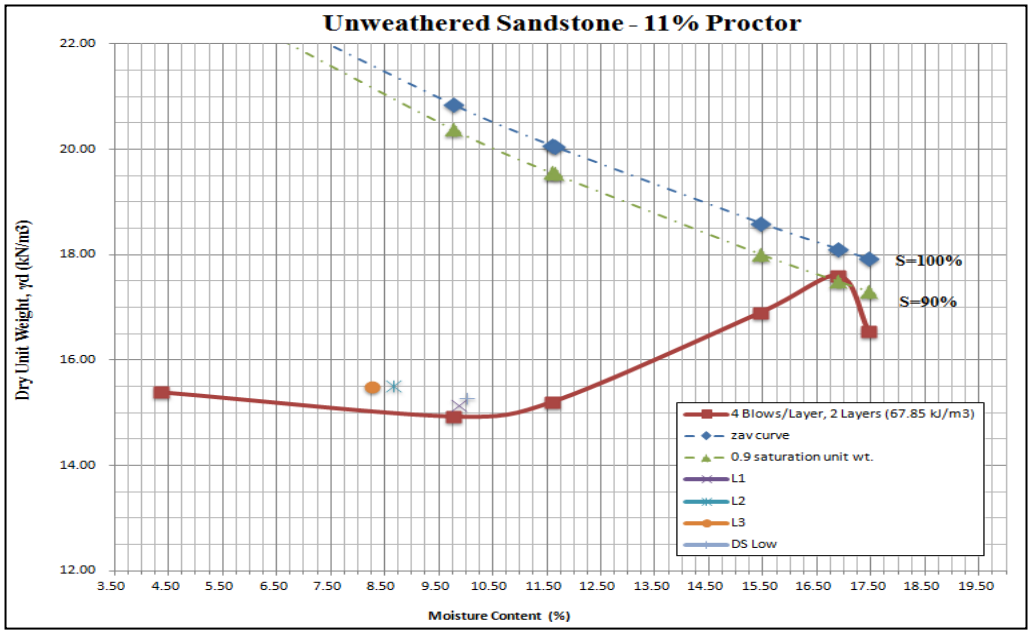

Figure 7.6 11% Proctor Compaction Energy (67.85 kJ/m^3): Variability in dry density

8. Strength Testing

The shear strength testing was performed on a GeoJac direct shear testing device. Each test was performed at a saturated, consolidated condition. The specimens were prepared as a standard proctor compaction sample, 34% Proctor compaction effort sample, and an 11% Proctor compaction effort sample. The angle of internal friction (ϕ) was calculated using Mohr-Coulomb failure criterion concepts. The tests were performed on the gray unweathered well graded sand with silt material to determine the shear strength properties of the material under specified normal stress conditions. These stress conditions were determined by multiplying the optimum density of the soil by the depth of a valley fill at the Coal MAC site in Logan, WV. The initial stresses were adjusted based on the capabilities of the testing equipment. The maximum normal stresses and shear strains of the equipment capability were sought to investigate thoroughly the residual strength of the material.

Unweathered Sandstone Overburden

The strength testing phase was organized into three different test specimens with predetermined specified compaction energies which each had unique void ratios. The compaction energies were at a standard proctor effort of 592.5 kJ/m^3, a 65.64% reduced compaction effort at 203.6 kJ/m^3 or 34.36% of a standard proctor effort, and an even further reduced compaction effort at 11.45% of standard proctor equal to 67.85 kJ/m^3 or 88.55% reduced. These three compaction energies will be referred to as "34% Proctor," "11% Proctor," and Standard Proctor. The specimens were prepared to target the optimum dry density for their respective compaction energies. Each compacted specimen was extruded approximately one third the length of the compaction mold. The three layers were captured in a direct shear specimen ring. The testing was performed on a GeoJac® direct shear testing device. The software used to reduce the data was DigiShear™. Loading schedules were determined from analyzing a valley fill at a surface mine in Logan, West Virginia. After the normal stress conditions were determined, they were modified to not exceed the loading limitations of the testing devices. The tests were run at a saturated condition. The data and results for the testing are shown in this chapter. Figure 8.1 and Figure 8.2 show the valley fill under inspection for this testing in plan and profile view.

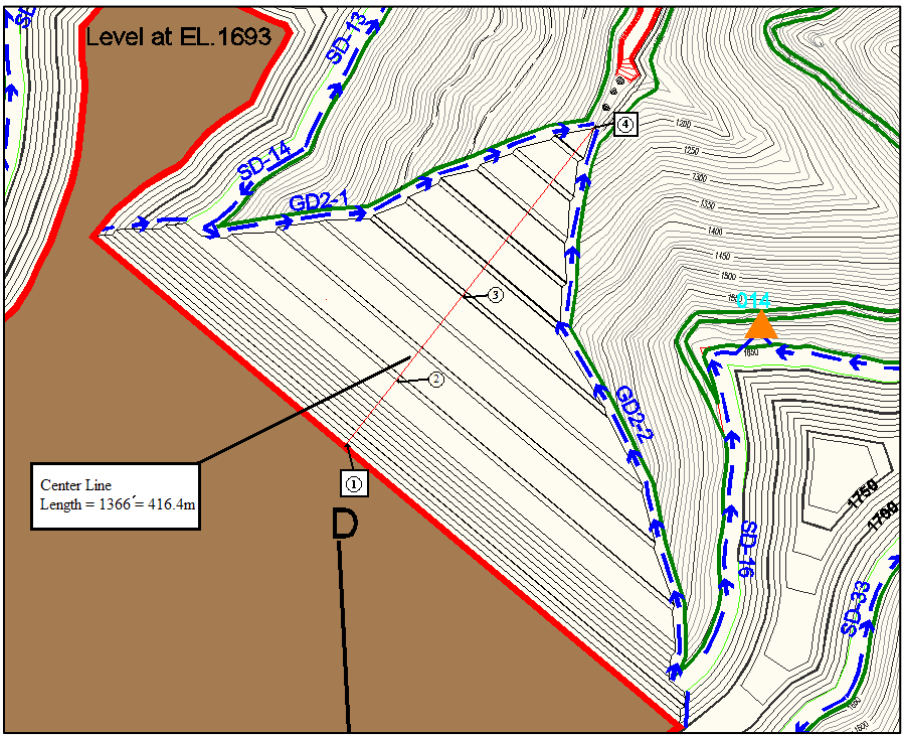

Figure 8.1 Shows the centerline and the points of evaluation on the valley fill under inspection in this section.

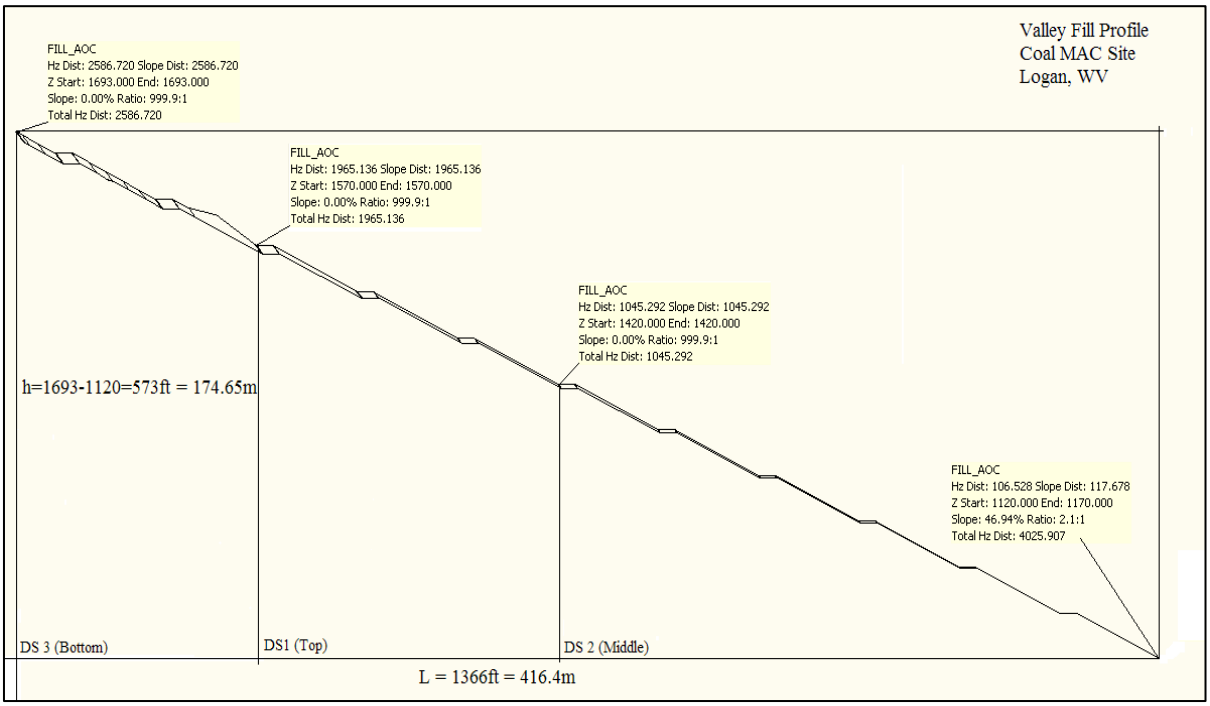

Figure 8.2 Slope profile of an AOC fill design illustrating determined stress evaluation points and slope dimensions.

Table 8.1 Stress conditions for direct shear test depths (DS1, DS2, DS3)

Compaction Condition	Test Points	Dry Density, γ_d [kN/m^2]	Depth, d [m]	Normal Stress, σ (γ_d*d) [kPa]
Standard Proctor	3	18.39	0.00	0.00
	2	18.39	97.02	1784.26
	1	18.39	145.54	2676.40
34% Proctor	DS31	18.56	32.33	600.07
	DS32	18.56	64.66	1200.14
	DS33	18.56	134.72	2500.32
11% Proctor	DSL1	16.81	35.69	600.00
	DSL2	16.81	71.39	1200.00
	DSL3	16.81	148.72	2500.00

The depths of the stress conditions varied as a result of equipment maximum loading. The 34% proctor sample dry density was in fact higher than the standard proctor sample. This was a function of climatic variability in the laboratory. Moisture content varied some throughout the testing, and the target dry densities were not fully achieved. For the standard proctor sample, the third point was made to be at the origin of the graph to demonstrate a zero cohesion condition. The maximum normal stress and shear strain conditions were sought to investigate the behavior of the residual strength of the unweathered sandstone. The objective of the residual strength investigation was to give insight into slope strength.

8.1 Standard Proctor (592.5 kJ/m^3)

A standard proctor compaction specimen was prepared and layer depths were each approximately 1/3 of the height of the compaction mold. After compaction, the specimen was extruded from the compaction mold approximately one third at a time. The center of each layer was captured in a direct shear ring mold. The remaining material for each layer was used for grain size distribution analysis. Direct shearing tests were performed on each ring specimen. The stress conditions for consolidation were found by multiplying the optimum dry density of the unweathered sandstone fill by the depth of the valley fill profile shown in Figure 8.2. It was determined that an additional point could be assumed on the Mohr-Coulomb failure envelope at the origin (0 kPa, 0 kPa) since the material was classified as a well graded sand with silt and would have little cohesion. The consolidation stress conditions were at a normal stress of 1784.26 kPa and 2676.40 kPa. The maximum shear stresses that occurred during the testing were 1029.95 kPa, and 1342.94 kPa, respectively. For DS1, the testing equipment reached its maximum loading capability before peak strength, but likely very near to it around a strain of approximately 7.5%. The maximum shear stress that was read was taken to be the maximum. The testing was performed at a saturated condition. An apparent cohesion resulted from graphing a best fit line to the data points. The apparent cohesion is understood to be the result of the creation of a negative pore pressure in the specimen during the shearing phase of the testing. The differences of φ' are shown for a best fit line and where cohesion equals zero. The data and results are shown in Figure 8.3 through Figure 8.7, and Table 8.2. The compaction information for the sheared specimens is in Appendix V.

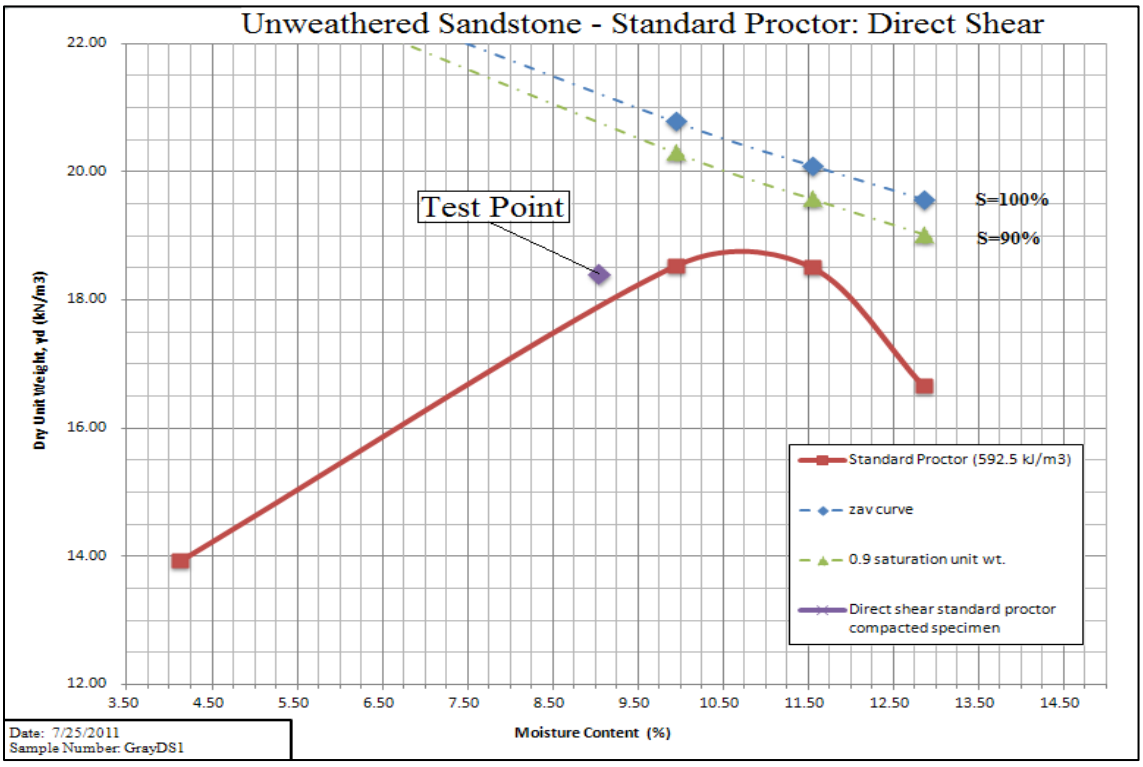

Figure 8.3 Comparison of the direct shear standard proctor compaction specimen and other standard proctor compaction data.

Table 8.2 Direct shear peak data and calculated values

Date	**Sample**	**Compaction**	**Material**
7/28/2011	GrayDS1	Standard Proctor	Passing No. 4
Specimen Number	**Max Shear Stress (ksf)**	**Max Shear Stress(psf)**	**Normal Stress (psf)**
1	28.04	28044	55890
2	21.51	21508	37260
3	0	0	0
Specimen Number	**Max Shear Stress(kPa)**	**Normal Stress (kPa)**	
1	1342.94	2676.4	
2	1029.95	1784.26	
3	0	0	
m =	0.51	m =	0.53
$\phi_{best\ fit}$'(degrees) =	27.14	$\phi_{c'=0}$'(degrees) =	27.7
c'(psf) =	602.57	c'(kPa) =	0
c'(kPa) =	28.86		

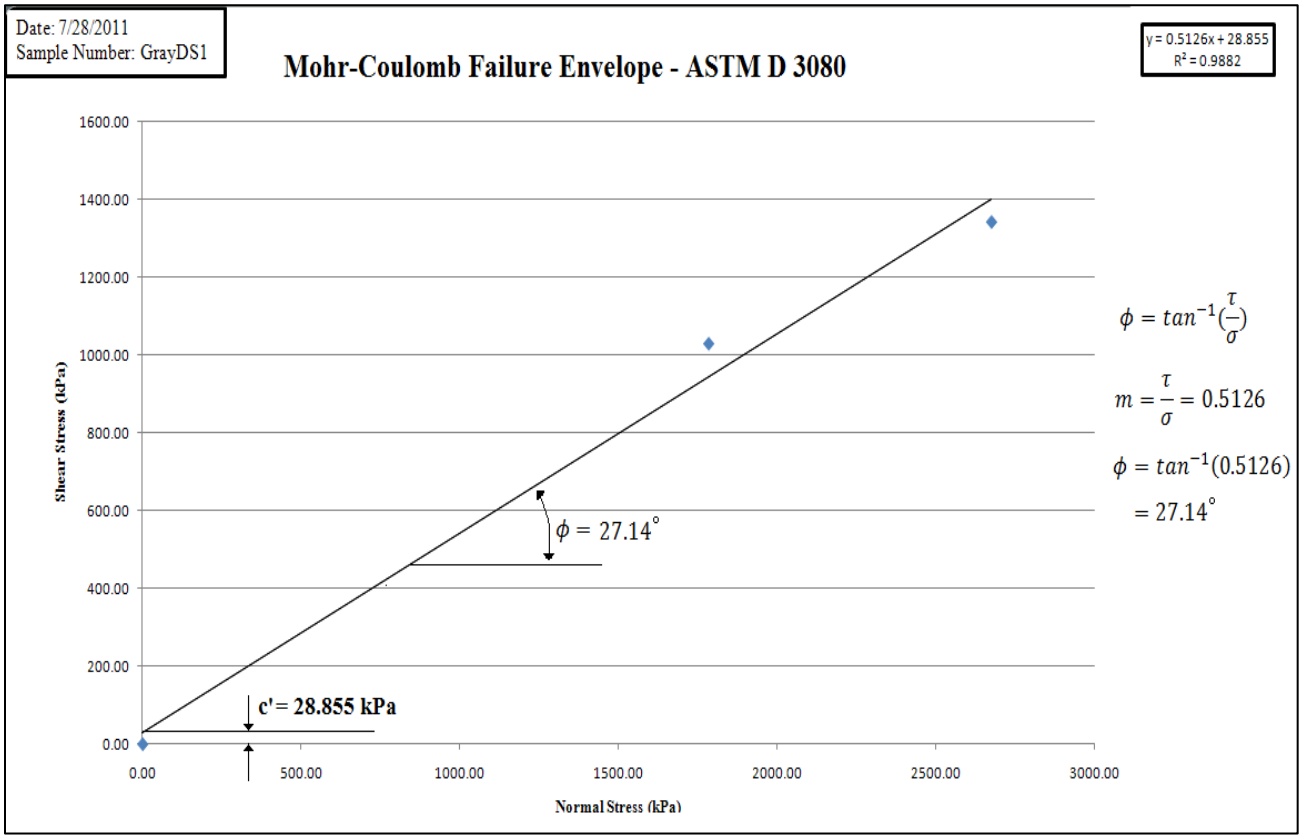

Figure 8.4 Shear stress versus normal stress plot of the standard proctor specimen

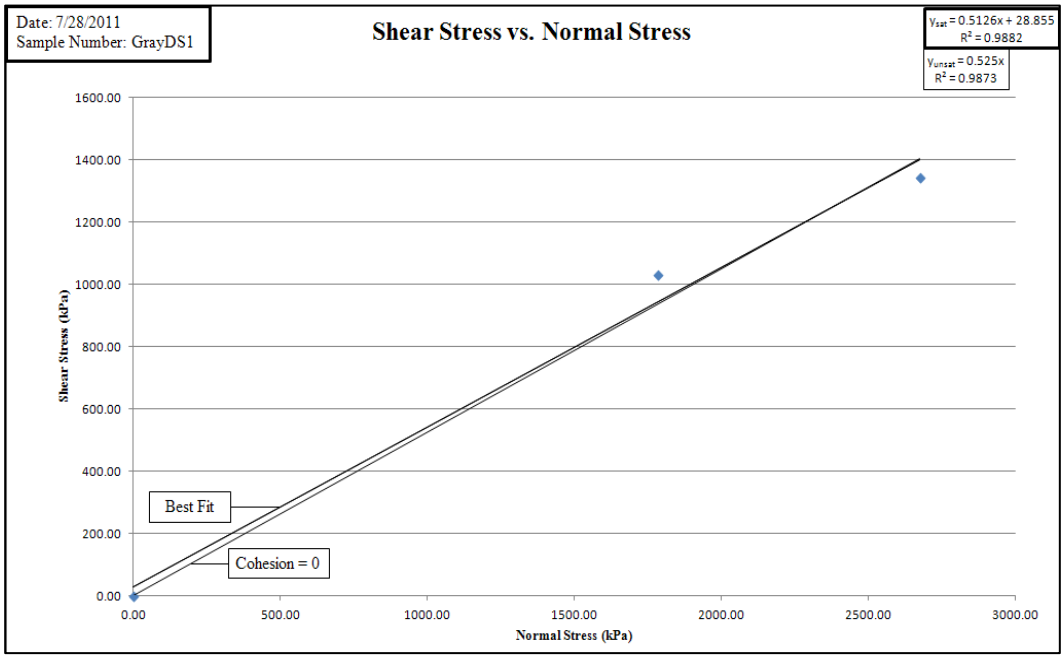

Figure 8.5 Shear stress versus normal stress saturated and unsaturated conditions of the standard proctor specimen

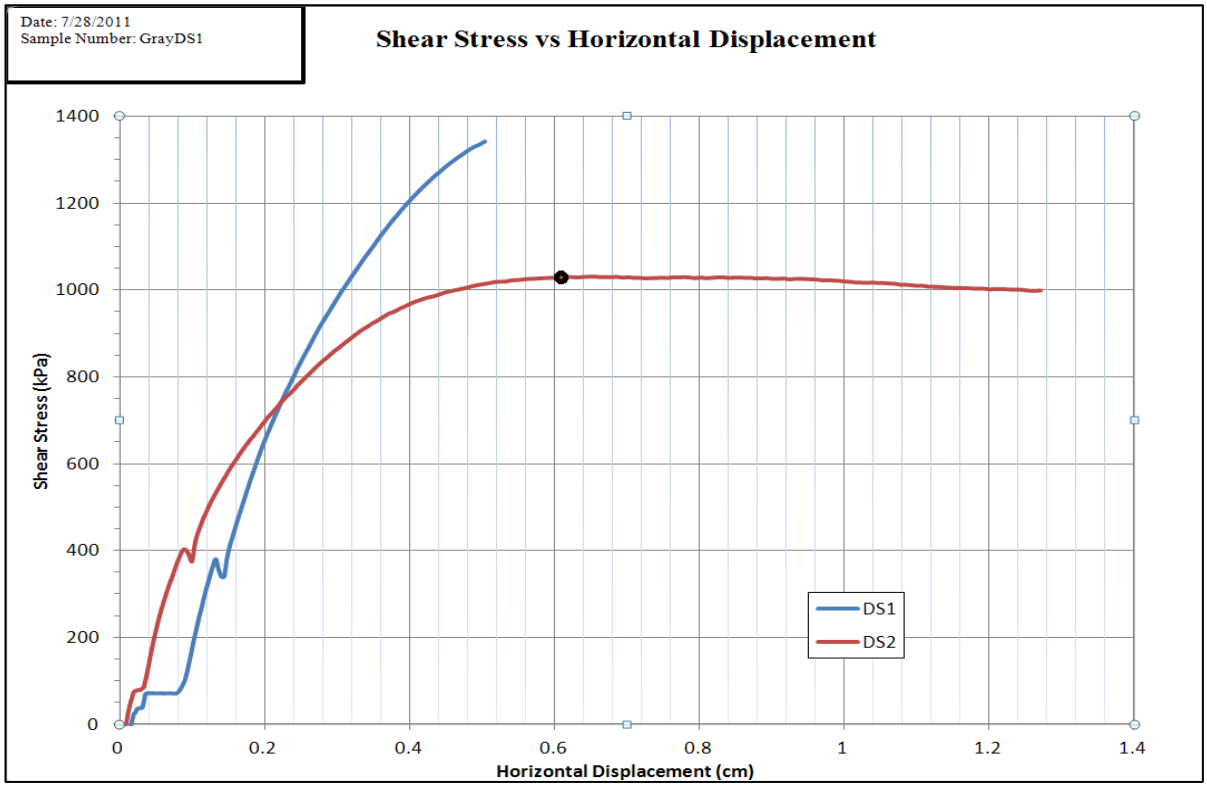

Figure 8.6 Shear stress versus horizontal displacement of test 1 (DS1) and test 2 (DS2).

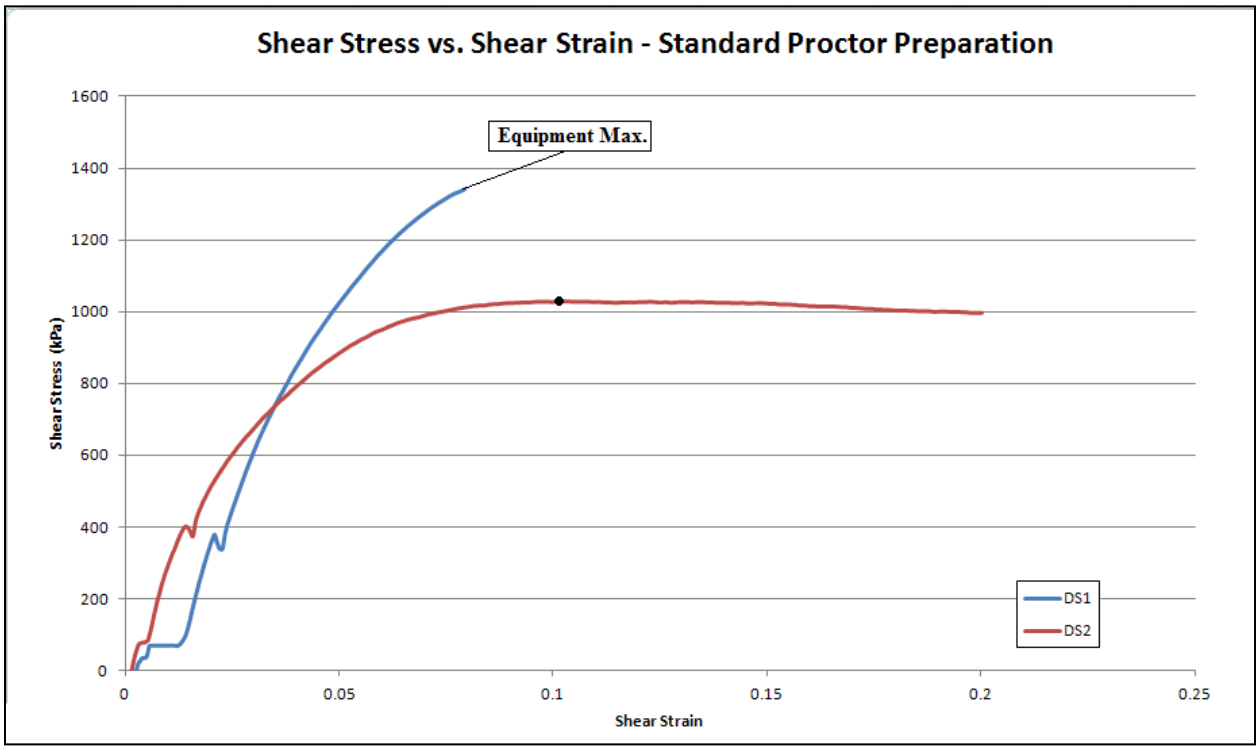

Figure 8.7 Shear stress versus shear strain of test 1 (DS1) and test 2 (DS2)

The jump on Figure 8.6 and Figure 8.7 represents a shear box set up error. The shearing pins used to separate the top and bottom of the shearing box 0.025in were not adequately loosened. The result is the jump between the shear stress of 200 and 400 kPa to overcome the friction caused by the pins on the shear box. The initial inconsistency of the curves also represents this error. The friction angle that was calculated using these data are consistent with the 34% and 11% proctor strength assessment data, however, its precision up to 0.2 cm displacement is approximate as a result of the error.

8.2 Proctor Compaction Energy at 34%: 12 Blows/Layer, 2 Layers (203.6 kJ/m^3)

A specimen was prepared at 34% Proctor with layer depths each approximately 1/3 of the height of the compaction mold. After compaction, the specimen was extruded from the compaction mold approximately one third at a time. The center of each layer was captured in a direct shear ring mold. The remaining material for each layer was used for grain size distribution analysis. Direct shearing tests were performed on each ring specimen. The stress conditions for consolidation were found by multiplying the optimum dry density of the unweathered sandstone material by the depth of the valley fill profile at the points shown Figure 8.8. For this test, it was determined that a forth point could be assumed on the Mohr-Coulomb failure envelope at the origin (0 kPa, 0 kPa) since the material was classified as a well graded sand, has a low plasticity index, and therefore little cohesion. The consolidation stress conditions were at normal stresses of 600 kPa, 1200 kPa, and 2500 kPa for the top, middle, and bottom layers, respectively. The maximum shear stresses that occurred during the testing were 365.71 kPa, 607.73 kPa, and 1078.41 kPa, respectively. The testing was performed at a saturated condition. An apparent cohesion resulted from graphing a best fit line to the data points. The apparent cohesion is understood to be the result of the creation of a negative pore pressure in the specimen during the shearing phase of the testing. The differences of φ' are shown for a best fit line and where the cohesion equals zero. The data and results are shown in Figure 8.8 through Figure 8.12 and Table 8.3. The compaction information for the sheared specimens is in Appendix V.

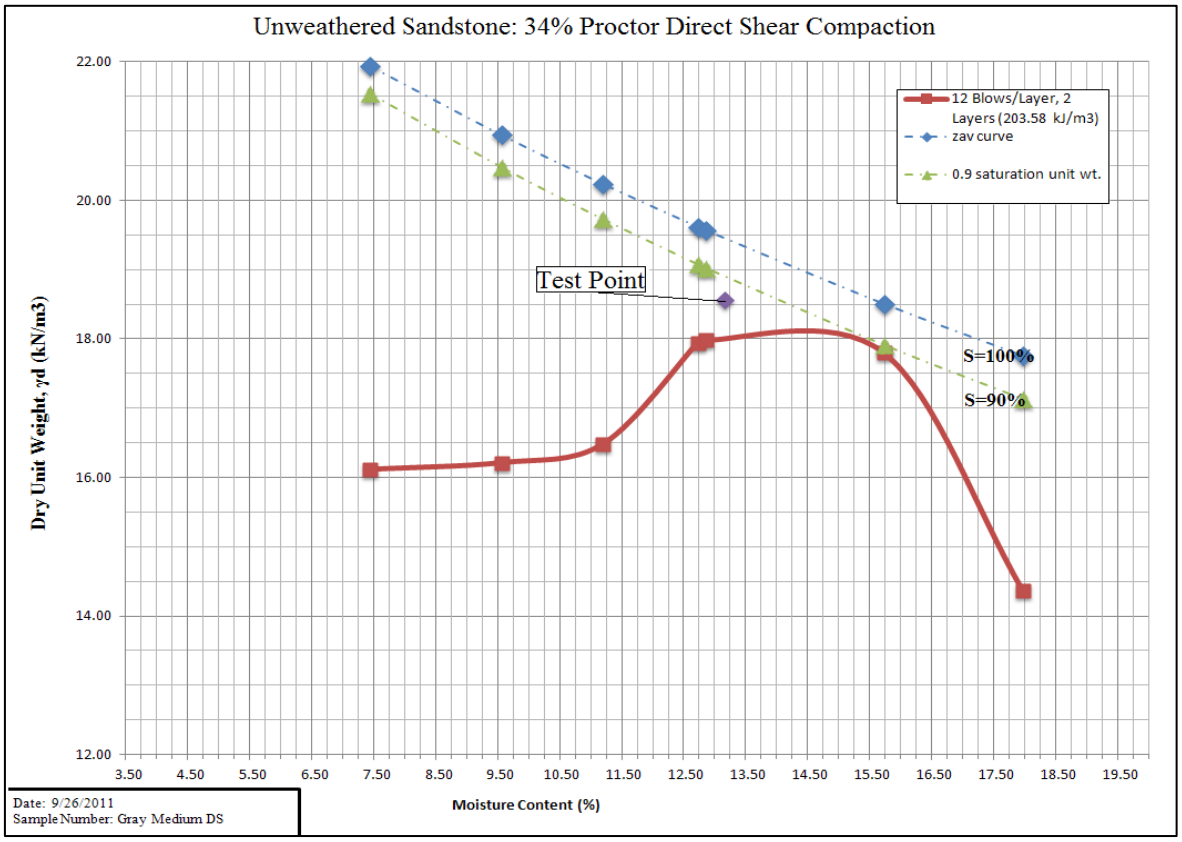

Figure 8.8 Comparison of the direct shear 34% Proctor compaction specimen and other 34% Proctor compaction energy specimen data.

Table 8.3 Direct shear peak data and calculated values

Date	Sample	Compaction	Material
9/26/2011	Gray M:DS31, DS32, DS33	12 Blows/Layer, 2 Layers (203.6 kJ/m3)	Passing No. 4
Specimen Number	**Max Shear Stress (ksf)**	**Max Shear Stress(psf)**	**Normal Stress (psf)**
DS31	7.64	7637	12531
DS32	12.69	12691	25062
DS33	22.52	22520	52213
4	0	0	0
Specimen Number	**Max Shear Stress(kPa)**	**Normal Stress (kPa)**	
DS31	365.71	600.07	
DS32	607.73	1200.14	
DS33	1078.41	2500.32	
4	0	0	
m =	0.42	m =	0.45
$\phi_{best\ fit}$'(degrees) =	22.77	$\phi_{c'=0}$'(degrees) =	24.36
c'(ksf) =	1287.42	c'(kPa) =	0
c'(kPa) =	61.642		

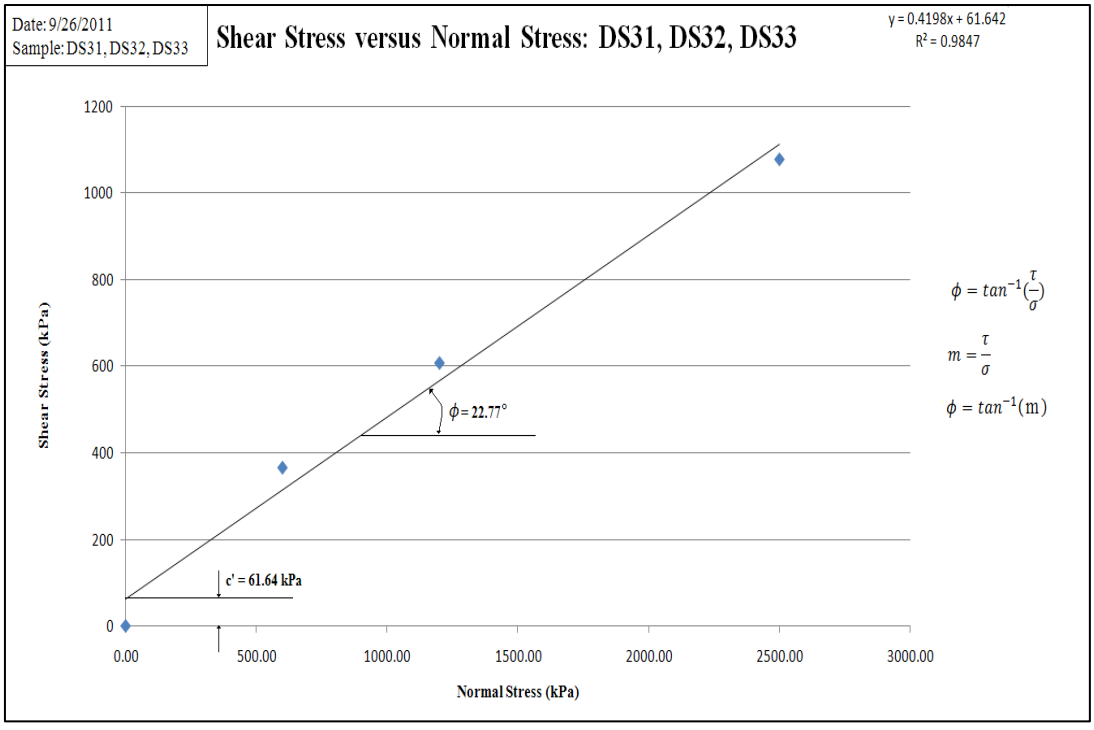

Figure 8.9 Shear stress versus normal stress plot of test 1 (DS31), test 2 (DS32), and test 3 (DS33)

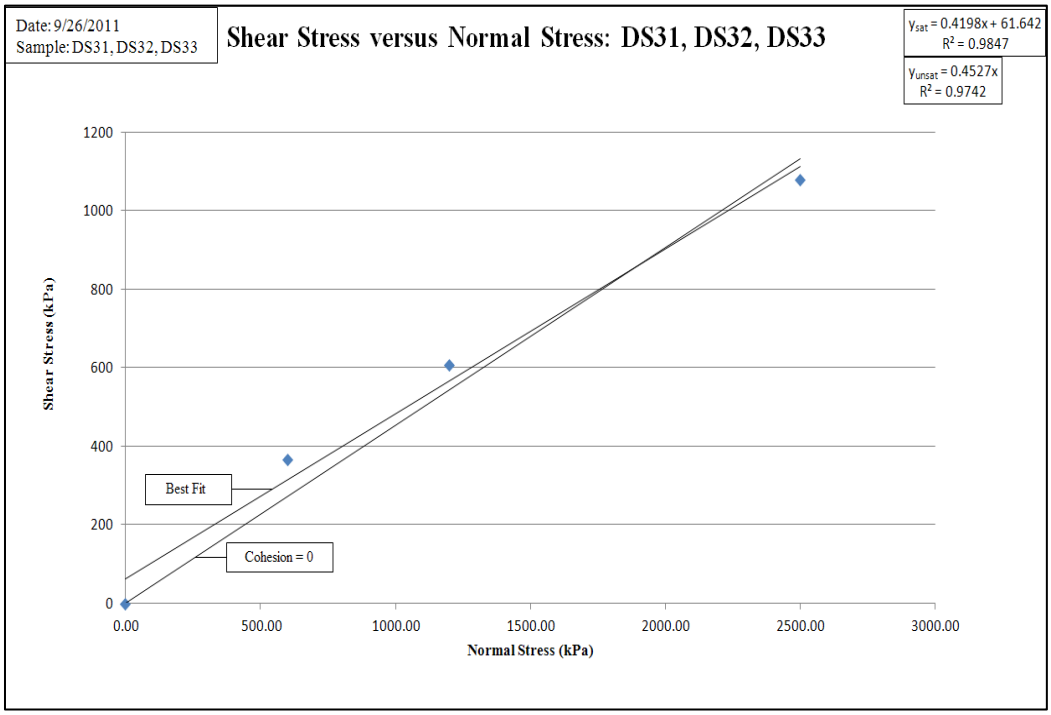

Figure 8.10 Shear stress versus normal stress saturated and unsaturated conditions of test 1 (DS31), test 2 (DS32), and test 3 (DS33)

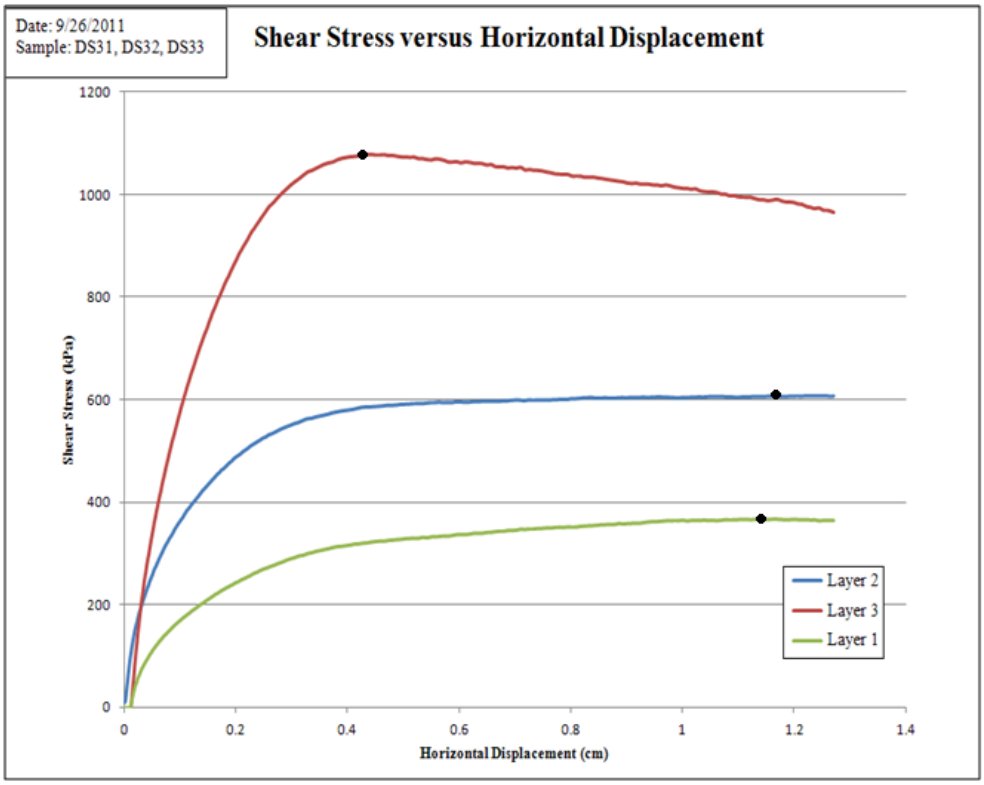

Figure 8.11 Shear stress versus horizontal displacement of layer 1, layer 2, and layer 3.

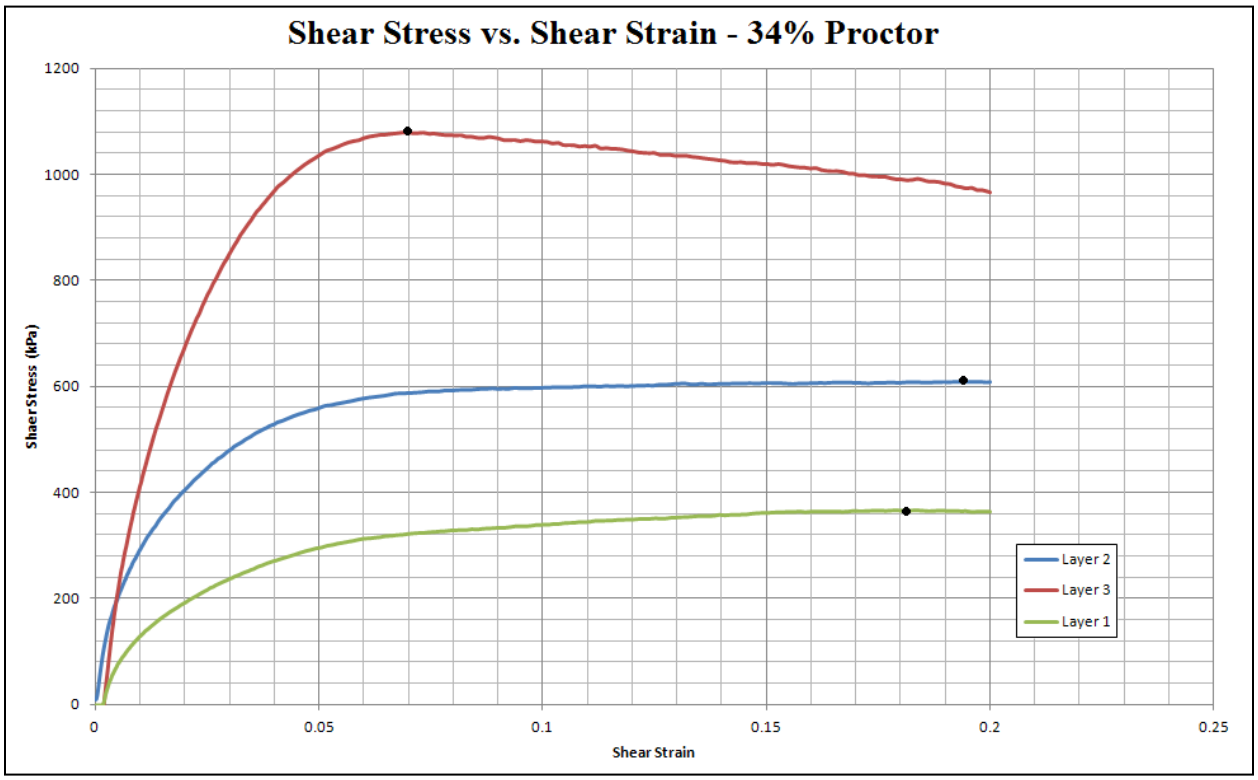

Figure 8.12 Shear stress versus shear strain of layer 1, layer 2, and layer 3.

8.3 Proctor Compaction Energy at 11%: 4 Blows/Layer, 2 Layers (67.85 kJ/m^3)

A specimen was prepared at the minimum dry density of the 11% Proctor compaction energy compaction curve. Layer depths were each approximately 1/3 of the height of the compaction mold. After compaction, the specimen was extruded from the compaction mold approximately one third at a time. The center of each layer was captured in a direct shear ring mold. The remaining material for each layer was used for grain size distribution analysis. Direct shearing tests were performed on each ring specimen. The stress conditions for consolidation were found by multiplying the optimum dry density of the unweathered sandstone material by the depth of the valley fill profile at the points shown below. For this test, it was determined that a forth point could be assumed on the Mohr-Coulomb failure envelope at the origin (0 kPa, 0 kPa) since the material was classified as a well graded sand with silt, has a low plasticity index, and therefore little cohesion. The consolidation stress conditions were at normal stresses of 600 kPa, 1200 kPa, and 2500 kPa for the top, middle, and bottom layers, respectively. The maximum shear stresses that occurred during the testing were 314.19 kPa, 595.62 kPa, and 1180.03 kPa, respectively. The testing was performed at a saturated condition. An apparent cohesion resulted from graphing a best fit line to the data points. The apparent cohesion is understood to be the result of the creation of a negative pore pressure in the specimen during the shearing phase of the testing. The differences of φ' are shown for a best fit line and where the cohesion equals zero. The data and results are shown in Figure 8.13 through Figure 8.17 and Table 8.4. The compaction information for the sheared specimens is in Appendix V.

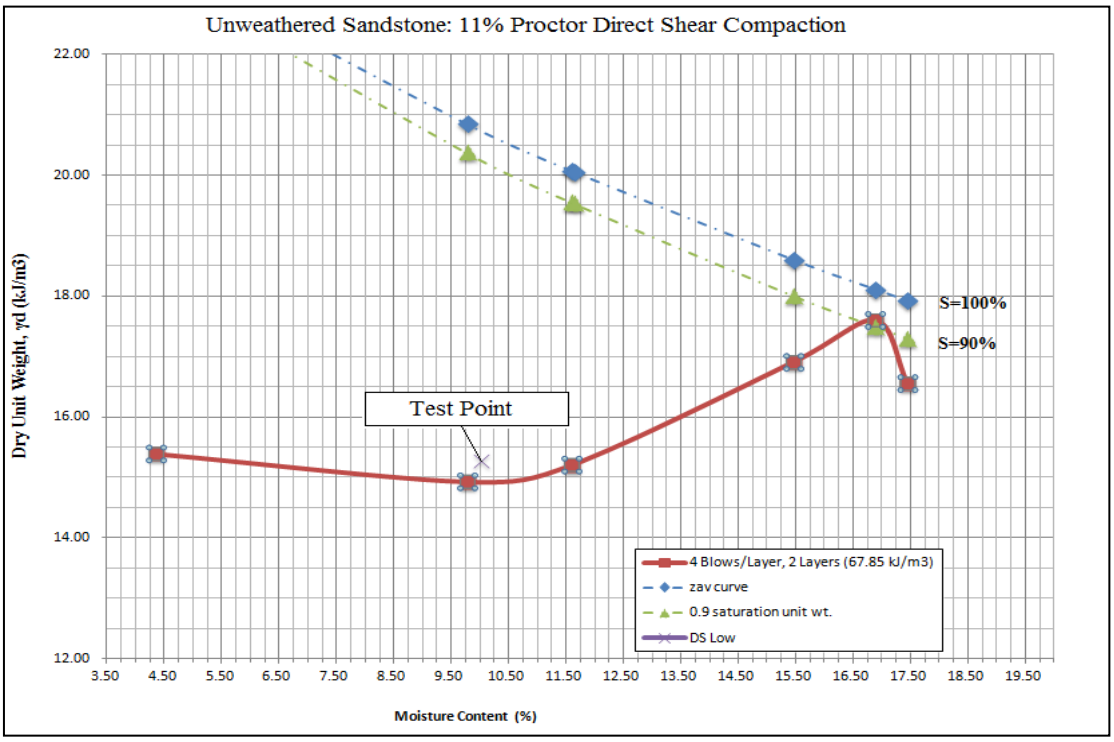

Figure 8.13 Comparison of the direct shear 11% Proctor compaction specimen and other 11% Proctor compaction data.

Table 8.4 Direct shear peak data and calculated values

Date	Sample	Compaction	Material
10/15/2011	11% Proctor:DSL1, DSL2, DSL3	4 Blows/Layer, 2 Layers (67.85 kJ/m^3)	Passing No. 4
Specimen Number	**Max Shear Stress (ksf)**	**Max Shear Stress(psf)**	**Normal Stress (psf)**
DSL1	6.56	6561	12531
DSL2	12.44	12438	25062
DSL3	24.64	24642	52213
4	0	0	0
Specimen Number	**Max Shear Stress(kPa)**	**Normal Stress (kPa)**	
DSL1	314.19	600	
DSL2	595.62	1200	
DSL3	1180.03	2500	
4	0	0	
m =	0.47	m =	0.48
$\phi_{best\ fit}$'(degrees) =	25.11	$\phi_{c'=0}$'(degrees) =	25.58
c'(ksf) =	386.76	c'(kPa) =	0
c'(kPa) =	18.52		

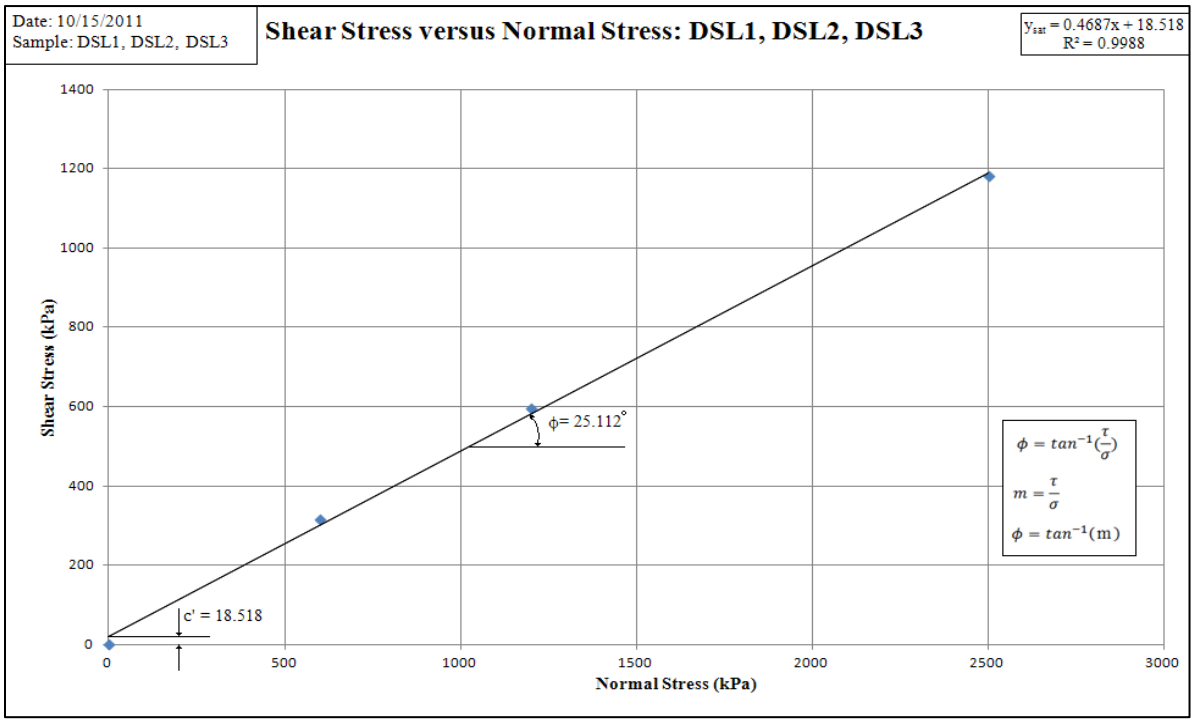

Figure 8.14 Shear stress versus normal stress plot of 11% Proctor compaction layer 1, layer 2, and layer 3

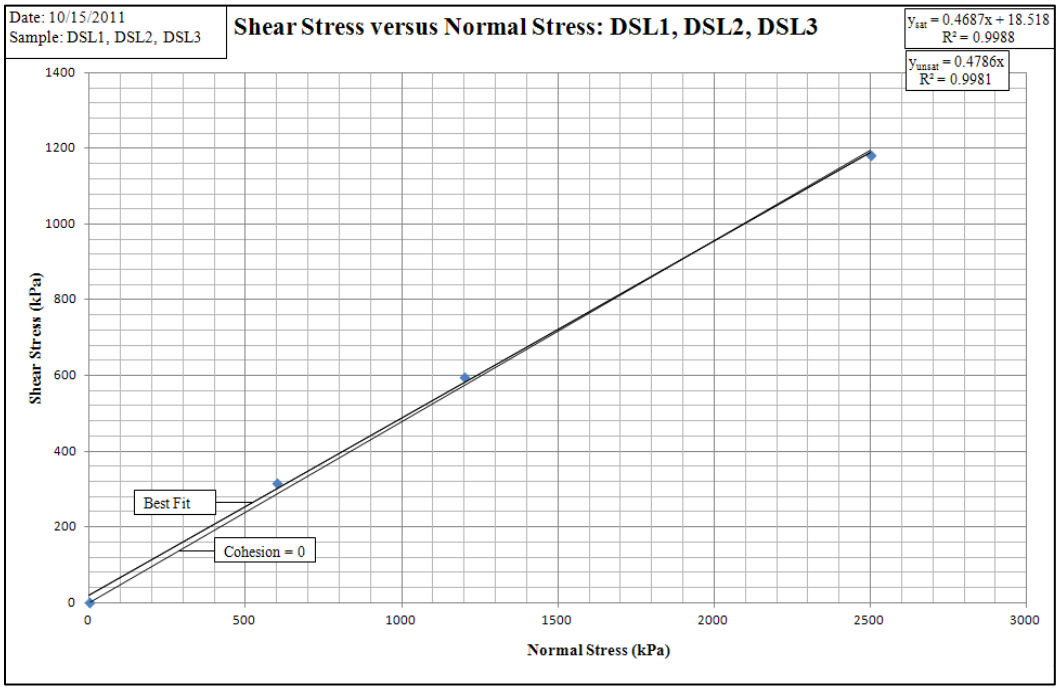

Figure 8.15 Shear stress versus normal stress saturated and unsaturated conditions of test 1 (DSL1), test 2 (DSL2), and test 3 (DSL3)

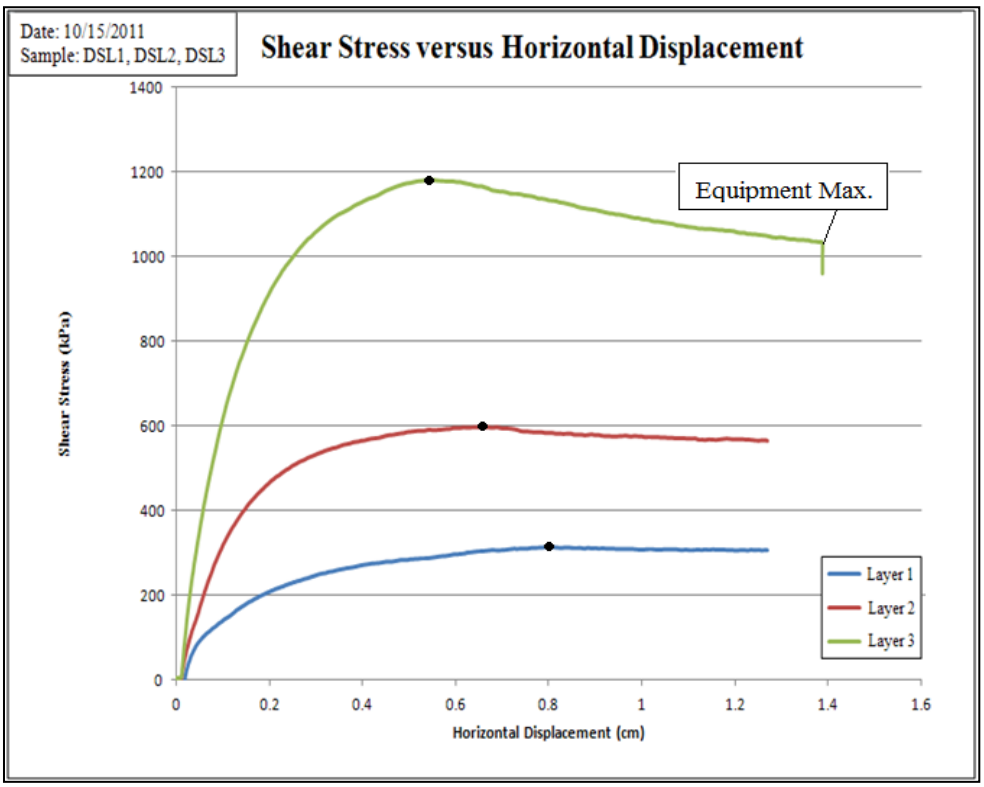

Figure 8.16 Shear stress versus horizontal displacement of layer 1, layer 2, and layer 3.

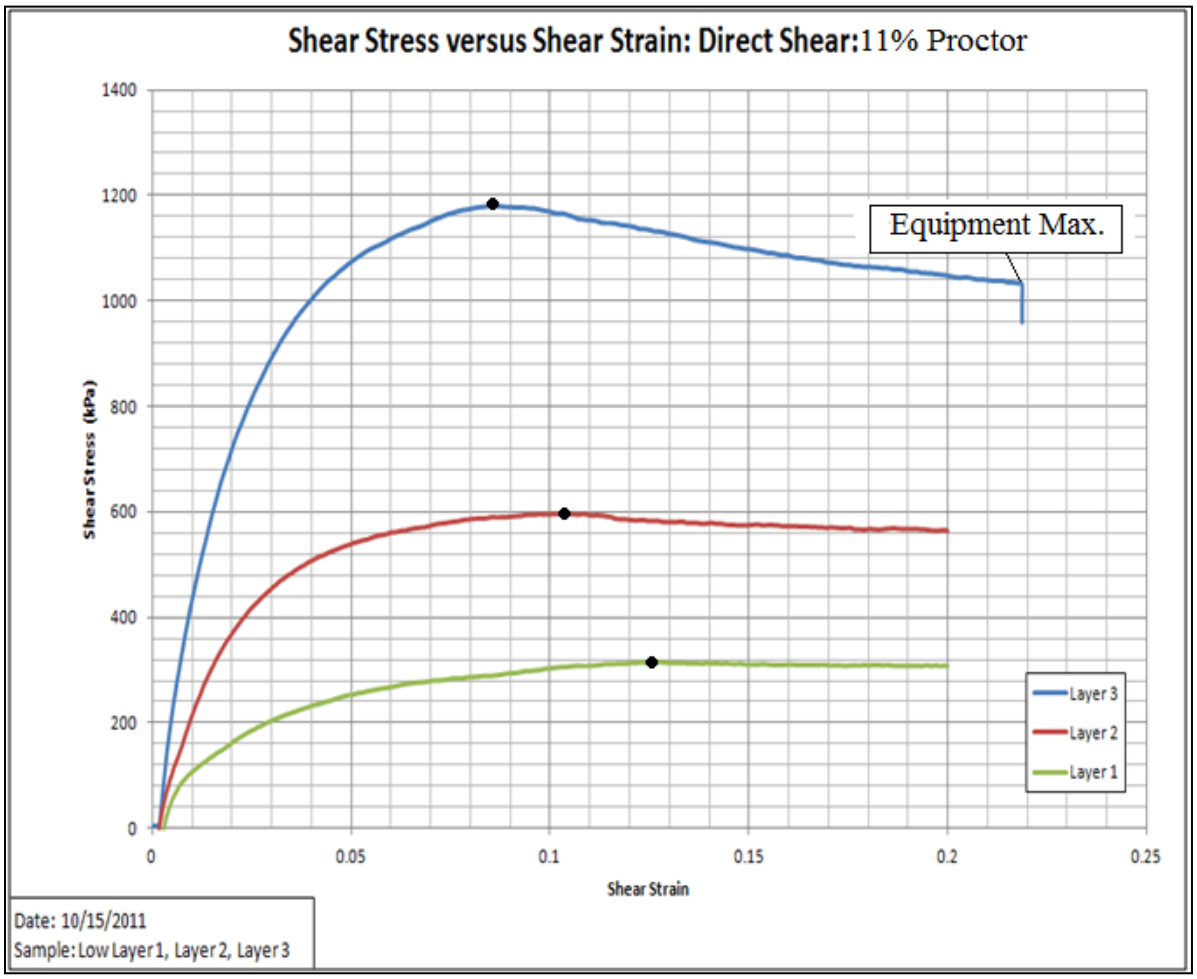

Figure 8.17 Shear stress versus shear strain

8.4 Strength Testing Results

The results of the strength testing performed in sections 8.1-8.3 were useful to determine the input parameter "φ" into GeoStudio™. The friction angle results are shown in Table 8.5.

Table 8.5 Friction angle results with shear stresses and normal stresses shown

Compaction Condition	Test Points	Normal Stress, σ (γ_d*d) [kPa]	Shear Stress, τ [kPa]	Friction Angle, φ (Best fit)	Friction Angle, φ (zero cohesion)
Standard Proctor	3	0.00	0.00	27.14°	27.70°
	2	1784.26	1029.95		
	1	2676.40	1342.94		
34% Proctor	DS31	600.07	365.71	22.77°	24.36°
	DS32	1200.14	607.73		
	DS33	2500.32	1078.41		
11% Proctor	DSL1	600.00	314.19	25.11°	25.58°
	DSL2	1200.00	595.62		
	DSL3	2500.00	1180.03		

The target shear strain for each sample was 20%. The shear strain curves revealed that much of the residual strength is retained within the sample. The reason the samples retained their strength is likely a result of the creation of the unweathered material. The geometry of the particles of the sample is angular. The material was blasted, unweathered sandstone. The angular nature of the material increases the friction between shear planes and resists displacement. This insight is beneficial when considering slope stability. Slopes constructed with this material should be strong and resistant to failure (FS<1).

9. Pre-Permeability Grain Size Distribution

The compacted specimens were tested using standard proctor compaction energy (592.5 kJ/m^3), 34% Proctor compaction energy (203.6 kJ/m^3), and an 11% Proctor compaction energy (67.85 kJ/m^3). Sieve analysis was performed on the compacted specimens for the remainder of each of three layers from which the direct shear specimens were taken. The objective of the testing was to determine the volume of created fines in the three layers due to the compaction effort, and compare their distribution within the mold with the distribution of fines in the post-permeability specimens. The desired outcome was to understand the creation, movement, and variability of fine particles in the specimens at a pre-permeability condition and later compare the results to a post-permeability condition grain size distribution analysis. The concept is that the testing will emulate field compaction energies and fine particle creation. Therefore, it will be possible to understand how to construct a valley fill in order to reduce the creation and movement of fine particles to prevent suffusion and internal erosion and ultimately increase the durability and prolong the lifetime of the structure. The results of the testing are shown in this chapter (Chapter 9).

9.1 Grain Size Distribution: Standard Proctor (592.5 kJ/m^3)

Grain size distribution testing was performed on three layers of a specimen that was prepared via standard proctor compaction. The specimen was used for direct shear testing, but the remainder of the soil per layer was used for grain size distribution testing. The third layer of the specimen could not be tested with our direct shear equipment because the second layer maxed out the load actuators on the GeoJac equipment. The normal stresses were intended to increase from the top layer to the bottom layer. Regardless, the grain size distribution analysis testing was performed on the third layer of the specimen. The layers varied very little in their gradations, as shown by the coefficient of variability for the uniformity coefficient at 0.068, and the coefficient of variation for the coefficient of gradation at 0.116. The specimen was oven dried prior to testing. The data are shown in Table 9.1, Table 9.2, Table 9.3, and Figure 9.1.

Table 9.1 Critical index values for the direct shear grain size distribution testing.

Results			
Critical Indices	**Layer 1**	**Layer 2**	**Layer 3**
D_{90}	3.75	3.30	3.80
D_{60}	1.65	1.05	1.80
D_{50}	1.15	0.69	1.35
D_{30}	0.48	0.35	0.55
D_{25}	0.40	0.29	0.44
D_{10}	0.15	0.10	0.15
Uniformity Coefficient, C_u	**11.00**	**10.50**	**12.00**
Coefficient of Gradation, C_c	**0.93**	**1.17**	**1.12**

Table 9.2 Uniformity coefficient statistics

Uniformity Coefficient, C_u	
Average Uniformity Coefficient	11.167
Sample Standard Deviation (s)	0.764
Coefficient of Variation (COV)	0.068

Table 9.3 Coefficient of gradation statistics

Coefficient of Gradation, C_c	
Average Coefficient of Gradation	1.073
Sample Standard Deviation (s)	0.125
Coefficient of Variation (COV)	0.116

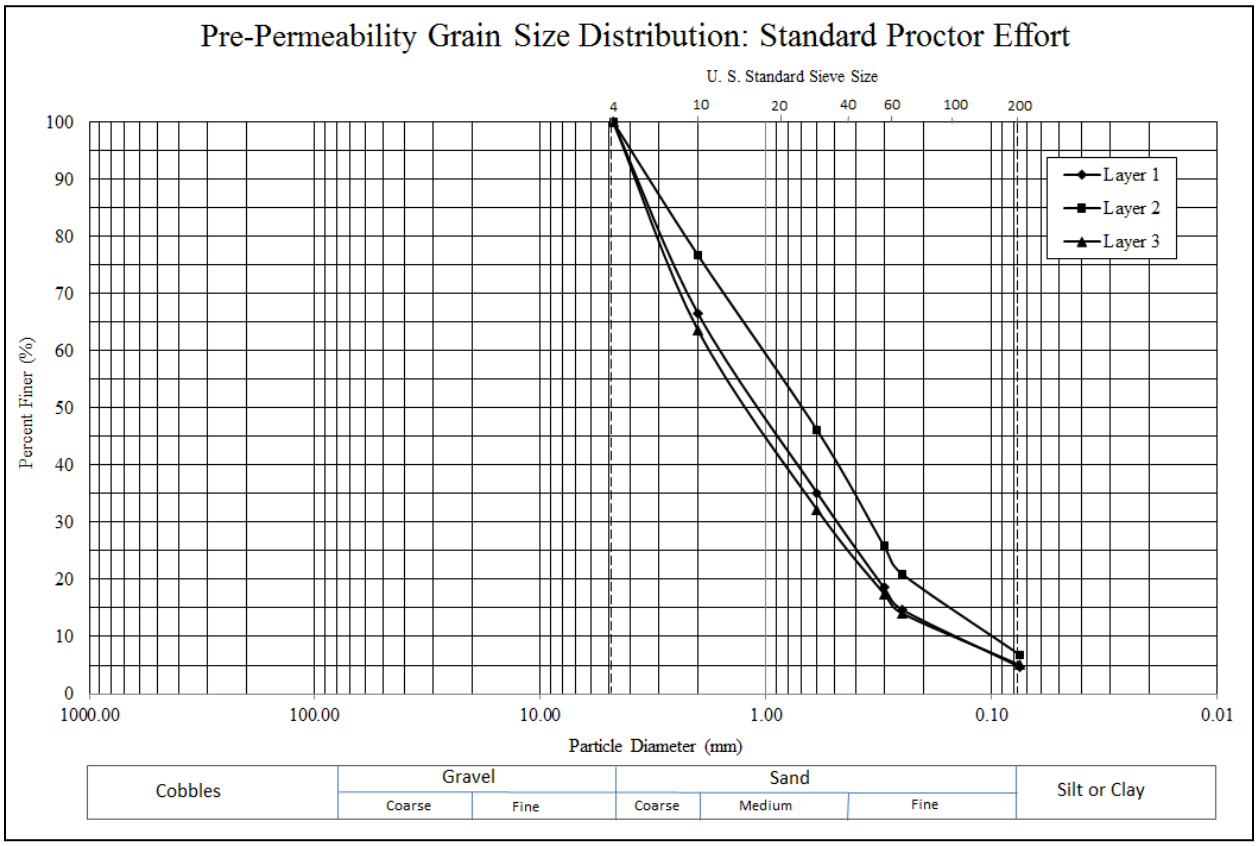

Figure 9.1 Grain size distribution of layer 1, layer 2, layer 3.

9.2 Grain Size Distribution: 34% Proctor Compaction Energy (203.6 kJ/m^3)

Grain size distribution testing was performed on a 34% Proctor specimen that was prepared for direct shear testing. The remainder of the soil for the 3 layers from which direct shear ring specimens were taken was used for the grain size distribution testing. The material was oven dried before testing. The three layers showed very little variability. The variability is shown by the coefficient of variability for the uniformity coefficient at 0.117, and a coefficient of variability for the coefficient of gradation at 0.048. The data are shown in Table 9.4, Table 9.5, Table 9.6, and Figure 9.2.

Table 9.4 Critical index values for the direct shear grain size distribution testing.

Results	Layer 1	Layer 2	Layer 3
D_{90}	3.80	3.80	3.80
D_{60}	1.80	1.70	1.70
D_{50}	1.40	1.30	1.30
D_{30}	0.69	0.58	0.56
D_{25}	0.56	0.45	0.44
D_{15}	0.28	0.22	0.24
D_{10}	0.17	0.13	0.13
Uniformity Coefficient, C_u	10.59	13.08	13.08
Coefficient of Gradation, C_c	1.56	1.52	1.42

Table 9.5 Uniformity coefficient statistics

Uniformity Coefficient, C_u	
Average Uniformity Coefficient	12.247
Sample Standard Deviation (s)	1.437
Coefficient of Variation (COV)	0.117

Table 9.6 Coefficient of gradation statistics

Coefficient of Gradation, C_c	
Average Coefficient of Gradation	1.499
Sample Standard Deviation (s)	0.071
Coefficient of Variation (COV)	0.048

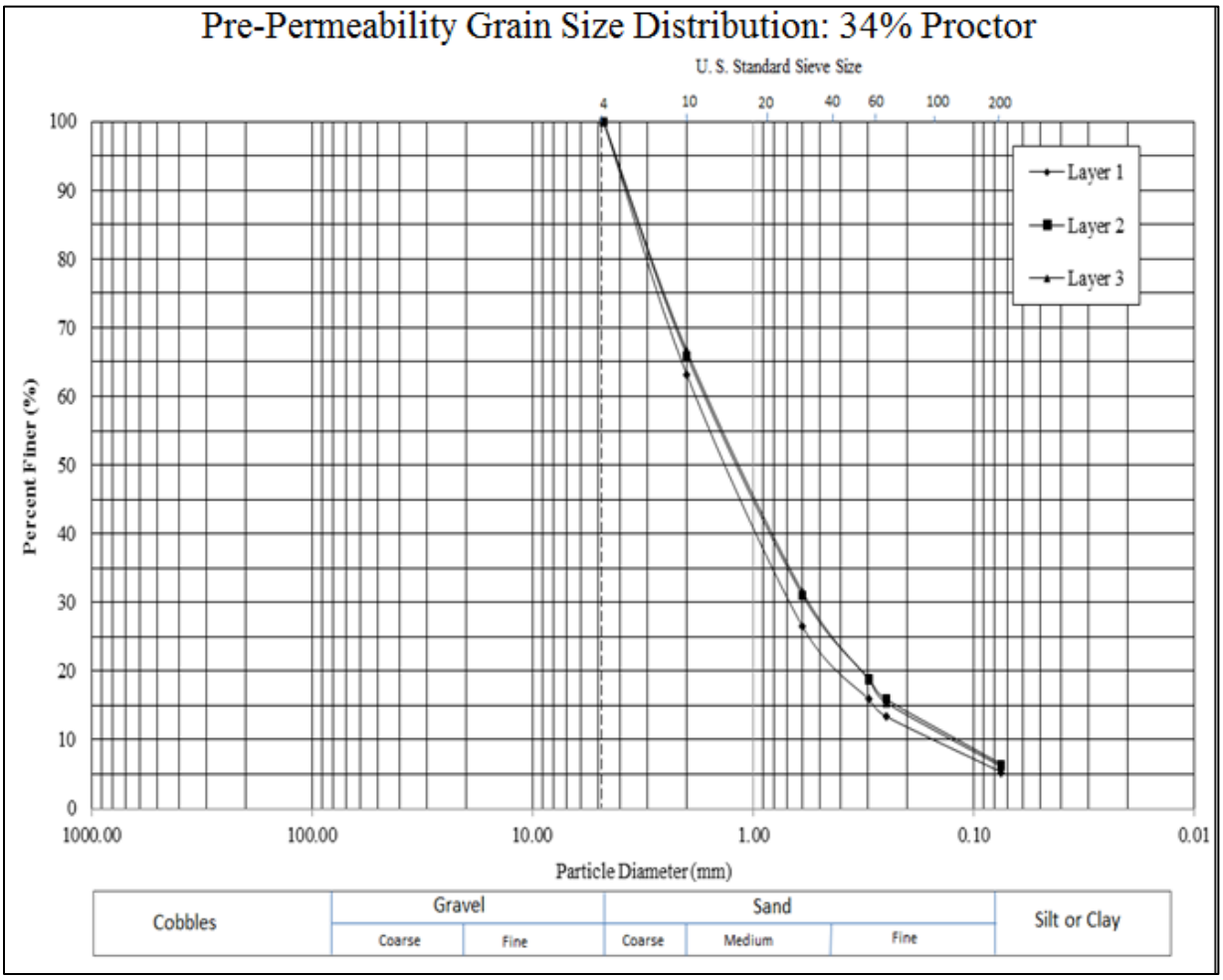

Figure 9.2 Grain size distribution of 34% Proctor compaction effort: layer 1 (test1), layer 2 (test 2), layer 3 (test 3)

9.3 Grain Size Distribution: 11% Proctor Compaction Energy (67.85 kJ/m^3)

Grain size distribution testing was performed on an 11% Proctor compaction energy specimen that was prepared for direct shear testing. The remainder of the soil for the 3 layers from which direct shear ring specimens were taken was used for the grain size distribution testing. The material was oven dried before testing. There was little variability in the data. The variability is expressed by the coefficient of variability. The coefficient of variability for the uniformity coefficient was 0.123. The coefficient of variability for the coefficient of gradation was 0.170. The data are shown in Table 9.7, Table 9.8, Table 9.9, and Figure 9.3.

Table 9.7 Critical index values for the direct shear grain size distribution testing.

Results	Layer 1	Layer 2	Layer 3
D_{90}	4.10	4.00	4.00
D_{60}	2.70	2.60	2.40
D_{50}	2.20	2.00	1.80
D_{30}	1.20	0.98	0.90
D_{25}	0.88	0.75	0.73
D_{15}	0.51	0.39	0.41
D_{10}	0.28	0.22	0.25
Uniformity Coefficient, C_u	9.64	11.82	9.60
Coefficient of Gradation, C_c	1.90	1.68	1.35

Table 9.8 Uniformity coefficient statistics

Uniformity Coefficient, C_u	
Average Uniformity Coefficient	10.354
Sample Standard Deviation (s)	1.268
Coefficient of Variation (COV)	0.123

Table 9.9 Coefficient of gradation statistics

Coefficient of Gradation, C_c	
Average Coefficient of Gradation	1.645
Sample Standard Deviation (s)	0.279
Coefficient of Variation (COV)	0.170

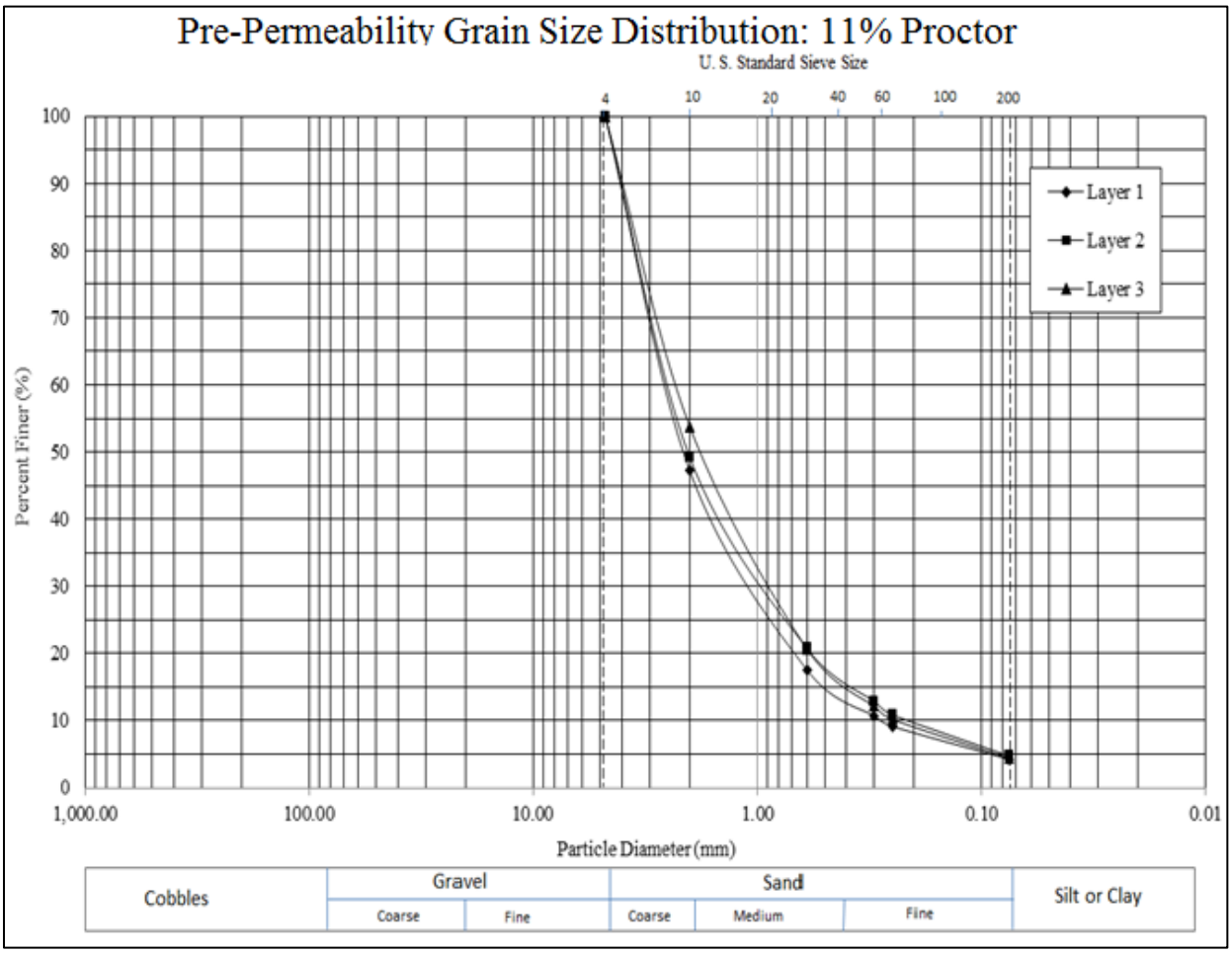

Figure 9.3 Grain size distribution of 11% Proctor compaction effort: layer 1, layer 2, layer 3

10. Hydraulic Conductivity

Hydraulic conductivity testing was performed using the ASTM standard test method D 5856. The target compaction density was the maximum dry density of the unweathered sandstone overburden for the standard proctor compaction specimen, and the 34% Proctor compaction specimen. The 11% Proctor compaction energy specimen was prepared for the minimum dry density to establish an upper limit for the hydraulic conductivity. The objective of the hydraulic conductivity testing was to determine the permeability of water through a test specimen at the maximum and minimum dry density of the material. Grain size distribution tests were performed on three approximately equal layers of the specimen after a gradient of i=100 for the standard proctor specimens, and a hydraulic gradient of i=15 for the 34% and 11% proctor specimens was permeated through each specimen for an adequate period of time, and the hydraulic conductivity had been determined. The high gradients were chosen to accelerate the testing process. The gradient of 100 was used on the standard proctor specimen as no hydraulic consolidation was expected, nor did it occur. The hydraulic gradient of 15 was chosen for the reduced proctor specimens to avoid hydraulic consolidation and accelerate the testing process as a low hydraulic conductivity was expected for the well graded sand with silt. The purpose of the grain size distribution testing was to track the movement of material particles, particularly the smaller diameter particles. The effort was meant to emulate field conditions replicating suffusion phenomena and internal erosion within an AOC valley fill. The results of the testing are shown in this chapter.

10.1 Hydraulic Conductivity: Standard Proctor (592.5 kJ/m^3)

Hydraulic conductivity testing was performed on a standard proctor compaction effort (592.5 kJ/m^3) standard proctor specimen. The target dry density was at optimum for the standard proctor compaction effort test data. The optimum dry density for the standard proctor compaction effort specimen was 18.75 kN/m^3. Triplicate testing was performed to ensure accuracy. The dry densities for tests 1, 2, and 3 were 18.14 kN/m^3, 18.15 kN/m^3, and 18.30 kN/m^3 respectively. The objective of the testing was to determine the hydraulic conductivity in order to better understand the rate at which water would permeate through the material under inspection. The purpose of the testing was to determine the fine particle movement within the specimen under the influence of a hydraulic gradient i=100. After the hydraulic conductivity readings reached equilibrium, the hydraulic conductivity was determined and the specimen was extruded approximately one third at a time. The hydraulic conductivity was determined after the data had become stable. In these cases, the average of the last five data points was taken to be the hydraulic conductivity of the specimens. The layers were saved and oven dried. Grain size analysis was run on three layers of each specimen. The hydraulic conductivity data for the standard proctor compaction energy specimens are presented in this section (10.1). The hydraulic conductivity data is presented in Appendix I.

Table 10.1 Hydraulic conductivty standard proctor compaction energy specimen data.

Test Number	**Test 1**	**Test 2**	**Test 3**
Assumed moisture content (%)	10.75	10.75	10.75
Mold Weight (g), M_{md}	614.90	616.62	618.11
Specimen+Mold Weight (g), M_t	2454.57	2318.32	2416.29
Volume of Mold (cm^3), V	888.52	837.04	888.52
Specific Gravity of Soil, G_s	2.69	2.69	2.69
Unit Weight of Water @ 20^{o}C(KN/m^3), ?w	9.79	9.79	9.79
Unit Weight of Water @ 20^{o}C(lb/ft^3), γ_w	62.34	62.34	62.34
Moist Unit Weight of Compacted Specimen (g/cm^3), γ_m	2.07	2.03	2.02
Dry Unit Weight of Compacted Specimen (g/cm^3), γ_d	1.85	1.85	1.87
Dry Unit Weight of Compacted Specimen (KN/m^3), γ_d	**18.14**	**18.15**	**18.30**
Dry Unit Weight of Compacted Specimen (lb/ft^3), γ_d	115.49	115.55	116.52
Dry Unit Weight at S=1.0 (KN/m^3),γ_d	**19.94**	**20.82**	**21.47**
Dry Unit Weight at S=0.9 (KN/m^3),γ_d	**19.42**	**20.35**	**21.03**
Dry Unit Weight at S=1.0 (lb/ft^3), γ_d	126.98	132.59	136.70
Dry Unit Weight at S=0.9 (lb/ft^3), γ_d	123.65	129.57	133.95
Void Ratio, $e=((G_s*\gamma_w)/\gamma_d)-1$	0.45	0.45	0.44
Degree of Saturation (%), $S=G_s*(w/e)$	0.71	0.59	0.52
Saturated Water Content, w_{sat} (%)	16.80	16.78	16.33
Assumed moisture content (%)	10.75	10.75	10.75
Container Mass (g), Mc	30.40	30.55	30.52
Container+Moist Specimen Mass (g), Mcms	70.12	58.00	69.62
Intial Container+Oven Dry Specimen Mass (g), Mcds	65.89	55.54	66.58
Mass of Water (g), Mw= Mcms-Mcds	4.23	2.46	3.04
Mass of Solids (g), Ms= Mcds-Mc	35.49	24.99	36.06
Water Content, (%) W= (Mw/Ms)x100	11.92	9.84	8.43
Compaction Energy kJ/m^3 ($ft\text{-}lb/ft^3$)	592.50 (12375)		

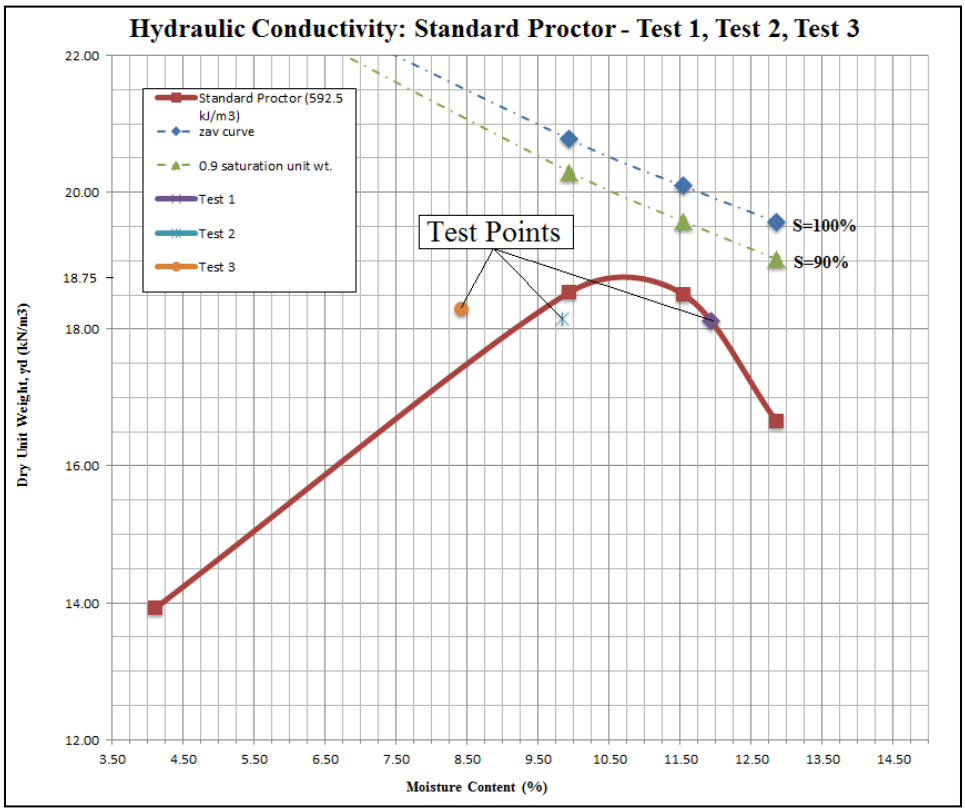

Figure 10.1 *Comparison of the hydraulic conductivity standard proctor compaction energy specimen and other standard proctor compaction energy compaction data.*

10.1.1. Test 1

The target dry density for the specimen was at optimum for standard proctor at 18.75 kN/m^3. The dry density of the specimen for test 1 was found to be 18.14 kN/m^3. The void ratio (e) was 0.45. The porosity (n) was 0.31. The average hydraulic conductivity of the last 5 points of test 1 was found to be 1.14E-09 m/s with a coefficient of variation of 0.073. The low coefficient of variability implies that a stable filter was reach as a result of little variability within the specimen. One pore volume was calculated to be 276.35 cm^3. It was calculated that 2.89 pore volumes were permeated through the specimen. Test 1 results are shown in Table 10.2 through Table 10.7, Figure 10.2, and Figure 10.3.

Table 10.2 Sample properties for the hydraulic conductivity specimen.

Sample Properties	
Molded Water Content, w (%)	11.92%
Specific Gravity, G_s	2.69
Volume of specimen (cm^3), V	888.05
Unit Weight of Water, γ_w	9.79
Target Dry Density (kN/m^3), γ_d	18.75
Dry density (lb/ft^3), γ_d	115.49
Dry density(KN/m^3), γ_d	18.14
Void Ratio, e	0.45
Porosity, n	0.31
Pore Volume, (cm^3) Vp	276.35
Volume of Water Needed for Saturation (mL)	295.34
Cylinder Water Level Change for Saturation (in)	12/16
Cylinder Water Level at Saturation (in)	9 1/2

Table 10.3 Sample characteristics for the hydraulic conductivity specimen

Sample Characteristics	
Height of Sample (cm)	10.95
Diameter of Sample (cm)	10.16
Area of Sample (cm^2)	81.07
Volume of Sample (cm^3)	888.05
Pressure (Inches water), P	375
Applied Pressure (PSI), P	16.48
Applied Pressure (kPa), P	113.61
Area of Pressure Cylinder (cm^2)	149.81

Table 10.4 Sample preparation information

Sample Preparation	
Sample used for compaction	Passing No. 4 Sieve
Density used for Compaction (% target γ_d)	97%
Corresponding Water Content	11.92% (Dry Side)

Table 10.5 Hydraulic gradient calculation information

Pressure calculation for a predetermined hydraulic gradient						
L (ft)	i	γ_w (lb/ft^3)	u (psf)	u (psi)	u (kPa)	γ_w (kN/m^3)
0.38	100	62.4	2372.5	16.48	113.61	9.79

Table 10.6 Equation Definitions

Definitions:
i = h/L: Hydraulic gradient (unitless)
$h = u/\gamma_w$: Pressure head according to Bernoulli's equation
u = Pressure (psi)
γ_w= 62.4 lb/ft^3 = 9.79 kN/m^3 : Unit weight of water
L = Length of specimen (height of cylinder) (cm or in)

Table 10.7 Hydraulic conductivity results – Statistics (Last 5 data points)

k Results: Last 5 Points	
Average Hydraulic Conductivity (m/s)	1.14E-09
Sample Standard Deviation (s)	8.33E-11
Coefficient of Variation (COV)	0.073

10.1.2. Test 2

The target dry density for the specimen was at optimum for standard proctor at 18.75 kN/m^3. The dry density of the specimen for test 2 was found to be 18.15 kN/m^3. The void ratio (e) was 0.45. The porosity (n) was 0.31. The average hydraulic conductivity of the last 5 points of test 2 was found to be 5.81E-10 m/s with a coefficient of variation of 0.243. The low coefficient of variability implies that a stable filter was reach as a result of little variability within the specimen. One pore volume was calculated to be 260.01 cm^3. It was calculated that 3.69 pore volumes were permeated through the specimen. Test 2 results are shown in Table 10.8 through Table 10.12, Figure 10.2, and Figure 10.3.

Table 10.8 Sample properties for the hydraulic conductivity specimen.

Sample Properties	
Molded Water Content, w (%)	11.92%
Specific Gravity, G_s	2.69
Volume of specimen (cm^3), V	836.57
Unit Weight of Water, γ_w	9.79
Target Dry Density (kN/m^3), γ_d	18.75
Dry density (lb/ft^3), γ_d	115.55
Dry density(KN/m^3), γ_d	18.15
Void Ratio, e	0.45
Porosity, n	0.31
Pore Volume, (cm^3) Vp	260.01
Volume of Water Needed for Saturation (mL)	277.55
Cylinder Water Level Change for Saturation (in)	12/16
Cylinder Water Level at Saturation (in)	10 1/4

Table 10.9 Sample characteristics for the hydraulic conductivity specimen

Sample Characteristics	
Height of Sample (cm)	10.32
Diameter of Sample (cm)	10.16
Area of Sample (cm^2)	81.07
Volume of Sample (cm^3)	836.57
Pressure (Inches water), P	375
Applied Pressure (PSI), P	16.48
Applied Pressure (kPa), P	113.61
Area of Pressure Cylinder (cm^2)	149.81

Table 10.10 Sample preparation information

Sample Preparation	
Sample used for compaction	Passing No. 4 Sieve
Density used for Compaction (% target γ_d)	97%
Corresponding Water Content	9.84% (Dry Side)

Table 10.11 Hydraulic gradient calculation information

Pressure calculation for a predetermined hydraulic gradient						
L (ft)	i	γ_w (lb/ft^3)	u (psf)	u (psi)	u (kPa)	γ_w (kN/m^3)
0.38	100	62.4	2372.5	16.48	113.61	9.79

Table 10.12 Hydraulic conductivity results – Statistics (Last 5 data points)

k Results: Last 5 Points	
Average Hydraulic Conductivity (m/s)	5.81E-10
Sample Standard Deviation (s)	1.41E-10
Coefficient of Variation (COV)	0.243

10.1.3. Test 3

The target dry density for the specimen was at optimum for standard proctor at 18.75 kN/m^3. The dry density of the specimen for test 3 was found to be 18.30 kN/m^3. The void ratio (e) was 0.44. The porosity (n) was 0.31. The average hydraulic conductivity of the last 5 points of test 3 was found to be 1.82E-09 m/s with a coefficient of variation of 0.062. The low coefficient of variability implies that a stable filter was reach as a result of little variability within the specimen. One pore volume was calculated to be 270.95 cm^3. It was calculated that 18.46 pore volumes were permeated through the specimen. Test 3 results are shown in Table 10.13 through Table 10.17, Figure 10.2, and Figure 10.3.

Table 10.13 Sample properties for the hydraulic conductivity specimen

Sample Properties	
Molded Water Content, w (%)	8.43%
Specific Gravity, G_s	2.69
Volume of specimen (cm^3), V	888.05
Unit Weight of Water, γ_w	9.79
Target Dry Density (kN/m^3), γ_d	18.75
Dry density (lb/ft^3), γ_d	115.55
Dry density(KN/m^3), γ_d	18.3
Void Ratio, e	0.44
Porosity, n	0.31
Pore Volume, (cm^3) Vp	270.95
Volume of Water Needed for Saturation (mL)	315.06
Cylinder Water Level Change for Saturation (in)	13/16
Cylinder Water Level at Saturation (in)	16

Table 10.14 Sample characteristics for the hydraulic conductivity specimen.

Sample Characteristics	
Height of Sample (cm)	10.95
Diameter of Sample (cm)	10.16
Area of Sample (cm^2)	81.07
Volume of Sample (cm^3)	888.05
Pressure (Inches water), P	375
Applied Pressure (PSI), P	16.48
Applied Pressure (kPa), P	113.61
Area of Pressure Cylinder (cm^2)	149.81

Table 10.15 Sample preparation information

Sample Preparation	
Sample used for compaction	Passing No. 4 Sieve
Density used for Compaction (% target γ_d)	98%
Corresponding Water Content	8.43% (Dry Side)

Table 10.16 Hydraulic gradient calculation information

Pressure calculation for a predetermined hydraulic gradient						
L (ft)	i	γ_w (lb/ft^3)	u (psf)	u (psi)	u (kPa)	γ_w (kN/m^3)
0.38	100	62.4	2372.5	16.48	113.61	9.79

Table 10.17 Hydraulic conductivity results – Statistics (Last 5 data points)

k Results: Last 5 Points	
Average Hydraulic Conductivity (m/s)	1.82E-09
Sample Standard Deviation (s)	1.13E-10
Coefficient of Variation (COV)	0.062

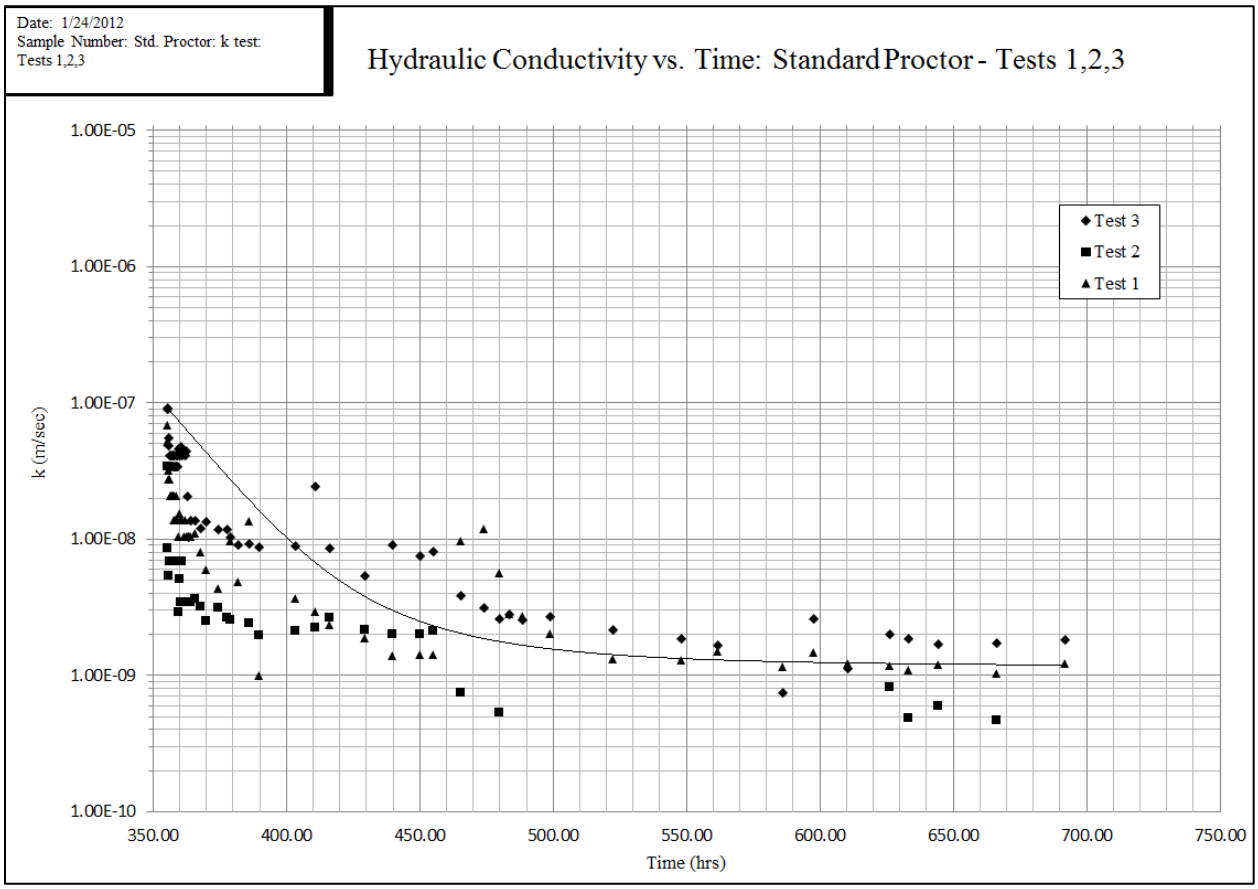

Figure 10.2 Hydraulic conductivity (k) versus time.

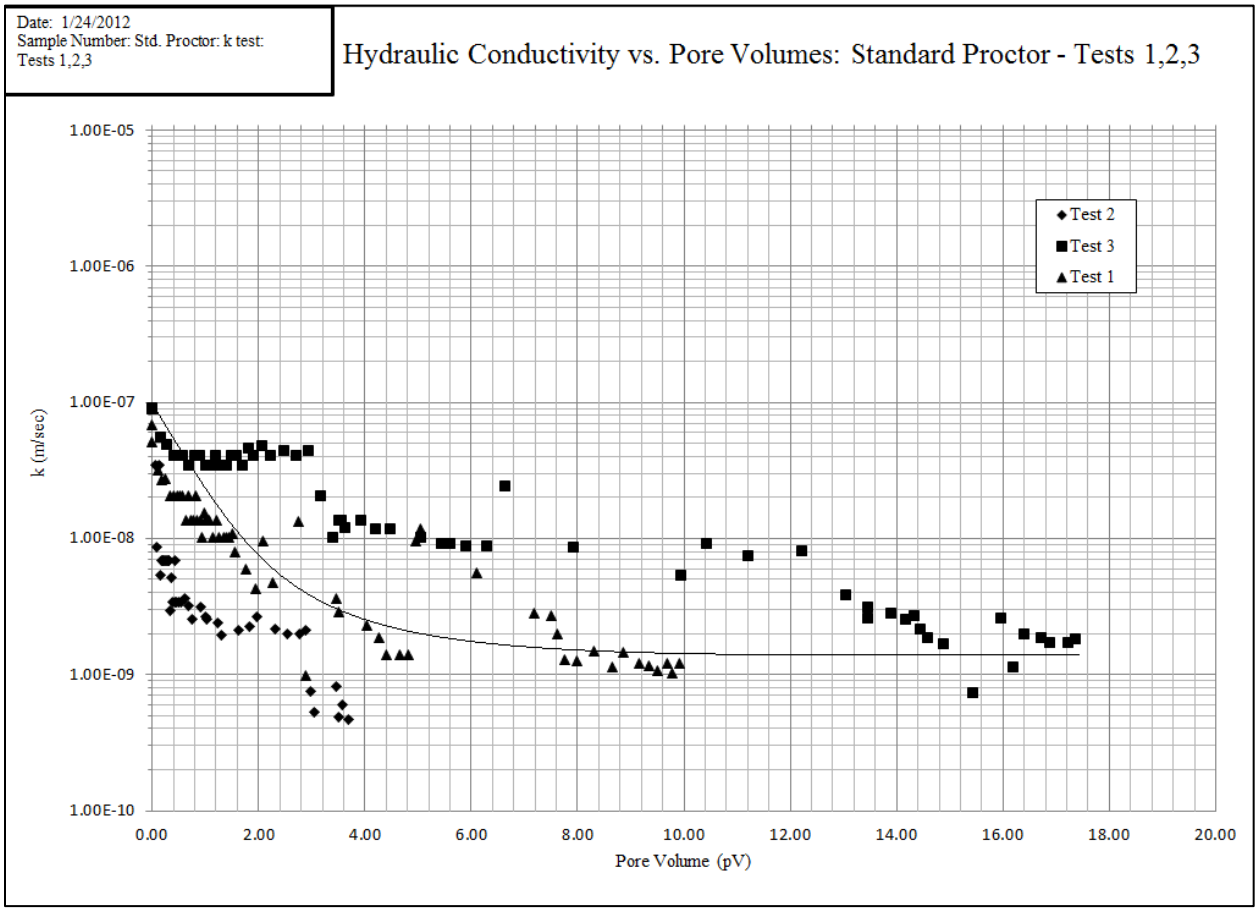

Figure 10.3 Hydraulic conductivity (k) versus pore volumes (pV).

Table 10.18 Summary values for tests 1, 2, and 3.

	i	$\gamma_{std.\ proctor}$ (kN/m^3)	$\gamma_{optimum}$ (kN/m^3)	e	n	k (m/s)	s (for k)	COV
Test 1	100	18.14	18.75	0.45	0.31	1.14E-09	8.33E-11	0.073
Test 2	100	18.15	18.75	0.45	0.31	5.81E-10	1.41E-10	0.243
Test 3	100	18.30	18.75	0.44	0.31	1.82E-09	1.13E-10	0.062
Average	--	18.20	--	0.45	0.31	1.18E-09	1.12E-10	0.126

10.2 Hydraulic Conductivity: 34% Proctor (203.6kJ/m^3)

Hydraulic conductivity testing was performed on a 34% Proctor compaction effort (203.6 kJ/m^3) specimen. The target dry density was at optimum for this compaction effort test data. The optimum dry density for the specimen was 18.1 kN/m^3. Triplicate testing was performed to ensure accuracy. The dry densities for tests 1, 2, and 3 were 16.32 kN/m^3, 16.44 kN/m^3, and 17.61 kN/m^3 respectively. The objective of the testing was to determine the hydraulic conductivity in order to better understand the rate at which water would permeate through the material under inspection. The purpose of the testing was to determine the fine particle movement within the specimen under the influence of a hydraulic gradient i=15. The hydraulic gradient of 15 was chosen for the 34% proctor specimens to avoid hydraulic consolidation and accelerate the testing process as a low hydraulic conductivity was expected for the well graded sand with silt. After the hydraulic conductivity readings reached equilibrium, the hydraulic conductivity was determined and the specimen was extruded approximately one third at a time. The hydraulic conductivity was determined after the data had become stable. In these cases, the average of the last five data points was taken to be the hydraulic conductivity of the specimens. The layers were saved and oven dried. Grain size analysis was run on three layers of each specimen. The hydraulic conductivity results are presented in this section (10.2). The hydraulic conductivity data is presented in Appendix I.

Table 10.19 Hydraulic conductivity 34% Proctor compaction energy specimen data.

Test Number	Test 1	Test 2	Test 3
Assumed moisture content (%)	14.5	14.5	14.5
Mold Weight (g), M_{md}	613.79	615.98	617.2
Specimen Weight (g)	1778.08	1803.46	1917.1
Specimen+Mold Weight (g), M_t	2391.87	2419.44	2534.3
Volume of Mold (cm^3), V	940	940	940
Specific Gravity of Soil, G_s	2.69	2.69	2.69
Unit Weight of Water @ 20°C (KN/m^3), γ_w	9.79	9.79	9.79
Unit Weight of Water @ 20°C (lb/ft^3), γ_w	62.34	62.34	62.34
Moist Unit Weight of Compacted Specimen (g/cm^3), γ_m	1.89	1.92	2.04
Dry Unit Weight of Compacted Specimen (g/cm^3), γ_d	1.66	1.67	1.79
Dry Unit Weight of Compacted Specimen (KN/m^3), γ_d	16.32	16.42	17.58
Dry Unit Weight of Compacted Specimen (lb/ft^3), γ_d	103.93	104.57	111.93
Dry Unit Weight at S=1.0 (KN/m^3),γ_d	19.27	18.93	19.22
Dry Unit Weight at S=0.9 (KN/m^3),γ_d	18.71	18.36	18.66
Dry Unit Weight at S=1.0 (lb/ft^3), γ_d	122.71	120.53	122.4
Dry Unit Weight at S=0.9 (lb/ft^3), γ_d	119.16	116.88	118.83
Void Ratio, $e=((G_s*\gamma_w)/\gamma_d)-1$	0.61	0.6	0.5
Degree of Saturation (%), $S=G_s*w/e$	0.6	0.65	0.74
Saturated Water Content, w_{sat} (%)	22.81	22.44	18.52
Assumed moisture content (%)	14.5	14.5	14.5
Container Mass (g), Mc	18.85	22.01	17.4
Container+Moist Specimen Mass(g), Mcms	66.63	83.67	74.62
Intial Container+Oven Dry Specimen Mass(g), Mcds	60.9	75.84	67.7
Mass of Water (g), Mw= Mcms-Mcds	5.73	7.83	6.92
Mass of Solids (g), Ms= Mcds-Mc	42.05	53.83	50.3
Water Content, % W= (Mw/Ms)x100	13.63	14.55	13.76

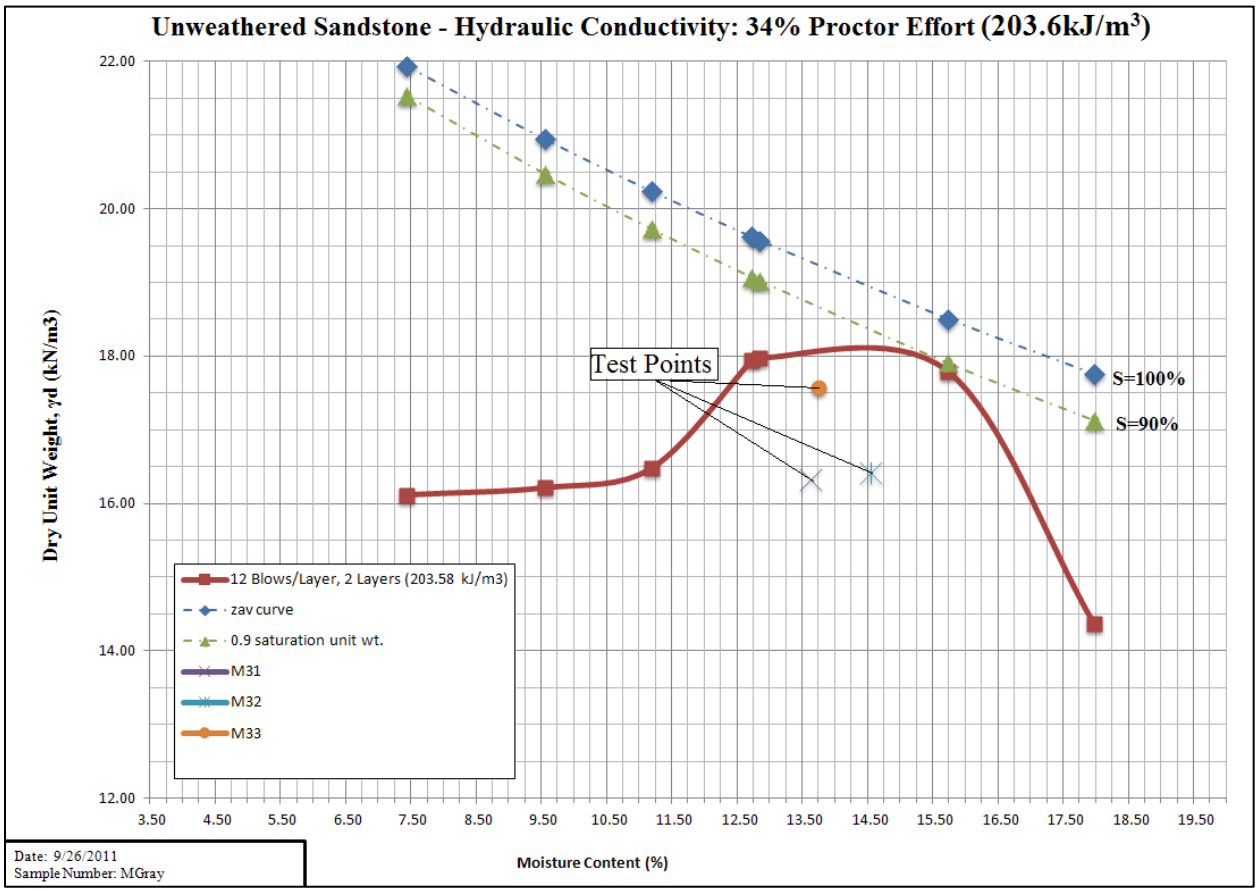

Figure 10.4 Comparison of the hydraulic conductivity 34% Proctor compaction energy specimen and other 34% Proctor specimen compaction data.

10.2.1 Test 1

The target dry density for the specimen was at optimum for 34% proctor at 18.1 kN/m^3. The dry density of the specimen for test 1 was found to be 16.32 kN/m^3. The void ratio (e) was 0.61. The porosity (n) was 0.38. The average hydraulic conductivity of the last 5 points of test 1 was found to be 2.02E-09 m/s with a coefficient of variation of 0.09. The low coefficient of variability implies that a stable filter was reach as a result of little variability within the specimen. The statistics are also shown for all of the test data to illustrate that the sample became a stable filter near the end of permeation. One pore volume was calculated to be 357.24 cm^3. It was calculated that 1.79 pore volumes were permeated through the specimen. Test 1 results are shown in Table 10.20 through Table 10.26, Figure 10.5 and Figure 10.6.

Table 10.20 Sample characteristics for the hydraulic conductivity specimen

Sample Characteristics	
Height of Sample (cm)	11.59
Diameter of Sample (cm)	10.16
Area of Sample (cm^2)	81.07
Volume of Sample (cm^3)	939.54
Pressure (Inches water), P	0.00
Applied Pressure (PSI), P	2.37
Applied Pressure (kPa), P	0.11

Table 10.21 Sample properties for the hydraulic conductivity specimen

Sample Properties	
Molded Water Content, w (%)	0.14
Specific Gravity, G_s	2.69
Volume of specimen (cm^3), V	939.54
Unit Weight of Water, γ_w	9.79
Dry density (lb/ft^3), γ_d	103.93
Dry density (kN/m^3), γ_d	16.32
Void Ratio, e	0.61
Porosity, n	0.38
Pore Volume, (cm^3) Vp	357.24

Table 10.22 Sample preparation information

Sample Preparation	
Sample used for compaction	Passing No. 4 Sieve
Density used for Compaction	90% max γ_d
Corresponding Water Content	13.63%(Dry Side)

Table 10.23 Hydraulic gradient calculation information

Pressure calculation for a predetermined hydraulic gradient						
L (ft)	i	γw (lb/ft^3)	u (psf)	u (psi)	u (kPa)	γw (kN/m^3)
0.38	15.00	62.40	355.88	2.47	17.04	9.79

Table 10.24 Equation Definitions

Definitions:
i = h/L: Hydraulic gradient (unitless)
$h = u/\gamma_w$: Pressure head according to Bernoulli's equation
u = Pressure (psi)
γ_w= 62.4 lb/ft^3 = 9.79 kN/m^3 : Unit weight of water
L = Length of specimen (height of cylinder) (cm or in)

Table 10.25 Hydraulic conductivity results – Statistics (All test 1 data)

Average Hydraulic Conductivity (m/s):	9.60E-08
Sample Standard Deviation (s)	4.92E-07
Coefficient of Variation (COV)	5.12

Table 10.26 Hydraulic conductivity results – Statistics (Last 5 data points)

Last 5 Points	
Average Hydraulic Conductivity (m/s):	2.02E-09
Sample Standard Deviation (s)	1.84E-10
Coefficient of Variation (COV)	0.09

10.2.2. Test 2

The target dry density for the specimen was at optimum for 34% proctor at 18.1 kN/m^3. The dry density of the specimen for test 2 was found to be 16.32 kN/m^3. The void ratio (e) was 0.60. The porosity (n) was 0.38. The average hydraulic conductivity of the last 5 points of test 2 was found to be 1.69E-09 m/s with a coefficient of variation of 0.21. The low coefficient of variability implies that a stable filter was reach as a result of little variability within the specimen. The statistics are also shown for all of the test data to illustrate that the sample became a stable filter near the end of permeation. One pore volume was calculated to be 352.96 cm^3. It was calculated that 0.751 pore volumes were permeated through the specimen. Test 2 results are shown in Table 10.27 through Table 10.32, Figure 10.5 and Figure 10.6.

Table 10.27 Sample characteristics for the hydraulic conductivity specimen

Sample Characteristics	
Height of Sample (cm)	11.59
Diameter of Sample (cm)	10.16
Area of Sample (cm^2)	81.07
Volume of Sample (cm^3)	939.54
Pressure (Inches water), P	56.25
Applied Pressure (PSI), P	2.37
Applied Pressure (kPa), P	0.11

Table 10.28 Sample properties for the hydraulic conductivity specimen

Sample Properties	
Molded Water Content, w (%)	0.15
Specific Gravity, G_s	2.69
Volume of specimen (cm^3), V	939.54
Unit Weight of Water, γ_w	9.79
Dry density (lb/ft^3), γ_d	104.69
Dry density(kN/m^3), γ_d	16.44
Void Ratio, e	0.60
Porosity, n	0.38
Pore Volume, (cm^3) V_p	352.96

Table 10.29 Sample preparation information

Sample Preparation	
Sample used for Compaction	Passing No. 4 Sieve
Density used for Compaction	90% max γ_d
Corresponding Water Content	14.55% (Wet Side)

Table 10.30 Hydraulic gradient calculation information

Pressure calculation for a predetermined hydraulic gradient						
L (ft)	**i**	**γ_w (lb/ft^3)**	**u (psf)**	**u (psi)**	**u (kPa)**	**γ_w (kN/m^3)**
0.38	15	62.40	355.88	2.47	17.04	9.79

Table 10.31 Hydraulic conductivity results – Statistics (All test 2 data)

Average Hydraulic Conductivity (m/s):	1.80E-09
Sample Standard Deviation (s)	1.87E-09
Coefficient of Variation (COV)	1.04E+00

Table 10.32 Hydraulic conductivity results – Statistics (Last 5 data points)

Last 5 Points	
Average Hydraulic Conductivity (m/s):	1.69E-09
Sample Standard Deviation (s)	3.52E-10
Coefficient of Variation (COV)	2.08E-01

10.2.3. Test 3

The target dry density for the specimen was at optimum for 34% proctor at 18.1 kN/m^3. The dry density of the specimen for test 3 was found to be 17.61 kN/m^3. The void ratio (e) was 0.50. The porosity (n) was 0.33. The average hydraulic conductivity of the last 5 points of test 3 was found to be 3.31E-09 m/s with a coefficient of variation of 0.07. The low coefficient of variability implies that a stable filter was reach as a result of little variability within the specimen. The statistics are also shown for all of the test data to illustrate that the sample became a stable filter near the end of permeation. One pore volume was calculated to be 311.21 cm^3. It was calculated that 2.22 pore volumes were permeated through the specimen. Test 3 results are shown in Table 10.33 through Table 10.38, Figure 10.5 and Figure 10.6.

Table 10.33 Sample characteristics for the hydraulic conductivity specimen

Sample Characteristics	
Height of Sample (cm)	11.59
Diameter of Sample (cm)	10.16
Area of Sample (cm^2)	81.07
Volume of Sample (cm^3)	939.54
Pressure (Inches water), P	56.25
Applied Pressure (PSI), P	2.37
Applied Pressure (kPa), P	0.11

Table 10.34 Sample properties for the hydraulic conductivity specimen

Sample Properties	
Molded Water Content, w (%)	14
Specific Gravity, G_s	2.69
Volume of specimen (cm^3), V	939.54
Unit Weight of Water, γ_w	9.79
Dry density (lb/ft^3), γ_d	112.12
Dry density(kN/m^3), γ_d	17.61
Void Ratio, e	0.50
Porosity, n	0.33
Pore Volume, (cm^3) V_p	311.21

Table 10.35 Sample preparation information

Sample Preparation	
Sample used for Compaction	Passing No. 4 Sieve
Density used for Compaction	97% max γd
Corresponding Water Content	13.76%(Dry Side)

Table 10.36 Hydraulic gradient calculation information

Pressure calculation for a predetermined hydraulic gradient						
L (ft)	**i**	**γ_w (lb/ft^3)**	**u (psf)**	**u (psi)**	**u (kPa)**	**γ_w (kN/m^3)**
0.38	15	62.40	355.88	2.47	17.04	9.79

Table 10.37 Hydraulic conductivity results – Statistics (All test 3 data)

Average Hydraulic Conductivity (m/s):	4.611E-09
Sample Standard Deviation (s)	2.650E-09
Coefficient of Variation (COV)	5.747E-01

Table 10.38 Hydraulic conductivity results – Statistics (Last 5 data points)

Last 5 Points	
Average Hydraulic Conductivity (m/s):	3.313E-09
Sample Standard Deviation (s)	2.298E-10
Coefficient of Variation (COV)	6.936E-02

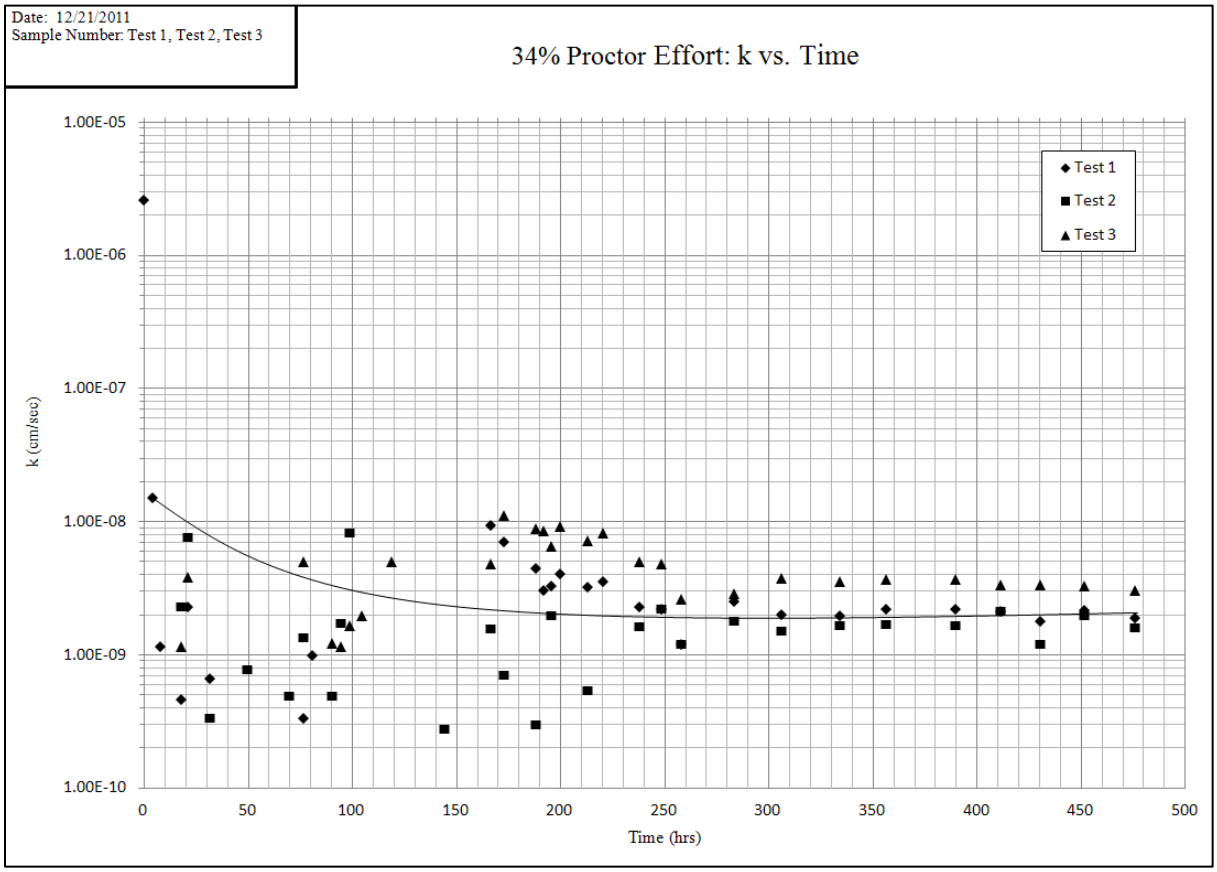

Figure 10.5 Hydraulic conductivity (k) versus time.

Table 10.39 Summary values for tests 1, 2, and 3.

	i	$\gamma_{34\%Proctor}$ (kN/m^3)	$\gamma_{optimum}$ (kN/m^3)	e	n	k (m/s)	s (for k)	COV
Test 1	15	16.32	18.1	0.61	0.38	2.02E-09	1.84E-10	0.09
Test 2	15	16.44	18.1	0.60	0.38	1.69E-09	3.52E-10	0.21
Test 3	15	17.61	18.1	0.50	0.33	3.31E-09	2.30E-10	0.07
Average	--	16.79	--	0.57	0.36	2.34E-09	2.55E-10	0.12

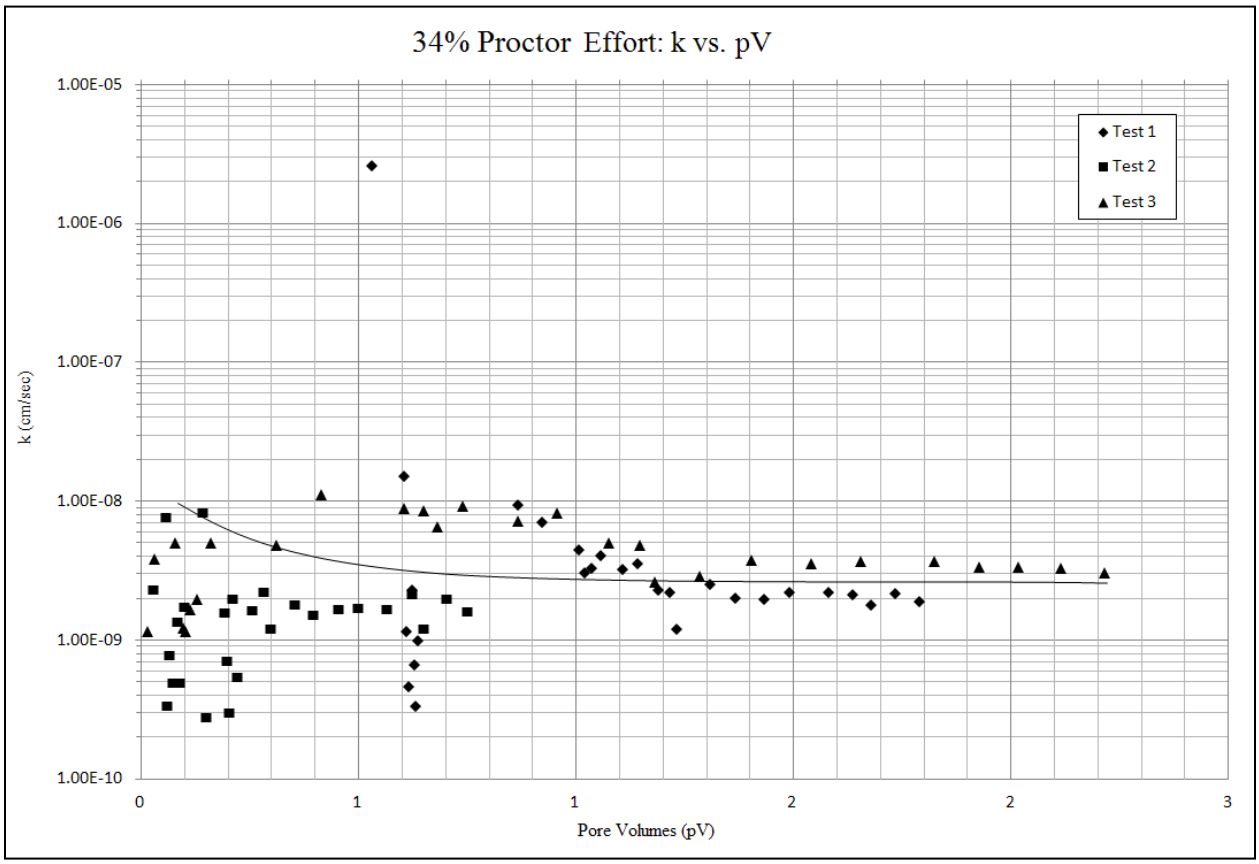

Figure 10.6 Hydraulic conductivity (k) versus pore volumes (pV).

10.3 Hydraulic Conductivity: 11% Proctor (67.85 kJ/m^3)

Hydraulic conductivity testing was performed on a 11% Proctor compaction effort (67.85 kJ/m^3) specimen. The target dry density was at the minimum for the 11% Proctor compaction effort test data. The minimum dry density for the 11% Proctor compaction effort specimen was 14.9 kN/m^3. Triplicate testing was performed to ensure accuracy. The dry densities for tests 1, 2, and 3 were 15.14 kN/m^3, 15.52 kN/m^3, and 15.49 kN/m^3 respectively. The objective of the testing was to determine the hydraulic conductivity in order to better understand the rate at which water would permeate through the material under inspection. The purpose of the testing was to determine the fine particle movement within the specimen under the influence of a hydraulic gradient i=15. The hydraulic gradient of 15 was chosen for the 11% proctor specimens to avoid hydraulic consolidation and accelerate the testing process as a low hydraulic conductivity was expected for the well graded sand with silt. After the hydraulic conductivity readings reached equilibrium, the hydraulic conductivity was determined and the specimen was extruded approximately one third at a time. The hydraulic conductivity was determined after the data had become stable. In these cases, the average of the last five data points was taken to be the hydraulic conductivity of the specimens. The layers were saved and oven dried. Grain size analysis was run on three layers of each specimen. The hydraulic conductivity data for the 11% Proctor compaction energy specimen are presented in this section (10.3). The hydraulic conductivity data is presented in Appendix I.

Table 10.40 Hydraulic conductivity 11% Proctor compaction energy specimen data.

Test Number	Test 1	Test 2	Test 3
Assumed moisture content (%)	10.5	10.5	10.5
Mold Weight(g), M_{md}	614.74	616.56	617.67
Specimen Weight (g)	1595.5	1616.54	1608.18
Specimen+Mold Weight (g), M_t	2210.24	2233.1	2225.85
Volume of Mold(cm^3), V	940	940	940
Specific Gravity of Soil, G_s	2.69	2.69	2.69
Unit Weight of Water @ 20°C(KN/m^3), γ_w	9.79	9.79	9.79
Unit Weight of Water @ 20°C(lb/ft^3), γ_w	62.34	62.34	62.34
Moist Unit Weight of Compacted Specimen(g/cm^3), γ_m	1.7	1.72	1.71
Dry Unit Weight of Compacted Specimen(g/cm^3), γ_d	1.54	1.58	1.58
Dry Unit Weight of Compacted Specimen(kN/m^3), γ_d	**15.14**	**15.52**	**15.49**
Dry Unit Weight of Compacted Specimen(lb/ft^3), γ_d	96.44	98.8	98.65
Dry Unit Weight at S=1.0 (kN/m^3),γ_d	**20.81**	**21.36**	**21.55**
Dry Unit Weight at S=0.9 (kN/m^3),γ_d	**20.33**	**20.92**	**21.12**
Dry Unit Weight at S=1.0 (lb/ft^3), γ_d	132.5	136.01	137.2
Dry Unit Weight at S=0.9 (lb/ft^3), γ_d	129.48	133.21	134.48
Void Ratio, $e=((Gs*g_w)/g_d)-1$	0.74	0.7	0.7
Degree of Saturation (%), S=Gs*w/e	0.36	0.33	0.32
Saturated Water content, W_{sat} (%)	27.47	25.92	26.02
Assumed moisture content (%)	10.5	10.5	10.5
Container Mass(g), M_c	30.65	30.47	30.56
Container+Moist Specimen Mass(g), M_{cms}	131	89.68	98.68
Intial Container+Oven Dry Specimen Mass(g), M_{cds}	121.98	84.96	93.48
Mass of Water(g), $M_w= M_{cms}-M_{cds}$	9.02	4.72	5.2
Mass of Solids(g), $M_s= M_{cds}-M_c$	91.33	54.49	62.92
Water Content, % $W= (M_w/M_s)x100$	**9.88**	**8.66**	**8.26**

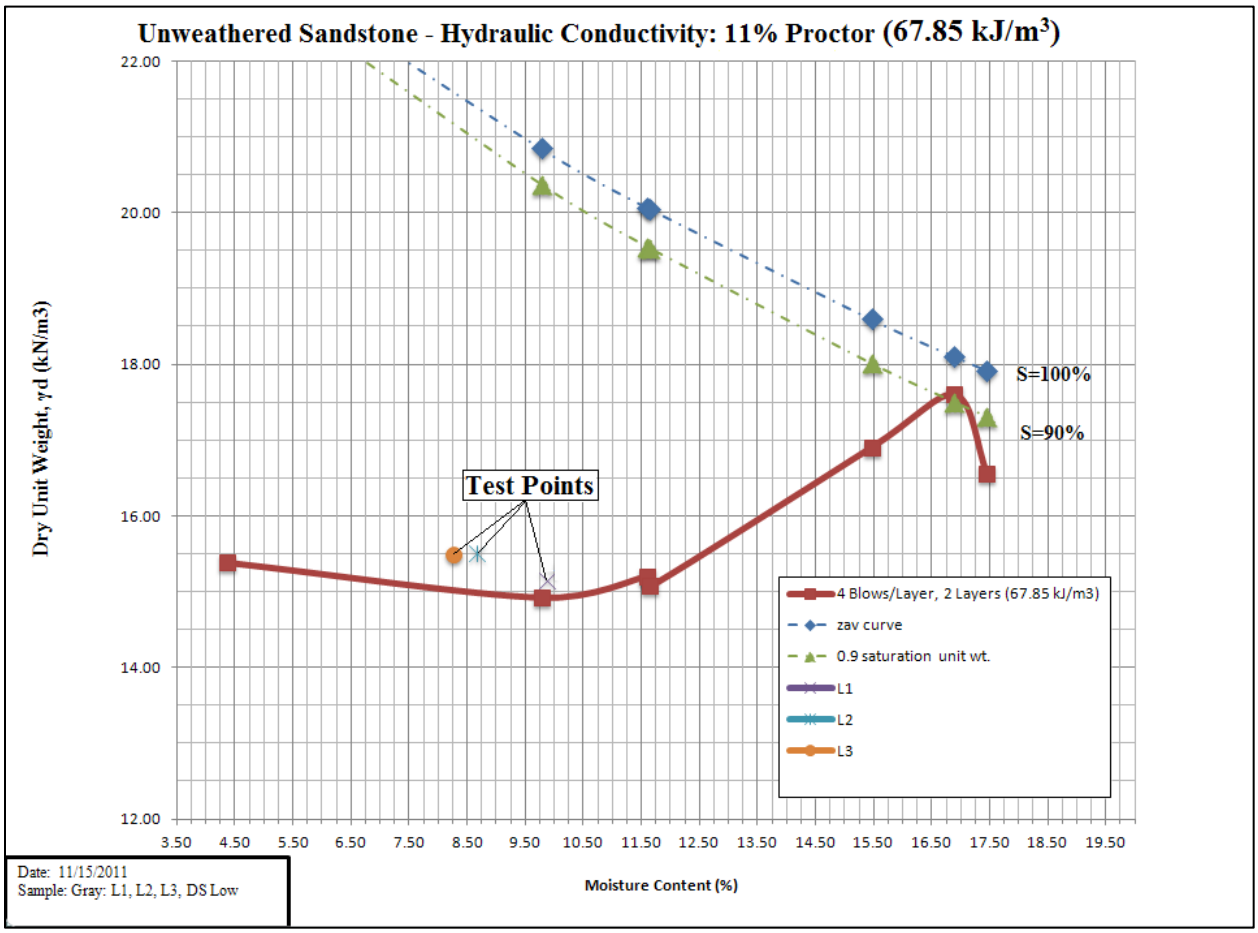

Figure 10.7 Comparison of the hydraulic conductivity 11% Proctor compaction energy specimen and other 11% Proctor compaction energy compaction data.

10.3.1. Test 1

The target dry density for the specimen was at minimum for 11% proctor at 14.90 kN/m^3. The dry density of the specimen for test 1 was found to be 15.14 kN/m^3. The void ratio (e) was 0.74. The porosity (n) was 0.43. The average hydraulic conductivity of the last 5 points of test 1 was found to be 1.89E-09 m/s with a coefficient of variation of 0.125. The low coefficient of variability implies that a stable filter was reach as a result of little variability within the specimen. The statistics are also shown for all of the test data to illustrate that the sample became a stable filter near the end of permeation. One pore volume was calculated to be 399.34 cm^3. It was calculated that 1.10 pore volumes were permeated through the specimen. Test 1 results are shown in Table 10.41 through Table 10.46, Figure 10.8 and Figure 10.9.

Table 10.41 Sample characteristics for the hydraulic conductivity specimen

Sample Characteristics	
Height of Sample (cm)	11.59
Diameter of Sample (cm)	10.16
Area of Sample (cm^2)	81.07
Volume of Sample (cm^3)	939.54
Pressure (Inches water), P	56.25
Applied Pressure (PSI), P	0.82
Applied Pressure (kPa), P	0.04

Table 10.42 Sample properties for the hydraulic conductivity specimen

Sample Properties	
Molded Water Content, w (%)	9.88%
Specific Gravity, G_s	2.69
Volume of specimen (cm^3), V	939.54
Unit Weight of Water, γ_w	9.79
Dry density (lb/ft^3), γ_d	96.44
Dry density(kN/m^3), γ_d	15.14
Void Ratio, e	0.74
Porosity, n	0.43
Pore Volume, (cm^3) V_p	399.34

Table 10.43 Sample preparation information

Sample Preparation	
Sample used for Compaction	Passing No. 4 Sieve
Density used for Compaction	101% min γ_d
Corresponding Water Content	9.88% (Dry Side)

Table 10.44 Hydraulic gradient calculation information

Pressure calculation for a predetermined hydraulic gradient						
L (ft)	i	γ_w (lb/ft^3)	u (psf)	u (psi)	u (kPa)	γ_w (kN/m^3)
0.38	15	62.4	355.88	2.47	17.04	9.79

Table 10.45 Hydraulic conductivity results – Statistics (All test 1 data)

Average Hydraulic Conductivity (m/s):	1.41E-08
Sample Standard Deviation (s)	2.23E-08
Coefficient of Variation (COV)	1.577

Table 10.46 Hydraulic conductivity results – Statistics (Last 5 data points)

Last 5 Points	
Average Hydraulic Conductivity (m/s)	1.89E-09
Sample Standard Deviation (s)	2.37E-10
Coefficient of Variation (COV)	0.125

10.3.2. Test 2

The target dry density for the specimen was at minimum for 11% proctor at 14.90 kN/m^3. The dry density of the specimen for test 2 was found to be 15.52 kN/m^3. The void ratio (e) was 0.70. The porosity (n) was 0.41. The average hydraulic conductivity of the last 5 points of test 2 was found to be 2.43E-09 m/s with a coefficient of variation of 0.133. The low coefficient of variability implies that a stable filter was reach as a result of little variability within the specimen. The statistics are also shown for all of the test data to illustrate that the sample became a stable filter near the end of permeation. One pore volume was calculated to be 385.79 cm^3. It was calculated that 7.61 pore volumes were permeated through the specimen. Test 2 results are shown in Table 10.47 through Table 10.52, Figure 10.8 and Figure 10.9.

Table 10.47 Sample characteristics for the hydraulic conductivity specimen

Sample Characteristics	
Height of Sample (cm)	11.59
Diameter of Sample (cm)	10.16
Area of Sample (cm^2)	81.07
Volume of Sample (cm^3)	939.54
Pressure (Inches water), P	56.25
Applied Pressure (PSI), P	0.82
Applied Pressure (kPa), P	0.04

Table 10.48 Sample properties for the hydraulic conductivity specimen

Sample Properties	
Molded Water Content, w(%)	8.66%
Specific Gravity, Gs	2.69
Volume of specimen (cm^3), V	939.54
Unit Weight of Water, γ_w	9.79
Dry density (lb/ft^3), γ_d	98.80
Dry density(kN/m^3), γ_d	15.52
Void Ratio, e	0.70
Porosity, n	0.41
Pore Volume, (cm^3) V_p	385.79

Table 10.49 Sample preparation information

Sample Preparation	
Sample used for Compaction	Passing No. 4 Sieve
Density used for Compaction	104% min γ_d
Corresponding Water Content	8.66%(Dry Side)

Table 10.50 Hydraulic gradient calculation information

Pressure calculation for a predetermined hydraulic gradient						
L (ft)	i	γ_w (lb/ft^3)	u (psf)	u (psi)	u (kPa)	γ_w (kN/m^3)
0.38	15	62.4	355.88	2.47	17.04	9.79

Table 10.51 Hydraulic conductivity results – Statistics (All test 1 data)

Average Hydraulic Conductivity (m/s):	2.05E-07
Sample Standard Deviation (s)	3.88E-07
Coefficient of Variation (COV)	1.889

Table 10.52 Hydraulic conductivity results – Statistics (Last 5 data points)

Last 5 Points	
Average Hydraulic Conductivity (m/s):	2.43E-09
Sample Standard Deviation (s)	3.22E-10
Coefficient of Variation (COV)	0.133

10.3.3. Test 3

The target dry density for the specimen was at minimum for 11% proctor at 14.90 kN/m^3. The dry density of the specimen for test 3 was found to be 15.49 kN/m^3. The void ratio (e) was 0.70. The porosity (n) was 0.41. The average hydraulic conductivity of the last 5 points of test 3 was found to be 3.60E-09 m/s with a coefficient of variation of 0.121. The low coefficient of variability implies that a stable filter was reach as a result of little variability within the specimen. The statistics are also shown for all of the test data to illustrate that the sample became a stable filter near the end of permeation. One pore volume was calculated to be 386.86 cm^3. It was calculated that 9.04 pore volumes were permeated through the specimen. Test 3 results are shown in Table 10.53 through Table 10.58, Figure 10.8 and Figure 10.9.

Table 10.53 Sample characteristics for the hydraulic conductivity specimen

Sample Characteristics	
Height of Sample (cm)	11.59
Diameter of Sample (cm)	10.16
Area of Sample (cm^2)	81.07
Volume of Sample (cm^3)	939.54
Pressure (Inches water), P	56.25
Applied Pressure (PSI), P	0.82
Applied Pressure (kPa), P	0.04

Table 10.54 Sample properties for the hydraulic conductivity specimen

Sample Properties	
Molded Water Content, w (%)	8.26%
Specific Gravity, Gs	2.69
Volume of specimen (cm^3), V	939.54
Unit Weight of Water, γ_w	9.79
Dry density (lb/ft^3), γ_d	98.65
Dry density(kN/m^3), γ_d	15.49
Void Ratio, e	0.70
Porosity, n	0.41
Pore Volume, (cm^3) V_p	386.86

Table 10.55 Sample preparation information

Sample Preparation	
Sample used for comapaction	Passing No. 4 Sieve
Density used for Comapaction	104% min γ_d
Corresponding Water Content	8.26%(Dry Side)

Table 10.56 Hydraulic gradient calculation information

Pressure calculation for a predetermined hydraulic gradient						
L (ft)	i	γ_w (lb/ft^3)	u (psf)	u (psi)	u (kPa)	γ_w (kN/m^3)
0.38	15	62.4	355.88	2.47	17.04	9.79

Table 10.57 Hydraulic conductivity results – Statistics (All test 1 data)

Average Hydraulic Conductivity (m/s):	1.09E-07
Sample Standard Deviation (s)	1.86E-07
Coefficient of Variation (COV)	1.703

Table 10.58 Hydraulic conductivity results – Statistics (Last 5 data points)

Last 5 Points	
Average Hydraulic Conductivity (m/s):	3.60E-09
Sample Standard Deviation (s)	4.35E-10
Coefficient of Variation (COV)	0.121

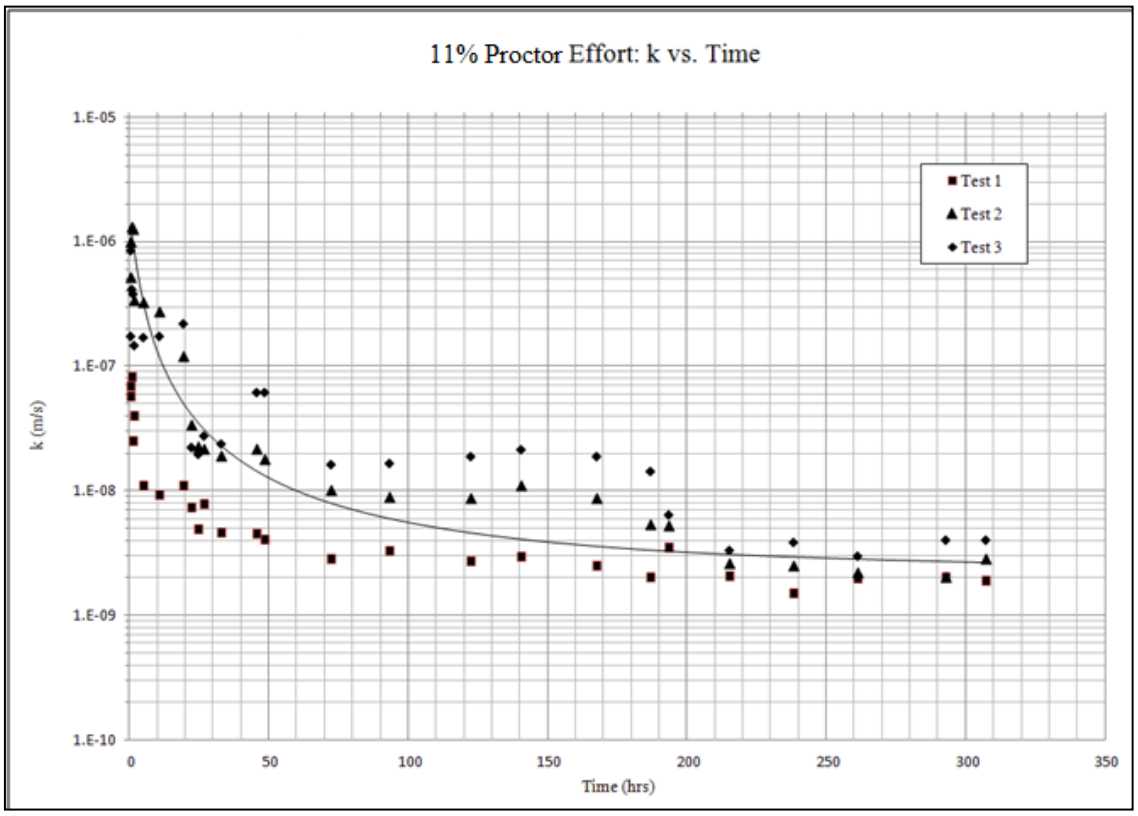

Figure 10.8 Hydraulic conductivity (k) versus time.

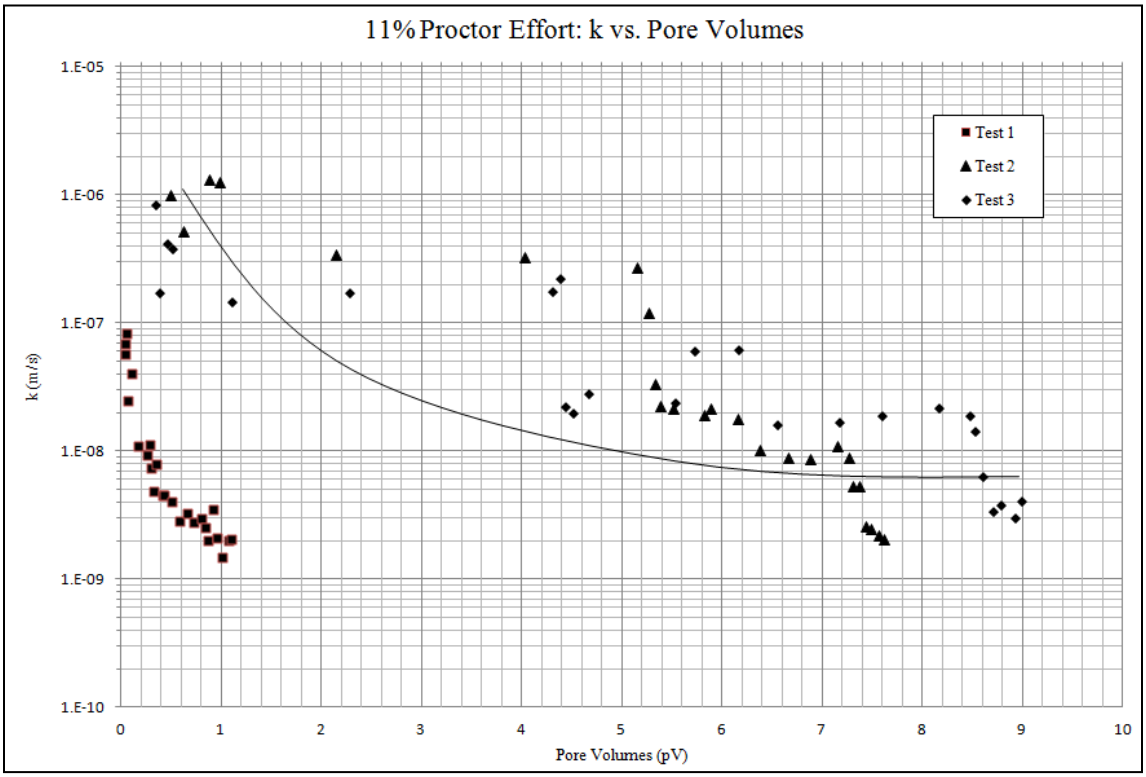

Figure 10.9 Hydraulic conductivity (k) versus pore volumes (pV).

Table 10.59 Summary values for tests 1, 2, and 3.

	i	$\gamma_{11\%Proctor}$ (kN/m^3)	$\gamma_{minimum}$ (kN/m^3)	e	n	k (m/s)	s (for k)	COV
Test 1	15	15.14	14.9	0.74	0.43	1.89E-09	2.37E-10	0.13
Test 2	15	15.52	14.9	0.70	0.41	2.43E-09	3.22E-10	0.13
Test 3	15	15.49	14.9	0.70	0.41	3.60E-09	4.35E-10	0.12
Average	--	15.38	--	0.71	0.42	2.64E-09	3.31E-10	0.13

Discussion

The hydraulic conductivity for each test performed for standard proctor, 34% proctor, and 11% proctor all remained in the order of 10^{-9} m/s. The neither the 34% proctor permeated specimens, nor the standard proctor specimens had hydraulic consolidation effects. Some hydraulic consolidation did occur for the 11% proctor specimens. The consolidation that occurred was the cause of the low hydraulic conductivity of the 11% proctor specimens. The soil structure could not retain its skeleton and void spaces collapsed under the hydraulic gradient of i=15. The standard proctor and 34% proctor specimens had low porosities in a range of n=0.31 to n=0.38 which resulted in low hydraulic conductivities. A summary table of the hydraulic conductivity results are shown in Table 10.60 below.

Table 10.60 Hydraulic conductivity summary

	Test Number	k (m/s)
Standard Proctor	Test 1	1.14E-09
	Test 2	5.81E-09
	Test 3	1.82E-09
34% Proctor	Test 1	2.02E-09
	Test 2	1.69E-09
	Test 3	3.31E-09
11% Proctor	Test 1	1.89E-09
	Test 2	2.43E-09
	Test 3	2.64E-09

11. Post-Permeability Grain Size Distribution

Triplicate testing was performed for three phases of hydraulic conductivity testing. The first phase was a triplicate testing of a standard proctor compacted specimen (592.5 kJ/m^3) with a hydraulic gradient of i=100. For the first phase, each specimen had a target density at the maximum dry density (18.75 kN/m^3) of the determined proctor curve. The second phase was a triplicate testing of a 34% Proctor compacted specimen (203.6 kJ/m^3) with a hydraulic gradient of i=15. For the second phase, each specimen had a target density at the maximum dry density (18.1 kN/m^3) of the determined proctor curve. The third phase was a triplicate testing of a 11% Proctor compacted specimen (67.85 kJ/m^3) with a hydraulic gradient of i=15. For the third phase, each specimen had a target density at the minimum dry density (14.9 kN/m^3) of the determined proctor curve. One hydraulic conductivity specimen was chosen for each phase for grain size distribution testing. Three approximately equal layers were cut from the specimen after the hydraulic conductivity had been determined. A sieve analysis was performed on each of these layers. The objective of this testing was to determine the movement of the particles with an applied hydraulic gradient that was comparable to the conditions that the material would experience in the field. These results have implications on the stability or instability of earthen structures built from the unweathered sandstone under inspection. The results of the testing are shown in this chapter.

11.1 Post-Permeability Grain Size Distribution: Standard Proctor (592.5kJ/m^3)

Three approximately equal layers were cut from the standard proctor Test 1 hydraulic conductivity specimen in Chapter 10, section 10.1 for the standard proctor post-permeability grain size distribution testing. The layers were tested separately to determine whether or not their gradations varied. The sought after variation is a result of particle movement during permeation. Only the sand portion (passing #4 sieve to #200 sieve) was permeated and tested. The results of the sieve analysis yielded a coefficient of variation of 0.036 for the uniformity coefficient and a coefficient of variation of 0.044 for the coefficient of gradation. This low coefficient of variation implies that the samples had very little variation in their gradations. Additional information about the properties of this specimen can be found in Appendix I and section 10.1. The data for the sieve analysis is shown in Table 11.1, Table 11.2, Table 11.3, and Figure 11.1.

Table 11.1 Critical index values for the hydraulic conductivity grain size distribution testing.

Critical Indices	Layer 1	Layer 2	Layer 3
D_{90}	3.90	4.00	4.00
D_{60}	2.00	2.40	2.30
D_{50}	1.60	1.80	1.75
D_{30}	0.74	0.83	0.81
D_{25}	0.60	0.65	0.65
D_{10}	0.14	0.16	0.15
Uniformity Coefficient, C_u	**14.29**	**15.00**	**15.33**
Coefficient of Gradation, C_c	**1.96**	**1.79**	**1.90**

Table 11.2 Uniformity coefficient statistics

Uniformity Coefficient, C_u	
Average Uniformity Coefficient	14.873
Sample Standard Deviation (s)	0.535
Coefficient of Variation (COV)	0.036

Table 11.3 Coefficient of gradation statistics

Coefficient of Gradation, C_c	
Average Coefficient of Gradation	1.884
Sample Standard Deviation (s)	0.082
Coefficient of Variation (COV)	0.044

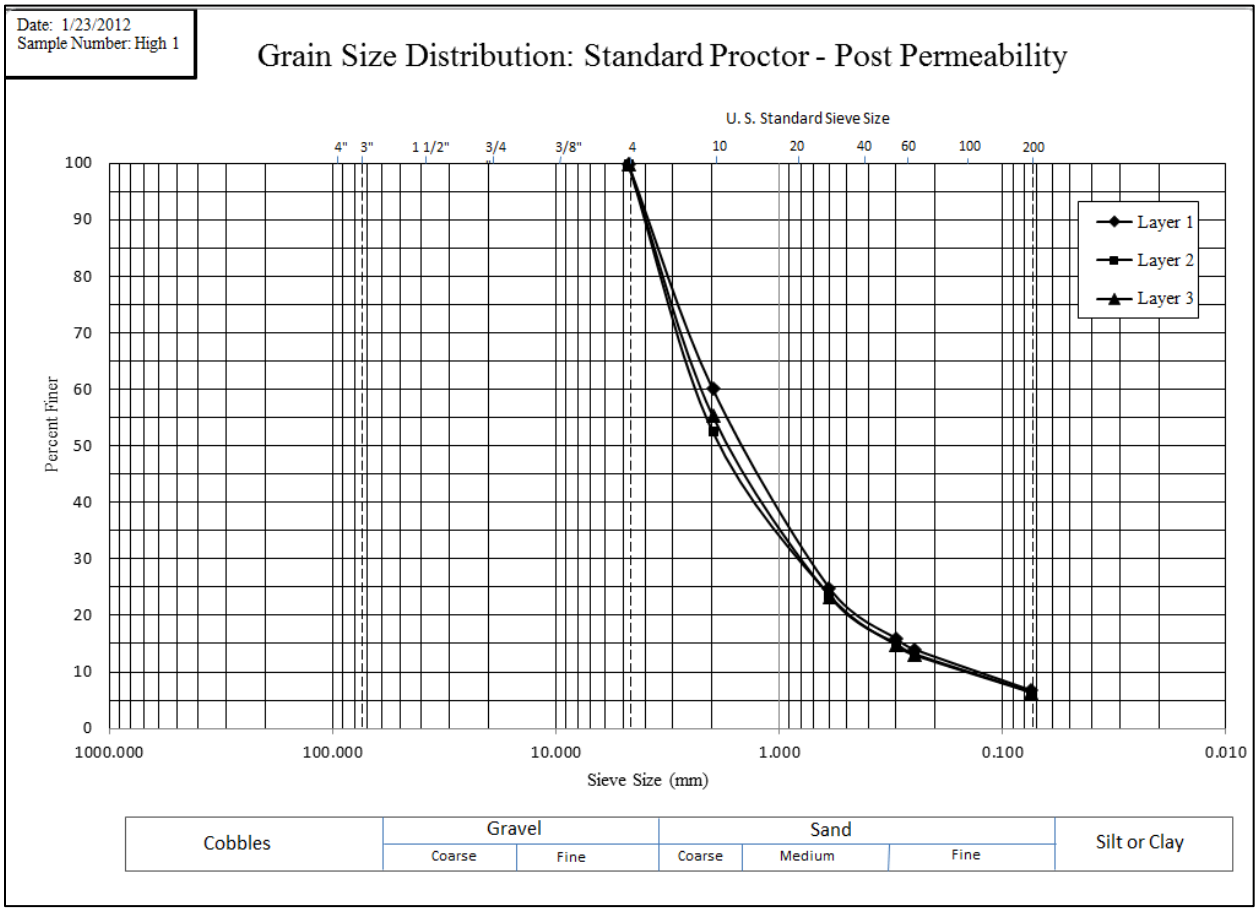

Figure 11.1 Grain size distribution of layer1, layer2, and layer3 of the hydraulic conductivity test specimen.

11.2 Post-Permeability Grain Size Distribution: 34% Proctor (203.6 kJ/m^3)

Three approximately equal layers were cut from the 34% proctor Test 1 hydraulic conductivity specimen in Chapter 10, section 10.2 for the standard proctor post-permeability grain size distribution testing. The layers were tested separately to determine whether or not their gradations varied. The sought after variation is a result of particle movement during permeation. Only the sand portion (passing #4 sieve to #200 sieve) was permeated and tested. The results of the sieve analysis yielded a coefficient of variation of 0.163 for the uniformity coefficient and a coefficient of variation of 0.050 for the coefficient of gradation. This low coefficient of variation implies that the samples had very little variation in their gradations. Additional information about the properties of this specimen can be found in Appendix I and section 10.2. The data for the sieve analysis is shown in Table 11.4, Table 11.5, Table 11.6, and Figure 11.2.

Table 11.4 Critical index values for the hydraulic conductivity grain size distribution testing.

Critical Indices	Layer 1	Layer 2	Layer 3
D_{90}	3.900	3.900	4.000
D_{60}	2.100	2.200	2.400
D_{50}	1.600	1.700	1.800
D_{30}	0.660	0.700	0. 880
D_{25}	0.500	0.550	0.700
D_{15}	0.230	0.260	0.350
D_{10}	0.110	0.130	0.175
Uniformity Coefficient, C_u	**19.09**	**16.92**	**13.71**
Coefficient of Gradation, C_c	**1.89**	**1.71**	**1.84**

Table 11.5 Uniformity coefficient statistics

Uniformity Coefficient, C_u	
Average Uniformity Coefficient	16.576
Sample Standard Deviation (s)	2.705
Coefficient of Variation (COV)	0.163

Table 11.6 Coefficient of gradation statistics

Coefficient of Gradation, C_c	
Average Coefficient of Gradation	1.814
Sample Standard Deviation (s)	0.090
Coefficient of Variation (COV)	0.050

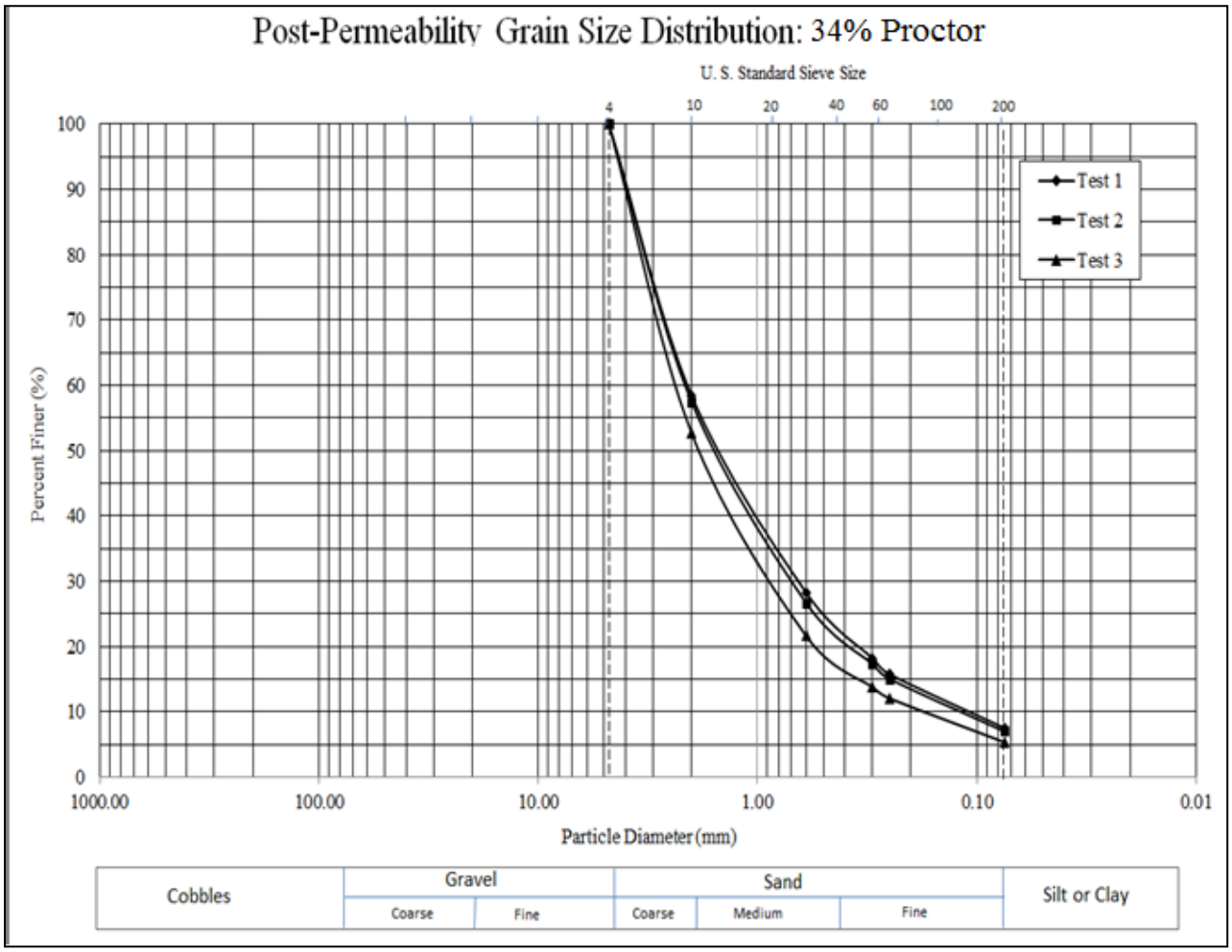

Figure 11.2 Grain size distribution of layer1, layer2, and layer3 of the hydraulic conductivity test specimen.

11.3 Post-Permeability Grain Size Distribution: 11% Proctor (67.85 kJ/m^3)

For 11% proctor hydraulic conductivity, a sieve analysis was performed for three permeated specimens with three layers each for additional precision in the testing. Test 1, Test 2, and Test 3 correspond to Tests 1, 2, and 3 in sections 10.3.1, 10.3.2, and 10.3.3, respectively. Compaction information, porosity (n), void ratio (e), and other properties of each specimen are given in each respective section as well as Appendix I. Three approximately equal layers were cut from the hydraulic conductivity specimen in Chapter 10 for the standard proctor post-permeability grain size distribution testing. The layers were tested separately to determine whether or not their gradations varied. The sought after variation is a result of particle movement during permeation. Only the sand portion (passing #4 sieve to #200 sieve) was permeated and tested. The results of this testing are shown in sections 11.3.1, 11.3.2, and 11.3.3.

11.3.1 Post-Permeability Grain Size Distribution: 11% Proctor - Test 1

The results of this sieve analysis yielded a coefficient of variation of 0.096 for the uniformity coefficient and a coefficient of variation of 0.067 for the coefficient of gradation. This low coefficient of variation implies that the samples had very little variation in their gradations. The data for the sieve analysis is shown in Table 11.7, Table 11.8, Table 11.9, and Figure 11.3.

Table 11.7 Critical index values for the hydraulic conductivity grain size distribution testing

Results			
Critical Indices	Layer 1	Layer 2	Layer 3
D_{90}	3.750	3.900	3.800
D_{60}	1.750	2.000	1.900
D_{50}	1.300	1.500	1.400
D_{30}	0.590	0.630	0.650
D_{25}	0.430	0.480	0.500
D_{15}	0.180	0.210	0.240
D_{10}	0.095	0.105	0.120
Uniformity Coefficient, C_u	**18.42**	**19.05**	**15.83**
Coefficient of Gradation, C_c	**2.09**	**1.89**	**1.85**

Table 11.8 Uniformity coefficient statistics

Uniformity Coefficient, C_u	
Average Uniformity Coefficient	17.767
Sample Standard Deviation (s)	1.704
Coefficient of Variation (COV)	0.096

Table 11.9 Coefficient of gradation statistics

Coefficient of Gradation, C_c	
Average Coefficient of Gradation	1.946
Sample Standard Deviation (s)	0.130
Coefficient of Variation (COV)	0.067

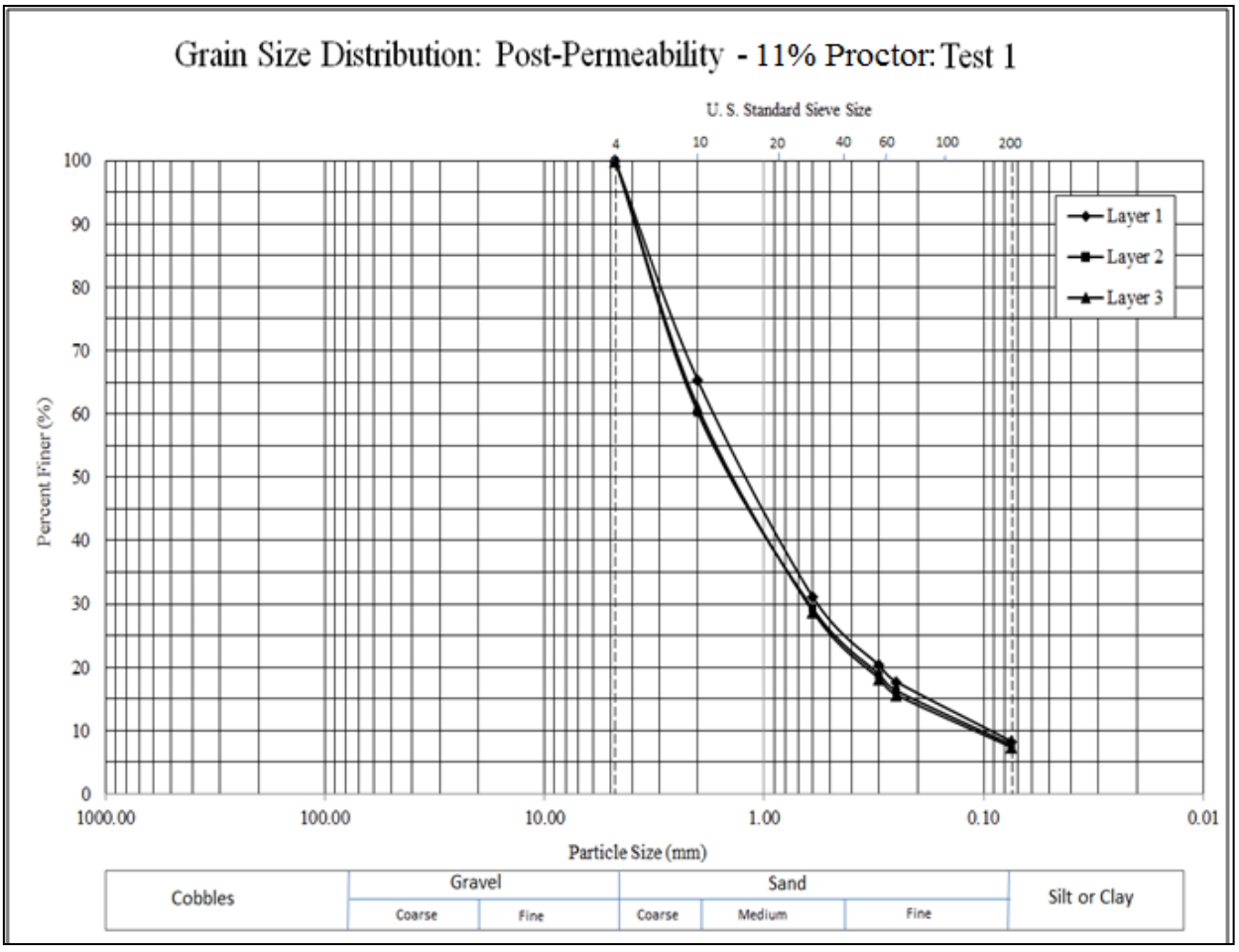

Figure 11.3 Grain size distribution of layer1, layer2, and layer3 of the hydraulic conductivity test specimen.

11.3.2 Post-Permeability Grain Size Distribution: 11% Proctor - Test 2

The results of this sieve analysis yielded a coefficient of variation of 0.065 for the uniformity coefficient and a coefficient of variation of 0.058 for the coefficient of gradation. This low coefficient of variation implies that the samples had very little variation in their gradations. The data for the sieve analysis is shown in Table 11.10, Table 11.11, Table 11.12, and Figure 11.4.

Table 11.10 Critical index values for the hydraulic conductivity grain size distribution testing.

Critical Indices	Layer 1	Layer 2	Layer 3
D_{90}	3.800	3.800	3.900
D_{60}	1.800	1.700	1.900
D_{50}	1.400	1.400	1.450
D_{30}	0.600	0.590	0.600
D_{25}	0.470	0.450	0.480
D_{15}	0.190	0.190	0.200
D_{10}	0.094	0.100	0.100
Uniformity Coefficient, C_u	**19.15**	**17.00**	**19.00**
Coefficient of Gradation, C_c	**2.13**	**2.05**	**1.89**

Table 11.11 Uniformity coefficient statistics

Uniformity Coefficient, C_u	
Average Uniformity Coefficient	18.383
Sample Standard Deviation (s)	1.200
Coefficient of Variation (COV)	0.065

Table 11.12 Coefficient of gradation statistics

Coefficient of Gradation, C_c	
Average Coefficient of Gradation	2.023
Sample Standard Deviation (s)	0.118
Coefficient of Variation (COV)	0.058

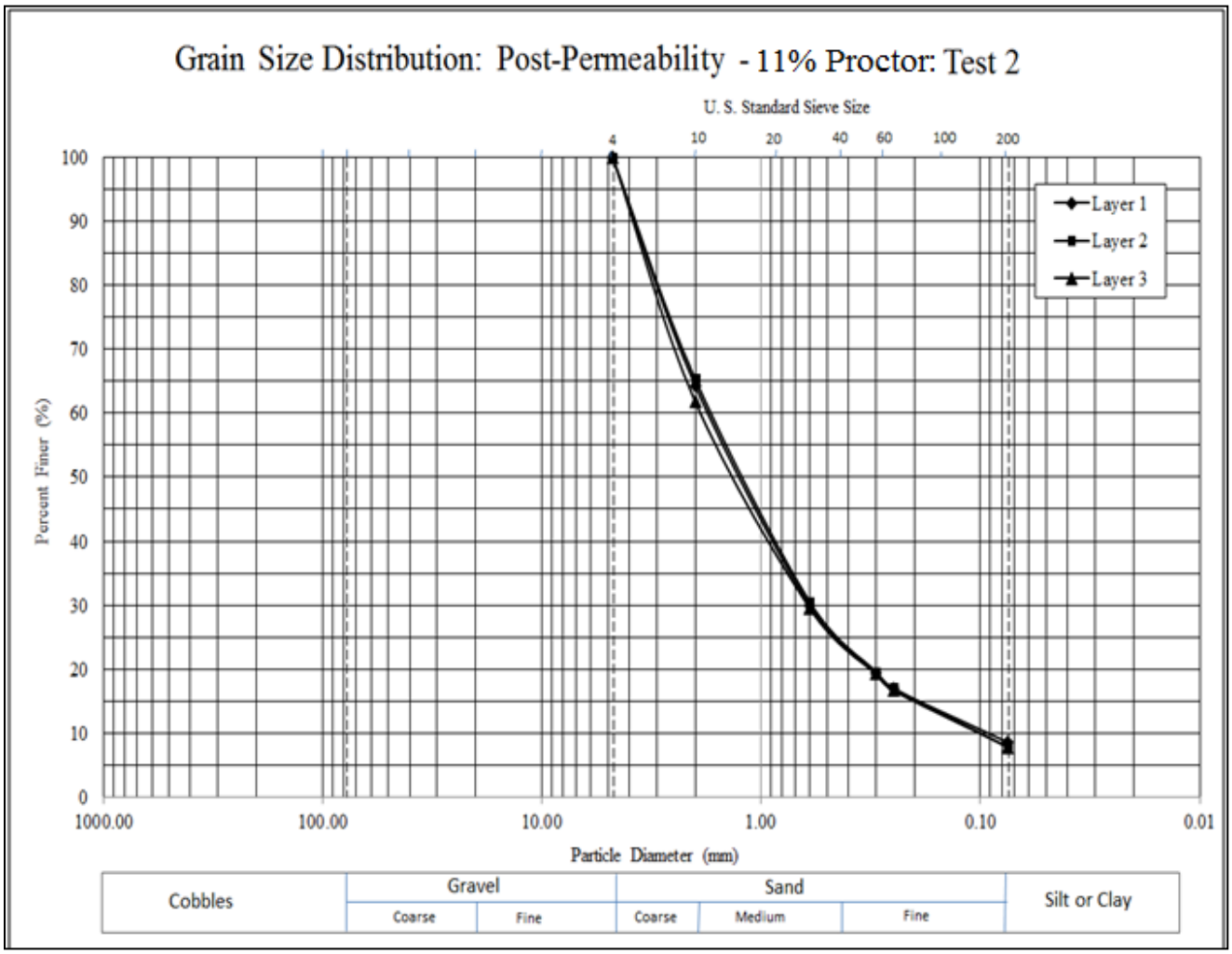

Figure 11.4 Grain size distribution of layer1, layer2, and layer3 of the hydraulic conductivity test specimen.

11.3.3 Post-Permeability Grain Size Distribution: 11% Proctor - Test 3

The results of this sieve analysis yielded a coefficient of variation of 0.121 for the uniformity coefficient and a coefficient of variation of 0.017 for the coefficient of gradation. This low coefficient of variation implies that the samples had very little variation in their gradations. The data for the sieve analysis is shown in Table 11.13, Table 11.14, Table 11.15, and Figure 11.5.

Table 11.13 Critical index values for the hydraulic conductivity grain size distribution testing.

Critical Indices	Layer 1	Layer 2	Layer 3
D_{90}	3.900	4.000	4.000
D_{60}	1.900	2.200	2.400
D_{50}	1.450	1.700	1.900
D_{30}	0.650	0.680	0.800
D_{25}	0.520	0.520	0.620
D_{15}	0.240	0.220	0.280
D_{10}	0.120	0.110	0.140
Uniformity Coefficient, C_u	**15.83**	**20.00**	**17.14**
Coefficient of Gradation, C_c	**1.85**	**1.91**	**1.90**

Table 11.14 Uniformity coefficient statistics

Uniformity Coefficient, C_u	
Average Uniformity Coefficient	17.659
Sample Standard Deviation (s)	2.131
Coefficient of Variation (COV)	0.121

Table 11.15 Coefficient of gradation statistics

Coefficient of Gradation, C_c	
Average Coefficient of Gradation	1.89
Sample Standard Deviation (s)	0.032
Coefficient of Variation (COV)	0.017

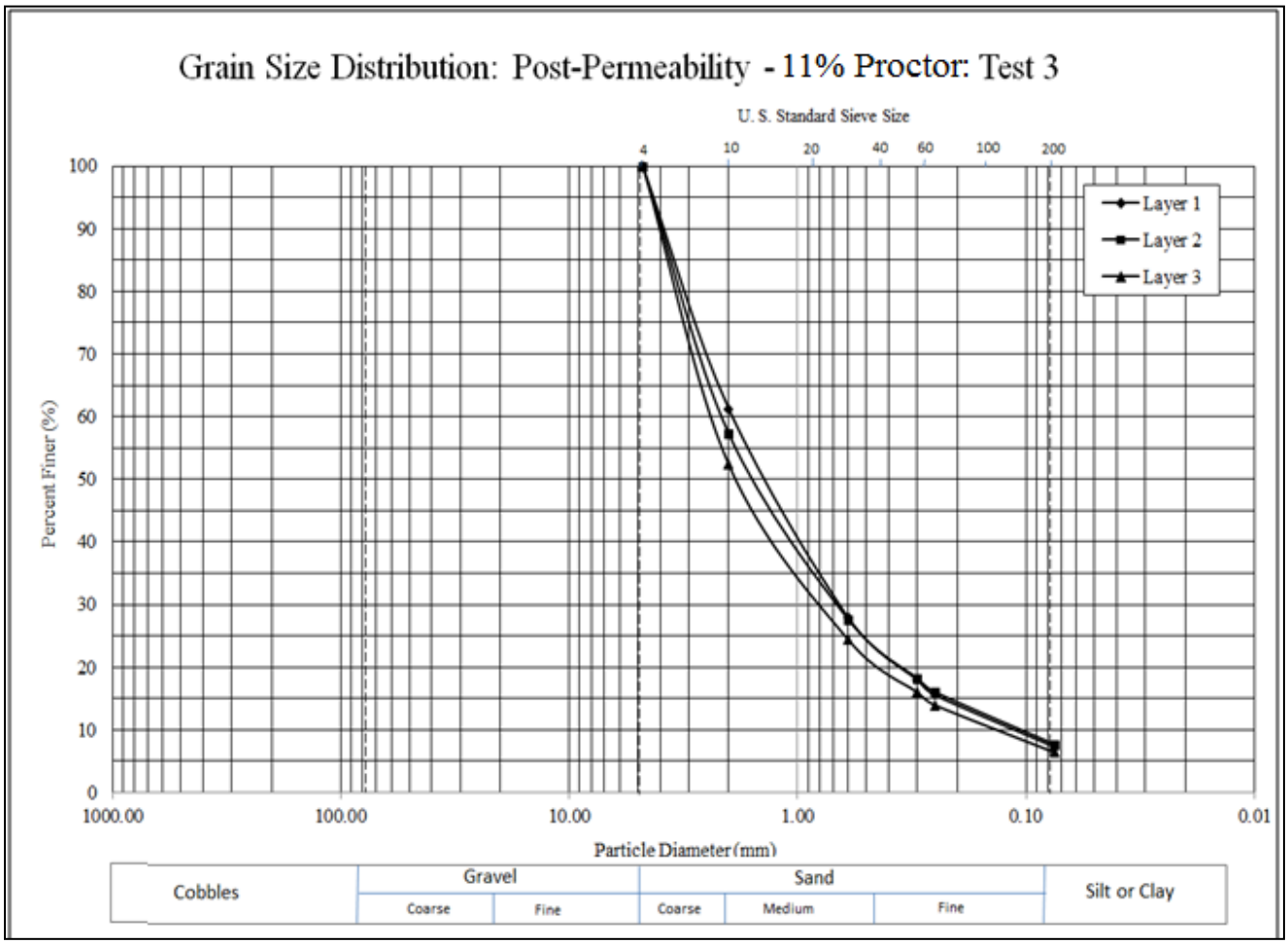

Figure 11.5 Grain size distribution of layer1, layer2, and layer3 of the hydraulic conductivity test specimen.

12. Grading Envelopes and Particle Transport

12.1. Introduction

The term "grading envelope" refers to the range, or variation, of particle size with respect to the percent finer of the material being observed. Grading envelopes can be a result of a phenomenon called suffusion. Suffosion is defined as the transportation of soil particles over significant distances through constrictions within a soil matrix. If the constrictions are larger than the particle, then the particle has the potential to be transported, and sometimes exit the soil body it is encased within. It is understood that particle transport can clog a filter if a soil is regarded as unstable. Unstable soils are those which have significant particle movement, where the soil acting as a filter will become more porous due to a loss of fine particles. An increase in porosity and a potential increase in pore pressure at the toe of a slope due to an accumulation of fine particles, or clogging of the filter, can compromise the stability of a slope structure. This section compiles data accrued in the laboratory testing performed for this project. The purpose of the data is to illustrate the movement of soil particles under several imposed conditions, or lack thereof, to determine whether or not suffusion has the potential to be a significant concern in the stability modeling of the unweathered sandstone overburden under inspection. The data on the nine graphs below show the results of grain size distribution testing performed on layering of compacted specimens at three predetermined compaction energies. The energy levels are referred to as standard proctor at a compaction energy of 592.5 kJ/m^3, a 65.64% reduced from standard proctor effort or 34.36% of standard proctor or 203.6 kJ/m^3), and an even further reduced energy at 88.55% reduced equal to 67.85 kJ/m^3 or 11.45% of standard proctor energy. Three tests are shown per graph. The three tests are as received GSD, pre-permeability GSD, and post-permeability GSD. Layer 1, 2, and 3 are approximately one-third the length of the compacted specimen, and are top one-third, middle one-third, and bottom one-third, respectively.

12.2. Standard Proctor GSD Results

The figures below show graphs of superimposed grain size distributions. The grain size distributions illustrate the process of as received to a compaction to condition to a permeated condition. The item "Δ" in the figures means simply "the change in" for each maximum aggregation compared to the as received grain size distribution for the critical index shown. This value is expressed as a percent difference. Smaller values of "Δ" are lesser aggregation conditions, and larger values refer to larger changes in aggregation. The two graphs shown below illustrate some interesting phenomena. Let us consider the first illustration showing the grain size distribution of three layers of a compacted sample prepared as a standard proctor specimen alongside the original grain size distribution of the material. The material had 9.04% water content added to it. The material aggregated some, and was not particularly isotropic. The second illustration had 8.43% water content after distilled water was added to the sample, and it was compacted. The post-permeability grain size distribution became more aggregated after being permeated by 18.46 pore volumes. The material aggregation seems to be a function of the compaction energy and the water content. The compaction energy applied in the first illustration likely broke up the aggregation of the material, where the aggregation could reconvene in the hydraulic conductivity cell in the second illustration. The grain size distribution curves are illustrated in Figure 12.1.

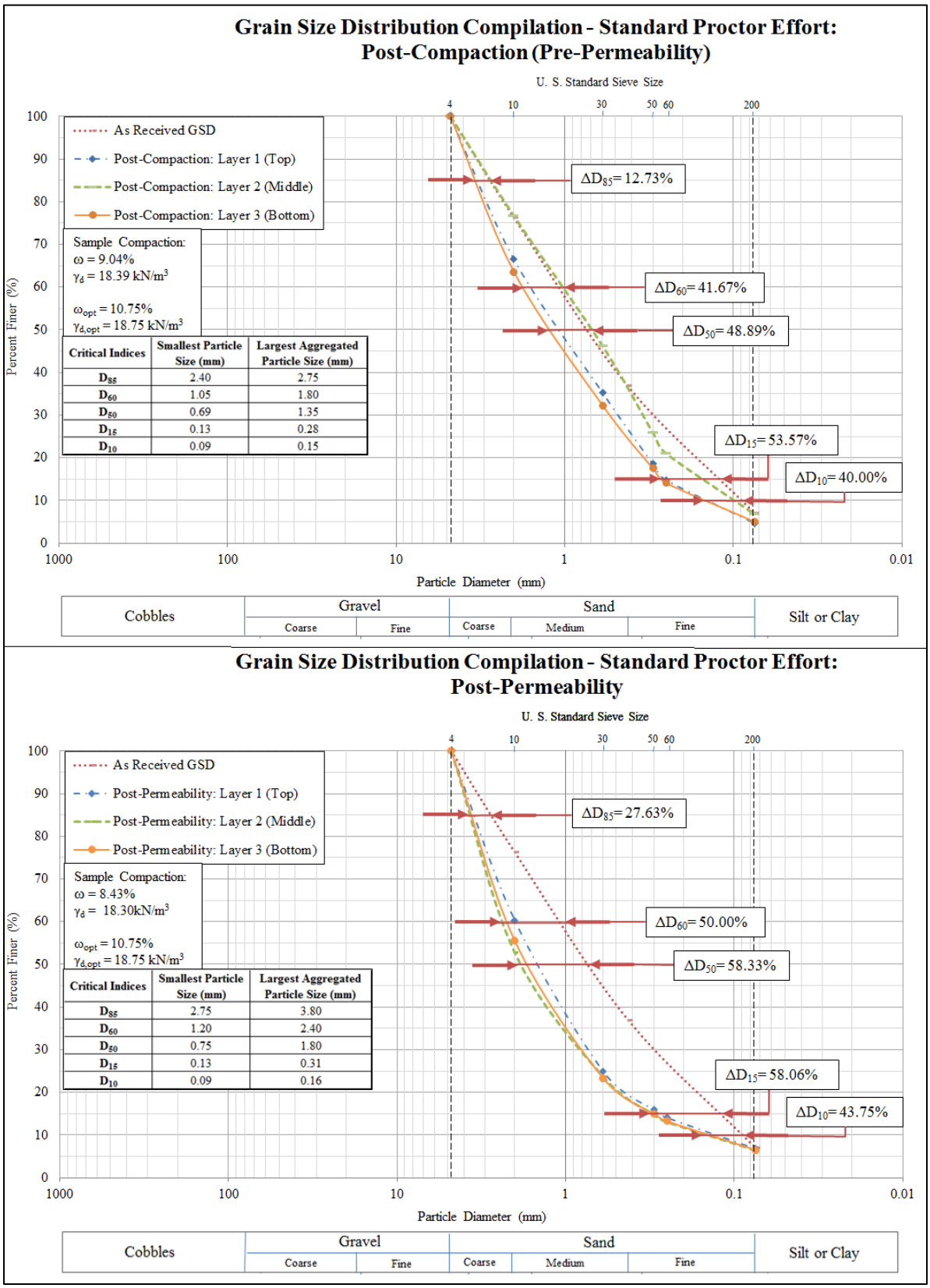

Critical Indices	Smallest Particle Size (mm)	Largest Aggregated Particle Size (mm)
D_{85}	2.40	2.75
D_{60}	1.05	1.80
D_{50}	0.69	1.35
D_{15}	0.13	0.28
D_{10}	0.09	0.15

Critical Indices	Smallest Particle Size (mm)	Largest Aggregated Particle Size (mm)
D_{85}	2.75	3.80
D_{60}	1.20	2.40
D_{50}	0.75	1.80
D_{15}	0.13	0.31
D_{10}	0.09	0.16

Figure 12.1. Standard Proctor grain size distribution compilation

12.3. Proctor Energy at 34% GSD Results

The two illustrations below depict the variations in gradation for two samples of a well graded sand with silt material compared to the original gradation of the material. The first graph is at a pre-permeability or pre-permeability state, and the second is at a post-permeability state. Both samples had a target dry density at optimum of a set 34% Proctor compaction effort of 203.6 kJ/m^3. The pre-permeability sample had a water content of 13.16%. The post-permeability sample had a pre-permeated water content of 14%. The permeated sample had 2.22 pore volumes run through it. The behavior of the material under these conditions seems to indicate that the compaction and added water increased the aggregation of the material. The permeation increased the aggregation more than the compaction alone. Similar behavior occurred in the standard proctor samples. The grain size distribution curves are illustrated in Figure 12.2.

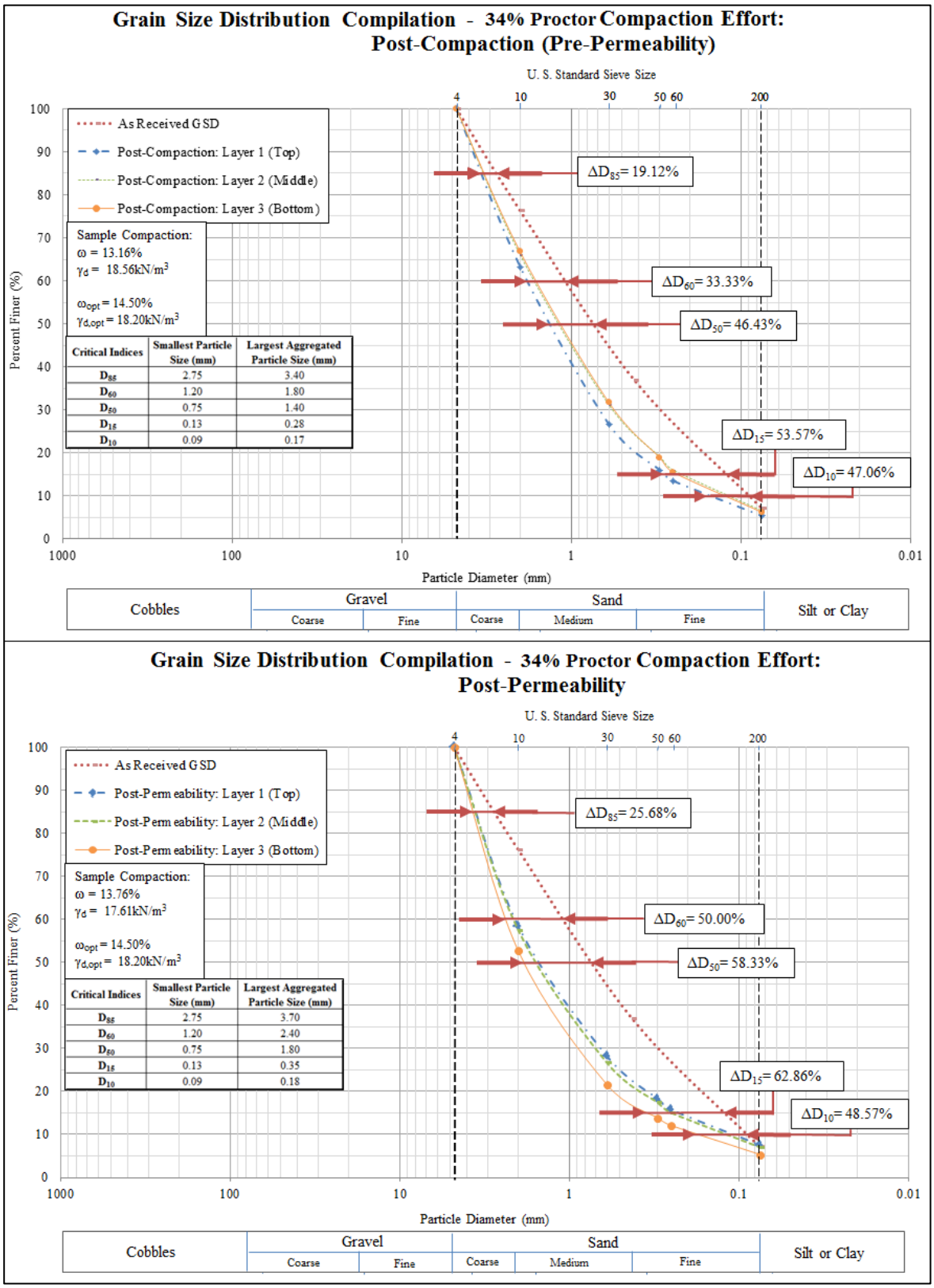

Critical Indices	Smallest Particle Size (mm)	Largest Aggregated Particle Size (mm)
D_{85}	2.75	3.40
D_{60}	1.20	1.80
D_{50}	0.75	1.40
D_{15}	0.13	0.28
D_{10}	0.09	0.17

Critical Indices	Smallest Particle Size (mm)	Largest Aggregated Particle Size (mm)
D_{85}	2.75	3.70
D_{60}	1.20	2.40
D_{50}	0.75	1.80
D_{15}	0.13	0.35
D_{10}	0.09	0.18

Figure 12.2. 34% Proctor compaction energy grain size distribution compilation

12.4. Proctor Energy at 11% GSD Results

The two illustrations below depict the variations in gradation for two samples of a well graded sand with silt material compared to the original gradation of the material. The first graph is at a pre-permeability or pre-permeability state, and the second is at a post-permeability state. Both samples had a target dry density at minimum of a set 11% Proctor compaction effort of 67.85kJ/m^3. The pre-permeability sample had a water content of 10.02%. The post-permeability sample had a pre-permeated water content of 8.26%. The permeated sample had 9.04 pore volumes run through it. The behavior of the material under these conditions seems to indicate that the compaction and added water increased the aggregation of the material. The permeation decreased the aggregation from the compacted state aggregation. The grain size distribution curves are illustrated in Figure 12.3

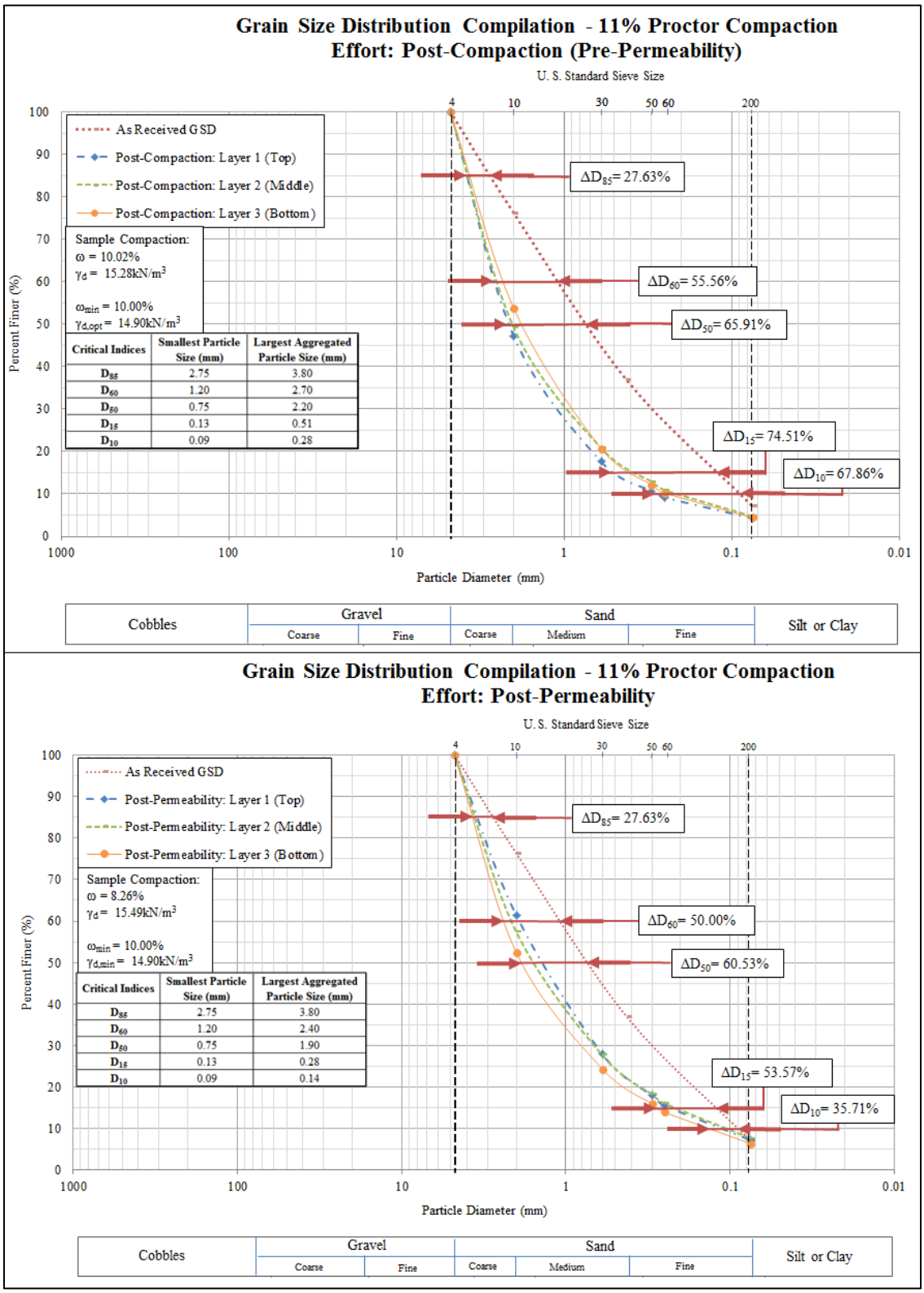

Critical Indices	Smallest Particle Size (mm)	Largest Aggregated Particle Size (mm)
D_{85}	2.75	3.80
D_{60}	1.20	2.70
D_{50}	0.75	2.20
D_{15}	0.13	0.51
D_{10}	0.09	0.28

Critical Indices	Smallest Particle Size (mm)	Largest Aggregated Particle Size (mm)
D_{85}	2.75	3.80
D_{60}	1.20	2.40
D_{50}	0.75	1.90
D_{15}	0.13	0.28
D_{10}	0.09	0.14

Figure 12.3. 11% Proctor compaction energy grain size distribution compilation

12.5. Discussion

Comparatively, taking into consideration all three compaction energies and the results shown above of the test scenarios performed it was found that particle movement varied significantly. The variation in gradation was a function of the moisture content added and the energy applied for preparation. The post-permeability results should be interpreted carefully as each specimen of different density varied in pore volume flux. The standard proctor specimens aggregated the most between D_{50} and D_{15} due to compaction, then aggregated more at a post-permeability condition. The 34% Proctor compaction specimens showed similar results as standard proctor, aggregating more at a post-permeability condition. The 11% Proctor compaction specimen results were opposite 34% Proctor compaction results and standard proctor compaction results. The 11% Proctor compaction specimen aggregated most at a pre-permeability condition, then became less aggregated at a post-permeability condition. The results indicate that the material reaches an aggregated equilibrium with very similar gradation after some pore volumes of water permeate through it. The results also imply that introducing a range of compaction energy can alter soil properties and have performance implications on earthen structures. Layered construction known as "lift construction" could assist in better quality control of the compaction energy applies to earthen structures to more precisely manage the aggregation phenomena. The amount of compaction energy for the 34% Proctor compaction and standard proctor samples seems to have broken up the aggregated particles, then when they were permeated, became more aggregated. After the permeation occurred, all three compaction energies approached a similar gradation, but diverged somewhat as the particle size decreased. The specimens began diverging in similarity around 40% finer. At D_{10} at a post-permeability condition, the 11% Proctor compaction energy compacted and permeated sample had the smallest particles, standard proctor had the next highest, and 34% Proctor energy specimens had the largest particle size. Overall the 11% proctor pre-permeability condition had the most aggregated particles, likely due to little compaction energy applied to break apart aggregated particles. At D_{10} at a pre-permeability condition, the standard proctor sample had the smallest particles, then 34% proctor, and 11% Proctor energy samples had the largest aggregated particles. The item "Δ" in the figures means simply "the change in" for each maximum aggregation compared to the as received grain size distribution for the critical index shown. This value is expressed as a percent difference. Smaller values of "Δ" are lesser aggregation conditions, and larger values refer to larger changes in aggregation. Table 12.1 shows a summary of the delta values for Figure 12.1, Figure 12.2, and Figure 12.3.

Table 12.1 Change in critical index summary table

Change in Critical Indices [%]	**ΔD_{85} (%)**	**ΔD_{60} (%)**	**ΔD_{50} (%)**	**ΔD_{15} (%)**	**ΔD_{10} (%)**
Standard Proctor Pre-Permeability	12.73	41.67	48.89	53.57	40.00
Standard Proctor Post-Permeability	27.63	50.00	58.33	58.06	43.75
34% Proctor Pre-Permeability	19.12	33.33	46.43	53.57	47.06
34% Proctor Post-Permeability	25.68	50.00	58.33	62.86	48.57
11% Proctor Pre-Permeability	27.63	55.56	65.91	74.51	67.86
11% Proctor Post-Permeability	27.63	50.00	60.53	53.57	35.71

13. Numerical Modeling

13.1 Introduction

In order to establish adequate results for slope stability modeling, it is important to consider utilizing computer software. Computer software can be used to perform multiple analysis operations and can permit parametric studies of soil property sensitivity. For this project, the modeling software used for the earthwork designs were GeoStudio™ and GeoFluv®. GeoStudio™ is an analysis tool for several earthwork functions. SLOPE/W, SIGMA/W and SEEP/W are the three modules of GeosStudio™ that were used for the modeling. The models that utilized SIGMA/W, SEEP/W, and SLOPE/W will be referred to as "cumulative analyses." SLOPE/W was the only module utilized on some models as a basic approach for comparison. This discussion will focus on targeted slope stability analysis of the earthwork designs that were produced by the GeoFluv® software as well as an AOC valley fill design.

GeoStudio™

GeoStudio is a finite element method analysis software that has the capacity to analyze slopes, earthen dams, and other earthwork structures. The results can be determined via probabilistic, sensitivity, seismic, or deterministic procedures for data input parameters. GeoStudio™ has several modules, all of which allow the user to view results via graphical representation which can be interpreted to look beyond the factor of safety. In SLOPE/W, the critical slice can be viewed to allow the user to determine methods of solution to the risk, or decide whether or not the risk is significant. Failure entry and exit points can be defined, as well as piezometric surfaces. There are many options available to the user, all of which can be explored to create more realistic scenarios for earth structure evaluation.

General Limit Equilibrium Theory and Method

The General Limit Equilibrium method commonly referred to as the "GLE method" uses statics equations to solve for a factor of safety. The GLE method of slope stability analysis was used for the modeling performed in this research. The following concepts for the equations were used as defined by GeoStudio SLOPE/W Engineering Methodology Book:

- The summation of forces in a vertical direction for each slice is used to compute the normal force at the base of the slice, N.
- The summation of forces in a horizontal direction for each slice is used to compute the interslice normal force, E. This equation is applied in an integration manner across the sliding mass (i.e., from left to right).
- The summation of moments about a common point for all slices. The equation can be rearranged and solved for the moment equilibrium factor of safety, F_m (eqn. 1).
- The summation of forces in a horizontal direction for all slices, giving rise to a force equilibrium factor of safety, F_f (eqn. 2).

$$F_m = \frac{\sum(c'\beta R + (N - u\beta)Rtan(\varphi'))}{\sum Wx - \sum Nf \pm \sum Dd} \quad (1)$$

$$F_f = \frac{\sum(c'\beta cos\alpha + (N - u\beta)tan\varphi' cos\alpha)}{\sum Nsin\alpha - \sum Dcos\omega} \quad (2)$$

where:

c' = effective cohesion

φ' = effective angle of friction

u = pore-water pressure

N = slice base normal force

W = slice weight

D = concentrated point load

β, R, x, f, d, ω = geometric parameters

α = inclination of slice base

In equation form, the base normal is defined as:

$$N = \frac{W + (X_R - X_L) - \frac{(c'\beta sin\alpha + u\beta sin\alpha tan\varphi')}{F}}{cos\alpha + \frac{sin\alpha tan\varphi'}{F}} \qquad (3)$$

One of the most beneficial aspects of the GLE method is the option to vary a variety of interslice force conditions. The equations used for the GLE method gives the user the opportunity to use several methods of analysis. The limit equilibrium method of slices is based on the principles of statics. As a result, there are limitations to the general limit equilibrium method.. The missing physics of the limit equilibrium formulation is that there is a lack of a stress-strain constitutive relationship to ensure displacement compatibility.

SIGMA/W was used along with SEEP/W to yield more precise pore pressure and head conditions, with the intent of reducing the implications of the method's limitations, and producing accurate *insitu* stresses within the structures analyzed.

For the cumulative analysis, finite element models were produced with a global element size of 10m. The factor of safety or "stability factor" (S.F.) produced by a finite element stress method is defined as a ratio of the summation of the resisting shear force S_r along a failure plane to the summation of the mobilized shear force S_m along a failure plane in the equation form:

$$S.F. = \frac{\sum S_r}{\sum S_m} \qquad (4)$$

$$S_r = s\beta = (c' + (\sigma_n - u_a)tan\varphi' + (u_a - u_w)tan\varphi^b)\beta \qquad (5)$$

$$S_m = \tau_m\beta \qquad (6)$$

where:

s = effective shear strength of the soil at the base center of a slice

β = base length of a slice

σ_n = normal stress at the base center of a slice

τ_m = mobilized shear stress

u_a = pore-air pressure

u_w = pore-water pressure

and,

$$Local\ S.F. = \frac{S_r}{S_m} = \frac{s\beta}{\tau\beta} \quad (7)$$

Material Strength

Geotechnical materials can be decribed in a legion of ways. One of the most common techniques to describe the strength of a geotechnical material is the Mohr-Coulomb model. The equation for this method is the following:

$$\tau = c + \sigma_n tan\varphi \quad (8)$$

$$\sigma_n = \frac{N}{\beta} \quad (9)$$

where:

τ = shear strength (i.e., shear at failure)

c = cohesion

σ_n = normal stress on shear plane

φ = angle of internal friction (phi)

β = the base length of each slice

N = the total normal force on the base of the slice

For all modeling, the input values were determined via geotechnical laboratory testing. Cohesion was taken to be zero as the gradation of the fill material under consideration was found to be sand with small volumes of fines. Details involving the internal friction angles produced for the range of stresses imposed and compaction energies performed for the specimen preparation can be found in Chapter 8.

Approach

The approach taken for the modeling was analyze slopes in order to understand and assess the risk involved in the construction of a valley fill slope as well as several of the more critical cases generated GeoFluv® slopes. First, the models were calibrated to verify the stability analysis in the AOC design for the valley fill. The AOC valley fill design was then analyzed using deterministic and sensitivity methods. The methods were applied to four failure modes: face, toe, deep, and crest.

The entry and exit points of each case were input as a range of the surface area for a more realistic assessment. For each of the four failure modes, two piezometric conditions were addressed. The first piezometric condition considered that the slope drained to the durable rock underdrain. The second piezometric condition considered an elevated water table at a 50ft vertical displacement from the upper elevation along the underdrain. The second case considers that the rate of infiltration is greater than the rate of seepage. This condition could take place for

several reasons, but we will consider that the rock underdrain could be clogged by small diameter particles.

A cumulative analysis was performed on the GeoFluv® valley fill alternative slope and the valley fill slope. The analysis included infiltration results over a 10 year period modeled in SEEP/W, insitu stress calculations performed in SIGMA/W, and deterministic and sensitivity slope stability analysis performed in SLOPE/W. The hydrologic infiltration information was modeled by considering practical hydraulic conductivity values for waste rock tailings. Piezometric lines locations were determined by utilizing the inspection of two conditions; condition 1 (or piez. 1) included a piezometric line at the top of the durable rock underdrain. Condition 2 (or piez. 2) included a piezometric line raised 50ft or 15.24m above the underdrain to encapsulate a range of elevation for the water table and produce more accurate results. No piezometric line was needed for the cumulative analysis. SEEP/W produced areas of increased pore pressures and hydraulic head, and the analysis used those results in lieu of a piezometric line. All models used the results produced at the end of a 10 year infiltration period.

Geometric Input

The valley fill under inspection is the mass body by which the GeoFluv® designs were built upon. The geometry of the slope was taken from the AOC contour information as well as the profile elevations and distances shown in Figures 13.1 and 13.2. The fill is referred to as "Fill #2." The figure below shows the profile that was emulated for the SLOPE/W designs.

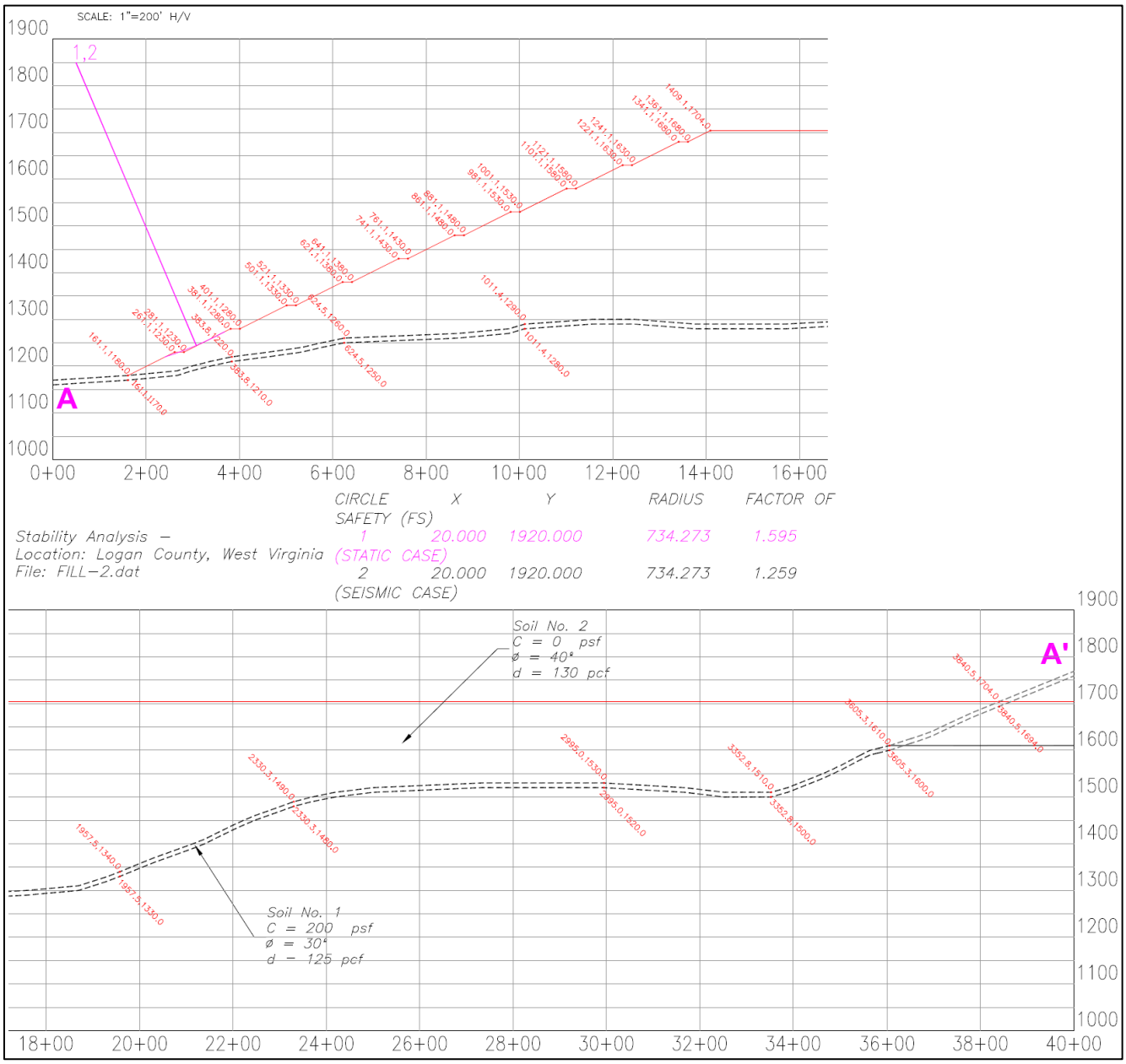

Figure 13.1. Slope profile used for valley fill modeling

Figure 13.2 shows the plan view with contour information for the proposed AOC valley fill design illustrated in Figure 13.1 (WVDEP, 2007).

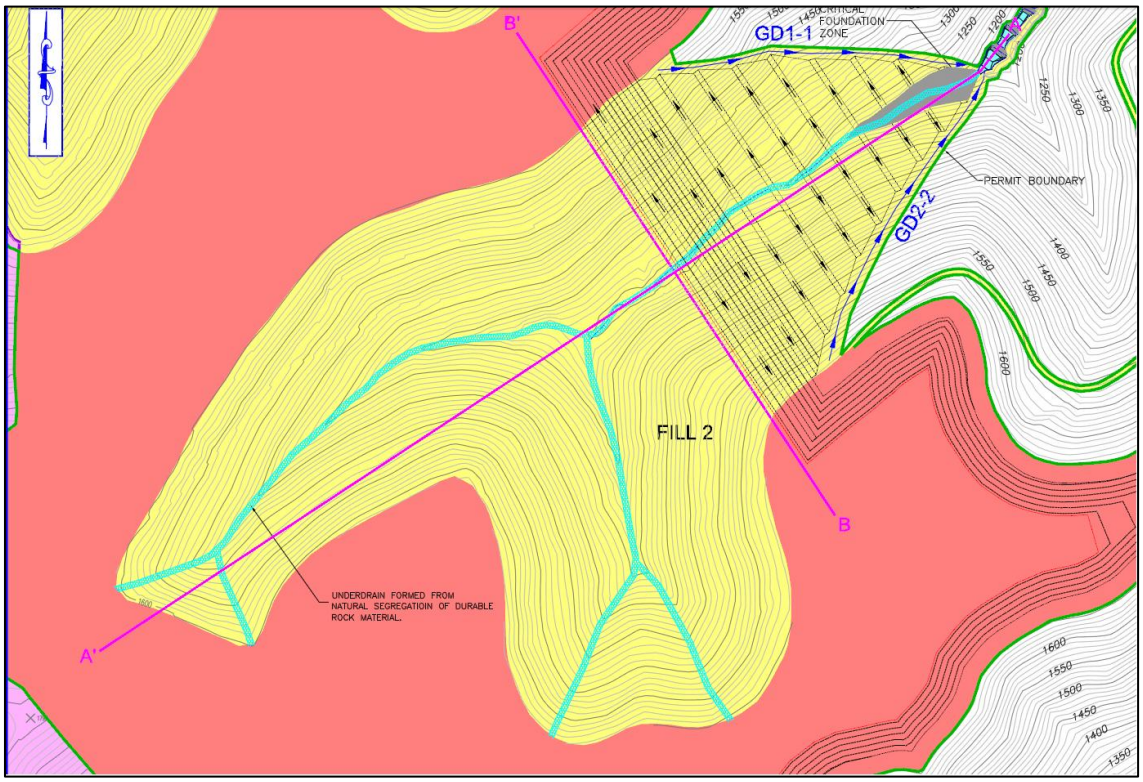

Figure 13.2. Valley fill plan view

The dimensions shown in Figure 13.1 and Figure 13.2 are in U.S. customary units. These files were taken from WVDEP permit File#S500809. The models that were created used metric dimensions and metric laboratory soil property values for consistency within the scope of this research. Two types of soil are presented in Figure 13.1. The blasted overburden fill referred to as unweathered sandstone (Soil No. 2) is used in the design for the slope construction, with a 10ft thick durable rock underdrain constructed by gravity segregation of the end dumped unweathered sandstone material. The factors of safety shown in Figure 13.1 were developed using Bishop's Simplified Method, without taking into account any piezometric surface within the fill. This is a result of the assumption that the slope is entirely free draining. The assessment in Figure 13.1 identifies the friction angle (φ) as 40^{o}, the unit weight (γ_d) as 130 psf, and the cohesion (c) as 0 psf.

This blasted material is considered as unweathered sandstone and is modeled to act as sand within the fill with an associated cohesive input value of 0 psf. Soil No. 1 refers to a cohesive, weathered undisturbed material. This material contours the original valley bottom and creates a more impermeable layer to line the lower elevation of the underdrain. A labeled illustration of the GeoStudio™ modeled slope is shown in Figure 13.3.

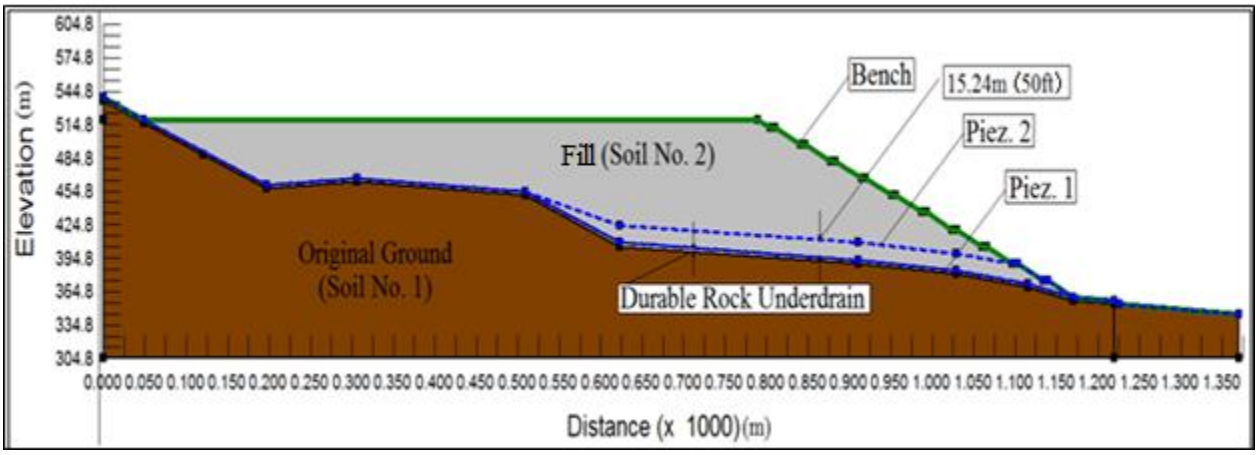

Figure 13.3. Actual modeled slope profile

SEEP/W Analysis: Valley Fill

Seepage was first modeled through a valley fill using "Approximate Original Contour" (AOC) design. The geometry of this fill was modeled under two cases. Case 1 used a drain that was modeled under a "saturated only" condition, and case 2 used a drain that was modeling under a "saturated/unsaturated" condition.

Geometry

The geometry for the profile view of the valley fill was taken from the fill cross-section details in the AOC valley fill design slope stability analysis. The information provided in Figure 13.1 was used for the coordinates of the AOC fill. Coordinates were given in U.S. customary units. These were converted to metric because distance in the model was measured in meters. The fill was modeled from an elevation of 304.8 m to 519.4 m with a length of 1370 m. The face of the fill was modeled at an elevation of 359.7 m to 519.4 m and from a horizontal location of 789.7 m to 1170.1 m. The curved line throughout the fill was a 10 foot core drain. The discharge pond of the fill was set at an elevation of 359.7 m. An approximate global mesh size of 10 m was used to create 386 nodes and 352 elements. Because SEEP/W creates models in two dimensions, one profile slice was extracted from the entire fill to be modeled. SEEP/W then uses a profile thickness of 1 m to model the fill. The profile modeled followed the centerline of the fill as to include the core drain. A plan view of the fill is shown in Figure 13.2 with section A-A denoted as the profile that was used for the modeling.

Materials

The valley fill model consisted of three materials. These materials can be seen in Figure 13.4.

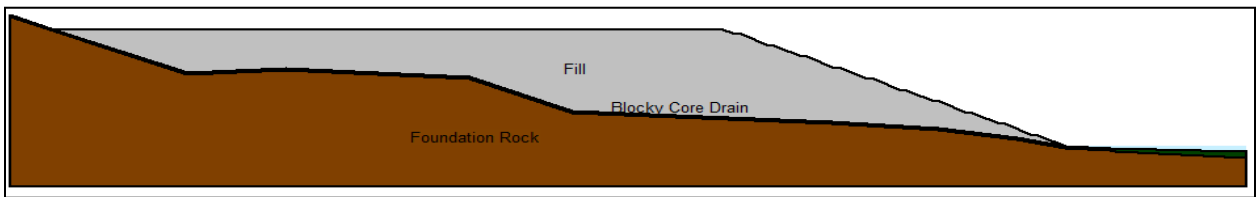

Figure 13.4. AOC fill materials

The first material, named "Fill", was the top layer of the valley fill comprised of waste rock tailings from mining. It was modeled under a saturated/unsaturated condition, which required a function for hydraulic conductivity and an additional function for the material's water content. Hydraulic conductivity (m/s) was plotted versus pore water pressure (kPa) by inputting a saturated hydraulic conductivity and using the Van Genuchten estimation method within Seep/W. A maximum suction was set at 0.01 kPa and a minimum set at 1000 kPa with 20 data points to produce a function. Hydraulic conductivity was chosen from a range values found from previous work done with waste rock tailings. These ranged from an unsaturated hydraulic conductivity of 1x10^-5 m/s (Abdelghani 2009) to a saturated hydraulic conductivity of 1x10^-7 m/s (Aubertin et al 1996). These previously published values were chosen instead of the values determined from laboratory testing because they represented more realistic values. Laboratory testing calculates hydraulic conductivity based on optimum water content and compaction values, which are difficult to obtain in the field. Previously published values for hydraulic conductivity of waste rock tailings provided a more practical value to be used in numerical modeling. The function is shown in Figure 13.5.

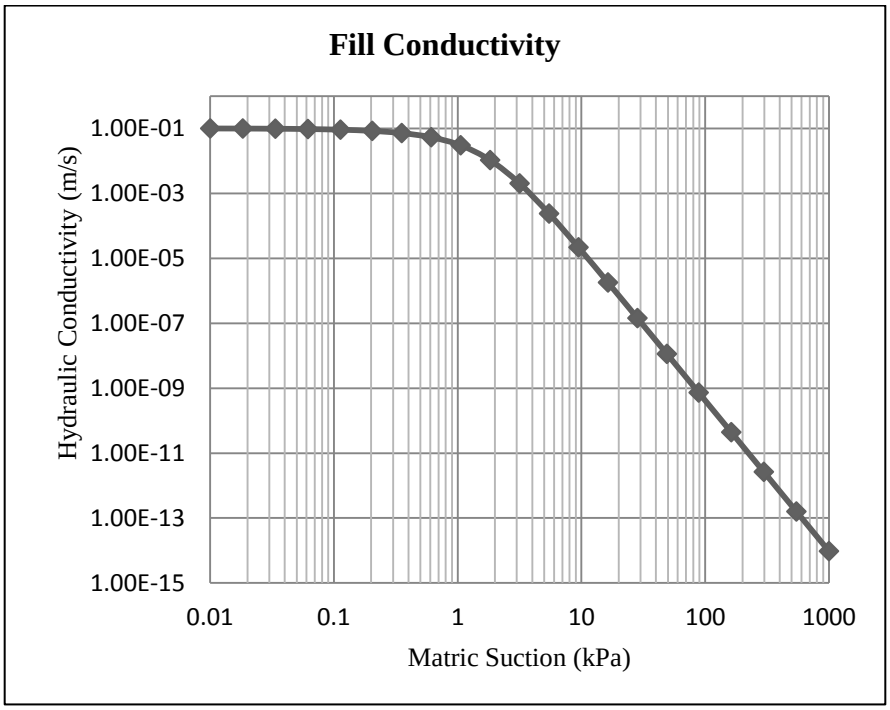

Figure 13.5. Fill conductivity function – AOC fill

This function was also compared to the function produced by Fredlund et. Al (1998) and found to be quite similar. The water content function was produced in a similar method. A saturated volumetric water content was input and the same parameters as the conductivity function were used to create a function. Gravel was chosen as the material type for this function. Saturated volumetric water content was taken to be 44%, the value used by Fredlund et al (1998). This function is shown in Figure 13.6.

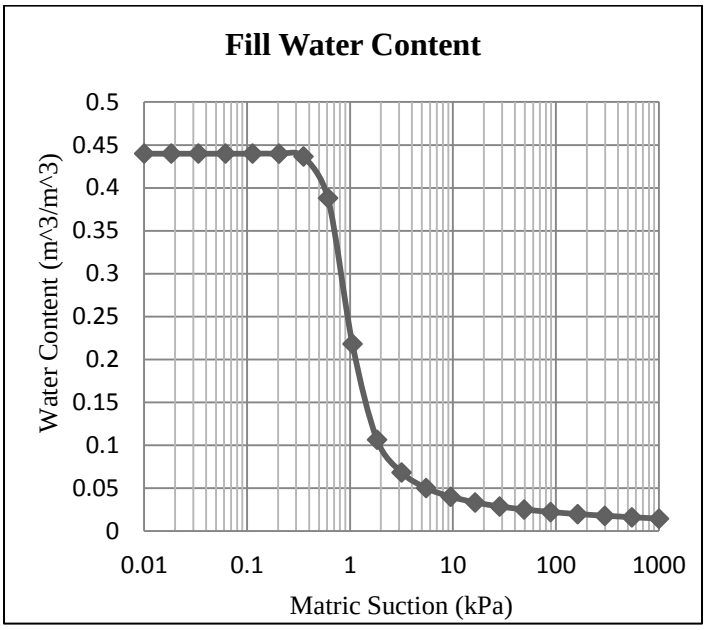

Figure 13.6. Fill water content function – AOC fill

The bottom layer of the valley fill, the "Foundation Rock" layer, was modeled in a saturated only condition with a very low hydraulic conductivity (2x10^12 m/s) to simulate an impermeable rock layer. Between the "Fill" layer and "Foundation Rock" layer, a 10-ft "Blocky Core Drain" material was placed. This layer was modeled under a saturated only condition with a constant hydraulic conductivity value of 0.1 m/s. This hydraulic conductivity was taken from the Das (2010) average value for gravel.

Boundary Conditions

Once materials were defined, boundary conditions were determined to fully define the model. A figure of the boundary conditions and their applied locations is shown in Figure 13.7.

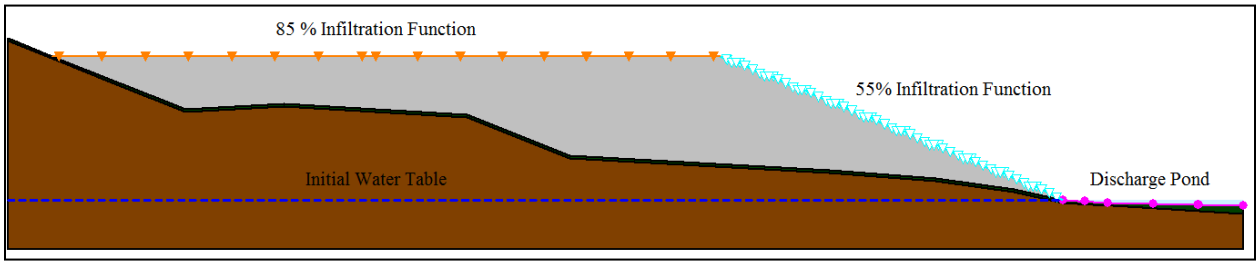

Figure 13.7. AOC fill boundary conditions

A step data point function for infiltration (unit flux vs. time) used the data points from the developed 10 year NOAA spreadsheet. The function developed from the 85% infiltration designation was applied to the top of the fill, and the function developed from the 55% infiltration designation was applied to the downstream sloped face of the fill. The 55% infiltration function boundary condition placed on the fill's downstream face was also analyzed as a potential seepage face. A constant head function was applied at the toe of the fill to model the discharge pond. The head value was input as the elevation of the discharge pond. Transient

modeling with SEEP/W also requires inputting an initial water table. Water table was placed at a constant level through the foundation rock at the elevation of the discharge pond.

SEEP/W Analysis: Geomorphic Fill

In addition to the fill geometry from the permit file, a fill using geomorphic design principles was analyzed. This fill used an altered geometry but the same boundary conditions as the AOC fill. The profile was taken from the design contours produced by GeoFluv® and is shown in Figure 13.10.

Geometry and Materials

The same geometry for the "Foundation Rock" and "Blocky Core Drain" were used. Only the surface geometry of the "Fill" material was altered. The profile slope was taken from a geomorphic design using the Carlson Natural Regrade software. A plan view of the fill with the location of profile slice (black line) is shown in Figure 13.10. As in the AOC fill, the 2-D model uses a profile thickness of 1 m. The same material properties were given to the three regions as in the AOC model. The two cases of modeling the drain in a saturated only condition and in an unsaturated/saturated condition were both modeled.

Boundary Conditions

The same boundary conditions were used to define this model as were used in the AOC model. For this case, however, the entire fill surface used the 55% infiltration boundary condition because it is sloped for its entire length. The sloped fill surface was also analyzed as a potential seepage face. Due to the altered surface profile, the initial water table and discharge pond were modeled at a height of 353.57 m, slightly lower than in the AOC fill. A figure showing the geomorphic profile with applied boundary conditions is illustrated in Figure 13.8 below.

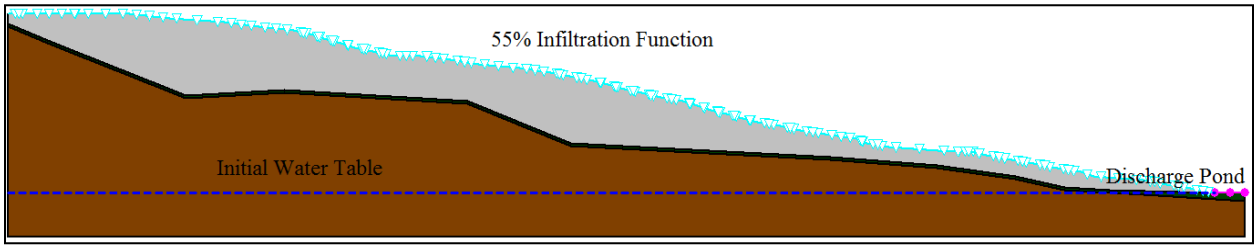

Figure 13.8. Geomorphic fill boundary conditions

Sensitivity Analysis

Sensitivity analysis is similar in comparison to probabilistic analysis. The difference is that instead of selecting variable parameters by a Monte Carlo simulation, the parameters are set with a mean value, a delta value, and a number of steps to set the range of sampling for each parameter. The delta value is input as equal steps from the mean input value for each property considered. Five steps of "delta" were used for each parameter in the sensitivity analysis. This analysis can be used to determine which parameter the design's stability is most sensitive. If the geometry and conditions happen to be more sensitive to a certain parameter, it means that small changes, or little variability, in the parameter can result in more significant result changes as compared to other parameters. It is valuable to know which parameter is the most critical. An example of a sensitivity output is shown in Figure 13.9.

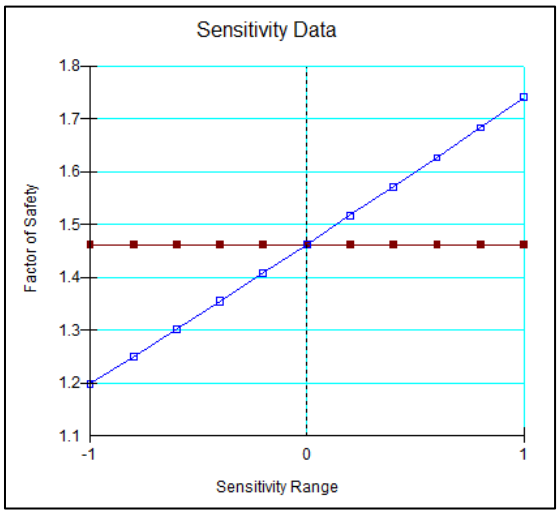

Figure 13.9. Sensitivity output example

This knowledge is important to determine the amount of risk involved in a specific earthwork design. The parameters taken into consideration for the sensitivity assessment were the friction angle (φ) and the unit weight (γ_d). The range of values chosen for the sensitivity analysis was targeted to emulate the values that would exists in a realistic three dimensional anisotropic structure with significant spatial variability. The sensitivity input parameters and outputs are shown in section 13.2.

Deterministic Analysis

Deterministic analysis was performed on all slopes considered in order to give a range of factors of safety to more accurately assess the stability of each slope. The method was also used in order to validate the model geometry and conditions by calibrating the analysis performed on the AOC design, and to input the soil's researched geotechnical laboratory test values to compare the analysis. The AOC valley fill design assessment found the static factor of safety to be 1.592 as shown in Figure 13.1. The analysis performed for this research found the factor of safety to be approximately the same under the similar conditions, but using the GLE method in lieu of Bishop's simplified method. This assessment did not consider any elevated water table.

The values used for the fill material were a friction angle of 40^o and a unit weight of 130 pcf. The cohesion was set to a value of 0 psf, assuming that the material acts as cohesionless free draining sand.

13.2 Data Input Parameters

This data input information has been accumulated from geotechnical laboratory testing on an unweathered sandstone overburden. The details of the testing performed to obtain these laboratory values can be found in Chapters 5-12. This overburden material is the fill material in all slope models presented. A summary of the values and their associated statistics are shown in the following tables. The delta values are equal to one fifth of the range for the data. The delta values were used in the sensitivity analysis. Five steps from the mean value were assessed in the sensitivity analysis each equal to the addition of one delta value. A summary of the input parameters for the GeoStudio™ modules are shown in Table 13.1 through Table 13.7.

Table 13.1. Laboratory friction angle values

φ (From ALL DATA)								
11% Proctor Compaction Energy			**34% Proctor Compaction Energy**			**Standard Proctor Compaction**		
Shear Stress (kPa)	**Normal Stress (kPa)**	**Φ°**	**Shear Stress (kPa)**	**Normal Stress (kPa)**	**Φ°**	**Shear Stress (kPa)**	**Normal Stress (kPa)**	**Φ°**
314.19	600	27.64	365.71	600	31.36	1342.94	2676.40	26.65
595.62	1200	26.39	607.73	1200	26.86	1029.95	1784.26	30.00
1180.03	2500	25.27	1078.41	2500	23.33			

Table 13.2. Laboratory friction angle statistics for sensitivity model input

Mean:	**27.19°**
Standard Deviation:	**2.54**
Coefficient of Variation	**0.09**
Ultimate Minimum:	**23.33°**
Ultimate Maximum:	**31.36°**
Range:	3.85
Delta:	0.77

Table 13.3. Laboratory dry unit weight (γ_d) values at predetermined compaction energies

	11% Proctor Energy	**34% Proctor Energy**	**Standard Proctor**
γ_d (From ALL DATA) [kN/m^3]	15.39	16.11	16.65
	16.90	16.21	18.51
	15.20	16.48	18.54
	14.93	17.98	13.92
	15.07	17.94	
	17.60	17.80	
	16.55	14.37	

Table 13.4. Laboratory dry unit weight (γ_d) statistics for sensitivity model input

Mean:	**16.45°**
Standard Deviation:	**1.42**
Coefficient of Variation	**0.09**
Ultimate Minimum:	**14.93°**
Ultimate Maximum:	**18.75°**
Range:	1.52
Delta:	0.30

Table 13.5. Deterministic SLOPE/W material input values

SLOPE/W					
Deterministic Inputs					
Blasted Fill		**Blocky Core Drain**		**Foundation Rock**	
γ (kN/m^3)	18.39	γ (kN/m^3)	19.64	γ (kN/m^3)	18.39
c (kPa)	0	c (kPa)	9.58	c (kPa)	0
φ	27.7°	φ	30°	φ	27.7°

Table 13.6. Sensitivity SLOPE/W material input values

SLOPE/W		
Sensitivity Inputs		
Unweathered Sandstone Fill	**Slip Surface Calculation Value**	**Mean**
γ (kN/m^3)	16.45	14.93
c (kPa)	0.00	0.00
φ	27.19^o	23.33^o
Blocky Core Drain		
γ (kN/m^3)	16.45	14.93
c (kPa)	0.00	0.00
φ	27.19^o	23.33^o
Foundation Rock	**No Sensitivity Values**	
γ (kN/m^3)	19.64	
c (kPa)	9.58	
φ	30.00^o	

Table 13.7. SIGMA/W material input values

SIGMA/W			
	Elastic Modulus, kPa	**Unit Weight, γ (kN/m^3)**	**Poisson's Ratio**
Blocky Core Drain	29868	18.39	0.34
Foundation Rock	1000000	26.48	0.38
Unweathered Fill	29868	18.39	0.34

13.3 Stability Analysis: AOC Valley Fill Design

The results of the limit equilibrium analysis yielded critical factors of safety found from the AOC valley fill (Fig. 13.3) deterministic SLOPE/W analysis are shown in the following tables. The two analysis methods shown below are deterministic and sensitivity each utilizing GLE theory. The failure modes assessed were: crest, toe, face, and deep foundation failures. The factor of safety (FS) results are shown in Table 13.8, Table 13.9, and Table 13.10. Two water table elevations were considered for each failure mode for precision:

- Piez. 1: Piezometric line at the top elevation of durable rock underdrain
- Piez. 2: Piezometric line at an elevated displacement (50ft or 15.24m) above the durable rock underdrain.

Table 13.8. Deterministic critical factors of safety (FOS) for selected scenarios using AOC valley fill input parameters

AOC Valley Fill Design Values		
Location		**Critical Deterministic FS**
Crest	**Piez. 1**	2.84
	Piez. 2	2.84
Toe	**Piez. 1**	1.51
	Piez. 2	0.91
Face	**Piez. 1**	2.13
	Piez. 2	2.13
Deep	**Piez. 1**	1.54
	Piez. 2	1.41

Table 13.9. Deterministic critical factors of safety for selected scenarios using laboratory value

Laboratory Values		
Location		**Critical Deterministic FS**
Crest	**Piez. 1**	1.78
	Piez. 2	1.78
Toe	**Piez. 1**	1.23
	Piez. 2	0.5
Face	**Piez. 1**	1.33
	Piez. 2	1.33
Deep	**Piez. 1**	1.37
	Piez. 2	1.21

Table 13.10. Sensitivity assessment: Critical factor of safety results for selected scenarios

Location		Critical Sensitivity Factor of Safety			
		Friction Angle, φ	FS for φ	Unit Wt., γ_d	FS for γ_d
Crest	**Piez. 1**	19.475	1.199	13.407	1.462
	Piez. 2	19.475	1.199	13.407	1.462
Toe	**Piez. 1**	19.475	0.815	13.407	0.979
	Piez. 2	19.475	0.223	13.407	0.198
Face	**Piez. 1**	19.475	0.898	13.407	1.095
	Piez. 2	19.475	0.898	13.407	1.095
Deep	**Piez. 1**	19.475	1.120	13.407	1.232
	Piez. 2	19.475	0.927	13.407	1.020

Discussion

The critical factor of safety results show that for an elevated water table in the AOC design, the factor of safety decreases below the regulatory requirement for a static case of 1.5. If a failure plane is taken entirely in the saturated zone; the factor of safety becomes less than 1.0.

Furthermore, the soil's laboratory values found differ from the AOC soil values used from the DEP permit file. The test results show that the blasted overburden has a lower friction angle, as well as a lower unit weight. It can be determined; however, that if the AOC design remains at a drained condition, the factor of safety will remain above 1.0.

The durability of the valley fill structure may be dependent on the limitation of the particle transport within the structure itself. Less internal erosion of fine particles could yield a more durable structure. Future research in modeling of this slope will shed more light to the limitations and shortcomings of the scenarios shown.

13.4 Stability Analysis: Geomorphic Valley Fill Alternative

Geomorphic design uses concepts derived from natural processes. Geomorphic landforms are designed with the intent of emulating a naturally occurring landform whose erosion potential is minimized. The minimized erosion potential is a function of drainage density. Drainage density is the ratio of the relationship between watershed area per channel length.

Some initial benefits can be observed when addressing geomorphic landform design from a slope stability, and earthen structure durability standpoint. Slope angles and lengths have the potential to be decreased. Smaller slopes give water runoff shorter distances to travel before being collected in a drainage channel. This analysis was performed to explore the stability capacity of the geomorphic landform design to be compared to the AOC valley fill design with regard to a factor of safety computed from GeoStudio™ by the general limit equilibrium (GLE) approach.

The geomorphic landform design shown in Figures 13.10 and 13.11 below was produced with GeoFluv® software. SLOPE/W was used for the slope stability analysis. The contours by which the profile dimensions were retrieved are shown in Figure 13.10. The geomorphic alternative dimensions were retrieved from a centerline cut at the identical dimensions as the valley fill centerline section A-A in Figure 13.2.

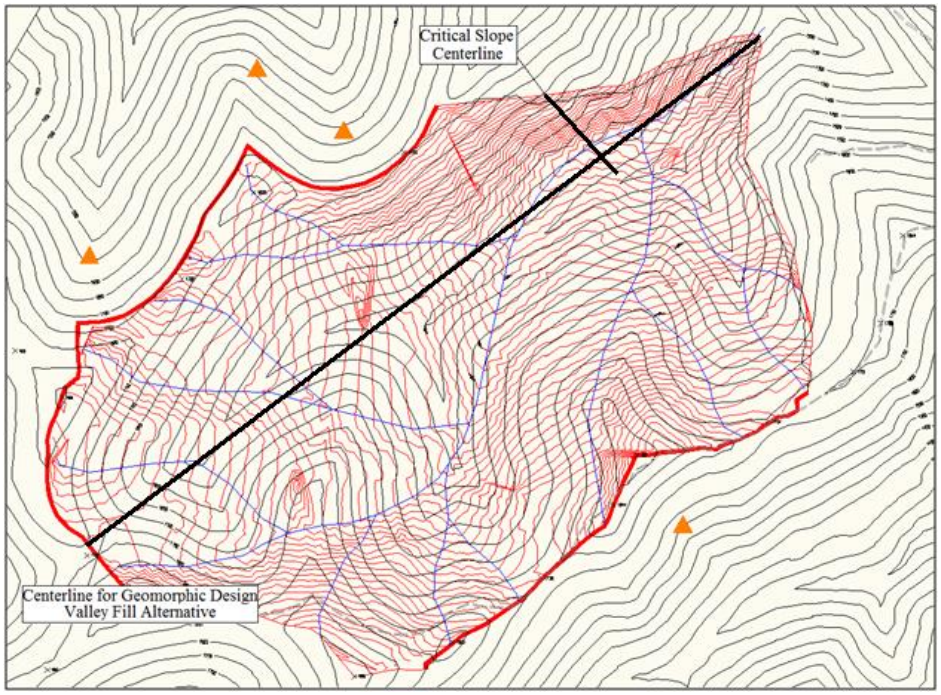

Figure 13.10. Geomorphic design contours superimposed on original ground contours

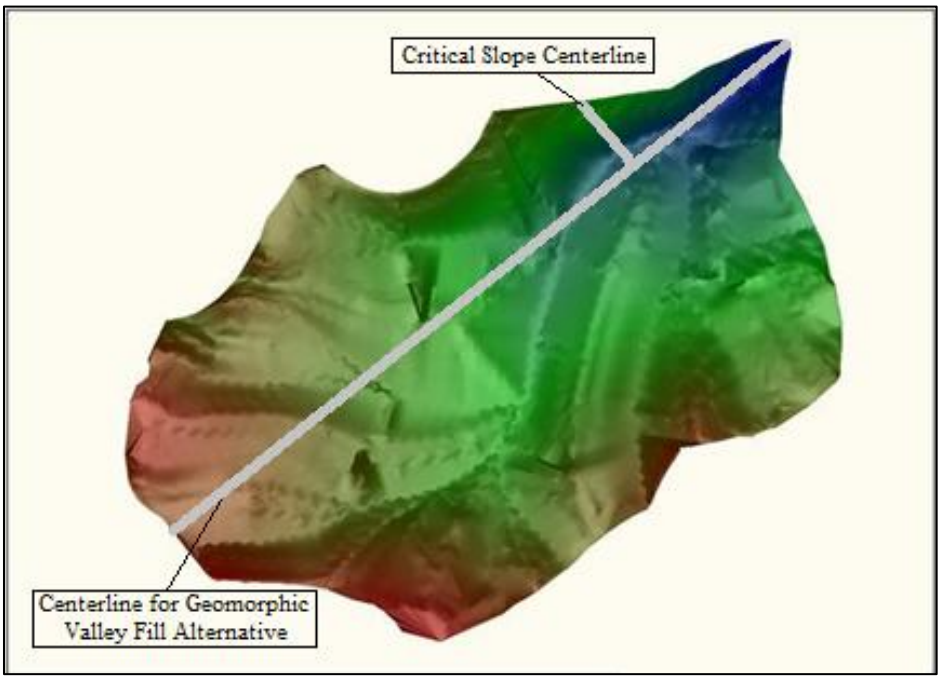

Figure 13.11. Geomorphic design surface generated from a triangulated irregular network (TIN)

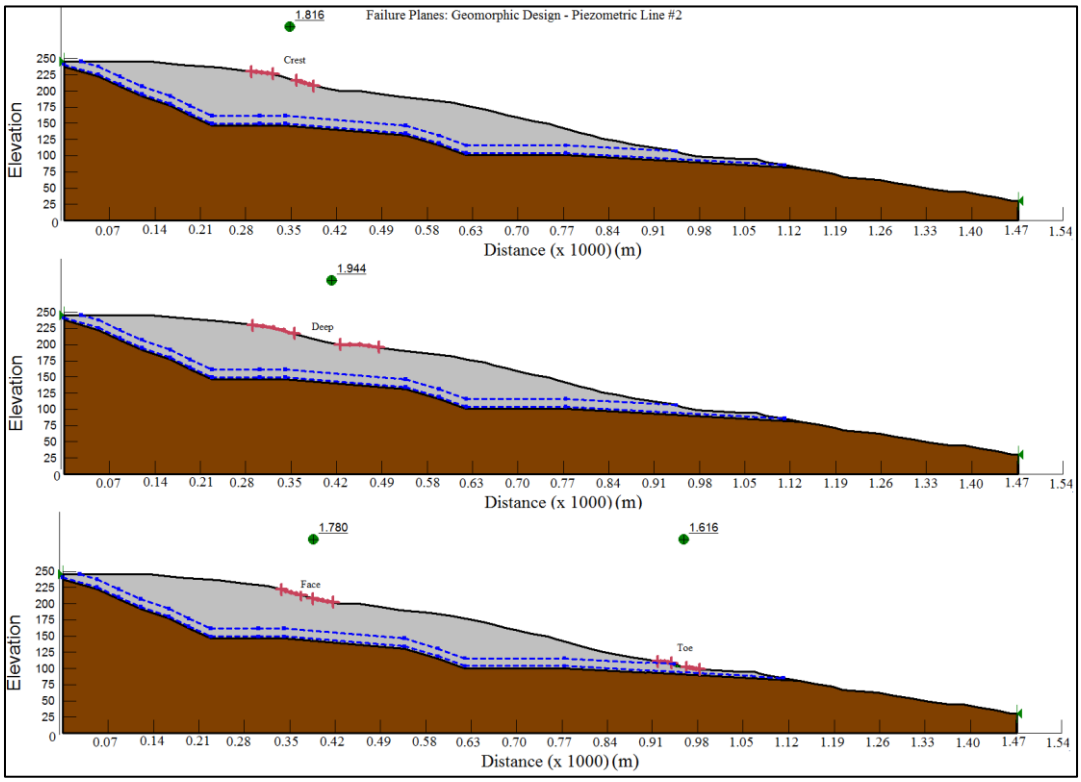

Figure 13.12. Geomorphic valley fill alternative failure planes along centerline shown in Fig. 13.10

Data Input Parameters

The data that was input into the model to identify the geometry of the slope was taken from the AOC contours in and the geomorphic design contours in Figure 13.10. The material's geotechnical properties were input identically to the data used for the AOC modeling in section 13.3 for accurate comparison. The failure planes were determines such that the most critical areas would be analyzed. The critical areas were identified as the steepest areas along the slope. From a slope stability standpoint, the steep slopes would have the highest driving forces for slope failure. These areas should have the lowest factors of safety. Four locations were chosen for analysis as shown in Figure 13.12. Two piezometric scenarios were assessed separately. The piezometric lines were at a 10ft thickness along the bottom of the fill to emulate a saturated gravity segregated durable rock underdrain, and a 50ft (15.24m) elevated water table to emulate a more critical condition. Slope angles are shown in Table 13.23. A summary of the results for the deterministic and sensitivity factors of safety are shown in Table 13.11 and Table 13.12.

Results

Table 13.11. Deterministic critical factors of safety for two piezometric scenarios

Laboratory Values		
Location		**Critical Deterministic Factor of Safety**
Crest	**Piez. 1**	1.816
	Piez. 2	1.816
Toe	**Piez. 1**	1.822
	Piez. 2	1.616
Face	**Piez. 1**	1.780
	Piez. 2	1.780
Deep	**Piez. 1**	1.944
	Piez. 2	1.944

Table 13.12. Sensitivity critical factors of safety for two piezometric scenarios

Location		Critical Sensitivity Factors of Safety				
		Friction Angle, φ^o	**FS for φ**	**Unit Wt., γ_d**	**FS for γ_d**	**FS**
Crest	**Piez. 1**	19.475	1.223	13.407	1.491	1.776
	Piez. 2	19.475	1.223	13.407	1.491	1.776
Toe	**Piez. 1**	19.475	1.227	13.407	1.497	1.783
	Piez. 2	19.475	1.058	13.407	1.267	1.559
Face	**Piez. 1**	19.475	1.199	13.407	1.462	1.741
	Piez. 2	19.475	1.199	13.407	1.462	1.741
Deep	**Piez. 1**	19.475	1.309	13.407	1.597	1.902
	Piez. 2	19.475	1.309	13.407	1.597	1.902

13.5 Cumulative Analysis: AOC Valley Fill Design

The modeling process undertaken for the valley fill under inspection in this section was for two scenarios. The first scenario run was for the durable rock underdrain to be initially dry or unsaturated. The second condition run was for the underdrain to be at an initially saturated state. The objective of the stability analysis performed for this valley fill profile geometry was intended to imitate more realistic in-field conditions. SEEP/W was first used to produce infiltration results over a 10 year period. The results from SEEP/W illustrated areas of storage, areas of increased hydraulic head, and elevated pore pressures. The results from this analysis were utilized as parent inputs to a SIGMA/W analysis. The SIGMA/W analysis, via finite element modeling techniques, calculated insitu stresses within the fill structure. The insitu stresses varied from previous piezometric head conditions by having spatially variable areas of increased total hydraulic head, as well as spatially variable areas of elevated pore pressures. Finally, the SIGMA/W results were used as parent input parameters for the finite element SLOPE/W analysis. The SLOPE/W analysis was run to produce factors of safety at several critical areas. The critical areas that were selected for failure plane entry and exit points were chosen to be identical to the valley fill modeling shown in section 13.3 for comparison. Slope profile with cumulative analysis results shown in Table 13.13 through Table 13.16, Figure 13.13, and Figure 13.14.

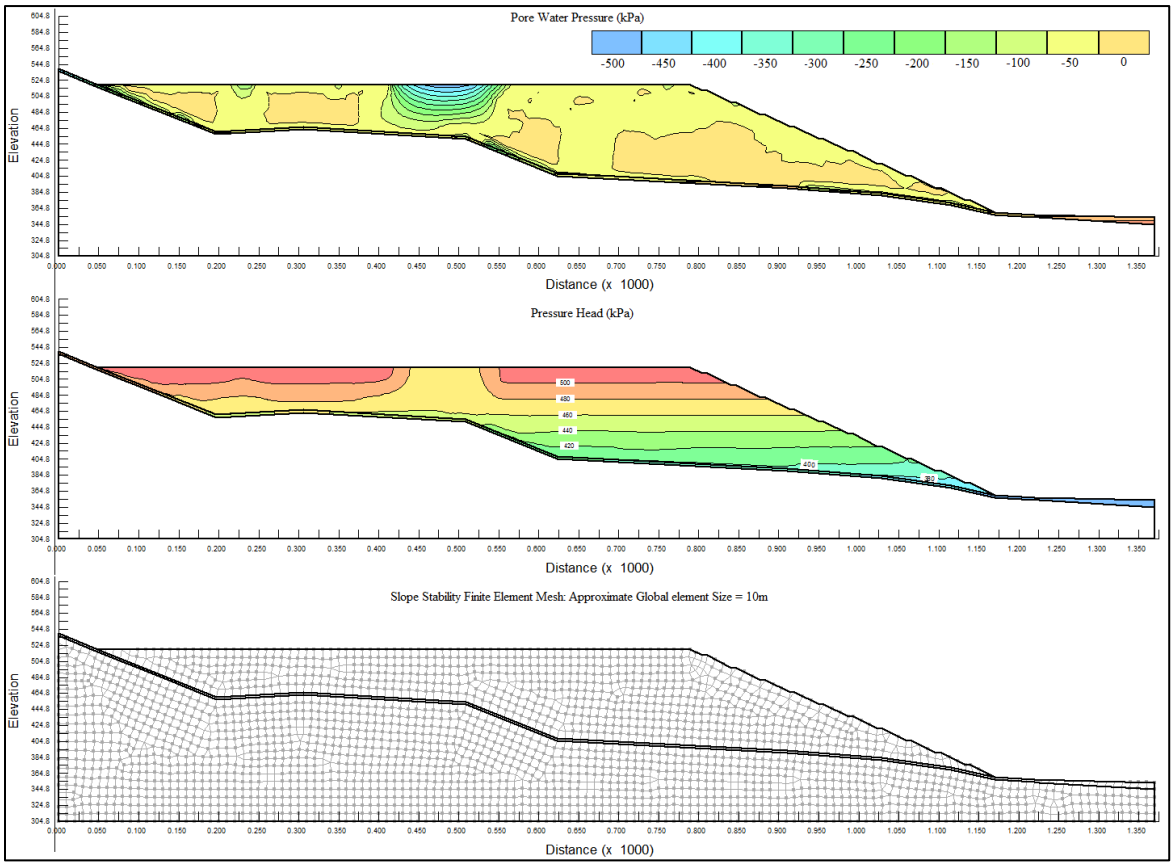

Figure 13.13. Valley fill diagrams of results from a cumulative analysis of SEEP/W, SIGMA/W, and SLOPE/W from GeoStudio™

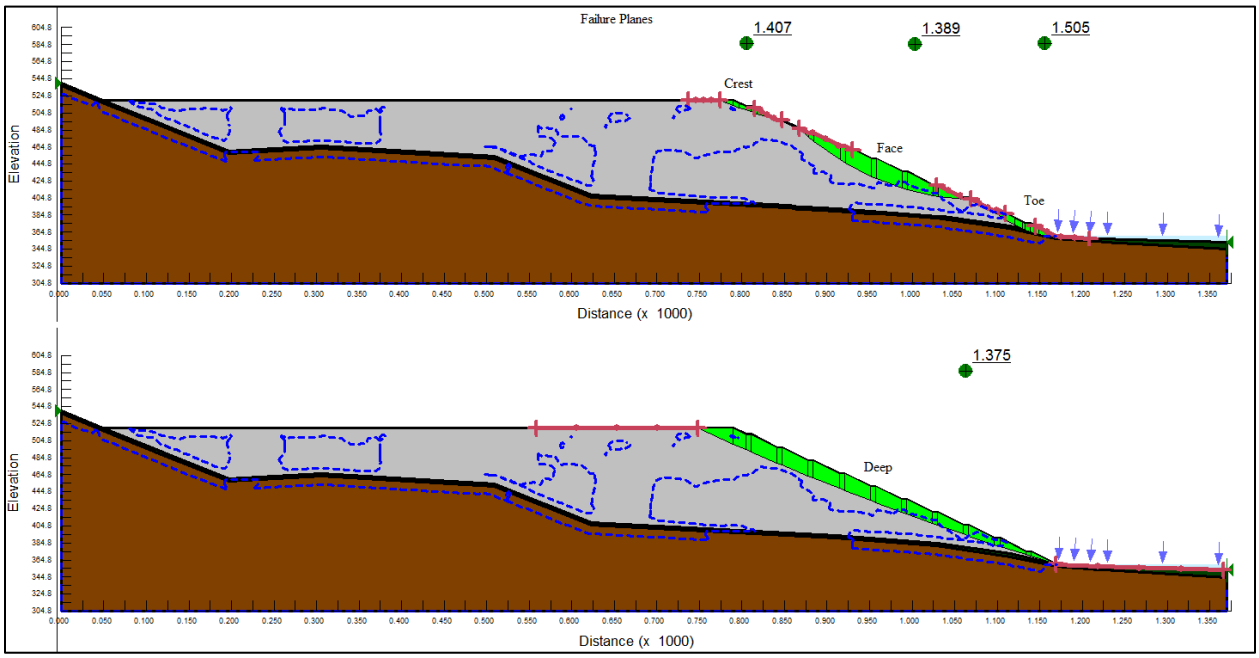

Figure 13.14. Failure entry and exit locations for saturated underdrain – Deterministic analysis results

Data Input Parameters

The geometry of this valley fill profile was taken from the image in Figure 13.1. The geometry is identical to the analysis described in section 13.3. The SEEP/W inputs are described in SEEP/W Analysis section in this chapter, or section 13.1. The SIGMA/W input parameters are shown in Table 13.7. The blocky underdrain material had its own unique hydraulic conductivity for the SEEP/W modeling, but had identical input parameters for strength, unit weight, and friction angle as the fill material. The original ground material was considered as a weak sandstone with an elastic modulus at the minimum for solid sandstone at 10^6 kPa.

Results

Table 13.13. Deterministic factor of safety results: Saturated Underdrain

Laboratory Values Valley Fill - Saturated	
Location	**Critical Deterministic Factor of Safety**
Crest	1.407
Toe	1.505
Face	1.389
Deep	1.375

Table 13.14. Deterministic factor of safety results: Unsaturated Underdrain

Laboratory Values Valley Fill - Unsaturated	
Location	**Critical Deterministic Factor of Safety**
Crest	1.673
Toe	1.246
Face	1.365
Deep	1.299

Table 13.15. Sensitivity factor of safety results: Saturated Underdrain

Location	**Sensitivity FS: Valley Fill - Saturated**		
	Friction Angle, φ	**Unit Wt., γ_d**	**FS**
Crest	19.475	13.407	1.377
Toe	19.475	13.407	1.472
Face	19.475	13.407	1.359
Deep	19.475	13.407	1.345

Table 13.16. Sensitivity factor of safety results: Unsaturated underdrain

Location	**Sensitivity FS: Valley Fill - Unsaturated**		
	Friction Angle, φ	**Unit Wt., γ_d**	**FS**
Crest	19.475	13.407	1.637
Toe	19.475	13.407	1.219
Face	19.475	13.407	1.335
Deep	19.475	13.407	1.271

13.6 Cumulative Analysis: Geomorphic Valley Fill Alternative

The objective of the stability analysis performed for this geomorphic design valley fill alternative profile geometry was intended to imitate more realistic in-field conditions than utilizing SLOPE/W alone. The modeling process undertaken for the geomorphic design valley fill alternative under inspection in this section was for two scenarios. The first scenario run was for the durable rock underdrain to be initially dry (unsaturated). The second condition run was for the underdrain to initially be at a fully saturated state. The cumulative analysis procedure was identical to the analysis run on the AOC valley fill design in the previous section (section 13.5), except for the failure plane entry and exit selection. SEEP/W was first used to produce infiltration results over a 10 year period. The results from SEEP/W illustrated areas of ground water storage, areas of increased hydraulic head, and elevated pore pressures. The results from this analysis were utilized as parent inputs to a SIGMA/W analysis.

The SIGMA/W analysis, via finite element modeling techniques, calculated *insitu* stresses within the fill structure. The *insitu* stresses varied from previous piezometric head conditions by having spatially variable areas of increased total hydraulic head, as well as spatially variable areas of elevated pore pressures. Finally, the SIGMA/W results were used as parent input parameters for the finite element SLOPE/W analysis. The SLOPE/W analysis was run to produce factors of safety at several critical areas. The critical areas that were selected for failure plane entry and exit points were chosen by considering areas where pore pressures were highest. Other failure plane entry and exit locations were selected by keeping in mind general limit equilibrium concepts of driving forces and resisting forces (or moments). The failure plane entry and exit location selection also involved keeping in mind the sometimes significant effects that steep slope angles can have on the stability of an earthen structure. The slope profile with cumulative analysis results are shown in the following figures and tables along with identified failure planes.

Figure 13.15 shows output from (top to bottom) SLOPE/W, SIGMA/W, SEEP/W, then finally the finite element mesh with a global element size of 10m. SEEP/W analysis was performed first to calculate the water storage through hydraulic conductivity and water content functions. SIGMA/W was then utilized to calculate the *insitu* stresses caused by the water storage and unit weight. SLOPE/W was lastly utilized to calculate factors of safety at three critical locations.

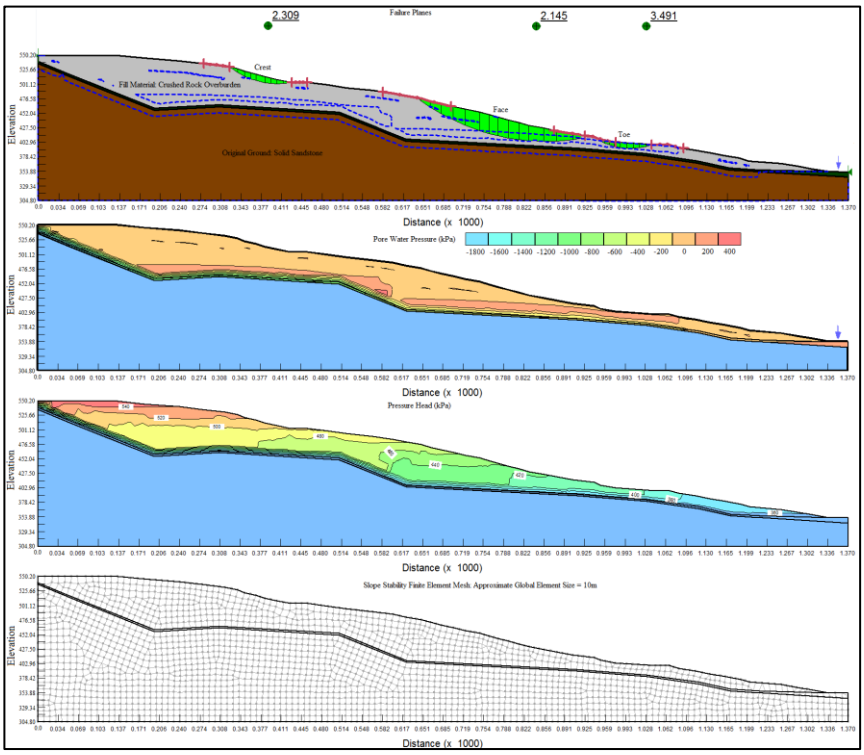

Figure 13.15. Geomorphic valley fill alternative cumulative analysis results for unsaturated underdrain conditions

Data Input Parameters

It is important to note that the profile geometry used for this model and the model described in section 13.10 vary slightly. The reason for this alteration is that the original ground input dimensions varied in discretization between the two illustrations in Figure 13.1 and Figure 13.10. Each geometry was chosen to be assessed in the manner laid out in this chapter. The SEEP/W inputs are described in SEEP/W Analysis section in this chapter, or section 13.1. The SIGMA/W input parameters are shown in Table 13.7. The blocky underdrain material had its own unique hydraulic conductivity for the SEEP/W modeling, but had identical input parameters for strength, unit weight, and friction angle as the fill material. The original ground material was considered as a weak sandstone with an elastic modulus at the minimum for solid sandstone at 10^6 kPa.

Results

Table 13.17. Deterministic critical factor of safety results for the geomorphic design valley fill alternative under an initial saturated underdrain condition

Laboratory Values Geomorphic Design - Saturated	
Location	**Critical Deterministic FS**
Crest	2.040
Toe	2.144
Face	2.242

Table 13.18. Sensitivity critical factor of safety results for the geomorphic design valley fill alternative under an initial saturated undedrain condition

Sensitivity: Geomorphic Design - Saturated			
Location	**Friction Angle, φ**	**Unit Wt., γ_d**	**FS**
Crest	19.475	13.407	1.997
Toe	19.475	13.407	2.097
Face	19.475	13.407	2.194

Table 13.19. Deterministic critical factor of safety results for the geomorphic design valley fill alternative under an initial unsaturated underdrain condition

Laboratory Values Geomorphic Design - Unsaturated	
Location	**Critical Deterministic FS**
Crest	2.309
Toe	3.491
Face	2.145

Table 13.20. Sensitivity critical factor of safety results for the geomorphic design valley fill alternative under an initial unsaturated undedrain condition

Sensitivity: Geomorphic Design - Unsaturated			
Location	**Friction Angle, φ**	**Unit Wt., γ_d**	**FS**
Crest	19.475	13.407	2.260
Toe	19.475	13.407	3.416
Face	19.475	13.407	2.099

13.7 Geomorphic Design Critical Slope Analysis

This slope analysis was performed to illustrate areas of concern for the GeoFluv® geomorphic design process. The geometry for these slopes were taken directly from the labeled location in the design in Figure 13.10. Since GeoFluv® does not have a slope stability module or assessment of any kind to reinsure the durability of the output, excessively steep slopes sometimes result. These excessively steep slopes result because the GeoFluv® program bases the design on the hydraulic factors involving surface precipitation runoff. These hydraulic factors include stream type, and stream slope. This particular slope was in a narrow part of the design. When inspecting Figure 13.10, one notices that the main channel and the design boundary are close to one another in proximity; however, their individual elevations vary greatly. In response to this scenario, the design software "ties in" the two elevations in a very short distance, producing a steep slope. Two piezometric conditions were modeled for this slope. The results prove that this slope is too steep to meet the factor of safety requirement for AOC of 1.5. None of the 16 models that were run produced a factor of safety over 1.0. One promising insight is that within GeoFluv®, the designer can mitigate these types of problems by changing the number of drainage channels, shifting the slope of the drainage channel, or by altering cut and fill volumes in specific areas. Designer customization in any of these areas will affect the calculated factor of safety. If a designer can identify critical slope areas accurately, then the low factors of safety can be increased by altering the geometry of the landform. The factor of safety results are presented in Figure 13.16 and Table 13.21.

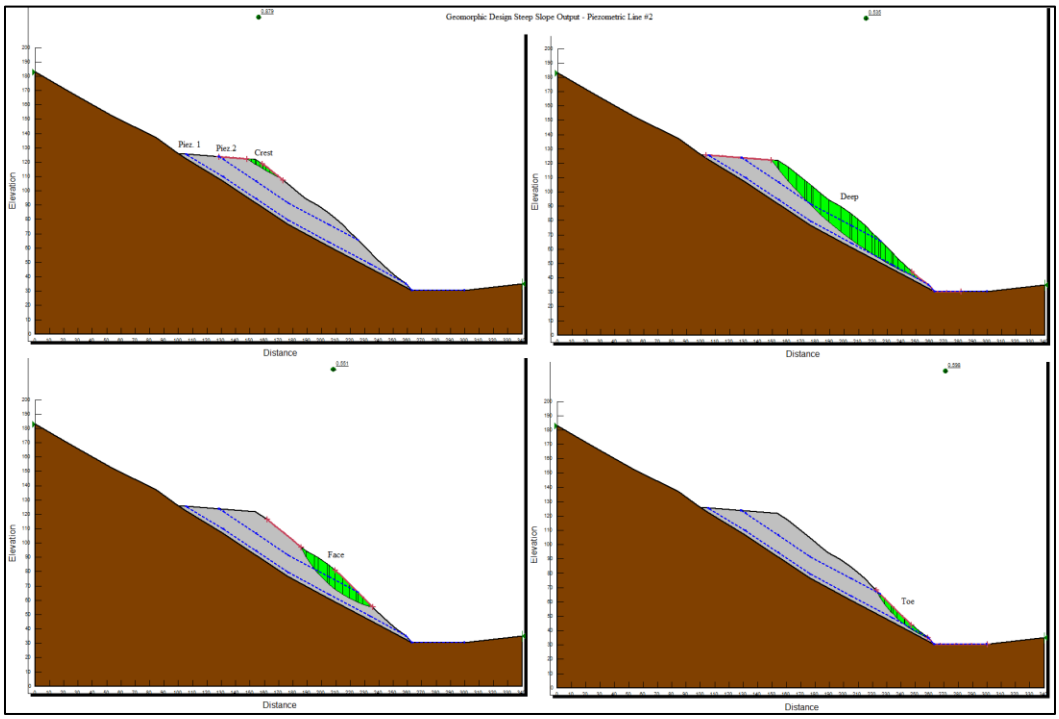

Figure 13.16. Critical slope profile with failure planes along centerline shown in Fig. 13.10. Pieziometric line #2 enabled – Deterministic analysis visual results

Data Input Parameters

The geometry of the model, as noted above, was retrieved from the AutoCad™ output contours of the original ground and the superimposed geomorphic design contours. The fill material and original ground material are defined identical to the previous models. The material's geotechnical properties were input according to Tables 13.1-13.7. The failure planes were determined such that the most critical areas would be analyzed along the fill surface. Two piezometric scenarios were assessed separately. The piezometric lines were at a 10ft thickness along the bottom of the fill to model a saturated gravity segregated durable rock underdrain, and a 50ft (15.24m) elevated water table to approximate a more critical condition. Tables summarizing the deterministic and sensitivity factors of safety are shown below in Table 13.21 and Table 13.22. Slope angles are shown in Table 13.23.

Results

Table 13.21. Sensitivity critical factor of safety results for the critical slope for two piezometric scenarios

Location		Critical Sensitivity Factor of Safety				
		Friction Angle, φ	FS for φ	Unit Wt., γ_d	FS for γ_d	FS
Crest	**Piez. 1**	19.475	0.611	13.407	0.745	0.887
	Piez. 2	19.475	0.611	13.407	0.745	0.887
Toe	**Piez. 1**	19.475	0.227	13.407	0.220	0.363
	Piez. 2	19.475	0.402	13.407	0.489	0.584
Face	**Piez. 1**	19.475	0.463	13.407	0.564	0.670
	Piez. 2	19.475	0.345	13.407	0.400	0.519
Deep	**Piez. 1**	19.475	0.468	13.407	0.570	0.677
	Piez. 2	19.475	0.338	13.407	0.396	0.506

Table 13.22. Deterministic critical factor of safety results for the critical slope for two piezometric scenarios

Laboratory Values		
Location		**Critical Deterministic Factor of Safety**
Crest	**Piez. 1**	0.879
	Piez. 2	0.879
Toe	**Piez. 1**	0.409
	Piez. 2	0.598
Face	**Piez. 1**	0.685
	Piez. 2	0.551
Deep	**Piez. 1**	0.679
	Piez. 2	0.535

AOC Valley Fill and Geomorphic Alternative Profiles

An additional assessment of the friction angle of the material was performed at a loose, as received condition. The friction angles were found through direct shear testing on GeoTac™ equipment. Figure 13.17 shows the direct shear information for an as received friction angle (phi). It was found that the friction angle for the cohesion case was 37.99°. The friction angle for the no cohesion case, or where the best fit line is forced through (0,0) was 39.75°. The WVDEP permit File#S500809 which was used to define the geometry of the AOC valley fill slope used a friction angle of 40° for the slope stability analysis performed on the valley fill. An analysis was performed in order to attain factors of safety for the same failure locations as defined for the AOC valley fill and geomorphic landform design alternative in Section 13.3 and Section 13.4. The results are shown in Figure 13.18 and Figure 13.19.

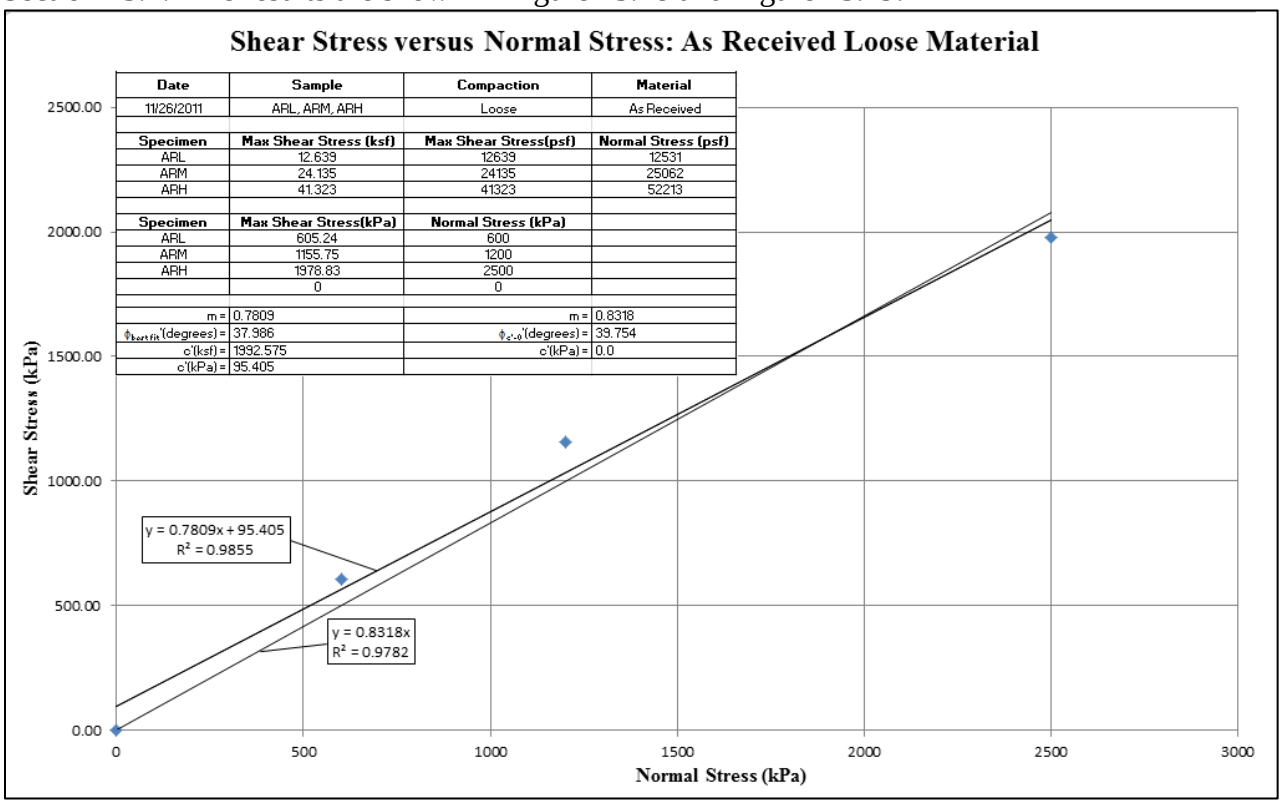

Date	Sample	Compaction	Material
11/26/2011	ARL, ARM, ARH	Loose	As Received

Specimen	Max Shear Stress (ksf)	Max Shear Stress(psf)	Normal Stress (psf)
ARL	12.639	12639	12531
ARM	24.135	24135	25062
ARH	41.323	41323	52213

Specimen	Max Shear Stress(kPa)	Normal Stress (kPa)	
ARL	605.24	600	
ARM	1155.75	1200	
ARH	1978.83	2500	
	0	0	

m =	0.7809	m =	0.8318
$\phi_{best\ fit}$'(degrees) =	37.986	$\phi_{c'=0}$'(degrees) =	39.754
c'(ksf) =	1992.575	c'(kPa) =	0.0
c'(kPa) =	95.405		

Figure 13.17. Direct shear information on as received testing

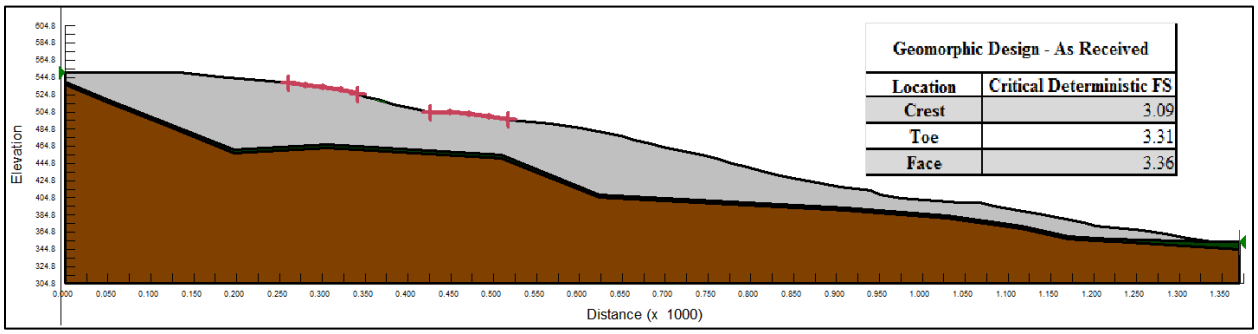

Figure 13.18. Geomorphic profile for as received models

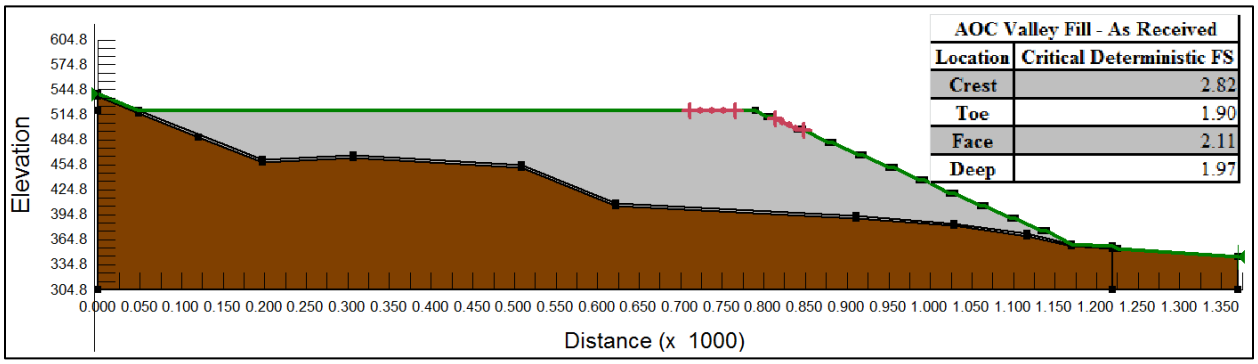

Figure 13.19. AOC valley fill profile for as received models

Discussion

The as received friction angle was modeled for the geomorphic and AOC valley fill profiles. It was found that the factors of safety increased significantly. The AOC factors of safety were all near 2.0 with a maximum of 2.82 and a minimum of 1.90. The geomorphic valley fill alternative profile also had very high factors of safety which increased from all previous models. All factors of safety were above 3.0 for the geomorphic models. For the geomorphic models, the maximum factor of safety was 3.36, and a minimum of 3.09. Regulatory requirements enforce that a factor of safety of 1.5 must be met for all valley fill slope faces. With this friction angle input parameter at 39.75^{o}, the factors of safety all greatly exceed the regulatory requirement. The material gradation considered as "as received" still had to be altered due to testing equipment limitations; however, the material passing the 3/8 in. sieve was used. These high factors of safety imply that the previously shown input parameter for a friction angle of 27.7^{o} was rather conservative at a gradation of the material passing the #4 sieve. Therefore, the factors of safety in Chapter 13 are conservative.

Summary and Comparison

Five separate assessments were performed in the modules available in GeoStudio™ for comparison. Through this rigorous analysis, it was found that slope angles, phreatic elevations, and areas of increased pore pressures greatly affected the factors of safety that were yielded by GeoStudio™ modules. The slope angles and associated coordinates for each failure plane assessed are shown in Table 13.23.

Table 13.23. Critical slip plane approximate exit point slope angles

Slope Angles							
	x (m)	y (m)	$\beta^0=\tan^{-1}(y/x)$	Top Left Coord.		Bottom Right Coord.	
				x (m)	y (m)	x (m)	y (m)
Valley Fill	30.40	15.20	**26.57**	920.20	466.30	950.60	451.10
Geomorphic Alternative: Contour Profile							
Face	19.81	4.57	**12.99**	383.88	208.79	403.69	204.22
Toe	25.05	4.57	**10.34**	950.76	103.63	975.81	99.06
Deep	22.62	4.58	**11.45**	403.69	204.22	426.31	199.64
Crest	18.96	4.57	**13.55**	349.49	217.93	368.45	213.36
Geomorphic Alternative: Plan Profile - Saturated							
Face	16.52	4.57	**15.47**	813.90	435.86	830.42	431.29
Toe	14.39	4.57	**17.63**	1188.21	376.43	1202.60	371.86
Crest	22.62	4.57	**11.43**	403.689	509.02	426.31	504.44
Geomorphic Alternative: Plan Profile - Unsaturated							
Face	35.48	4.57	**7.34**	904.86	417.58	940.33	413.00
Toe	68.09	4.57	**3.84**	975.82	403.86	1043.91	399.29
Crest	22.62	4.57	**11.43**	403.69	509.02	426.31	504.44
Geomorphic Critical Slope							
Face	4.74	4.57	**43.95**	228.62	62.48	233.36	57.91
Toe	104.59	56.39	**28.33**	154.45	91.44	259.04	35.05
Deep	6.48	4.57	**35.19**	252.56	39.62	259.04	35.05
Crest	5.82	4.57	**38.14**	172.3	108.2	178.12	103.63

The height of the piezometric line had a profound influence on the factors of safety. When an area was saturated, the factor of safety decreased, sometimes below 1.0 as in the piez. 2 toe scenario of the AOC valley fill design (Table 13.24). If the piezometric line was not elevated to the area of the selected failure plane, then the factor of safety remained unchanged. Additionally, steeper slope angles decreased factors of safety. Two initial saturation conditions were modeled for the cumulative analysis. The saturation conditions were applied in SEEP/W, and SIGMA/W computed *insitu* stresses to be input into SLOPE/W for a factor of safety computation. The initial saturation condition of the gravity segregated durable rock underdrain was significant. The initial saturation altered the volume of water retained within the structure,

and ultimately altered the factors of safety that resulted. Tables 13.24 and 13.25 show the factors of safety for both the saturated and unsaturated initial hydraulic condition. The factors of safety vary from one hydraulic condition to the next, but do not necessarily increase or decrease accordingly. The result is an effect of the varying areas of increased pore pressure. The result of the SEEP/W analysis produced outputs that accumulated water storage within each fill in different areas, which resulted in varying factors of safety. Both cumulative analysis that were run for the geomorphic design and the valley fill proved that the initial condition could vary the factor of safety. The change in the factor of safety was not always in favor of either condition from a structural standpoint. The significance of the initial saturation condition was that the water storage areas within the fill changed, and altered the factors of safety. It is important to note that the fills may be built in lifts or by end dumping. Sometimes when contractors build slopes, they cut into the original ground, and may use compaction equipment to help integrate the components of the structure. These considerations would likely alter the factors of safety. Additionally, spatial variability was only taken into account in these models as a sensitivity analysis. Field conditions of a slope structure would have a great deal of spatial variability both in compaction and in initial water content affecting soil strength and phreatic surface elevations.

By far, the cumulative analysis for the geomorphic valley fill alternative design yielded the highest factors of safety. Most cases produced factors of safety over 2.0. The most likely reason for these high factors of safety is that the geomorphic design has shallower slopes, and drains well. Geomorphic landform design can be utilized to reduce infiltration volumes by shortening runoff travel distances, increasing runoff water removal from a design site. A completed design should retain less water than the modeled results show because of vegetative cover and quick surface runoff. Both initial saturated and unsaturated conditions yielded high factors of safety. The failure locations were sought out to find the lowest factors of safety for the structure. The geomorphic stability analysis described in section 13.4 yielded high factors of safety (Table 13.25) also; however, the water tables were exaggerated. The profile described in section 13.4 still retains its structural integrity even when high volumes of water are being stored within it. None of the factors of safety even under the most critical circumstances tested yielded factors of safety under 1.0. Even though the original ground dimensions vary for the two profiles, the surface dimensions are identical except for the near the toe. The results prove that the geomorphic design can remain very stable under different conditions and geometries.

The weakest structure was by far the critical slope described in section 13.7. None of the factors of safety under any scenario analyzed yielded a factor of safety over 1.0. The factors of safety of this structure were expected to be low. The analysis of the critical slope was intended to illustrate that GeoFluv® does not consider slope stability, and can produce slopes that are not stable. As discussed in section 13.7, GeoFluv® does enable the designer to alter many components of the design to mitigate the slope stability problems that may occur due to rapid elevation changes.

The AOC design was typical with its bench cuts and planar slopes. Regulations require that slope factors of safety must remain above 1.5. The analysis performed showed that the design could withstand *insitu* loads and slope angle under most conditions analyzed. Elevated pore pressures tended to result at the toe of the slope, and decreased the factor of safety. The most critical scenario was a totally saturated toe which yielded a factor of safety of 0.50 as shown in the piez. 2 toe AOC valley fill design model summary in Table 13.24.

The SEEP/W analysis yielded results that implied that the structure drained well for the AOC valley fill design. There were small areas of water storage accumulation and elevated pore water pressures, but nothing which caused the factor of safety to drop below 1.0 for the cumulative analysis. For the cumulative analysis, the lowest factor of safety for the AOC valley fill design was 1.22 at the toe of the slope at an initially unsaturated durable rock underdrain condition.

Geomorphic design decreases erosion potential and therefore decreases maintenance demands. The proposed AOC design would be adequate if it remained sufficiently drained. If particle transport can occur and alter toe pore pressures, it is possible that some small slope failure may occur. The gradations that were found in the fill material in Chapter 9 and Chapter 12 show that particle transport probably would not be a concern for the laboratory tested unweathered sandstone.

Table 13.24. AOC valley fill slope summary

Slope Angles and Correlating Factors of Safety				
Failure Plane	Hydraulic Condition	**$\beta^{o}=\tan^{-1}(y/x)$**	**Critical Deterministic FS**	**Critical Sensitivity Factor of Safety**
AOC Valley Fill Design (Permit Values)				
Crest	Piez. 1	26.57	2.84	-
	Piez. 2	26.57	2.84	-
Toe	Piez. 1	26.57	1.51	-
	Piez. 2	26.57	0.91	-
Face	Piez. 1	26.57	2.13	-
	Piez. 2	26.57	2.13	-
Deep	Piez. 1	26.57	1.54	-
	Piez. 2	26.57	1.41	-
AOC Valley Fill Design (Laboratory Values)				
Face	Piez. 1	26.57	1.78	1.74
	Piez. 2	26.57	1.78	1.74
Toe	Piez. 1	26.57	1.23	1.20
	Piez. 2	26.57	0.50	0.40
Deep	Piez. 1	26.57	1.33	1.31
	Piez. 2	26.57	1.33	1.31
Crest	Piez. 1	26.57	1.37	1.35
	Piez. 2	26.57	1.21	1.18
Cumulative Analysis: AOC Valley Fill Design - Saturated				
Crest	Saturated	26.57	1.41	1.38
Toe	Saturated	26.57	1.51	1.47
Face	Saturated	26.57	1.39	1.36
Deep	Saturated	26.57	1.38	1.35
Cumulative Analysis: AOC Valley Fill Design - Unsaturated				
Crest	Unsaturated	26.57	1.67	1.64
Toe	Unsaturated	26.57	1.25	1.22
Face	Unsaturated	26.57	1.37	1.34
Deep	Unsaturated	26.57	1.30	1.27

Table 13.25. Geomorphic valley fill alternative slope summary

Slope Angles and Correlating Factors of Safety				
Failure Plane	Hydraulic Condition	$\beta^{o}=\tan^{-1}(y/x)$	**Critical Deterministic FS**	**Critical Sensitivity Factor of Safety**
Stability Analysis: Geomorphic Valley Fill Alternative				
Face	Piez. 1	12.99	1.82	1.78
	Piez. 2	12.99	1.82	1.78
Toe	Piez. 1	10.34	1.82	1.78
	Piez. 2	10.34	1.62	1.56
Deep	Piez. 1	11.45	1.78	1.74
	Piez. 2	11.45	1.78	1.74
Crest	Piez. 1	13.55	1.94	1.90
	Piez. 2	13.55	1.94	1.90
Cumulative Analysis: Geomorphic Valley Fill Alternative - Saturated				
Crest	Saturated	11.43	2.04	2.00
Toe	Saturated	17.63	2.14	2.10
Face	Saturated	15.47	2.42	2.19
Cumulative Analysis: Geomorphic Valley Fill Alternative - Unsaturated				
Crest	Unsaturated	11.43	2.31	2.26
Toe	Unsaturated	3.84	3.49	3.42
Face	Unsaturated	7.34	2.15	2.10
Geomorphic Critical Slope				
Face	Piez. 1	43.95	0.88	0.89
	Piez. 2	43.95	0.88	0.89
Toe	Piez. 1	28.33	0.41	0.36
	Piez. 2	28.33	0.60	0.58
Deep	Piez. 1	35.19	0.69	0.67
	Piez. 2	35.19	0.55	0.52
Crest	Piez. 1	38.14	0.68	0.68
	Piez. 2	38.14	0.54	0.51

14. Conclusions and Practical Significance

The objective of this research was to sample and identify a surface mine spoil in southern West Virginia, characterize its associated physical properties as well as the strength aspects for appropriate input parameter key in into a slope stability software analysis tool to compare stability results of an AOC valley fill and a geomorphic landform design with regard to a factor of safety computed by the general limit equilibrium method. The significant conclusions of this research are as follows:

By rigorous analysis of the laboratory testing for the unweathered sandstone overburden material, the following conclusions were identified:

- The standard proctor curve is a typical bell shaped curve with an optimum dry unit weight of 18.75 kN/m^3 at a moisture content of approximately 10.75%. The 34% proctor curve resembles a transition between standard proctor and 11% proctor curves. The optimum dry density of the 34% proctor curve was 18.1 kN/m^3 at a moisture content of 14.50%. The 11% proctor curve shows a compaction curve resembling a standard behavior for a well graded sand. The optimum dry density of the 11% proctor was at 17.6 kN/m^3 with a moisture content of approximately 17.00%. The minimum dry density of the 11% curve was at 10.50% moisture content at a value of 14.90 kN/m^3. The compaction energy applied in these three scenarios varied from 592.5 kJ/m^3 (standard proctor), 203.6 kJ/m^3(34% proctor), and 67.85 kJ/m^3 (11% proctor). The optimum dry densities did not increase by much, only a difference of 1.15 kN/m^3 between standard proctor and 11% proctor compaction. The corresponding moisture contents for these maximums varied from 10.75% (standard proctor) to 17.00% (11% proctor) at a difference of 6.25%. By observation of the data, the material does not need a significant amount of compaction in order to achieve a high dry density, but it does need the accompanying moisture content to achieve it.

- The shear strain curves revealed that much of the residual strength is retained within the sample. The reason the samples retained their strength is likely a result of the creation of the unweathered material. The geometry of the particles of the sample is angular. The material was blasted, unweathered sandstone. The angular nature of the material increases the friction between shear planes and resists displacement. This insight is beneficial when considering slope stability. Slopes constructed with this material should be strong and resistant to failure (FS<1). Regulations require a factor of safety of 1.5 or greater.

- The hydraulic conductivity for each test performed for standard proctor, 34% proctor, and 11% proctor all remained in the order of 10^{-9} m/s. The neither the 34% proctor permeated specimens, nor the standard proctor specimens had hydraulic consolidation effects. Some hydraulic consolidation did occur for the 11% proctor specimens. The consolidation that occurred was the cause of the low hydraulic conductivity of the 11% proctor specimens. The soil structure could not retain its skeleton and void spaces collapsed under the hydraulic gradient of i=15. The standard proctor and 34% proctor specimens had low porosities in a range of n=0.31 to n=0.38 which resulted in low hydraulic conductivities.

While observing the summary of the gradations produced by the as received grain size distribution, the pre-permeability test specimens, and the post-permeability specimens, the following conclusions were formed:

- Comparatively, taking into consideration all three compaction energies and the results shown above of the test scenarios performed it was found that particle movement varied significantly. The variation in gradation was a function of the moisture content added and the energy applied for preparation. The post-permeability results should be interpreted carefully as each specimen of different density varied in pore volume flux. The standard proctor specimens aggregated the most between D_{50} and D_{15} due to compaction, then aggregated more at a post-permeability condition. The 34% Proctor compaction specimens showed similar results as standard proctor, aggregating more at a post-permeability condition. The 11% Proctor compaction specimen results were opposite 34% Proctor compaction results and standard proctor compaction results. The 11% Proctor compaction specimen aggregated most at a pre-permeability condition, then became less aggregated at a post-permeability condition.

- The results of the particle transport analysis indicate that the unweathered sandstone material reaches an aggregated equilibrium with very similar gradation after some pore volumes of water permeate through it. The results also imply that introducing a range of compaction energy can alter soil properties and have performance implications on earthen structures. Layered construction known as "lift construction" could assist in better quality control of the compaction energy applies to earthen structures to more precisely manage the aggregation phenomena. The amount of compaction energy for the 34% Proctor compaction and standard proctor samples seems to have broken up the aggregated particles, then when they were permeated, became more aggregated. After the permeation occurred, all three compaction energies approached a similar gradation, but diverged somewhat as the particle size decreased. The specimens began diverging in similarity around 40% finer.

- Through rigorous grain size distribution analysis of the pre and post-permeability test specimens, it was found that at a D_{10} post-permeability condition, the 11% Proctor compaction energy compacted and permeated sample had the smallest particles, standard proctor had the next highest, and 34% Proctor energy specimens had the largest particle size. Overall the 11% proctor pre-permeability condition had the most aggregated particles, likely due to little compaction energy applied to break apart aggregated particles. At D_{10} at a pre-permeability condition, the standard proctor sample had the smallest particles, then 34% proctor, and 11% Proctor energy samples had the largest aggregated particles.

The numerical modeling of the AOC valley fill design juxtaposed with the geomorphic landform design alternative, the following significant conclusions were drawn:

- The height of the piezometric line had a profound influence on the factors of safety. When an area was saturated, the factor of safety decreased, sometimes below 1.0 as in the piez. 2 toe scenario of the AOC valley fill design (Table 13.24). If the piezometric line was not elevated to the area of the selected failure plane, then the factor of safety remained unchanged. Steep slope angles also decreased the factors of safety.

- Two initial saturation conditions were modeled for the cumulative analysis. The saturation conditions were applied in SEEP/W, and SIGMA/W computed *insitu* stresses to be input into SLOPE/W for a factor of safety computation. The initial saturation condition of the gravity segregated durable rock underdrain was significant. The initial saturation condition altered the volume of water retained within the structure, and ultimately altered the factors of safety that resulted.

- In the cumulative analysis, the change in the factor of safety was not always in favor of either saturation condition from a structural standpoint. The significance of the initial saturation condition was that the water storage areas within the fill changed, and altered the factors of safety. It is important to note that the fills may be built in lifts or by end dumping. Sometimes when contractors build slopes, they cut into the original ground, and may use compaction equipment to help integrate the components of the structure. These considerations would likely alter the factors of safety.

- The cumulative analysis for the geomorphic valley fill alternative design yielded the highest factors of safety. Most cases produced factors of safety over 2.0. The most likely reason for these high factors of safety is that the geomorphic design has shallower slopes, and drains well. Geomorphic landform design can be utilized to reduce infiltration volumes by shortening runoff travel distances, increasing runoff water removal from a design site. A completed design should retain less water than the modeled results show because of vegetative cover and quick surface runoff.

- The geomorphic stability analysis described in section 13.4 yielded high factors of safety between 1.56 and 1.92 (Table 13.25) also; however, the water tables were exaggerated. The geomorphic profile described in section 13.4 still retains its structural integrity even when high volumes of water are being stored within it. None of the factors of safety even under the most critical circumstances tested yielded factors of safety under 1.0. The results prove that the geomorphic design can remain stable under extreme hydraulic conditions and varying geometries.

- The weakest structure assessed was by far the critical slope described in section 13.7. None of the factors of safety under any scenario analyzed yielded a factor of safety over 1.0. The factors of safety of this structure were expected to be low. The analysis of the critical slope was intended to illustrate that GeoFluv® does not consider slope stability, and can produce slopes that are not stable. As discussed in section 13.7, GeoFluv® does enable the designer to alter many components of the design to mitigate the slope stability problems that may occur due to rapid elevation changes.

- The analysis performed for the AOC valley fill design showed that the design could withstand *insitu* loads and slope angle under most conditions analyzed. Elevated pore pressures tended to result at the toe of the slope, and decreased the factor of safety. The most critical scenario was a totally saturated toe which yielded a factor of safety of 0.50 as shown in the piez. 2 toe AOC valley fill design model summary in Table 13.24.

- In the cumulative analysis, the SEEP/W assessment yielded results that implied that the structure drained well for the AOC valley fill design. There were small areas of water storage accumulation and elevated pore water pressures, but nothing which caused the factor of safety to drop below 1.0. For the cumulative analysis, the lowest factor of safety for the AOC valley fill design was 1.22 at the toe of the slope at an initially unsaturated durable rock underdrain condition.

- The as received material (material passing the 3/8 in. sieve) achieved a friction angle of 39.75^{o}, which implies that the factors of safety which were produced for the friction angle of 27.7^{o} were conservative. The as received AOC valley fill achieved a maximum factor of safety of 2.82, and a minimum factor of safety of 1.90. The as received geomorphic landform design achieved a maximum factor of safety of 3.36, and a minimum factor of safety of 3.09.

The conclusions pointed to supporting the idea of the geomorphic design of valley fills having advantages over Approximate Original Contour design applied to valley fills from a slope stability perspective.

A geomorphic fill showed a distinct advantage in the durability of the earthen structure geometry addressed. To further analyze the comparison between a geomorphic and AOC fill, probabilistic analyses could be performed to more thoroughly account for spatial variability. Spatial variability was only taken into account in these models as a sensitivity analysis. Field conditions of a slope structure would have a great deal of spatial variability both in compaction and in initial water content affecting soil strength and phreatic surface elevations.

The AOC valley fill design would be adequate if it remained sufficiently drained. If particle transport can occur and alter toe pore pressures, it is possible that some small slope failure may occur. The gradations that were found in the fill material in Chapter 9 and Chapter 12 show that particle transport probably would not be a concern for the laboratory tested unweathered sandstone.

Geomorphic design decreases erosion potential and therefore decreases maintenance demands theoretically, however, in order to fully address this potential benefit of geomorphic landform design, a thorough cost analysis with regard to construction techniques in AOC and geomorphic landform design would need to be investigated.

With the very limited amount of work that has been done with geomorphic fills in the region of central Appalachia, this research has provided a sound initial analysis to compare with previously used design techniques. Further research must be done as a thorough cost analysis, and different overburden property stability analysis local to Appalachia in order to make a fully informed decision as to whether or not geomorphic design would be feasible to implement in the reclamation of surface mines in central Appalachia.

References

Abdelghani, F.B., Simon, R., Aubertin, M, Molson, J. & Therrien, R. (2009). "Use of the hydrogeosphere code to simulate water flow and contaminants transport through mining wastes disposed in a symmetric open pit within fractured rock." *Proc. Tailings and Mine Waste*. Taylor and Francis Group. Vail, CO. 601-611.

ASTM Designation D422. (2007). "Standard Test Method for Particle-Size Analysis of Soils." *Annual Book of ASTM Standards, American Society of Testing Materials*, Easton, MD.

ASTM Designation D698. (2007). "Standard Test Methods for Laboratory Compaction Characteristics of Soil Using Standard Effort (12400 ft-lbf/ft^3 (600 KN-m/m^3))." *Annual Book of ASTM Standards, American Society of Testing Materials*, Easton, MD.

ASTM Designation D854. (2007). "Standard Test Methods for Specific Gravity of Soil Solids by Water Pycnometer." *Annual Book of ASTM Standards, American Society of Testing Materials*, Easton, MD.

ASTM Designation D2216. (2007). "Standard Test Methods for Laboratory Determination of Water (Moisture) Content of Soil and Rock by Mass." *Annual Book of ASTM Standards, American Society of Testing Materials*, Easton, MD.

ASTM Designation D2487. (2010). "Standard Practice for Classification of Soils for Engineering Purposes (Unified Soil Classification System)." *Annual Book of ASTM Standards, American Society of Testing Materials*, Easton, MD.

ASTM Designation D3080. (2007). "Standard Test Methods for.Direct Shear Test of Soils Under Consolidated Drained Conditions." *Annual Book of ASTM Standards, American Society of Testing Materials*, Easton, MD

ASTM Designation D4318. (2007). "Standard Test Methods for Liquid Limit, Plastic Limit, and Plasticity Index of Soils." *Annual Book of ASTM Standards, American Society of Testing Materials*, Easton, MD

ASTM Designation D-5856. (2007). "Standard test Method for Measurement of Hydraulic Conductivity of Porous Material using a Rigid-Wall, Compaction-Mold Permeameter." *Annual Book of ASTM Standards, American Society of Testing Materials*, Easton, MD.

Aubertin, M., Bussierre, B. & Chapuis, R. (1996). "Hydraulic conductivity of homogenized tailings from hard rock mines." *Can. Geotech. J.*, 33: 470-482.

Bugosh, N. 2004. Computerizing the fluvial geomorphic approach to land reclamation. National Meeting of the American Society of Mining and Reclamation and The 25th West Virginia Surface Mine Drainage Task Force, April 18-24, 240-258.

Bugosh N. 2009. A summary of some land surface and water quality monitoring results for constructed GeoFluv® landforms. *Revitalizing the Environment: Proven Solutions and Innovative Approaches*, National Meeting of the American Society of Mining and Reclamation, Billings, MT, May 30 – June 5, 153-175.

Das, Braja M. (2006). *Principles of Geotechnical Engineering* (7th ed.). Canada: Nelson Education Ltd.

Davis ED, Duffy RJ. 2009. King coal vs. reclamation: Federal regulation of mountaintop removal mining in Appalachia. *Administration and Society*, 41(6), 674692.

Eckels, R, Bugosh N. 2010. Natural approach to mined land reclamation. FIG Congress 2010.

Ferrari JR, Lookingbill TR, McCormick B, Townsend PA. 2009. Surface mining and reclamation effects on flood response of watersheds in the central Appalachian Plateau region. *Water Resources Research*, 45, W04407.

Fredlund, M.D., Wilson, G.W. & Fredlund, D.G. (1998). "Estimation of hydraulic properties of an unsaturated soil using a knowledge-based system." *Proc., Second Inter. Conf. on Unsat. Soils*. Beiling, China.

GEO-SLOPE International Ltd. (2007). *Stability Modeling with SLOPE/W 2007 Version.* Calgary, Alberta, Canada.

H. Gercek. April 22, 2006. "Poisson's ratio values for rocks." Elsevier. International Journal of Rock Mechanics & Mining Sciences 44 (2007) 1-13.

Hartman KJ, Kaller MD, Howell JW, Sweka JA. 2005. How much do valley fills influence headwater streams? *Hydrobiologia*, 532, 91-102.

Hasselman, M. 2002. Bragg v. W-Va. Coal Ass'n and the unfortunate limitation of citizen suits against the state in cooperative federalism regimes. *Ecol. Law Quart.* 29: 205-229.

Martin-Duque JF, Sanz MA, Bodoque JM, Lucia A, Martin-Moreno C. 2009. Restoring earth surface processes through landform design. A 13-year monitoring of a geomorphic reclamation model for quarries on slopes. *Earth Surface Processes and Landforms*, 35, 531-548.

Martin-Moreno C, Martin-Duque JF, Nicolau JM, Sanchez L, Ruiz R, Sanz MA, Lucia A, Zapico I. 2008. A geomorphic approach for the ecological restoration of kaolin mines at the Upper Tagus Natural Park (Spain). *6th European Conference on Ecological Restoration*, Ghent, Belgium, August 8-12.

Measles D., Bugosh N. 2007. Making and building a fluvial geomorphic reclamation design at an active dragline mine using the GeoFluv® design method. *30 Years of SMCRA and Beyond*, National Meeting of the American Society of Mining and Reclamation, Gillette, WY, June 2-7, 2007, 449-456.

Michael PR, Superfesky MJ, Uranowski LJ. 2010. "Challenges to applying the geomorphic and stream reclamation methodologies to mountaintop mining and excess spoil fill construction in steep-slope topography (e.g. Central Appalachia)." 2010 National Meeting of the American Society of Mining and Reclamation, Pittsburgh, PA *Bridging Reclamation, Science and the Community* June 5 - 11, 2010. R.I. Barnhisel (Ed.) Published by ASMR, 3134 Montavesta Rd., Lexington, KY 40502.

National Oceanic and Atmospheric Administration. (2012). "Precipitation Frequency Data Server (PFDS)." *Hydrometeorological Design Studies Center*, <http://hdsc.nws.noaa.gov> (Feb. 10, 2012).

Pond GJ, Passmore ME, Borsuk FA, Reynolds L, Rose CJ. 2008. Downstream effects of mountaintop coal mining: comparing biological conditions using family- and genus-level macroinvertebrate bioassessment tools. *J. N. Am. Benthol. Soc.*, 27(3), 717-737.

Robson M, Spotts R, Wade R, Erickson W. 2009. A case history: Limestone quarry reclamation using fluvial geomorphic design techniques.

Rosgen DL. 1994. A classification of natural rivers. *Catena*, 22, 169-199.

Rosgen, D. 1996. Applied River Morphology. Wildland Hydrology, Pagosa Springs, Colorado.

Superfesky, M., Michael P. (2007). "Excess Spoil Minimization and Fill Stability." Proc., SME Annual Meeting, SME, Denver, CO, 1-13.

Toy TJ, Chuse WR. 2005. " Topographic reconstruction: a geomorphic approach." *Ecological Engineering*, 24, 29-35.

USEPA. 2005. *Final Programmatic Environmental Impact Statement (PEIS) on Mountaintop Mining/Valley Fills in Appalachia* (EPA 9-03-R-05002). U.S. Environmental Protection Agency. http://www.epa.gov/region03/mtntop/eis2005.htm

West Virginia Department of Environmental Protection, Division of Mining and Reclamation. (1999). Permit Handbook: AOC and excess spoil disposal.

West Virginia Department of Environmental Protection (WVDEP), Permit ID S500809. Pine Creek No. 2 Surface Mine (July 12, 2007).

Appendices

Appendix I - Hydraulic Conductivity Data Tables

Hydraulic Conductivity: Test 1 – Standard Proctor Compaction (592.5 kJ/m^3)

Time	Vol (ml)	Δt (min)	Time (Seconds) Δt	Cumulative (Seconds) Δt	Time (Hours)	Δt (hours)
					Cumulative	
12/21/11 3:00 PM	0	0	0	0	0	0
1/3/11 12:45 PM	0	0	0	0	0	0
1/5/12 10:16 AM	0	21316	1278960	1278960	355.27	355.27
1/5/12 10:25 AM	30	21325	540	1279500	355.42	0.15
1/5/12 10:33 AM	50	21333	480	1279980	355.55	0.13
1/5/12 10:46 AM	70	21346	780	1280760	355.77	0.22
1/5/12 11:05 AM	95	21365	1140	1281900	356.08	0.32
1/5/12 11:20 AM	115	21380	900	1282800	356.33	0.25
1/5/12 11:35 AM	130	21395	900	1283700	356.58	0.25
1/5/12 11:50 AM	145	21410	900	1284600	356.83	0.25
1/5/12 12:05 PM	160	21425	900	1285500	357.08	0.25
1/5/12 12:20 PM	175	21440	900	1286400	357.33	0.25
1/5/12 12:35 PM	190	21455	900	1287300	357.58	0.25
1/5/12 12:50 PM	200	21470	900	1288200	357.83	0.25
1/5/12 1:05 PM	215	21485	900	1289100	358.08	0.25

1/5/12 1:20 PM	225	21500	900	1290000	358.33	0.25
1/5/12 1:35 PM	235	21515	900	1290900	358.58	0.25
1/5/12 1:50 PM	250	21530	900	1291800	358.83	0.25
1/5/12 2:05 PM	260	21545	900	1292700	359.08	0.25
1/5/12 2:20 PM	270	21560	900	1293600	359.33	0.25
1/5/12 2:40 PM	280	21580	1200	1294800	359.67	0.33
1/5/12 3:00 PM	295	21600	1200	1296000	360.00	0.33
1/5/12 3:30 PM	315	21630	1800	1297800	360.50	0.50
1/5/12 4:00 PM	335	21660	1800	1299600	361.00	0.50
1/5/12 4:30 PM	350	21690	1800	1301400	361.50	0.50
1/5/12 5:00 PM	370	21720	1800	1303200	362.00	0.50
1/5/12 5:30 PM	385	21750	1800	1305000	362.50	0.50
1/5/12 6:00 PM	400	21780	1800	1306800	363.00	0.50
1/5/12 6:30 PM	415	21810	1800	1308600	363.50	0.50
1/5/12 7:00 PM	430	21840	1800	1310400	364.00	0.50
1/5/12 8:53 PM	490	21953	6780	1317180	365.88	1.88
1/5/12 11:02 PM	540	22082	7740	1324920	368.03	2.15
1/6/12 1:04 AM	575	22204	7320	1332240	370.07	2.03
1/6/12 5:28 AM	630	22468	15840	1348080	374.47	4.40
1/6/12 10:08 AM	760	22748	16800	1364880	379.13	4.67
1/6/12 1:00 PM	800	22920	10320	1375200	382.00	2.87

Hydraulic Conductivity: Test 1 – Standard Proctor Compaction (592.5 kJ/m^3): Continued

Time	Vol (ml)	Δt (min)	Time (Seconds) Δt	Cumulative (Seconds) Δt	Time (Hours) Cumulative	Δt (hours)
1/6/12 8:35 PM	970	23375	12600	1402500	389.58	3.50
1/7/12 10:15 AM	1115	24195	49200	1451700	403.25	13.67
1/7/12 5:55 PM	1180	24655	27600	1479300	410.92	7.67
1/7/12 11:07 PM	1215	24967	18720	1498020	416.12	5.20
1/8/12 12:30 PM	1288	25770	48180	1546200	429.50	13.38
1/8/12 10:50 PM	1330	26390	37200	1583400	439.83	10.33
1/9/12 9:09 AM	1372	27009	37140	1620540	450.15	10.32
1/9/12 2:01 PM	1392	27301	17520	1638060	455.02	4.87
1/10/12 12:30 AM	1685	27930	37740	1675800	465.50	10.48
1/10/12 9:15 AM	1985	28455	31500	1707300	474.25	8.75
1/10/12 2:45 PM	2075	28785	19800	1727100	479.75	5.50
1/10/12 6:24 PM	2105	29004	13140	1740240	483.40	3.65
1/10/12 11:30 PM	2145	29310	18360	1758600	488.50	5.10
1/11/12 9:50 AM	2205	29930	37200	1795800	498.83	10.33
1/12/12 9:35 AM	2295	31355	85500	1881300	522.58	23.75
1/13/12 11:12 AM	2390	32892	92220	1973520	548.20	25.62
1/14/12 12:30 AM	2448	33690	47880	2021400	561.50	13.30

1/15/12 1:00 AM	2530	35160	88200	2109600	586.00	24.50
1/15/12 12:45 PM	2580	35865	42300	2151900	597.75	11.75
1/16/12 1:30 AM	2625	36630	45900	2197800	610.50	12.75
1/16/12 5:00 PM	2678	37560	55800	2253600	626.00	15.50
1/17/12 12:00 AM	2700	37980	25200	2278800	633.00	7.00
1/17/12 11:25 AM	2740	38665	41100	2319900	644.42	11.42
1/18/12 9:15 AM	2805	39975	78600	2398500	666.25	21.83
1/19/12 10:45 AM	2895	41505	91800	2490300	691.75	25.50

Hydraulic Conductivity: Test 1 – Standard Proctor Compaction (592.5 kJ/m^3): Continued

ΔV (cm^3)	i	Area (cm^2)	q_{in} (cm^3/sec)	q_{out} (cm^3/sec)	k (cm/sec)	k (m/sec)	Height of Water (cm)	Height of Water (in)	Time Step	N_{PV}	Qin (mL) Cumulative
0	100	81.07	0	0	0	0.00E+00	26.04	10.25	0	0	0
0	100	81.07	0	0	0	0.00E+00	25.08	9.88	1	0	0
0	100	81.07	3.80E-05	0.00E+00	0.00E+00	0.00E+00	23.18	9.13	2	0	0
30	100	81.07	4.50E-02	5.56E-02	6.85E-06	6.85E-08	22.86	9.00	3	0.11	30
20	100	81.07	5.07E-02	4.17E-02	5.14E-06	5.14E-08	22.70	8.94	4	0.18	50
20	100	81.07	3.12E-02	2.56E-02	3.16E-06	3.16E-08	22.54	8.88	5	0.25	70
25	100	81.07	0.00E+00	2.19E-02	2.70E-06	2.70E-08	22.38	8.81	6	0.34	95
20	100	81.07	2.70E-02	2.22E-02	2.74E-06	2.74E-08	22.38	8.81	7	0.42	115
15	100	81.07	2.70E-02	1.67E-02	2.06E-06	2.06E-08	22.23	8.75	8	0.47	130
15	100	81.07	2.70E-02	1.67E-02	2.06E-06	2.06E-08	22.07	8.69	9	0.52	145
15	100	81.07	0.00E+00	1.67E-02	2.06E-06	2.06E-08	21.91	8.63	10	0.58	160
15	100	81.07	0.00E+00	1.67E-02	2.06E-06	2.06E-08	21.91	8.63	11	0.63	175
15	100	81.07	2.70E-02	1.67E-02	2.06E-06	2.06E-08	21.91	8.63	12	0.69	190
10	100	81.07	2.70E-02	1.11E-02	1.37E-06	1.37E-08	21.75	8.56	13	0.72	200
15	100	81.07	0.00E+00	1.67E-02	2.06E-06	2.06E-08	21.59	8.50	14	0.78	215
10	100	81.07	0.00E+00	1.11E-02	1.37E-06	1.37E-08	21.59	8.50	15	0.81	225
10	100	81.07	2.70E-02	1.11E-02	1.37E-06	1.37E-08	21.59	8.50	16	0.85	235
15	100	81.07	2.70E-02	1.67E-02	2.06E-06	2.06E-08	21.43	8.44	17	0.90	250
10	100	81.07	0.00E+00	1.11E-02	1.37E-06	1.37E-08	21.27	8.38	18	0.94	260
10	100	81.07	0.00E+00	1.11E-02	1.37E-06	1.37E-08	21.27	8.38	19	0.98	270
10	100	81.07	2.03E-02	8.33E-03	1.03E-06	1.03E-08	21.27	8.38	20	1.01	280
15	100	81.07	0.00E+00	1.25E-02	1.54E-06	1.54E-08	21.11	8.31	21	1.07	295
20	100	81.07	1.35E-02	1.11E-02	1.37E-06	1.37E-08	21.11	8.31	22	1.14	315
20	100	81.07	1.35E-02	1.11E-02	1.37E-06	1.37E-08	20.96	8.25	23	1.21	335
15	100	81.07	1.35E-02	8.33E-03	1.03E-06	1.03E-08	20.80	8.19	24	1.27	350
20	100	81.07	1.35E-02	1.11E-02	1.37E-06	1.37E-08	20.64	8.13	25	1.34	370

15	100	81.07	1.35E-02	8.33E-03	1.03E-06	1.03E-08	20.48	8.06	26	1.39	385
15	100	81.07	0.00E+00	8.33E-03	1.03E-06	1.03E-08	20.32	8.00	27	1.45	400
15	100	81.07	0.00E+00	8.33E-03	1.03E-06	1.03E-08	20.32	8.00	28	1.50	415
15	100	81.07	4.05E-02	8.33E-03	1.03E-06	1.03E-08	20.32	8.00	29	1.56	430
60	100	81.07	7.17E-03	8.85E-03	1.09E-06	1.09E-08	19.84	7.81	30	1.77	490
50	100	81.07	6.28E-03	6.46E-03	7.97E-07	7.97E-09	19.53	7.69	31	1.95	540
35	100	81.07	9.97E-03	4.78E-03	5.90E-07	5.90E-09	19.21	7.56	32	2.08	575
55	100	81.07	3.07E-03	3.47E-03	4.28E-07	4.28E-09	18.73	7.38	33	2.28	630
130	100	81.07	5.79E-03	7.74E-03	9.54E-07	9.54E-09	18.42	7.25	34	2.75	760
40	100	81.07	4.71E-03	3.88E-03	4.78E-07	4.78E-09	17.78	7.00	35	2.89	800

Hydraulic Conductivity: Test 1 – Standard Proctor Compaction (592.5 kJ/m^3): Continued

ΔV (cm^3)	i	Area (cm^2)	q_{in} (cm^3/sec)	q_{out} (cm^3/sec)	k (cm/sec)	k (m/sec)	Height of Water (cm)	Height of Water (in)	Time Step	N_{PV}	Qin (mL) Cumulative
160	100	81.07	3.31E-03	1.09E-02	1.34E-06	1.34E-08	17.46	6.88	36	3.47	960
10	100	81.07	9.65E-03	7.94E-04	9.79E-08	9.79E-10	17.15	6.75	37	3.51	970
145	100	81.07	1.48E-03	2.95E-03	3.64E-07	3.64E-09	16.35	6.44	38	4.03	1115
65	100	81.07	8.81E-04	2.36E-03	2.90E-07	2.90E-09	15.88	6.25	39	4.27	1180
35	100	81.07	5.20E-03	1.87E-03	2.31E-07	2.31E-09	15.72	6.19	40	4.40	1215
73	100	81.07	1.01E-03	1.52E-03	1.87E-07	1.87E-09	15.08	5.94	41	4.66	1288
42	100	81.07	6.54E-04	1.13E-03	1.39E-07	1.39E-09	14.76	5.81	42	4.81	1330
42	100	81.07	3.27E-03	1.13E-03	1.39E-07	1.39E-09	14.61	5.75	43	4.96	1372
20	100	81.07	1.67E-02	1.14E-03	1.41E-07	1.41E-09	13.81	5.44	44	5.04	1392
293	100	81.07	7.73E-03	7.76E-03	9.58E-07	9.58E-09	11.91	4.69	45	6.10	1685
300	100	81.07	3.86E-03	9.52E-03	1.17E-06	1.17E-08	10.00	3.94	46	7.18	1985
90	100	81.07	1.23E-03	4.55E-03	5.61E-07	5.61E-09	9.21	3.63	47	7.51	2075
30	100	81.07	3.70E-03	2.28E-03	2.82E-07	2.82E-09	9.05	3.56	48	7.62	2105
40	100	81.07	2.65E-03	2.18E-03	2.69E-07	2.69E-09	8.73	3.44	49	7.76	2145
60	100	81.07	2.62E-03	1.61E-03	1.99E-07	1.99E-09	8.41	3.31	50	7.98	2205
90	100	81.07	1.42E-03	1.05E-03	1.30E-07	1.30E-09	7.78	3.06	51	8.30	2295

95	100	81.07	-1.21E-02	1.03E-03	1.27E-07	1.27E-09	6.99	2.75	52	8.65	2390
58	100	81.07	2.64E-02	1.21E-03	1.49E-07	1.49E-09	14.29	5.63	53	8.86	2448
82	100	81.07	5.51E-04	9.30E-04	1.15E-07	1.15E-09	6.03	2.38	54	9.16	2530
50	100	81.07	1.15E-03	1.18E-03	1.46E-07	1.46E-09	5.72	2.25	55	9.34	2580
45	100	81.07	1.06E-03	9.80E-04	1.21E-07	1.21E-09	5.40	2.13	56	9.50	2625
53	100	81.07	4.36E-04	9.50E-04	1.17E-07	1.17E-09	5.08	2.00	57	9.69	2678
22	100	81.07	9.65E-04	8.73E-04	1.08E-07	1.08E-09	4.92	1.94	58	9.77	2700
40	100	81.07	1.18E-03	9.73E-04	1.20E-07	1.20E-09	4.76	1.88	59	9.91	2740
65	100	81.07	8.66E-03	8.27E-04	1.02E-07	1.02E-09	4.45	1.75	60	10.15	2805
90	100	81.07	6.36E-03	9.80E-04	1.21E-07	1.21E-09	3.81	1.50	61	10.48	2895

Hydraulic Conductivity: Test 2 - Standard Proctor Compaction (592.5 kJ/m^3)

Time	Vol (ml)	Δt (min)	Time (Seconds) Δt	Cumulative (Seconds) Δt	Time (Hours) Cumulative	Δt (hours)
12/21/11 3:00 PM	0	0	0	0	0	0
1/3/12 12:35 AM	0	17855	1071300	1071300	297.58	297.58
1/5/12 10:16 AM	0	21316	207660	1278960	355.27	57.68
1/5/12 10:25 AM	15	21325	540	1279500	355.42	0.15
1/5/12 10:37 AM	20	21337	720	1280220	355.62	0.20
1/5/12 10:46 AM	35	21346	540	1280760	355.77	0.15
1/5/12 11:05 AM	40	21365	1140	1281900	356.08	0.32
1/5/12 11:20 AM	45	21380	900	1282800	356.33	0.25
1/5/12 11:35 AM	50	21395	900	1283700	356.58	0.25
1/5/12 11:50 AM	55	21410	900	1284600	356.83	0.25
1/5/12 12:05 PM	60	21425	900	1285500	357.08	0.25
1/5/12 12:20 PM	60	21440	900	1286400	357.33	0.25
1/5/12 12:35 PM	65	21455	900	1287300	357.58	0.25
1/5/12 12:50 PM	70	21470	900	1288200	357.83	0.25
1/5/12 1:05 PM	70	21485	900	1289100	358.08	0.25
1/5/12 1:20 PM	75	21500	900	1290000	358.33	0.25
1/5/12 1:35 PM	75	21515	900	1290900	358.58	0.25

1/5/12 1:50 PM	80	21530	900	1291800	358.83	0.25
1/5/12 2:05 PM	85	21545	900	1292700	359.08	0.25
1/5/12 2:40 PM	90	21580	2100	1294800	359.67	0.58
1/5/12 3:00 PM	95	21600	1200	1296000	360.00	0.33
1/5/12 3:30 PM	100	21630	1800	1297800	360.50	0.50
1/5/12 4:00 PM	110	21660	1800	1299600	361.00	0.50
1/5/12 4:30 PM	115	21690	1800	1301400	361.50	0.50
1/5/12 5:00 PM	120	21720	1800	1303200	362.00	0.50
1/5/12 6:00 PM	130	21780	3600	1306800	363.00	1.00
1/5/12 7:00 PM	140	21840	3600	1310400	364.00	1.00
1/5/12 8:53 PM	160	21953	6780	1317180	365.88	1.88
1/5/12 11:02 PM	180	22082	7740	1324920	368.03	2.15
1/6/12 1:04 AM	195	22204	7320	1332240	370.07	2.03
1/6/12 5:28 AM	235	22468	15840	1348080	374.47	4.40
1/6/12 8:40 AM	260	22660	11520	1359600	377.67	3.20
1/6/12 10:00 AM	270	22740	4800	1364400	379.00	1.33
1/6/12 5:05 PM	320	23165	25500	1389900	386.08	7.08

Hydraulic Conductivity: Test 2 - Standard Proctor Compaction (592.5 kJ/m^3): Continued

Time	Vol (ml)	Δt (min)	Time (Seconds) Δt	Cumulative (Seconds) Δt	Time (Hours)	Δt (hours)
					Cumulative	
1/6/12 8:35 PM	340	23375	12600	1402500	389.58	3.50
1/7/12 10:15 AM	425	24195	49200	1451700	403.25	13.67
1/7/12 5:55 PM	475	24655	27600	1479300	410.92	7.67
1/7/12 11:05 PM	515	24965	18600	1497900	416.08	5.17
1/8/12 12:30 PM	600	25770	48300	1546200	429.50	13.42
1/8/12 10:50 PM	660	26390	37200	1583400	439.83	10.33
1/9/12 9:09 AM	720	27009	37140	1620540	450.15	10.32
1/9/12 2:01 PM	750	27301	17520	1638060	455.02	4.87
1/10/12 12:30 AM	773	27930	37740	1675800	465.50	10.48
1/10/12 2:45 PM	795	28785	51300	1727100	479.75	14.25
1/16/12 5:00 PM	900	37560	55800	2253600	626.00	15.50
1/17/12 12:00 AM	910	37980	25200	2278800	633.00	7.00
1/17/12 11:25 AM	930	38665	41100	2319900	644.42	11.42
1/18/12 9:15 AM	960	39975	78600	2398500	666.25	21.83

Hydraulic Conductivity: Test 2 - Standard Proctor Compaction (592.5 kJ/m^3): Continued

ΔV (cm^3)	i	Area (cm^2)	q_{in} (cm^3/sec)	q_{out} (cm^3/sec)	k (cm/sec)	k (m/sec)	Height of Water (cm)	Height of Water (in)	Time Step	N_{PV}	Qin (mL) Cumulative
0	100	81.07	0	0	0	0.00E+00	27.94	11.00	1	0	0
0	100	81.07	1.14E-03	0.00E+00	0.00E+00	0.00E+00	26.83	10.56	2	0.00	0
0	100	81.07	-3.51E-04	0.00E+00	0.00E+00	0.00E+00	18.89	7.44	3	0.00	0
15	100	81.07	4.50E-02	2.78E-02	3.43E-06	3.43E-08	19.37	7.63	4	0.06	15
5	100	81.07	0.00E+00	6.94E-03	8.57E-07	8.57E-09	19.21	7.56	5	0.08	20
15	100	81.07	0.00E+00	2.78E-02	3.43E-06	3.43E-08	19.21	7.56	6	0.13	35
5	100	81.07	0.00E+00	4.39E-03	5.41E-07	5.41E-09	19.21	7.56	7	0.15	40
5	100	81.07	2.70E-02	5.56E-03	6.85E-07	6.85E-09	19.21	7.56	8	0.17	45
5	100	81.07	0.00E+00	5.56E-03	6.85E-07	6.85E-09	19.05	7.50	9	0.19	50
5	100	81.07	0.00E+00	5.56E-03	6.85E-07	6.85E-09	19.05	7.50	10	0.21	55
5	100	81.07	0.00E+00	5.56E-03	6.85E-07	6.85E-09	19.05	7.50	11	0.23	60
0	100	81.07	0.00E+00	0.00E+00	0.00E+00	0.00E+00	19.05	7.50	12	0.23	60
5	100	81.07	0.00E+00	5.56E-03	6.85E-07	6.85E-09	19.05	7.50	13	0.25	65
5	100	81.07	0.00E+00	5.56E-03	6.85E-07	6.85E-09	19.05	7.50	14	0.27	70
0	100	81.07	0.00E+00	0.00E+00	0.00E+00	0.00E+00	19.05	7.50	15	0.27	70
5	100	81.07	2.70E-02	5.56E-03	6.85E-07	6.85E-09	19.05	7.50	16	0.29	75
0	100	81.07	0.00E+00	0.00E+00	0.00E+00	0.00E+00	18.89	7.44	17	0.29	75
5	100	81.07	0.00E+00	5.56E-03	6.85E-07	6.85E-09	18.89	7.44	18	0.31	80
5	100	81.07	0.00E+00	5.56E-03	6.85E-07	6.85E-09	18.89	7.44	19	0.33	85
5	100	81.07	0.00E+00	2.38E-03	2.94E-07	2.94E-09	18.89	7.44	20	0.35	90
5	100	81.07	0.00E+00	4.17E-03	5.14E-07	5.14E-09	18.89	7.44	21	0.37	95
5	100	81.07	0.00E+00	2.78E-03	3.43E-07	3.43E-09	18.89	7.44	22	0.38	100
10	100	81.07	1.35E-02	5.56E-03	6.85E-07	6.85E-09	18.89	7.44	23	0.42	110
5	100	81.07	0.00E+00	2.78E-03	3.43E-07	3.43E-09	18.73	7.38	24	0.44	115
5	100	81.07	1.35E-02	2.78E-03	3.43E-07	3.43E-09	18.73	7.38	25	0.46	120
10	100	81.07	0.00E+00	2.78E-03	3.43E-07	3.43E-09	18.57	7.31	26	0.50	130

10	100	81.07	6.76E-03	2.78E-03	3.43E-07	3.43E-09	18.57	7.31	27	0.54	140
20	100	81.07	3.59E-03	2.95E-03	3.64E-07	3.64E-09	18.42	7.25	28	0.62	160
20	100	81.07	0.00E+00	2.58E-03	3.19E-07	3.19E-09	18.26	7.19	29	0.69	180
15	100	81.07	0.00E+00	2.05E-03	2.53E-07	2.53E-09	18.26	7.19	31	0.75	195
40	100	81.07	4.61E-03	2.53E-03	3.11E-07	3.11E-09	18.26	7.19	32	0.90	235
25	100	81.07	0.00E+00	2.17E-03	2.68E-07	2.68E-09	17.78	7.00	33	1.00	260
10	100	81.07	1.01E-02	2.08E-03	2.57E-07	2.57E-09	17.78	7.00	34	1.04	270
50	100	81.07	9.54E-04	1.96E-03	2.42E-07	2.42E-09	17.46	6.88	35	1.23	320

Hydraulic Conductivity: Test 2 - Standard Proctor Compaction (592.5 kJ/m^3): Continued

ΔV (cm^3)	i	Area (cm^2)	q_{in} (cm^3/sec)	q_{out} (cm^3/sec)	k (cm/sec)	k (m/sec)	Height of Water (cm)	Height of Water (in)	Time Step	N_{PV}	Qin (mL) Cumulative
20	100	81.07	7.72E-03	1.59E-03	1.96E-07	1.96E-09	17.30	6.81	36	1.31	340
85	100	81.07	9.89E-04	1.73E-03	2.13E-07	2.13E-09	16.67	6.56	37	1.63	425
50	100	81.07	1.76E-03	1.81E-03	2.23E-07	2.23E-09	16.35	6.44	38	1.83	475
40	100	81.07	3.92E-03	2.15E-03	2.65E-07	2.65E-09	16.03	6.31	39	1.98	515
85	100	81.07	2.01E-03	1.76E-03	2.17E-07	2.17E-09	15.56	6.13	40	2.31	600
60	100	81.07	6.54E-04	1.61E-03	1.99E-07	1.99E-09	14.92	5.88	41	2.54	660
60	100	81.07	1.96E-03	1.62E-03	1.99E-07	1.99E-09	14.76	5.81	42	2.77	720
30	100	81.07	0.00E+00	1.71E-03	2.11E-07	2.11E-09	14.29	5.63	43	2.88	750
23	100	81.07	1.29E-03	6.09E-04	7.52E-08	7.52E-10	14.29	5.63	44	2.97	773
22	100	81.07	4.74E-04	4.29E-04	5.29E-08	5.29E-10	13.97	5.50	45	3.06	795
37	100	81.07	4.36E-04	6.63E-04	8.18E-08	8.18E-10	13.02	5.13	51	3.46	900
10	100	81.07	0.00E+00	3.97E-04	4.89E-08	4.89E-10	12.86	5.06	52	3.50	910
20	100	81.07	4.79E-02	4.87E-04	6.00E-08	6.00E-10	12.86	5.06	53	3.58	930
30	100	81.07	2.48E-02	3.82E-04	4.71E-08	4.71E-10	12.70	5.00	54	3.69	960

Hydraulic Conductivity: Test 3- Standard Proctor Compaction (592.5 kJ/m^3)

Time	Vol (ml)	Δt (min)	Time (Seconds) Δt	Cumulative (Seconds) Δt	Time (Hours) Cumulative	Δt (hours)
12/21/11 3:00 PM	0	0	0	0	0	0
1/3/12 12:45 PM	0	18585	1115100	1115100	309.75	309.75
1/5/12 10:16 AM	0	21316	163860	1278960	355.27	45.52
1/5/12 10:25 AM	40	21325	540	1279500	355.42	0.15
1/5/12 10:33 AM	75	21333	480	1279980	355.55	0.13
1/5/12 10:46 AM	110	21346	780	1280760	355.77	0.22
1/5/12 11:05 AM	155	21365	1140	1281900	356.08	0.32
1/5/12 11:20 AM	185	21380	900	1282800	356.33	0.25
1/5/12 11:35 AM	215	21395	900	1283700	356.58	0.25
1/5/12 11:50 AM	240	21410	900	1284600	356.83	0.25
1/5/12 12:05 PM	270	21425	900	1285500	357.08	0.25
1/5/12 12:20 PM	300	21440	900	1286400	357.33	0.25
1/5/12 12:35 PM	325	21455	900	1287300	357.58	0.25
1/5/12 12:50 PM	350	21470	900	1288200	357.83	0.25
1/5/12 1:05 PM	380	21485	900	1289100	358.08	0.25
1/5/12 1:20 PM	405	21500	900	1290000	358.33	0.25
1/5/12 1:35 PM	430	21515	900	1290900	358.58	0.25

1/5/12 1:50 PM	460	21530	900	1291800	358.83	0.25
1/5/12 2:05 PM	490	21545	900	1292700	359.08	0.25
1/5/12 2:20 PM	515	21560	900	1293600	359.33	0.25
1/5/12 2:40 PM	560	21580	1200	1294800	359.67	0.33
1/5/12 3:00 PM	600	21600	1200	1296000	360.00	0.33
1/5/12 3:30 PM	670	21630	1800	1297800	360.50	0.50
1/5/12 4:00 PM	730	21660	1800	1299600	361.00	0.50
1/5/12 4:30 PM	795	21690	1800	1301400	361.50	0.50
1/5/12 5:00 PM	855	21720	1800	1303200	362.00	0.50
1/5/12 5:30 PM	920	21750	1800	1305000	362.50	0.50
1/5/12 6:00 PM	950	21780	1800	1306800	363.00	0.50
1/5/12 6:30 PM	965	21810	1800	1308600	363.50	0.50
1/5/12 7:00 PM	985	21840	1800	1310400	364.00	0.50
1/5/12 8:53 PM	1060	21953	6780	1317180	365.88	1.88
1/5/12 11:02 PM	1135	22082	7740	1324920	368.03	2.15
1/6/12 1:04 AM	1215	22204	7320	1332240	370.07	2.03
1/6/12 5:28 AM	1365	22468	15840	1348080	374.47	4.40
1/6/12 8:40 AM	1475	22660	11520	1359600	377.67	3.20

Hydraulic Conductivity: Test 3- Standard Proctor Compaction (592.5 kJ/m^3): Continued

Time	Vol (ml)	Δt (min)	Time (Seconds) Δt	Cumulative (Seconds) Δt	Time (Hours) Cumulative	Δt (hours)
1/6/12 10:00 AM	1515	22740	4800	1364400	379.00	1.33
1/6/12 1:00 PM	1595	22920	10800	1375200	382.00	3.00
1/6/12 5:05 PM	1705	23165	14700	1389900	386.08	4.08
1/6/12 8:35 PM	1795	23375	12600	1402500	389.58	3.50
1/7/12 10:15 AM	2148	24195	49200	1451700	403.25	13.67
1/7/12 5:55 PM	2693	24655	27600	1479300	410.92	7.67
1/7/12 11:07 PM	2823	24967	18720	1498020	416.12	5.20
1/8/12 12:30 PM	3033	25770	48180	1546200	429.50	13.38
1/8/12 10:50 PM	3308	26390	37200	1583400	439.83	10.33
1/9/12 9:09 AM	3533	27009	37140	1620540	450.15	10.32
1/9/12 2:01 PM	3648	27301	17520	1638060	455.02	4.87
1/10/12 12:30 AM	3761	27930	36000	1675800	465.50	10.00
1/10/12 9:15 AM	3841	28455	31500	1707300	474.25	8.75
1/10/12 2:45 PM	3883	28785	19800	1727100	479.75	5.50
1/10/12 6:24 PM	3913	29004	13140	1740240	483.40	3.65
1/10/12 11:30 PM	3951	29310	18360	1758600	488.50	5.10
1/11/12 9:50 AM	4033	29930	37200	1795800	498.83	10.33
1/12/12 9:30 AM	4183	31350	85200	1881000	522.50	23.67
1/13/12 11:12	4323	32892	92520	1973520	548.20	25.70

AM						
1/14/12 12:30 AM	4388	33690	47880	2021400	561.50	13.30
1/15/12 1:00 AM	4441	35160	88200	2109600	586.00	24.50
1/15/12 12:45 PM	4531	35865	42300	2151900	597.75	11.75
1/16/12 1:30 AM	4573	36630	45900	2197800	610.50	12.75
1/16/12 5:00 PM	4663	37560	55800	2253600	626.00	15.50
1/17/12 12:00 AM	4701	37980	25200	2278800	633.00	7.00
1/17/12 11:25 AM	4758	38665	41100	2319900	644.42	11.42
1/18/12 9:15 AM	4868	39975	78600	2398500	666.25	21.83
1/19/12 10:45 AM	5003	41505	91800	2490300	691.75	25.50

Hydraulic Conductivity: Test 3- Standard Proctor Compaction (592.5 kJ/m^3): Continued

ΔV (cm^3)	i	Area (cm^2)	q_{in} (cm^3/sec)	q_{out} (cm^3/sec)	k (cm/sec)	k (m/sec)	Height of Water (cm)	Height of Water (in)	Time Step	N_{PV}	Qin (mL) Cumulative
0	100	81.07	0	0	0	0.00E+00	42.70	16.81	1	0	0
0	100	81.07	1.96E-04	0.00E+00	0.00E+00	0.00E+00	41.43	16.31	2	0.00	0
0	100	81.07	2.97E-04	0.00E+00	0.00E+00	0.00E+00	40.01	15.75	3	0.00	0
40	100	81.07	9.01E-02	7.41E-02	9.14E-06	9.14E-08	39.69	15.63	4	0.15	40
35	100	81.07	5.07E-02	7.29E-02	8.99E-06	8.99E-08	39.37	15.50	5	0.28	75
35	100	81.07	9.35E-02	4.49E-02	5.53E-06	5.53E-08	39.21	15.44	6	0.41	110
45	100	81.07	0.00E+00	3.95E-02	4.87E-06	4.87E-08	38.74	15.25	7	0.57	155
30	100	81.07	2.70E-02	3.33E-02	4.11E-06	4.11E-08	38.74	15.25	8	0.68	185
30	100	81.07	5.40E-02	3.33E-02	4.11E-06	4.11E-08	38.58	15.19	9	0.79	215
25	100	81.07	2.70E-02	2.78E-02	3.43E-06	3.43E-08	38.26	15.06	10	0.89	240
30	100	81.07	2.70E-02	3.33E-02	4.11E-06	4.11E-08	38.10	15.00	11	1.00	270
30	100	81.07	2.70E-02	3.33E-02	4.11E-06	4.11E-08	37.94	14.94	12	1.11	300
25	100	81.07	5.40E-02	2.78E-02	3.43E-06	3.43E-08	37.78	14.88	13	1.20	325
25	100	81.07	0.00E+00	2.78E-02	3.43E-06	3.43E-08	37.47	14.75	14	1.29	350
30	100	81.07	5.40E-02	3.33E-02	4.11E-06	4.11E-08	37.47	14.75	15	1.40	380
25	100	81.07	0.00E+00	2.78E-02	3.43E-06	3.43E-08	37.15	14.63	16	1.49	405
25	100	81.07	5.40E-02	2.78E-02	3.43E-06	3.43E-08	37.15	14.63	17	1.59	430
30	100	81.07	0.00E+00	3.33E-02	4.11E-06	4.11E-08	36.83	14.50	18	1.70	460
30	100	81.07	5.40E-02	3.33E-02	4.11E-06	4.11E-08	36.83	14.50	19	1.81	490
25	100	81.07	5.40E-02	2.78E-02	3.43E-06	3.43E-08	36.51	14.38	20	1.90	515
45	100	81.07	2.03E-02	3.75E-02	4.63E-06	4.63E-08	36.20	14.25	21	2.07	560
40	100	81.07	4.05E-02	3.33E-02	4.11E-06	4.11E-08	36.04	14.19	22	2.21	600
70	100	81.07	4.05E-02	3.89E-02	4.80E-06	4.80E-08	35.72	14.06	23	2.47	670
60	100	81.07	4.05E-02	3.33E-02	4.11E-06	4.11E-08	35.24	13.88	24	2.69	730
65	100	81.07	4.05E-02	3.61E-02	4.45E-06	4.45E-08	34.77	13.69	25	2.93	795
60	100	81.07	2.70E-02	3.33E-02	4.11E-06	4.11E-08	34.29	13.50	26	3.16	855

65	100	81.07	1.35E-02	3.61E-02	4.45E-06	4.45E-08	33.97	13.38	27	3.40	920
30	100	81.07	1.35E-02	1.67E-02	2.06E-06	2.06E-08	33.81	13.31	28	3.51	950
15	100	81.07	1.35E-02	8.33E-03	1.03E-06	1.03E-08	33.66	13.25	29	3.56	965
20	100	81.07	4.05E-02	1.11E-02	1.37E-06	1.37E-08	33.50	13.19	30	3.64	985
75	100	81.07	1.08E-02	1.11E-02	1.36E-06	1.36E-08	33.02	13.00	31	3.91	1060
75	100	81.07	9.43E-03	9.69E-03	1.20E-06	1.20E-08	32.54	12.81	32	4.19	1135
80	100	81.07	1.99E-02	1.09E-02	1.35E-06	1.35E-08	32.07	12.63	33	4.48	1215
150	100	81.07	7.68E-03	9.47E-03	1.17E-06	1.17E-08	31.12	12.25	34	5.04	1365
110	100	81.07	4.22E-03	9.55E-03	1.18E-06	1.18E-08	30.32	11.94	35	5.44	1475

Hydraulic Conductivity: Test 3- Standard Proctor Compaction (592.5 kJ/m^3): Continued

ΔV (cm^3)	i	Area (cm^2)	q_{in} (cm^3/sec)	q_{out} (cm^3/sec)	k (cm/sec)	k (m/sec)	Height of Water (cm)	Height of Water (in)	Time Step	N_{PV}	Qin (mL) Cumulative
40	100	81.07	1.52E-02	8.33E-03	1.03E-06	1.03E-08	30.00	11.81	36	5.59	1515
80	100	81.07	9.01E-03	7.41E-03	9.14E-07	9.14E-09	29.53	11.63	37	5.89	1595
110	100	81.07	6.62E-03	7.48E-03	9.23E-07	9.23E-09	28.89	11.38	38	6.29	1705
90	100	81.07	2.70E-02	7.14E-03	8.81E-07	8.81E-09	28.26	11.13	39	6.62	1795
353	100	81.07	3.95E-03	7.17E-03	8.85E-07	8.85E-09	26.04	10.25	40	7.93	2148
545	100	81.07	5.29E-03	1.97E-02	2.44E-06	2.44E-08	24.77	9.75	41	9.94	2693
130	100	81.07	1.69E-02	6.94E-03	8.57E-07	8.57E-09	23.81	9.38	42	10.42	2823
210	100	81.07	1.51E-03	4.36E-03	5.38E-07	5.38E-09	21.75	8.56	43	11.19	3033
275	100	81.07	9.81E-03	7.39E-03	9.12E-07	9.12E-09	21.27	8.38	44	12.21	3308
225	100	81.07	3.27E-03	6.06E-03	7.47E-07	7.47E-09	18.89	7.44	45	13.04	3533
115	100	81.07	0.00E+00	6.56E-03	8.10E-07	8.10E-09	18.10	7.13	46	13.46	3648
113	100	81.07	1.35E-03	3.14E-03	3.87E-07	3.87E-09	17.15	6.75	48	13.88	3761
80	100	81.07	1.54E-03	2.54E-03	3.13E-07	3.13E-09	16.83	6.63	49	14.18	3841
42	100	81.07	1.23E-03	2.12E-03	2.62E-07	2.62E-09	16.51	6.50	50	14.33	3883
30	100	81.07	3.70E-03	2.28E-03	2.82E-07	2.82E-09	16.35	6.44	51	14.44	3913
38	100	81.07	3.97E-03	2.07E-03	2.55E-07	2.55E-09	16.03	6.31	52	14.58	3951

82	100	81.07	4.58E-03	2.20E-03	2.72E-07	2.72E-09	15.56	6.13	53	14.88	4033
150	100	81.07	1.71E-03	1.76E-03	2.17E-07	2.17E-09	14.45	5.69	54	15.44	4183
140	100	81.07	1.05E-03	1.51E-03	1.87E-07	1.87E-09	13.49	5.31	55	15.95	4323
65	100	81.07	2.54E-03	1.36E-03	1.67E-07	1.67E-09	12.86	5.06	56	16.19	4388
53	100	81.07	5.51E-04	6.01E-04	7.41E-08	7.41E-10	12.07	4.75	57	16.39	4441
90	100	81.07	1.15E-03	2.13E-03	2.62E-07	2.62E-09	11.75	4.63	58	16.72	4531
42	100	81.07	2.12E-03	9.15E-04	1.13E-07	1.13E-09	11.43	4.50	59	16.88	4573
90	100	81.07	4.36E-04	1.61E-03	1.99E-07	1.99E-09	10.80	4.25	60	17.21	4663
38	100	81.07	9.65E-04	1.51E-03	1.86E-07	1.86E-09	10.64	4.19	61	17.35	4701
57	100	81.07	3.91E-02	1.39E-03	1.71E-07	1.71E-09	10.48	4.13	62	17.56	4758
110	100	81.07	1.92E-02	1.40E-03	1.73E-07	1.73E-09	9.84	3.88	63	17.97	4868
135	100	81.07	1.48E-02	1.47E-03	1.81E-07	1.81E-09	8.89	3.50	64	18.46	5003

Hydraulic Conductivity: Test 1 – 34% Proctor Compaction (203.6 kJ/m^3)

Time	Vol(ml)	Δt (min)	Time (Seconds) Δt	Cumulative	Time (Hours) Cumulative	Δt (hours)
9/22/11 4:22 PM	0.00	0.00	0.00	0.00	0.00	0.00
9/22/11 4:32 PM	190.00	10.00	600.00	600.00	0.17	0.17
9/22/11 8:30 PM	216.00	248.00	14280.00	14880.00	4.13	3.97
9/23/11 12:30 AM	218.00	488.00	14400.00	29280.00	8.13	4.00
9/23/11 10:30 AM	220.00	1088.00	36000.00	65280.00	18.13	10.00
9/23/11 1:30 PM	223.00	1268.00	10800.00	76080.00	21.13	3.00
9/23/11 5:05 PM	223.00	1483.00	12900.00	88980.00	24.72	3.58
9/24/11 12:00 AM	225.00	1898.00	24900.00	113880.00	31.63	6.92
9/24/11 12:00 PM	225.00	2618.00	43200.00	157080.00	43.63	12.00
9/24/11 6:00 PM	225.00	2978.00	21600.00	178680.00	49.63	6.00
9/25/11 12:00 AM	225.00	3338.00	21600.00	200280.00	55.63	6.00
9/25/11 2:00 PM	225.00	4178.00	50400.00	250680.00	69.63	14.00
9/25/11 8:50 PM	226.00	4588.00	24600.00	275280.00	76.47	6.83
9/26/11 1:30 AM	228.00	4868.00	16800.00	292080.00	81.13	4.67
9/26/11 11:00 AM	228.00	5438.00	34200.00	326280.00	90.63	9.50
9/26/11 3:00 PM	228.00	5678.00	14400.00	340680.00	94.63	4.00
9/26/11 7:10 PM	228.00	5928.00	15000.00	355680.00	98.80	4.17
9/27/11 1:00 AM	228.00	6278.00	21000.00	376680.00	104.63	5.83
9/27/11 11:00 AM	228.00	6878.00	36000.00	412680.00	114.63	10.00
9/27/11 3:35 PM	228.00	7153.00	16500.00	429180.00	119.22	4.58
9/28/11 4:30 PM	220.00	8648.00	89700.00	518880.00	144.13	24.92
9/29/11 2:45 PM	310.00	9983.00	80100.00	598980.00	166.38	22.25
9/29/11 9:20 PM	330.00	10378.00	23700.00	622680.00	172.97	6.58
9/30/11 12:45 PM	360.00	11303.00	55500.00	678180.00	188.38	15.42
9/30/11 4:30 PM	365.00	11528.00	13500.00	691680.00	192.13	3.75
9/30/11 8:00 PM	370.00	11738.00	12600.00	704280.00	195.63	3.50
10/1/11 12:30 AM	378.00	12008.00	16200.00	720480.00	200.13	4.50
10/1/11 1:15 PM	396.00	12773.00	45900.00	766380.00	212.88	12.75
10/1/11 9:02 PM	408.00	13240.00	28020.00	794400.00	220.67	7.78
10/2/11 2:10 PM	425.00	14268.00	61680.00	856080.00	237.80	17.13

10/3/11 12:40 AM	435.00	14898.00	37800.00	893880.00	248.30	10.50
10/3/11 10:20 AM	440.00	15478.00	34800.00	928680.00	257.97	9.67
10/4/11 12:00 PM	468.00	17018.00	92400.00	1021080.00	283.63	25.67
10/5/11 10:45 AM	488.00	18383.00	81900.00	1102980.00	306.38	22.75
10/6/11 2:45 PM	512.00	20063.00	100800.00	1203780.00	334.38	28.00
10/7/11 12:45 PM	533.00	21383.00	79200.00	1282980.00	356.38	22.00
10/8/11 10:00 PM	565.00	23378.00	119700.00	1402680.00	389.63	33.25
10/9/11 7:45 PM	585.00	24683.00	78300.00	1480980.00	411.38	21.75
10/10/11 3:00 PM	600.00	25838.00	69300.00	1550280.00	430.63	19.25
10/11/11 12:10 PM	620.00	27108.00	76200.00	1626480.00	451.80	21.17
10/12/11 12:30 PM	640.00	28568.00	87600.00	1714080.00	476.13	24.33

$\Delta V(cm^3)$	i	Area (cm^2)	q_{in} (cm^3/sec)	q_{out} (cm^3/sec)	k (cm/sec)	k (m/sec)	Height of Water (cm)	Height of Water (in)	Time Step	N_{PV}	Qin (mL) Cumulative
0.00	15	81.07	0.00	0.00	0.00	0.000E+00	23.65	9.31	1.00	0.00	0
190.00	15	81.07	0.08	0.32	0.00	2.604E-06	22.23	8.75	2.00	0.53	190
26.00	15	81.07	0.00	0.00	0.00	1.497E-08	21.91	8.63	3.00	0.60	216
2.00	15	81.07	0.00	0.00	0.00	1.142E-09	21.91	8.63	4.00	0.61	218
2.00	15	81.07	0.00	0.00	0.00	4.568E-10	21.59	8.50	5.00	0.62	220
3.00	15	81.07	0.00	0.00	0.00	2.284E-09	21.59	8.50	6.00	0.62	223
0.00	15	81.07	0.00	0.00	0.00	0.000E+00	21.59	8.50	7.00	0.62	223
2.00	15	81.07	0.00	0.00	0.00	6.605E-10	21.59	8.50	8.00	0.63	225
0.00	15	81.07	0.00	0.00	0.00	0.000E+00	21.59	8.50	9.00	0.63	225
0.00	15	81.07	0.00	0.00	0.00	0.000E+00	21.59	8.50	10.00	0.63	225
0.00	15	81.07	0.00	0.00	0.00	0.000E+00	21.59	8.50	11.00	0.63	225
0.00	15	81.07	0.00	0.00	0.00	0.000E+00	21.59	8.50	12.00	0.63	225
1.00	15	81.07	0.00	0.00	0.00	3.343E-10	21.43	8.44	13.00	0.63	226
2.00	15	81.07	0.00	0.00	0.00	9.789E-10	21.43	8.44	14.00	0.64	228
0.00	15	81.07	0.00	0.00	0.00	0.000E+00	21.43	8.44	15.00	0.64	228
0.00	15	81.07	0.00	0.00	0.00	0.000E+00	21.43	8.44	16.00	0.64	228
0.00	15	81.07	0.00	0.00	0.00	0.000E+00	21.43	8.44	17.00	0.64	228
0.00	15	81.07	0.00	0.00	0.00	0.000E+00	21.43	8.44	18.00	0.64	228
0.00	15	81.07	0.00	0.00	0.00	0.000E+00	21.27	8.38	19.00	0.64	228
0.00	15	81.07	0.00	0.00	0.00	0.000E+00	21.27	8.38	20.00	0.64	228
-8.00	15	81.07	0.00	0.00	0.00	-7.334E-10	21.27	8.38	21.00	0.62	220
90.00	15	81.07	0.00	0.00	0.00	9.239E-09	20.64	8.13	22.00	0.87	310
20.00	15	81.07	0.00	0.00	0.00	6.939E-09	20.48	8.06	23.00	0.92	330
30.00	15	81.07	0.00	0.00	0.00	4.445E-09	20.32	8.00	24.00	1.01	360
5.00	15	81.07	0.00	0.00	0.00	3.046E-09	20.16	7.94	25.00	1.02	365
5.00	15	81.07	0.00	0.00	0.00	3.263E-09	20.16	7.94	26.00	1.04	370
8.00	15	81.07	0.00	0.00	0.00	4.061E-09	20.16	7.94	27.00	1.06	378

18.00	15	81.07	0.00	0.00	0.00	3.225E-09	20.00	7.88	28.00	1.11	396
12.00	15	81.07	0.00	0.00	0.00	3.522E-09	20.00	7.88	29.00	1.14	408
17.00	15	81.07	0.00	0.00	0.00	2.266E-09	19.69	7.75	30.00	1.19	425
10.00	15	81.07	0.00	0.00	0.00	2.175E-09	19.69	7.75	31.00	1.22	435
5.00	15	81.07	0.00	0.00	0.00	1.181E-09	19.69	7.75	32.00	1.23	440
28.00	15	81.07	0.00	0.00	0.00	2.492E-09	19.37	7.63	33.00	1.31	468
20.00	15	81.07	0.00	0.00	0.00	2.008E-09	19.37	7.63	34.00	1.37	488
24.00	15	81.07	0.00	0.00	0.00	1.958E-09	19.05	7.50	35.00	1.43	512
21.00	15	81.07	0.00	0.00	0.00	2.180E-09	19.05	7.50	36.00	1.49	533
32.00	15	81.07	0.00	0.00	0.00	2.198E-09	18.73	7.38	37.00	1.58	565
20.00	15	81.07	0.00	0.00	0.00	2.100E-09	18.73	7.38	38.00	1.64	585
15.00	15	81.07	0.00	0.00	0.00	1.780E-09	18.57	7.31	39.00	1.68	600
20.00	15	81.07	0.00	0.00	0.00	2.158E-09	18.42	7.25	40.00	1.74	620
20.00	15	81.07	0.03	0.00	0.00	1.877E-09	18.26	7.19	41.00	1.79	640

Back pressure saturation was attempted on September 28 at 4:30 p.m. for a duration of 22 hours and 15 minutes. The effort was an attempt to remove additional air trapped in the specimen.

Hydraulic Conductivity: Test 2 – 34% Proctor Compaction (203.6 kJ/m^3)

Sample - GrayPermM32: Test Started on 9/22/2011 at 4:22:00 p.m.								
Time	Vol (ml)	Δt (min)	Time (Seconds)		Time (Hours)		ΔV (cm^3)	i
			Δt	Cumulative	Cumulative	Δt		
9/22/11 4:22 PM	0	0	0	0	0.00	0.00	0	15
9/22/11 4:32 PM	0	10	600	600	0.17	0.17	0	15
9/22/11 8:30 PM	0	248	14280	14880	4.13	3.97	0	15
9/23/11 12:30 AM	0	488	14400	29280	8.13	4.00	0	15
9/23/11 10:30 AM	10	1088	36000	65280	18.13	10.00	10	15
9/23/11 1:30 PM	20	1268	10800	76080	21.13	3.00	10	15
9/23/11 5:05 PM	20	1483	12900	88980	24.72	3.58	0	15
9/24/11 12:00 AM	21	1898	24900	113880	31.63	6.92	1	15
9/24/11 12:00 PM	21	2618	43200	157080	43.63	12.00	0	15
9/24/11 6:00 PM	23	2978	21600	178680	49.63	6.00	2	15
9/25/11 12:00 AM	23	3338	21600	200280	55.63	6.00	0	15
9/25/11 2:00 PM	26	4178	50400	250680	69.63	14.00	3	15
9/25/11 8:50 PM	30	4588	24600	275280	76.47	6.83	4	15
9/26/11 1:30 AM	30	4868	16800	292080	81.13	4.67	0	15
9/26/11 11:00 AM	32	5438	34200	326280	90.63	9.50	2	15
9/26/11 3:00 PM	35	5678	14400	340680	94.63	4.00	3	15
9/26/11 7:10 PM	50	5928	15000	355680	98.80	4.17	15	15
9/27/11 1:00 AM	50	6278	21000	376680	104.63	5.83	0	15
9/27/11 11:00 AM	50	6878	36000	412680	114.63	10.00	0	15
9/27/11 3:35 PM	50	7153	16500	429180	119.22	4.58	0	15
9/28/11 4:30 PM	53	8648	89700	518880	144.13	24.92	3	15
9/29/11 2:45 PM	68	9983	80100	598980	166.38	22.25	15	15
9/29/11 9:20 PM	70	10378	23700	622680	172.97	6.58	2	15
9/30/11 12:45 PM	72	11303	55500	678180	188.38	15.42	2	15
9/30/11 4:30 PM	72	11528	13500	691680	192.13	3.75	0	15
9/30/11 8:00 PM	75	11738	12600	704280	195.63	3.50	3	15
10/1/11 12:30 AM	75	12008	16200	720480	200.13	4.50	0	15

10/1/11 1:15 PM	78	12773	45900	766380	212.88	12.75	3	15
10/1/11 9:02 PM	78	13240	28020	794400	220.67	7.78	0	15
10/2/11 2:10 PM	90	14268	61680	856080	237.80	17.13	12	15
10/3/11 12:40 AM	100	14898	37800	893880	248.30	10.50	10	15
10/3/11 10:20 AM	105	15478	34800	928680	257.97	9.67	5	15
10/4/11 12:00 PM	125	17018	92400	1021080	283.63	25.67	20	15
10/5/11 10:45 AM	140	18383	81900	1102980	306.38	22.75	15	15
10/6/11 2:45 PM	160	20063	100800	1203780	334.38	28.00	20	15
10/7/11 12:45 PM	176	21383	79200	1282980	356.38	22.00	16	15
10/8/11 10:00 PM	200	23378	119700	1402680	389.63	33.25	24	15
10/9/11 7:45 PM	220	24683	78300	1480980	411.38	21.75	20	15
10/10/11 3:00 PM	230	25838	69300	1550280	430.63	19.25	10	15
10/11/11 12:10 PM	248	27108	76200	1626480	451.80	21.17	18	15
10/12/11 12:30 PM	265	28568	87600	1714080	476.13	24.33	17	15

Area (cm^2)	qin (cm^3/sec)	qout (cm^3/sec)	k (cm/sec)	k (m/sec)	Height of Water (cm)	Height of Water (in)	Time Step	N_{PV}	Qin (mL) Cumulative
81.07	0.000E+00	0.000E+00	0.00E+00	0.00E+00	28.89	11.38	1	0.000	0
81.07	8.107E-02	0.000E+00	0.00E+00	0.00E+00	28.89	11.38	2	0.000	0
81.07	0.000E+00	0.000E+00	0.00E+00	0.00E+00	28.58	11.25	3	0.000	0
81.07	3.378E-03	0.000E+00	0.00E+00	0.00E+00	28.58	11.25	4	0.000	0
81.07	0.000E+00	2.778E-04	2.28E-07	2.28E-09	28.26	11.13	5	0.028	10
81.07	2.252E-03	9.259E-04	7.61E-07	7.61E-09	28.26	11.13	6	0.057	20
81.07	0.000E+00	0.000E+00	0.00E+00	0.00E+00	28.10	11.06	7	0.057	20
81.07	0.000E+00	4.016E-05	3.30E-08	3.30E-10	28.10	11.06	8	0.059	21
81.07	0.000E+00	0.000E+00	0.00E+00	0.00E+00	28.10	11.06	9	0.059	21
81.07	0.000E+00	9.259E-05	7.61E-08	7.61E-10	28.10	11.06	10	0.065	23
81.07	0.000E+00	0.000E+00	0.00E+00	0.00E+00	28.10	11.06	11	0.065	23
81.07	4.826E-04	5.952E-05	4.89E-08	4.89E-10	28.10	11.06	12	0.074	26
81.07	0.000E+00	1.626E-04	1.34E-07	1.34E-09	27.94	11.00	13	0.085	30
81.07	0.000E+00	0.000E+00	0.00E+00	0.00E+00	27.94	11.00	14	0.085	30
81.07	0.000E+00	5.848E-05	4.81E-08	4.81E-10	27.94	11.00	15	0.091	32
81.07	1.689E-03	2.083E-04	1.71E-07	1.71E-09	27.94	11.00	16	0.099	35
81.07	0.000E+00	1.000E-03	8.22E-07	8.22E-09	27.78	10.94	17	0.142	50
81.07	0.000E+00	0.000E+00	0.00E+00	0.00E+00	27.78	10.94	18	0.142	50
81.07	0.000E+00	0.000E+00	0.00E+00	0.00E+00	27.78	10.94	19	0.142	50
81.07	1.327E-02	0.000E+00	0.00E+00	0.00E+00	27.78	10.94	20	0.142	50
81.07	2.711E-04	3.344E-05	2.75E-08	2.75E-10	26.35	10.38	21	0.150	53
81.07	0.000E+00	1.873E-04	1.54E-07	1.54E-09	26.19	10.31	22	0.193	68
81.07	0.000E+00	8.439E-05	6.94E-08	6.94E-10	26.19	10.31	23	0.198	70
81.07	0.000E+00	3.604E-05	2.96E-08	2.96E-10	26.19	10.31	24	0.204	72
81.07	0.000E+00	0.000E+00	0.00E+00	0.00E+00	26.19	10.31	25	0.204	72
81.07	0.000E+00	2.381E-04	1.96E-07	1.96E-09	26.19	10.31	26	0.212	75
81.07	0.000E+00	0.000E+00	0.00E+00	0.00E+00	26.19	10.31	27	0.212	75
81.07	0.000E+00	6.536E-05	5.37E-08	5.37E-10	26.19	10.31	28	0.221	78
81.07	8.680E-04	0.000E+00	0.00E+00	0.00E+00	26.19	10.31	29	0.221	78
81.07	3.943E-04	1.946E-04	1.60E-07	1.60E-09	26.04	10.25	30	0.255	90
81.07	0.000E+00	2.646E-04	2.18E-07	2.18E-09	25.88	10.19	31	0.283	100

81.07	6.989E-04	1.437E-04	1.18E-07	1.18E-09	25.88	10.19	32	0.297	105
81.07	2.632E-04	2.165E-04	1.78E-07	1.78E-09	25.72	10.13	33	0.354	125
81.07	2.970E-04	1.832E-04	1.51E-07	1.51E-09	25.56	10.06	34	0.397	140
81.07	2.413E-04	1.984E-04	1.63E-07	1.63E-09	25.40	10.00	35	0.453	160
81.07	3.071E-04	2.020E-04	1.66E-07	1.66E-09	25.24	9.94	36	0.499	176
81.07	2.032E-04	2.005E-04	1.65E-07	1.65E-09	25.08	9.88	37	0.567	200
81.07	0.000E+00	2.554E-04	2.10E-07	2.10E-09	24.92	9.81	38	0.623	220
81.07	3.509E-04	1.443E-04	1.19E-07	1.19E-09	24.92	9.81	39	0.652	230
81.07	3.192E-04	2.362E-04	1.94E-07	1.94E-09	24.77	9.75	40	0.703	248
81.07	4.303E-02	1.941E-04	1.60E-07	1.60E-09	24.61	9.69	41	0.751	265

Hydraulic Conductivity: Test 3 – 34% Proctor Compaction (203.6 kJ/m^3)

Sample - GrayPermM33: Test Started on 9/22/2011 at 4:22:00 p.m.									
Time	Vol (ml)	Δt (min)	Time (Seconds)		Time (Hours)		ΔV (cm^3)	i	Area (cm^2)
			Δt	Cumulative	Cumulative	Δt			
9/22/11 4:22 PM	0	0	0	0	0.00	0.00	0	15	81.07
9/22/11 4:32 PM	0	10	600	600	0.17	0.17	0	15	81.07
9/22/11 8:30 PM	0	248	14280	14880	4.13	3.97	0	15	81.07
9/23/11 12:30 AM	0	488	14400	29280	8.13	4.00	0	15	81.07
9/23/11 10:30 AM	5	1088	36000	65280	18.13	10.00	5	15	81.07
9/23/11 1:30 PM	10	1268	10800	76080	21.13	3.00	5	15	81.07
9/23/11 5:05 PM	10	1483	12900	88980	24.72	3.58	0	15	81.07
9/24/11 12:00 AM	10	1898	24900	113880	31.63	6.92	0	15	81.07
9/24/11 12:00 PM	10	2618	43200	157080	43.63	12.00	0	15	81.07
9/24/11 6:00 PM	10	2978	21600	178680	49.63	6.00	0	15	81.07
9/25/11 12:00 AM	10	3338	21600	200280	55.63	6.00	0	15	81.07
9/25/11 2:00 PM	10	4178	50400	250680	69.63	14.00	0	15	81.07
9/25/11 8:50 PM	25	4588	24600	275280	76.47	6.83	15	15	81.07
9/26/11 1:30 AM	25	4868	16800	292080	81.13	4.67	0	15	81.07
9/26/11 11:00 AM	30	5438	34200	326280	90.63	9.50	5	15	81.07
9/26/11 3:00 PM	32	5678	14400	340680	94.63	4.00	2	15	81.07
9/26/11 7:10 PM	35	5928	15000	355680	98.80	4.17	3	15	81.07
9/27/11 1:00 AM	40	6278	21000	376680	104.63	5.83	5	15	81.07
9/27/11 11:00 AM	40	6878	36000	412680	114.63	10.00	0	15	81.07
9/27/11 3:35 PM	50	7153	16500	429180	119.22	4.58	10	15	81.07
9/28/11 4:30 PM	50	8648	89700	518880	144.13	24.92	0	15	81.07
9/29/11 2:45 PM	97	9983	80100	598980	166.38	22.25	47	15	81.07
9/29/11 9:20 PM	129	10378	23700	622680	172.97	6.58	32	15	81.07
9/30/11 12:45 PM	188	11303	55500	678180	188.38	15.42	59	15	81.07
9/30/11 4:30 PM	202	11528	13500	691680	192.13	3.75	14	15	81.07
9/30/11 8:00 PM	212	11738	12600	704280	195.63	3.50	10	15	81.07
10/1/11 12:30 AM	230	12008	16200	720480	200.13	4.50	18	15	81.07
10/1/11 1:15 PM	270	12773	45900	766380	212.88	12.75	40	15	81.07
10/1/11 9:02 PM	298	13240	28020	794400	220.67	7.78	28	15	81.07

10/2/11 2:10 PM	335	14268	61680	856080	237.80	17.13	37	15	81.07
10/3/11 12:40 AM	357	14898	37800	893880	248.30	10.50	22	15	81.07
10/3/11 10:20 AM	368	15478	34800	928680	257.97	9.67	11	15	81.07
10/4/11 12:00 PM	400	17018	92400	1021080	283.63	25.67	32	15	81.07
10/5/11 10:45 AM	437	18383	81900	1102980	306.38	22.75	37	15	81.07
10/6/11 2:45 PM	480	20063	1E+05	1203780	334.38	28.00	43	15	81.07
10/7/11 12:45 PM	515	21383	79200	1282980	356.38	22.00	35	15	81.07
10/8/11 10:00 PM	568	23378	1E+05	1402680	389.63	33.25	53	15	81.07
10/9/11 7:45 PM	600	24683	78300	1480980	411.38	21.75	32	15	81.07
10/10/11 3:00 PM	628	25838	69300	1550280	430.63	19.25	28	15	81.07
10/11/11 12:10 PM	658	27108	76200	1626480	451.80	21.17	30	15	81.07
10/12/11 12:30 PM	690	28568	87600	1714080	476.13	24.33	32	15	81.07

qin (cm^3/sec)	qout (cm^3/sec)	k (cm/sec)	k (m/sec)	Height of Water (cm)	Height of Water (in)	Time Step	N_{PV}	Q_{in} (mL) Cumulative
0.00E+00	0.00E+00	0.00E+00	0.00E+00	29.37	11.56	1	0.00	0
0.00E+00	0.00E+00	0.00E+00	0.00E+00	29.21	11.50	2	0.00	0
0.00E+00	0.00E+00	0.00E+00	0.00E+00	29.21	11.50	3	0.00	0
6.76E-03	0.00E+00	0.00E+00	0.00E+00	29.21	11.50	4	0.00	0
0.00E+00	1.39E-04	1.14E-07	1.14E-09	28.58	11.25	5	0.02	5
2.25E-03	4.63E-04	3.81E-07	3.81E-09	28.58	11.25	6	0.03	10
0.00E+00	0.00E+00	0.00E+00	0.00E+00	28.42	11.19	7	0.03	10
0.00E+00	0.00E+00	0.00E+00	0.00E+00	28.42	11.19	8	0.03	10
0.00E+00	0.00E+00	0.00E+00	0.00E+00	28.42	11.19	9	0.03	10
0.00E+00	0.00E+00	0.00E+00	0.00E+00	28.42	11.19	10	0.03	10
0.00E+00	0.00E+00	0.00E+00	0.00E+00	28.42	11.19	11	0.03	10
9.65E-04	0.00E+00	0.00E+00	0.00E+00	28.42	11.19	12	0.03	10
0.00E+00	6.10E-04	5.01E-07	5.01E-09	28.10	11.06	13	0.08	25
0.00E+00	0.00E+00	0.00E+00	0.00E+00	28.10	11.06	14	0.08	25
0.00E+00	1.46E-04	1.20E-07	1.20E-09	28.10	11.06	15	0.10	30
1.69E-03	1.39E-04	1.14E-07	1.14E-09	28.10	11.06	16	0.10	32
0.00E+00	2.00E-04	1.64E-07	1.64E-09	27.94	11.00	17	0.11	35
0.00E+00	2.38E-04	1.96E-07	1.96E-09	27.94	11.00	18	0.13	40
0.00E+00	0.00E+00	0.00E+00	0.00E+00	27.94	11.00	19	0.13	40
2.95E-03	6.06E-04	4.98E-07	4.98E-09	27.94	11.00	20	0.16	50
2.98E-03	0.00E+00	0.00E+00	0.00E+00	27.62	10.88	21	0.16	50
3.04E-04	5.87E-04	4.82E-07	4.82E-09	25.88	10.19	22	0.31	97
3.08E-03	1.35E-03	1.11E-06	1.11E-08	25.72	10.13	23	0.41	129
4.38E-04	1.06E-03	8.74E-07	8.74E-09	25.24	9.94	24	0.60	188
0.00E+00	1.04E-03	8.53E-07	8.53E-09	25.08	9.88	25	0.65	202
1.93E-03	7.94E-04	6.53E-07	6.53E-09	25.08	9.88	26	0.68	212
1.50E-03	1.11E-03	9.14E-07	9.14E-09	24.92	9.81	27	0.74	230
5.30E-04	8.71E-04	7.17E-07	7.17E-09	24.77	9.75	28	0.87	270
2.60E-03	9.99E-04	8.22E-07	8.22E-09	24.61	9.69	29	0.96	298
0.00E+00	6.00E-04	4.93E-07	4.93E-09	24.13	9.50	30	1.08	335
6.43E-04	5.82E-04	4.79E-07	4.79E-09	24.13	9.50	31	1.15	357

1.40E-03	3.16E-04	2.60E-07	2.60E-09	23.97	9.44	32	1.18	368
5.26E-04	3.46E-04	2.85E-07	2.85E-09	23.65	9.31	33	1.29	400
5.94E-04	4.52E-04	3.71E-07	3.71E-09	23.34	9.19	34	1.40	437
2.41E-04	4.27E-04	3.51E-07	3.51E-09	23.02	9.06	35	1.54	480
9.21E-04	4.42E-04	3.63E-07	3.63E-09	22.86	9.00	36	1.65	515
2.03E-04	4.43E-04	3.64E-07	3.64E-09	22.38	8.81	37	1.83	568
3.11E-04	4.09E-04	3.36E-07	3.36E-09	22.23	8.75	38	1.93	600
3.51E-04	4.04E-04	3.32E-07	3.32E-09	22.07	8.69	39	2.02	628
6.38E-04	3.94E-04	3.24E-07	3.24E-09	21.91	8.63	40	2.11	658
3.78E-02	3.65E-04	3.00E-07	3.00E-09	21.59	8.50	41	2.22	690

Hydraulic Conductivity: Test 1 – 11% Proctor Compaction (67.85 kJ/m^3)

Sample - GrayPermL1: Test Started on 10/18/2011 at 2:40:00 p.m.									
Time	**Vol(ml)**	**Δt (min)**	**Time (Seconds)**		**Time (Hours)**		**ΔV(cm^3)**	**i**	**Area (cm^2)**
			Δt	**Cumulative**	**Cumulative**	**Δt**			
10/18/11 2:40 PM	0	0.00	0	0	0.00	0	0	15	81.07
10/18/11 3:00 PM	10	20.00	1200	1200	0.33	0.33	10	15	81.07
10/18/11 3:12 PM	15	32.00	720	1920	0.53	0.20	5	15	81.07
10/18/11 3:27 PM	18	47.00	900	2820	0.78	0.25	3	5	81.07
10/18/11 4:00 PM	20	80.00	1980	4800	1.33	0.55	2	5	81.07
10/18/11 4:17 PM	25	97.00	1020	5820	1.62	0.28	5	15	81.07
10/18/11 7:24 PM	40	284.00	11220	17040	4.73	3.12	15	15	81.07
10/19/11 1:30 AM	65	650.00	21960	39000	10.83	6.10	25	15	81.07
10/19/11 9:45 AM	105	1145.00	29700	68700	19.08	8.25	40	15	81.07
10/19/11 12:50 PM	115	1330.00	11100	79800	22.17	3.08	10	15	81.07
10/19/11 3:10 PM	120	1470.00	8400	88200	24.50	2.33	5	15	81.07
10/19/11 5:30 PM	128	1610.00	8400	96600	26.83	2.33	8	15	81.07
10/19/11 11:30 PM	140	1970.00	21600	118200	32.83	6.00	12	15	81.07
10/20/11 12:10 PM	165	2730.00	45600	163800	45.50	12.67	25	15	81.07
10/20/11 3:00 PM	170	2900.00	10200	174000	48.33	2.83	5	15	81.07
10/21/11 3:00 PM	200	4340.00	86400	260400	72.33	24.00	30	15	81.07
10/22/11 12:00 PM	230	5600.00	75600	336000	93.33	21.00	30	15	81.07
10/23/11 5:10 PM	265	7350.00	105000	441000	122.50	29.17	35	15	81.07
10/24/11 10:55 AM	288	8415.00	63900	504900	140.25	17.75	23	15	81.07
10/25/11 2:15 PM	318	10055.00	98400	603300	167.58	27.33	30	15	81.07
10/26/11 9:30 AM	335	11210.00	69300	672600	186.83	19.25	17	15	81.07
10/26/11 4:00 PM	345	11600.00	23400	696000	193.33	6.50	10	15	81.07
10/27/11 2:00 PM	365	12920.00	79200	775200	215.33	22.00	20	15	81.07
10/28/11 1:00 PM	380	14300.00	82800	858000	238.33	23.00	15	15	81.07
10/29/11 12:00 PM	400	15680.00	82800	940800	261.33	23.00	20	15	81.07
10/30/11 7:30 PM	428	17570.00	113400	1054200	292.83	31.50	28	15	81.07
10/31/11 10:00 AM	440	18440.00	52200	1106400	307.33	14.50	12	15	81.07

q_{in} (cm^3/sec)	q_{out} (cm^3/sec)	k (cm/sec)	k (m/sec)	Height of Water (cm)	Height of Water (in)	Time Step	N_{PV}	Q_{in} (mL) Cumulative
0	0	0.00	0.00	30.32	11.938	1	0.00	0
2.03E-02	8.33E-03	6.85E-06	6.85E-08	30.16	11.875	2	0.03	10
0.00E+00	6.94E-03	5.71E-06	5.71E-08	30.00	11.813	3	0.04	15
2.70E-02	3.33E-03	8.22E-06	8.22E-08	30.00	11.813	4	0.05	18
0.00E+00	1.01E-03	2.49E-06	2.49E-08	29.85	11.750	5	0.05	20
0.00E+00	4.90E-03	4.03E-06	4.03E-08	29.85	11.750	6	0.06	25
4.34E-03	1.34E-03	1.10E-06	1.10E-08	29.85	11.750	7	0.10	40
1.11E-03	1.14E-03	9.36E-07	9.36E-09	29.53	11.625	8	0.16	65
8.19E-04	1.35E-03	1.11E-06	1.11E-08	29.37	11.563	9	0.26	105
0.00E+00	9.01E-04	7.41E-07	7.41E-09	29.21	11.500	10	0.29	115
0.00E+00	5.95E-04	4.89E-07	4.89E-09	29.21	11.500	11	0.30	120
5.79E-03	9.52E-04	7.83E-07	7.83E-09	29.21	11.500	12	0.32	128
1.13E-03	5.56E-04	4.57E-07	4.57E-09	28.89	11.375	13	0.35	140
0.00E+00	5.48E-04	4.51E-07	4.51E-09	28.73	11.313	14	0.41	165
-2.38E-03	4.90E-04	4.03E-07	4.03E-09	28.73	11.313	15	0.43	170
8.44E-04	3.47E-04	2.86E-07	2.86E-09	28.89	11.375	16	0.50	200
6.43E-04	3.97E-04	3.26E-07	3.26E-09	28.42	11.188	17	0.58	230
2.32E-04	3.33E-04	2.74E-07	2.74E-09	28.10	11.063	18	0.66	265
7.61E-04	3.60E-04	2.96E-07	2.96E-09	27.94	11.000	19	0.72	288
2.47E-04	3.05E-04	2.51E-07	2.51E-09	27.62	10.875	20	0.80	318
3.51E-04	2.45E-04	2.02E-07	2.02E-09	27.46	10.813	21	0.84	335
1.04E-03	4.27E-04	3.51E-07	3.51E-09	27.31	10.750	22	0.86	345
3.07E-04	2.53E-04	2.08E-07	2.08E-09	27.15	10.688	23	0.91	365
2.94E-04	1.81E-04	1.49E-07	1.49E-09	26.99	10.625	24	0.95	380
2.94E-04	2.42E-04	1.99E-07	1.99E-09	26.83	10.563	25	1.00	400
4.29E-04	2.47E-04	2.03E-07	2.03E-09	26.67	10.500	26	1.07	428
7.73E-02	2.30E-04	1.89E-07	1.89E-09	26.35	10.375	27	1.10	440

Hydraulic Conductivity: Test 2 – 11% Proctor Compaction (67.85 kJ/m^3)

Sample - GrayPermL2: Test Started on 10/18/2011 at 2:40:00 p.m.									
Time	**Vol(ml)**	**Δt (min)**	**Time (Seconds)**		**Time (Hours)**		**ΔV (cm^3)**	**i**	**Area (cm^2)**
			Δt	**Cumulative**	**Cumulative**	**Δt**			
10/18/11 2:40 PM	0	0.00	0	0	0.00	0	0	15	81.07
10/18/11 3:00 PM	145	20.00	1200	1200	0.33	0.33	145	15	81.07
10/18/11 3:12 PM	190	32.00	720	1920	0.53	0.20	45	15	81.07
10/18/11 3:27 PM	238	47.00	900	2820	0.78	0.25	48	5	81.07
10/18/11 4:00 PM	338	80.00	1980	4800	1.33	0.55	100	5	81.07
10/18/11 4:17 PM	380	97.00	1020	5820	1.62	0.28	42	15	81.07
10/18/11 7:24 PM	825	284.00	11220	17040	4.73	3.12	445	15	81.07
10/19/11 1:30 AM	1555	650.00	21960	39000	10.83	6.10	730	15	81.07
10/19/11 9:45 AM	1988	1145.00	29700	68700	19.08	8.25	433	15	81.07
10/19/11 12:50 PM	2033	1330.00	11100	79800	22.17	3.08	45	15	81.07
10/19/11 3:10 PM	2056	1470.00	8400	88200	24.50	2.33	23	15	81.07
10/19/11 5:30 PM	2078	1610.00	8400	96600	26.83	2.33	22	15	81.07
10/19/11 11:30 PM	2128	1970.00	21600	118200	32.83	6.00	50	15	81.07
10/20/11 12:10 PM	2248	2730.00	45600	163800	45.50	12.67	120	15	81.07
10/20/11 3:00 PM	2270	2900.00	10200	174000	48.33	2.83	22	15	81.07
10/21/11 3:00 PM	2376	4340.00	86400	260400	72.33	24.00	106	15	81.07
10/22/11 12:00 PM	2458	5600.00	75600	336000	93.33	21.00	82	15	81.07
10/23/11 5:10 PM	2568	7350.00	105000	441000	122.50	29.17	110	15	81.07
10/24/11 10:55 AM	2653	8415.00	63900	504900	140.25	17.75	85	15	81.07
10/25/11 2:15 PM	2758	10055.00	98400	603300	167.58	27.33	105	15	81.07
10/26/11 9:30 AM	2803	11210.00	69300	672600	186.83	19.25	45	15	81.07
10/26/11 4:00 PM	2818	11600.00	23400	696000	193.33	6.50	15	15	81.07
10/27/11 2:00 PM	2843	12920.00	79200	775200	215.33	22.00	25	15	81.07
10/28/11 1:00 PM	2868	14300.00	82800	858000	238.33	23.00	25	15	81.07
10/29/11 12:00 PM	2890	15680.00	82800	940800	261.33	23.00	22	15	81.07
10/30/11 7:30 PM	2918	17570.00	113400	1054200	292.83	31.50	28	15	81.07
10/31/11 10:00 AM	2936	18440.00	52200	1106400	307.33	14.50	18	15	81.07

q_{in} (cm^3/sec)	q_{out} (cm^3/sec)	k (cm/sec)	k (m/sec)	Height of Water (cm)	Height of Water (in)	Time Step	N_{PV}	Q_{in} (mL) Cumulative
0	0	0.00	0.00	30.16	11.875	1	0.00	0
4.05E-02	1.21E-01	9.94E-05	9.94E-07	29.21	11.500	2	0.38	145
6.76E-02	6.25E-02	5.14E-05	5.14E-07	28.89	11.375	3	0.49	190
1.35E-01	5.33E-02	1.32E-04	1.32E-06	28.58	11.250	4	0.62	238
1.23E-02	5.05E-02	1.25E-04	1.25E-06	27.78	10.938	5	0.88	338
4.29E-01	4.12E-02	3.39E-05	3.39E-07	27.62	10.875	6	0.99	380
6.72E-02	3.97E-02	3.26E-05	3.26E-07	24.77	9.750	7	2.14	825
3.99E-02	3.32E-02	2.73E-05	2.73E-07	19.84	7.813	8	4.03	1555
1.64E-03	1.46E-02	1.20E-05	1.20E-07	14.13	5.563	9	5.15	1988
2.19E-03	4.05E-03	3.33E-06	3.33E-08	13.81	5.438	10	5.27	2033
0.00E+00	2.74E-03	2.25E-06	2.25E-08	13.65	5.375	11	5.33	2056
8.69E-03	2.62E-03	2.15E-06	2.15E-08	13.65	5.375	12	5.39	2078
-1.24E-02	2.31E-03	1.90E-06	1.90E-08	13.18	5.188	13	5.52	2128
9.07E-03	2.63E-03	2.16E-06	2.16E-08	14.92	5.875	14	5.83	2248
1.19E-02	2.16E-03	1.77E-06	1.77E-08	12.22	4.813	15	5.88	2270
8.44E-04	1.23E-03	1.01E-06	1.01E-08	11.43	4.500	16	6.16	2376
1.61E-03	1.08E-03	8.92E-07	8.92E-09	10.95	4.313	17	6.37	2458
9.27E-04	1.05E-03	8.61E-07	8.61E-09	10.16	4.000	18	6.66	2568
1.52E-03	1.33E-03	1.09E-06	1.09E-08	9.53	3.750	19	6.88	2653
4.94E-04	1.07E-03	8.77E-07	8.77E-09	8.89	3.500	20	7.15	2758
3.51E-04	6.49E-04	5.34E-07	5.34E-09	8.57	3.375	21	7.27	2803
0.00E+00	6.41E-04	5.27E-07	5.27E-09	8.41	3.313	22	7.30	2818
6.14E-04	3.16E-04	2.60E-07	2.60E-09	8.41	3.313	23	7.37	2843
2.94E-04	3.02E-04	2.48E-07	2.48E-09	8.10	3.188	24	7.43	2868
5.87E-04	2.66E-04	2.18E-07	2.18E-09	7.94	3.125	25	7.49	2890
0.00E+00	2.47E-04	2.03E-07	2.03E-09	7.62	3.000	26	7.56	2918
2.24E-02	3.45E-04	2.84E-07	2.84E-09	7.62	3.000	27	7.61	2936

Hydraulic Conductivity: Test 3 – 11% Proctor Compaction (67.85 kJ/m^3)

Sample - GrayPermL3: Test Started on 10/18/2011 at 2:40:00 p.m.									
Time	**Vol(ml)**	**Δt (min)**	**Time (Seconds)**		**Time (Hours)**		**ΔV (cm^3)**	**i**	**Area (cm^2)**
			Δt	**Cumulative**	**Cumulative**	**Δt**			
10/18/11 2:40 PM	0	0.00	0	0	0.00	0	0	15	81.07
10/18/11 3:00 PM	122	20.00	1200	1200	0.33	0.33	122	15	81.07
10/18/11 3:12 PM	137	32.00	720	1920	0.53	0.20	15	15	81.07
10/18/11 3:27 PM	152	47.00	900	2820	0.78	0.25	15	5	81.07
10/18/11 4:00 PM	182	80.00	1980	4800	1.33	0.55	30	5	81.07
10/18/11 4:17 PM	200	97.00	1020	5820	1.62	0.28	18	15	81.07
10/18/11 7:24 PM	430	284.00	11220	17040	4.73	3.12	230	15	81.07
10/19/11 1:30 AM	890	650.00	21960	39000	10.83	6.10	460	15	81.07
10/19/11 9:45 AM	1678	1145.00	29700	68700	19.08	8.25	788	15	81.07
10/19/11 12:50 PM	1708	1330.00	11100	79800	22.17	3.08	30	15	81.07
10/19/11 3:10 PM	1728	1470.00	8400	88200	24.50	2.33	20	15	81.07
10/19/11 5:30 PM	1756	1610.00	8400	96600	26.83	2.33	28	15	81.07
10/19/11 11:30 PM	1818	1970.00	21600	118200	32.83	6.00	62	15	81.07
10/20/11 12:10 PM	2153	2730.00	45600	163800	45.50	12.67	335	15	81.07
10/20/11 3:00 PM	2228	2900.00	10200	174000	48.33	2.83	75	15	81.07
10/21/11 3:00 PM	2396	4340.00	86400	260400	72.33	24.00	168	15	81.07
10/22/11 12:00 PM	2548	5600.00	75600	336000	93.33	21.00	152	15	81.07
10/23/11 5:10 PM	2788	7350.00	105000	441000	122.50	29.17	240	15	81.07
10/24/11 10:55 AM	2953	8415.00	63900	504900	140.25	17.75	165	15	81.07
10/25/11 2:15 PM	3178	10055.00	98400	603300	167.58	27.33	225	15	81.07
10/26/11 9:30 AM	3298	11210.00	69300	672600	186.83	19.25	120	15	81.07
10/26/11 4:00 PM	3316	11600.00	23400	696000	193.33	6.50	18	15	81.07
10/27/11 2:00 PM	3348	12920.00	79200	775200	215.33	22.00	32	15	81.07
10/28/11 1:00 PM	3386	14300.00	82800	858000	238.33	23.00	38	15	81.07
10/29/11 12:00 PM	3416	15680.00	82800	940800	261.33	23.00	30	15	81.07
10/30/11 7:30 PM	3471	17570.00	113400	1054200	292.83	31.50	55	15	81.07
10/31/11 10:00 AM	3496	18440.00	52200	1106400	307.33	14.50	25	15	81.07

q_{in} (cm^3/sec)	q_{out} (cm^3/sec)	k (cm/sec)	k (m/sec)	Height of Water (cm)	Height of Water (in)	Time Step	N_{PV}	Q_{in} (mL) Cumulative
0	0	0.00	0.00	26.51	10.438	1	0.00	0
2.03E-02	1.02E-01	8.36E-05	8.36E-07	26.35	10.375	2	0.32	122
0.00E+00	2.08E-02	1.71E-05	1.71E-07	26.19	10.313	3	0.35	137
5.40E-02	1.67E-02	4.11E-05	4.11E-07	26.19	10.313	4	0.39	152
1.23E-02	1.52E-02	3.74E-05	3.74E-07	25.88	10.188	5	0.47	182
1.91E-01	1.76E-02	1.45E-05	1.45E-07	25.72	10.125	6	0.52	200
4.34E-02	2.05E-02	1.69E-05	1.69E-07	24.45	9.625	7	1.11	430
3.21E-02	2.09E-02	1.72E-05	1.72E-07	21.27	8.375	8	2.30	890
1.64E-03	2.65E-02	2.18E-05	2.18E-07	16.67	6.563	9	4.34	1678
2.19E-03	2.70E-03	2.22E-06	2.22E-08	16.35	6.438	10	4.42	1708
2.90E-03	2.38E-03	1.96E-06	1.96E-08	16.19	6.375	11	4.47	1728
8.69E-03	3.33E-03	2.74E-06	2.74E-08	16.03	6.313	12	4.54	1756
1.46E-02	2.87E-03	2.36E-06	2.36E-08	15.56	6.125	13	4.70	1818
1.60E-03	7.35E-03	6.04E-06	6.04E-08	13.49	5.313	14	5.57	2153
1.67E-02	7.35E-03	6.05E-06	6.05E-08	13.02	5.125	15	5.76	2228
1.69E-03	1.94E-03	1.60E-06	1.60E-08	11.91	4.688	16	6.19	2396
2.90E-03	2.01E-03	1.65E-06	1.65E-08	10.95	4.313	17	6.59	2548
1.85E-03	2.29E-03	1.88E-06	1.88E-08	9.53	3.750	18	7.21	2788
3.81E-03	2.58E-03	2.12E-06	2.12E-08	8.26	3.250	19	7.63	2953
9.89E-04	2.29E-03	1.88E-06	1.88E-08	6.67	2.625	20	8.21	3178
7.02E-04	1.73E-03	1.42E-06	1.42E-08	6.03	2.375	21	8.53	3298
1.04E-03	7.69E-04	6.33E-07	6.33E-09	5.72	2.250	22	8.57	3316
9.21E-04	4.04E-04	3.32E-07	3.32E-09	5.56	2.188	23	8.65	3348
2.94E-04	4.59E-04	3.77E-07	3.77E-09	5.08	2.000	24	8.75	3386
5.87E-04	3.62E-04	2.98E-07	2.98E-09	4.92	1.938	25	8.83	3416
2.14E-04	4.85E-04	3.99E-07	3.99E-09	4.60	1.813	26	8.97	3471
1.30E-02	4.79E-04	3.94E-07	3.94E-09	4.45	1.750	27	9.04	3496

Appendix II – Compaction Data

Standard Proctor Compaction (592.5 kJ/m^3)

Compaction Energy kJ/m^3 (ft-lb/ft^3)	592.5 (12375)			
Test Number	1	2	3	4
Assumed moisture content (%)	14.00	11.00	8.00	6.00
Mold Weight (g), M_{md}	2044.62	2044.62	2044.62	2044.62
Specimen+Mold Weight (g), M_t	3846.50	4024.33	3998.61	3434.61
Volume of Mold (cm^3), V	940.00	940.00	940.00	940.00
Specific Gravity of Soil, G_s	2.69	2.69	2.69	2.69
Unit Weight of Water @ 20°C(KN/m^3), γ_w	9.79	9.79	9.79	9.79
Unit Weight of Water @ 20°C(lb/ft^3), γ_w	62.34	62.34	62.34	62.34
Moist Unit Weight of Compacted Specimen(g/cm^3), γ_m	1.92	2.11	2.08	1.48
Dry Unit Weight of Compacted Specimen(g/cm^3), γ_d	1.70	1.89	1.89	1.42
Dry Unit Weight of Compacted Specimen(KN/m^3), γ_d	**16.65**	**18.51**	**18.54**	**13.92**
Dry Unit Weight of Compacted Specimen(lb/ft^3), γ_d	106.04	117.87	118.04	88.67
Dry Unit Weight at S=1.0 (KN/m^3),γ_d	**19.57**	**20.09**	**20.78**	**23.71**
Dry Unit Weight at S=0.9 (KN/m^3),γ_d	**19.03**	**19.58**	**20.30**	**23.45**
Dry Unit Weight at S=1.0 (lb/ft3), γd	124.61	127.96	132.32	150.98
Dry Unit Weight at S=0.9 (lb/ft^3), γ_d	121.15	124.68	129.29	149.32
Void Ratio, e=((G_s*γ_w)/γ_d)-1	0.58	0.42	0.42	0.89
Degree of Saturation (%), S=G_s*w/e	0.59	0.73	0.64	0.12
Saturated Water Content, w_{sat}(%)	21.62	15.71	15.64	33.14

Moisture Content:				
Test Number	1	2	3	4
Assumed moisture content (%)	14.00	11.00	8.00	6.00
Container Mass (g), M_c	30.03	17.27	30.55	18.84
Container+Moist Specimen Mass (g), M_{cms}	90.43	70.70	77.78	41.60
Intial Container+Oven Dry Specimen Mass (g), M_{cds}	83.55	65.17	73.51	40.70
Mass of Water(g), M_w= M_{cms}-M_{cds}	6.88	5.53	4.27	0.90
Mass of Solids (g), M_s= M_{cds}-M_c	53.52	47.90	42.96	21.86

Water Content, $w=(M_w/M_s)x100(\%)$	12.86	11.54	9.94	4.12

34% Proctor Compaction Energy: (203.6 kJ/m^3)

Compaction Energy kJ/m^3 (ft-lb/ft^3)	203.6 (4252)						
Test Number	1	2	3	4	5	6	7
Assumed moisture content (%)	3.00	6.00	9.00	14.00	12.00	15.00	12.00
Mold Weight (g), M_{md}	1985.84	1985.84	1985.84	1985.84	1985.84	1985.84	1985.84
Specimen Weight (g)	1660.06	1703.00	1757.33	1945.49	1939.41	1974.56	1625.31
Specimen+Mold Weight (g), M_t	3645.90	3688.84	3743.17	3931.33	3925.25	3960.40	3611.15
Volume of Mold (cm^3), V	940.00	940.00	940.00	940.00	940.00	940.00	940.00
Specific Gravity of Soil, G_s	2.69	2.69	2.69	2.69	2.69	2.69	2.69
Unit Weight of Water @ 20^{o}C (KN/m^3), γ_w	9.79	9.79	9.79	9.79	9.79	9.79	9.79
Unit Weight of Water @ 20^{o}C (lb/ft^3), γ_w	62.34	62.34	62.34	62.34	62.34	62.34	62.34
Moist Unit Weight of Compacted Specimen (g/cm^3), γ_m	1.77	1.81	1.87	2.07	2.06	2.10	1.73
Dry Unit Weight of Compacted Specimen (g/cm^3), γ_d	1.64	1.65	1.68	1.83	1.83	1.82	1.47
Dry Unit Weight of Compacted Specimen (KN/m^3), γ_d	**16.11**	**16.21**	**16.48**	**17.98**	**17.94**	**17.80**	**14.37**
Dry Unit Weight of Compacted Specimen (lb/ft^3), γ_d	102.61	103.23	104.96	114.49	114.26	113.32	91.50
Dry Unit Weight at S=1.0 (KN/m^3),γ_d	21.94	20.95	20.24	19.57	19.62	18.51	17.75
Dry Unit Weight at S=0.9 (KN/m^3),γ_d	21.54	20.48	19.73	19.03	19.08	17.91	17.13
Dry Unit Weight at S=1.0 (lb/ft^3), γ_d	139.72	133.38	128.87	124.61	124.92	117.84	113.05
Dry Unit Weight at S=0.9 (lb/ft^3), γ_d	137.17	130.41	125.63	121.15	121.48	114.07	109.10
Void Ratio, e=((G_s*γ_w)/γ_d)-1	0.63	0.62	0.60	0.46	0.47	0.48	0.83
Degree of Saturation (%), S=G_s*w/e	0.32	0.41	0.50	0.74	0.73	0.88	0.58
Saturated Water Content, w_{sat} (%)	23.58	23.22	22.22	17.28	17.39	17.84	30.96

Moisture Content:							
Test Number	1	2	3	4	5	6	7
Assumed moisture content (%)	3.00	6.00	9.00	14.00	12.00	14.00	12.00
Container Mass (g), M_c	16.74	30.45	30.69	18.73	17.40	22.00	30.11
Container+Moist Specimen Mass (g), M_{cms}	68.55	128.84	128.77	78.87	85.68	99.55	131.87
Intial Container+Oven Dry Specimen Mass (g), M_{cds}	64.96	120.25	118.89	72.02	77.97	89.01	116.37
Mass of Water (g), $M_w= M_{cms}-M_{cds}$	3.59	8.59	9.88	6.85	7.71	10.54	15.50
Mass of Solids (g), $M_s= M_{cds}-M_c$	48.22	89.80	88.20	53.29	60.57	67.01	86.26
Water Content, (%) $W= (M_w/M_s)x100$	**7.45**	**9.57**	**11.20**	**12.85**	**12.73**	**15.73**	**17.97**

11% Proctor Compaction Energy: (67.85 kJ/m^3)

Compaction Energy kJ/m^3 (ft-lb/ft^3)	67.85 (1417)						
Test Number	1	2	3	4	5	6	7
Assumed moisture content (%)	3.00	9.00	8.00	12.00	6.00	12.00	17.00
Mold Weight (g), M_{md}	1985.84	1985.84	1985.84	1985.84	1985.84	1985.84	1985.84
Specimen Weight (g)	1539.63	1871.31	1626.85	1571.22	1613.3	1972.17	1864
Specimen+Mold Weight (g), M_t	3525.47	3857.15	3612.69	3557.06	3599.14	3958.01	3849.84
Volume of Mold (cm^3), V	940.00	940.00	940.00	940.00	940.00	940.00	940.00
Specific Gravity of Soil, G_s	2.69	2.69	2.69	2.69	2.69	2.69	2.69
Unit Weight of Water @ 20°C (KN/m^3), γ_w	9.79	9.79	9.79	9.79	9.79	9.79	9.79
Unit Weight of Water @ 20°C (lb/ft^3), γ_w	62.34	62.34	62.34	62.34	62.34	62.34	62.34
Moist Unit Weight of Compacted Specimen (g/cm^3), γ_m	1.64	1.99	1.73	1.67	1.72	2.10	1.98
Dry Unit Weight of Compacted Specimen (g/cm^3), γ_d	1.57	1.72	1.55	1.52	1.54	1.79	1.69
Dry Unit Weight of Compacted Specimen (KN/m^3), γ_d	**15.39**	**16.90**	**15.20**	**14.93**	**15.07**	**17.60**	**16.55**
Dry Unit Weight of Compacted Specimen (lb/ft^3), γ_d	97.98	107.64	96.82	95.05	95.97	112.05	105.40
Dry Unit Weight at S=1.0 (KN/m^3),γ_d	23.57	18.60	20.07	20.85	20.05	18.11	17.92
Dry Unit Weight at S=0.9 (KN/m^3),γ_d	23.30	18.01	19.55	20.38	19.53	17.50	17.31
Dry Unit Weight at S=1.0 (lb/ft^3), γ_d	150.09	118.43	127.81	132.76	127.68	115.31	114.12
Dry Unit Weight at S=0.9 (lb/ft^3), γ_d	148.36	114.68	124.52	129.75	124.38	111.44	110.20
Void Ratio, $e=((G_s*\gamma_w)/\gamma_d)-1$	0.71	0.56	0.73	0.76	0.75	0.50	0.59
Degree of Saturation (%), $S=G_s*w/e$	0.16	0.75	0.43	0.34	0.42	0.92	0.79
Saturated Water Content, w_{sat} (%)	26.45	20.74	27.22	28.41	27.79	18.46	21.97

Moisture Content:							
Test Number	1	2	3	4	5	6	7
Assumed moisture content (%)	3.00	9.00	8.00	12.00	6.00	12.00	17.00
Container Mass (g), M_c	17.42	18.86	18.84	17.42	18.77	30.59	30
Container+Moist Specimen Mass (g), M_{cms}	71.98	84.78	100.32	102.02	83.17	155.85	85.92
Intial Container+Oven Dry Specimen Mass (g), M_{cds}	69.70	75.95	91.85	94.48	76.45	137.75	77.61
Mass of Water (g), $M_w = M_{cms} - M_{cds}$	2.28	8.83	8.47	7.54	6.72	18.10	8.31
Mass of Solids (g), $M_s = M_{cds} - M_c$	52.28	57.09	73.01	77.06	57.68	107.16	47.61
Water Content, (%) $W = (M_w/M_s)x100$	**4.36**	**15.47**	**11.60**	**9.78**	**11.65**	**16.89**	**17.45**

Appendix III – Grain Size Distribution Testing Data

Post-Permeability Grain Size Distribution Data

Standard Proctor Effort – Sieve analysis data for layer 1 and layer 2

Sieve Analysis													
Sieve No.	**Particle dia. (mm)**	**Empty Pan**		**Wt. Retained+pan**		**Wt. Retained**		**% Retained**		**Cumulative %**		**Percent Finer**	
		Layer 1	**Layer 2**	**Layer 1**	**Layer 2**	**Layer 1**	**Layer 2**	**Layer 1**	**Layer 2**	**Layer 1**	**Layer 2**	**Layer 1**	**Layer 2**
2''	50.80	775.71	775.71	775.71	775.71	0.00	0.00	0.00	0.00	0.00	0.00	100.00	100.00
No. 4	4.76	557.13	557.13	557.13	557.13	0.00	0.00	0.00	0.00	0.00	0.00	100.00	100.00
No. 10	2.00	469.11	469.11	680.54	768.01	211.43	298.90	39.74	47.31	39.74	47.31	60.26	52.69
No.30	0.60	396.30	396.30	584.04	579.53	187.74	183.23	35.29	29.00	75.03	76.31	24.97	23.69
No. 50	0.30	370.07	370.07	418.28	426.73	48.21	56.66	9.06	8.97	84.10	85.28	15.90	14.72
No.60	0.25	317.98	317.98	327.81	328.64	9.83	10.66	1.85	1.69	85.94	86.96	14.06	13.04
No.200	0.08	293.88	293.88	332.48	335.74	38.60	41.86	7.26	6.63	93.20	93.59	6.80	6.41
Pan		369.66	369.66	405.53	406.74	35.87	37.08	6.74	5.87	99.94	99.46	0.06	0.54
					Total	531.68	628.39	99.94	99.46				

	Layer 1	**Layer 2**	**Layer 3**
Mass of Sample	531.98	631.81	489.78
Mass Loss(%)	0.06	0.54	0.00

Standard Proctor Effort – Sieve analysis data for layer 3

Sieve Analysis							
Sieve No.	**Particle dia. (mm)**	**Empty Pan**	**Wt. Retained+pan**	**Wt. Retained**	**% Retained**	**Cumulative %**	**Percent Finer**
		Layer 3	**Layer 3**	**Layer 3**	**Layer 3**	**Layer 3**	**Layer 3**
2''	50.80	775.71	775.71	0.00	0.00	0.00	100.00
No. 4	4.76	557.13	557.13	0.00	0.00	0.00	100.00
No. 10	2.00	469.11	687.10	217.99	44.51	44.51	55.49
No.30	0.60	396.30	553.63	157.33	32.12	76.63	23.37
No. 50	0.30	370.07	411.06	40.99	8.37	85.00	15.00
No.60	0.25	317.98	326.60	8.62	1.76	86.76	13.24
No.200	0.08	293.88	326.84	32.96	6.73	93.49	6.51
Pan		369.66	401.56	31.90	6.51	100.00	0.00
			Total	489.79	100.00		

34% Proctor Compaction Effort

Sieve Analysis

ve o.	Particle dia. (mm)	Empty Pan			Wt Retained+pan			Wt Retained			% Retained			Cumulative %			Percent Fine	
		Layer 1	Layer 2	Layer 3	Layer 1	Layer 2	Layer 3	Layer 1	Layer 2	Layer 3	Layer 1	Layer 2	Layer 3	Layer 1	Layer 2	Layer 3	Layer 1	Layer 2
"	50.8	775.88	775.88	775.88	775.88	775.88	775.88	0	0	0	0.00	0.00	0.00	0.00	0.00	0.00	100.00	100
. 4	4.76	557.33	557.33	557.33	557.33	557.33	557.33	0	0	0	0.00	0.00	0.00	0.00	0.00	0.00	100.00	100.00
10	2.00	479.24	479.31	479.23	664.52	733.52	719.19	185.28	254.21	239.96	41.51	42.48	47.26	41.51	42.48	47.26	58.49	57.52
30	0.39	482.31	482.21	482.32	617.17	666.66	640.22	134.86	184.45	157.9	30.21	30.82	31.10	71.73	73.30	78.35	28.27	26.70
50	0.30	370.94	371.14	371	415.61	427.04	410.72	44.67	55.9	39.72	10.01	9.34	7.82	81.73	82.64	86.18	18.27	17.36
60	0.25	367.1	367.26	367.26	378.21	381.11	376.06	11.11	13.85	8.8	2.49	2.31	1.73	84.22	84.95	87.91	15.78	15.05
200	0.08	338.1	338.09	338.09	374.84	386.07	372.26	36.74	47.98	34.17	8.23	8.02	6.73	92.45	92.97	94.64	7.55	7.03
n		370.93	370.96	370.91	404.34	411.82	397.85	33.41	40.86	26.94	7.49	6.83	5.31	99.94	99.80	99.94	0.06	0.20
							Total	**446.07**	**597.25**	**507.49**	**99.94**	**99.80**	**99.94**					

		Layer 1	Layer 2	Layer 3
ss of Sample		446.34	598.45	507.78
ass Loss(%)		0.06	0.20	0.06

11% Proctor Compaction Effort – Test 1

e Analysis

ve .	Particle dia. (mm)	Empty Pan			Wt Retained+pan			Wt Retained			% Retained			Cumulative %			Percent Fin	
		Layer 1	Layer 2	Layer 3	Layer 1	Layer 2	Layer 3	Layer 1	Layer 2	Layer 3	Layer 1	Layer 2	Layer 3	Layer 1	Layer 2	Layer 3	Layer 1	Layer 2
	50.8	775.73	775.73	775.73	775.73	775.73	775.73	0	0	0	0.00	0.00	0.00	0.00	0.00	0.00	100.00	100
4	4.76	557.2	557.2	557.2	557.2	557.2	557.2	0	0	0	0.00	0.00	0.00	0.00	0.00	0.00	100.00	100.00
10	2.00	479.34	479.26	479.18	597.1	656.21	673.85	117.76	176.95	194.67	34.73	39.86	38.95	34.73	39.86	38.95	65.27	60.14
0	0.39	482.35	482.37	482.02	598.08	619.30	643.07	115.73	136.93	161.05	34.13	30.84	32.22	68.86	70.70	71.17	31.14	29.30
50	0.30	370.97	370.99	370.71	407.53	417.06	423.44	36.56	46.07	52.73	10.78	10.38	10.55	79.64	81.07	81.72	20.36	18.93
0	0.25	367.13	367.13	366.83	375.93	378.62	379.78	8.8	11.49	12.95	2.60	2.59	2.59	82.24	83.66	84.31	17.76	16.34
00	0.08	337.99	338.01	337.78	369.86	375.70	379	31.87	37.69	41.22	9.40	8.49	8.25	91.64	92.15	92.56	8.36	7.85
		370.97	370.94	370.72	399.2	404.12	408.19	28.23	33.18	37.47	8.33	7.47	7.50	99.96	99.62	100.06	0.04	0.38
							Total	**338.95**	**442.31**	**500.09**	**99.96**	**99.62**	**100.06**					

		Layer 1	Layer 2	Layer 3
s of Sample		339.07	443.98	499.80
ss Loss(%)		0.04	0.38	-0.06

11% Proctor Compaction Effort – Test 2

Sieve Analysis

ve o.	Particle dia. (mm)	Empty Pan			Wt Retained+pan			Wt Retained			% Retained			Cumulative %			Percent Fine	
		Layer 1	Layer 2	Layer 3	Layer 1	Layer 2	Layer 3	Layer 1	Layer 2	Layer 3	Layer 1	Layer 2	Layer 3	Layer 1	Layer 2	Layer 3	Layer 1	Layer 2
	50.8	775.73	775.73	775.88	775.73	775.73	775.88	0	0	0	0.00	0.00	0.00	0.00	0.00	0.00	100.00	100
4	4.76	557.2	557.2	557.33	557.2	557.2	557.33	0	0	0	0.00	0.00	0.00	0.00	0.00	0.00	100.00	100.00
10	2.00	478.99	478.99	479.08	608.67	657.90	673.45	129.68	178.91	194.37	35.65	34.63	38.16	35.65	34.63	38.16	64.35	65.37
30	0.39	482.15	482.02	482.13	607.49	662.23	646.79	125.34	180.21	164.66	34.46	34.88	32.32	70.11	69.50	70.48	29.89	30.50
50	0.30	370.7	370.78	370.8	409.15	426.85	422.96	38.45	56.07	52.16	10.57	10.85	10.24	80.68	80.36	80.72	19.32	19.64
60	0.25	366.9	366.95	366.96	375.5	380.20	380.11	8.6	13.25	13.15	2.36	2.56	2.58	83.04	82.92	83.30	16.96	17.08
200	0.08	337.82	337.87	337.8	368.23	385.64	382.81	30.41	47.77	45.01	8.36	9.25	8.84	91.40	92.17	92.14	8.60	7.83
		370.75	370.77	370.75	401.03	411.13	410.62	30.28	40.36	39.87	8.32	7.81	7.83	99.73	99.98	99.96	0.27	0.02
							Total	**362.76**	**516.57**	**509.22**	**99.73**	**99.98**	**99.96**					

		Layer 1	Layer 2	Layer 3
ss of Sample		363.75	516.69	509.40
ass Loss(%)		0.27	0.02	0.04

11% Proctor Compaction Effort – Test 3

Sieve Analysis

	Particle dia. (mm)	Empty Pan			Wt Retained+pan			Wt Retained			% Retained			Cumulative %			Percent F	
		Layer 1	Layer 2	Layer 3	Layer 1	Layer 2	Layer 3	Layer 1	Layer 2	Layer 3	Layer 1	Layer 2	Layer 3	Layer 1	Layer 2	Layer 3	Layer 1	Layer 2
	50.8	775.73	775.73	775.73	775.73	775.73	775.73	0	0	0	0.00	0.00	0.00	0.00	0.00	0.00	100.00	10
	4.76	557.2	557.2	557.2	557.2	557.2	557.2	0	0	0	0.00	0.00	0.00	0.00	0.00	0.00	100.00	100.0
	2.00	479.19	479.23	479.26	647.7	693.04	677.5	168.51	213.81	198.24	38.73	42.72	47.67	38.73	42.72	47.67	61.27	57.2
	0.39	481.98	482.17	482.24	626.92	630.48	598.4	144.94	148.31	116.16	33.31	29.63	27.93	72.05	72.35	75.60	27.95	27.6
	0.30	370.93	370.96	370.92	414.12	417.82	405.7	43.19	46.86	34.78	9.93	9.36	8.36	81.97	81.72	83.96	18.03	18.2
	0.25	367.15	367.1	367.03	377.85	378.20	375.67	10.7	11.1	8.64	2.46	2.22	2.08	84.43	83.93	86.04	15.57	16.0
)	0.08	337.94	337.97	338	374.02	379.76	369.35	36.08	41.79	31.35	8.29	8.35	7.54	92.73	92.28	93.58	7.27	7.7
		370.94	370.89	370.85	402.67	409.82	397.53	31.73	38.93	26.68	7.29	7.78	6.42	100.02	100.06	100.00	-0.02	-0.0
							Total	**435.15**	**500.8**	**415.85**	**100.02**	**100.06**	**100.00**					

	Layer 1	Layer 2	Layer 3
of Sample	435.06	500.49	415.87
Loss(%)	-0.02	-0.06	0.00

Pre-Permeability Grain Size Distribution Data

Standard Proctor Compaction Effort – Sieve analysis data for layer 1 and layer 2

Sieve No.	Particle dia. (mm)	Empty Pan		Wt Retained+pan		Wt Retained		% Retained		Cumulative %		Percent Finer	
		Layer 1	Layer 2	Layer 1	Layer 2	Layer 1	Layer 2	Layer 1	Layer2	Layer 1	Layer2	Layer 1	Layer2
						0	0	0	0	0	0	100	100
2"	50.80	637.46	637.46	637.46	637.46	0	0	0	0	0	0	100	100
No. 4	4.760	556.79	556.7	556.79	556.7	0	0	0	0	0	0	100	100
No. 10	2.000	468.86	468.78	631.62	546.41	162.76	77.63	33.53	23.34	33.53	23.34	66.47	76.66
No. 30	0.595	409.52	409.38	561.44	510.89	151.92	101.51	31.3	30.52	64.83	53.86	35.17	46.14
No. 50	0.300	370.72	370.66	451.42	438.17	80.7	67.51	16.63	20.3	81.46	74.16	18.54	25.84
No. 60	0.250	366.81	366.87	385.25	383.01	18.44	16.14	3.8	4.85	85.26	79.01	14.74	20.99
No. 200	0.075	335.07	334.96	383.89	382.17	48.82	47.21	10.06	14.19	95.31	93.2	4.69	6.8
Pan		371.62	371.73	395.12	396.68	23.5	24.95	4.84	7.5	100.15	100.7	-0.15	-0.7
					Total	486.14	334.95	100.15	100.7				

Standard Proctor Compaction Effort - Sieve analysis data for layer 3

Sieve No.	Particle dia. (mm)	Empty Pan	Wt Retained+pan	Wt Retained	% Retained	Cumulative %	Percent Finer
		Layer 3	Layer 3	Layer 3	Layer 3	Layer 3	Layer 3
				0	0	0	100
2"	50.800	637.46	637.46	0	0	0	100
No. 4	4.760	556.82	556.82	0	0	0	100
No. 10	2.000	468.77	571.22	102.45	36.45	36.45	63.55
No. 30	0.595	409.53	497.56	88.03	31.32	67.76	32.24
No. 50	0.300	370.61	412.06	41.45	14.75	82.51	17.49
No. 60	0.250	366.91	376.47	9.56	3.4	85.91	14.09
No. 200	0.075	334.92	360.41	25.49	9.07	94.98	5.02
Pan		371.69	386.66	14.97	5.33	100.3	-0.3
			Total	281.95	100.3		

		Layer 1	Layer 2	Layer 3
Mass of Sample		485.39	332.61	281.10
Mass Loss(%)		-0.15	-0.70	-0.30

34% Proctor Compaction Effort – Sieve analysis data for layer 1 and layer 2

Sieve Analysis													
Sieve No.	**Particle dia. (mm)**	**Empty Pan**		**Wt. Retained+pan**		**Wt. Retained**		**% Retained**		**Cumulative %**		**Percent Finer**	
		Layer 1	**Layer 2**	**Layer 1**	**Layer 2**	**Layer 1**	**Layer 2**	**Layer 1**	**Layer 2**	**Layer 1**	**Layer 2**	**Layer 1**	**Layer 2**
2''	50.80	775.71	775.71	775.71	775.71	0	0	0	0	0	0	100	100
No. 4	4.76	557.43	557.43	557.43	557.43	0	0	0	0	0	0	100	100
No. 10	2.00	479.26	479.26	586.59	575.84	107.33	96.58	36.78	34.00	36.78	34.00	63.22	66.00
No.30	0.60	481.97	481.97	588.68	580.94	106.71	98.97	36.57	34.84	73.34	68.83	26.66	31.17
No. 50	0.30	370.89	370.95	402.09	405.43	31.2	34.48	10.69	12.14	84.04	80.97	15.96	19.03
No.60	0.25	367.06	367.09	374.34	375.76	7.28	8.67	2.49	3.05	86.53	84.02	13.47	15.98
No.200	0.08	338.03	338.03	361.75	364.91	23.72	26.88	8.13	9.46	94.66	93.48	5.34	6.52
Pan		370.9	370.91	388.55	392.06	17.65	21.15	6.05	7.44	100.71	100.93	-0.71	-0.93
					Total	293.89	286.73	100.71	100.93				

	Layer 1	**Layer 2**	**Layer 3**
Mass of Sample	291.83	284.09	535.42
Mass Loss(%)	-0.71	-0.93	-0.97

34% Proctor Compaction Effort - Sieve analysis data for layer 3

Sieve Analysis							
Sieve No.	**Particle dia. (mm)**	**Empty Pan**	**Wt. Retained+pan**	**Wt. Retained**	**% Retained**	**Cumulative %**	**Percent Finer**
		Layer 3	**Layer 3**	**Layer 3**	**Layer 3**	**Layer 3**	**Layer 3**
2''	50.80	775.71	775.71	0	0	0	100
No. 4	4.76	557.43	557.43	0	0	0	100
No. 10	2.00	479.26	657.49	178.23	33.29	33.29	66.71
No.30	0.60	482.09	669.48	187.39	35.00	68.29	31.71
No. 50	0.30	370.94	440.01	69.07	12.90	81.19	18.81
No.60	0.25	367.04	384.94	17.9	3.34	84.53	15.47
No.200	0.08	338.02	387.83	49.81	9.30	93.83	6.17
Pan		370.95	409.14	38.19	7.13	100.97	-0.97
			Total	540.59	100.97		

11% Proctor Compaction Effort – Sieve analysis data for layer 1 and layer 2

Sieve Analysis													
Sieve No.	**Particle dia. (mm)**	**Empty Pan**		**Wt. Retained+pan**		**Wt. Retained**		**% Retained**		**Cumulative %**		**Percent Finer**	
		Layer 1	**Layer 2**	**Layer 1**	**Layer 2**	**Layer 1**	**Layer 2**	**Layer 1**	**Layer 2**	**Layer 1**	**Layer 2**	**Layer 1**	**Layer 2**
2''	50.80	775.63	775.63	775.63	775.63	0	0	0	0	0	0	100	100
No. 4	4.76	557.18	557.18	557.18	557.18	0	0	0	0	0	0	100	100
No. 10	2.00	479.14	479.31	600.53	597.30	121.39	117.99	52.78	50.77	52.78	50.77	47.22	49.23
No.30	0.60	482.20	482.10	550.37	548.19	68.17	66.09	29.64	28.44	82.42	79.21	17.58	20.79
No. 50	0.30	371.00	370.96	386.83	389.37	15.83	18.41	6.88	7.92	89.31	87.13	10.69	12.87
No.60	0.25	367.15	367.15	370.65	371.72	3.50	4.57	1.52	1.97	90.83	89.10	9.17	10.90
No.200	0.08	338.08	337.99	349.37	352.36	11.29	14.37	4.91	6.18	95.74	95.28	4.26	4.72
Pan		369.65	369.6	379.23	380.99	9.58	11.39	4.17	4.90	99.90	100.18	0.10	-0.18
					Total	229.76	232.82	99.90	100.18				

	Layer 1	**Layer 2**	**Layer 3**
Mass of Sample	229.98	284.09	535.42
Mass Loss(%)	0.10	-0.93	-0.97

11% Proctor Compaction Effort - Sieve analysis data for layer 3

Sieve Analysis							
Sieve No.	**Particle dia. (mm)**	**Empty Pan**	**Wt. Retained+pan**	**Wt. Retained**	**% Retained**	**Cumulative %**	**Percent Finer**
		Layer 3	**Layer 3**	**Layer 3**	**Layer 3**	**Layer 3**	**Layer 3**
2''	50.80	775.63	775.63	0	0	0	100
No. 4	4.76	557.18	557.18	0	0	0	100
No. 10	2.00	479.30	604.95	125.65	46.21	46.21	53.80
No.30	0.60	482.04	572.07	90.03	33.11	79.31	20.69
No. 50	0.30	370.96	394.28	23.32	8.58	87.89	12.11
No.60	0.25	367.07	372.22	5.15	1.89	89.78	10.22
No.200	0.075	338.04	353.88	15.84	5.82	95.61	4.39
Pan		369.67	381.82	12.15	4.47	100.07	-0.07
			Total	272.14	100.07		

As-Received Grain Size Distribution Data: Weathered Sandstone Material

As Received Grain Size Distribution: Weathered Sandstone Material: Test 1, Test 2

Sieve No.	Particle dia. (mm)	Cumulative %		Percent Finer	
		Test 1	Test 2	Test 1	Test 2
2"	50.8	0	0	100	100
1"	25.4	7.29	15.04	92.71	84.96
3/4"	19.05	18.27	17.95	81.73	82.05
3/8"	9.5	37.24	30.42	62.76	69.58
No. 4	4.76	55.99	51.7	44.01	48.3
No. 10	2	70.08	68.04	29.92	31.96
No. 40	0.43	84.42	86.76	15.58	13.24
No. 200	0.08	96.13	97.87	3.87	2.13
Pan		99.72	99.77	0.28	0.23

Empty Pan		Wt Retained+pan		Wt Retained		% Retained	
Test 1	Test 2	Test 1	Test 2	Test 1	Test 2	Test 1	Test 2
638.02	638.02	638.02	638.02	0	0	0	0
584.26	584.22	620.73	659.4	36.47	75.18	7.29	15.04
587.77	587.8	642.66	602.37	54.89	14.57	10.98	2.91
556.02	555.83	650.86	618.2	94.84	62.37	18.97	12.47
517.72	585.78	611.47	692.18	93.75	106.4	18.75	21.28
472.55	472.51	543	554.2	70.45	81.69	14.09	16.34
375.02	374.98	446.74	468.58	71.72	93.6	14.34	18.72
337.9	337.93	396.45	393.45	58.55	55.52	11.71	11.1
371.84	372.52	389.75	382.03	17.91	9.51	3.58	1.9
			Total	**498.58**	**498.84**	**99.72**	**99.77**

As-Received Grain Size Distribution Data: Unweathered Sandstone Overburden

As Received Grain Size Distribution: Unweathered Sandstone Overburden: Test 1, Test 2

Sieve No.	Particle dia. (mm)	Cumulative %		Percent Finer	
		Test 1	Test 2	Test 1	Test 2
2"	50.8	0	0	100	100
1"	25.4	0	0	100	100
3/4"	19.05	1.11	7.14	98.89	92.86
3/8"	9.5	14.24	20.4	85.76	79.6
No. 4	4.76	28.83	32.19	71.17	67.81
No. 10	2	45.73	46.62	54.27	53.38
No. 40	0.43	73.73	74.03	26.27	25.97
No. 200	0.08	94.97	95.38	5.03	4.62
Pan		99.88	99.91	0.12	0.09

Empty Pan		Wt Retained+pan		Wt Retained		% Retained	
Test 1	Test 2	Test 1	Test 2	Test 1	Test 2	Test 1	Test 2
638.02	638.02	638.02	638.02	0	0	0	0
584.36	584.4	584.36	584.4	0	0	0	0
587.78	587.83	593.31	623.53	5.53	35.7	1.11	7.14
555.97	556.05	621.65	622.34	65.68	66.29	13.14	13.26
517.73	517.68	590.68	576.62	72.95	58.94	14.59	11.79
472.58	472.5	557.05	544.68	84.47	72.18	16.89	14.44
375.07	374.97	515.11	512	140.04	137.03	28.01	27.41
337.93	337.92	444.1	444.66	106.17	106.74	21.23	21.35
371.87	371.81	396.44	394.46	24.57	22.65	4.91	4.53
			Total	**499.41**	**499.53**	**99.88**	**99.91**

		Test 1	Test 2

Mass of Sample	500	500
Mass Loss(%)	0.12	0.09

Appendix IV – Specific Gravity and Atterberg Limit Data

Weathered Sandstone – Specific Gravity – Test 1 Data

Test Number	1	2	3
Temperature, T (^oC)	22.5	22.5	22.5
Density of Water, ρ_w (g/ML)	0.99766	0.99766	0.99766
Temperature Coefficient, K	0.99945	0.99945	0.99945
Volume of Pycnometer, V_p (mL)	500	500	500
Wt. of Pycnometer, M_p (g)	166.15	167.96	160.61
Sample+Pycnomter+Water, $M_{pws,t}$ (g)	693.76	695.76	687.47
Pycnometer+Water, $M_{pw,t}$ (g)	664.35	666.04	657.59
Dry Sample Mass, M_s (g)	46.09	46.09	46.09
Wt. of Sample (g)	50.00	50.00	50.00
Specific Gravity of soil solids, G_t	**2.76**	**2.82**	**2.84**
Specific Gravity at Test Temp., G_{tt}	**2.76**	**2.81**	**2.84**

Specific gravity test 1 results

Test Number	1
Empty Container, $M_{c,}$ (g)	30.00
Container + Wet Sample, M_{cms}, (g)	86.48
Container + Dry Sample, M_{cds}, (g)	82.66
Moisture content w (%)	**7.25**
Average Moisture Content (%):	**7.81**

Water content for determining the dry mass of the test specimen.

Weathered Sandstone – Specific Gravity – Test 2 Data

Test Number	1	2	3
Temperature, T (^oC)	22.00	22.00	22.00
Density of Water, $\rho_{w,t}$ (g/ML)	0.99777	0.99777	0.99777
Temperature Coefficient, K	0.99957	0.99957	0.99957
Volume of Pycnometer, V_p (mL)	500.00	500.00	500.00
Wt. of Pycnometer, M_p (g)	168.09	168.29	160.72
Sample+Pycnomter+Water, $M_{pws,t}$ (g)	693.51	695.3	687.21
Pycnometer+Water, $M_{pw,t}$ (g)	664.23	666.06	657.92
Dry Sample Mass, M_s (g)	45.97	45.97	45.97
Wt. of Sample (g)	50.00	50.00	50.00
Specific Gravity of soil solids, G_t	**2.75**	**2.75**	**2.76**
Specific Gravity at Test Temp., G_{tt}	**2.75**	**2.75**	**2.76**

Specific gravity test 2 results

Test Number	1	2	3
Empty Container, $M_{c,}$ (g)	17.41	17.3	18.77
Container + Wet Sample, M_{cms}, (g)	73.92	80.97	80.85
Container + Dry Sample, M_{cds}, (g)	69.63	76.29	76.22
Moisture content w (%)	**8.22**	**7.93**	**8.06**
Average Moisture Content (%):	**8.07**		

Water content for determining the dry mass of the test specimen

Weathered Sandstone – Atterberg Limit Data

Liquid Limit Test			
Test Number	1	3	5
Empty Container (g)	16.87	17.44	30.68
Container + Wet Sample (g)	28.12	29.4	43.81
Container + Dry Sample (g)	25.95	26.93	41.04
Moisture content, w (%)	**23.9**	**26.03**	**26.74**
Weight of Water (g)	2.17	2.47	2.77
Number of Blows:	38	26	19

Liquid Limit test results

Plastic Limit Test			
Test Number	2	4	6
Empty Container (g)	16.81	30.54	30.41
Container + Wet Sample (g)	20.36	32.31	33.87
Container + Dry Sample (g)	19.73	31.98	33.23
Moisture content, w (%)	**21.58**	**22.92**	**22.7**
Weight of Water (g)	0.63	0.33	0.64

Plastic Limit test results

Unweathered Sandstone – Specific Gravity Data

Test Number	1	2	3	4	5	6
Temperature, T (^oC)	22.00	22.00	22.00	22.00	22.00	22.00
Density of Water, ρ_w (g/mL)	0.99777	0.99777	0.99777	0.99777	0.99777	0.99777
Temperature Coefficient, K	0.99957	0.99957	0.99957	0.99957	0.99957	0.99957
Volume of Pycnometer, V_p (mL)	500.00	500.00	500.00	500.00	500.00	500.00
Wt. of Pycnometer, M_p (g)	167.27	169.04	160.62	159.74	152.74	154.85
Sample+Pycnomter+Water, $M_{pws,t}$ (g)	694.88	696.16	688.03	688.90	681.95	683.68
Pycnometer+Water, $M_{pw,t}$ (g)	663.42	666.03	657.71	657.82	650.84	653.13
Dry Sample Mass, M_s (g)	48.58	48.55	48.69	49.42	49.38	49.34
Wt. of Sample (g)	50.00	50.00	50.00	50.00	50.00	50.00
Specific Gravity of soil solids, G_t	2.84	2.64	2.65	2.69	2.70	2.63
Specific Gravity at Test Temp., G_{tt}	2.84	2.63	2.65	2.69	2.70	2.62

Specific gravity test results

Test Number	1	2	3	4	5	6
Empty Container, M_c, (g)	16.89	21.79	30.03	30.47	16.76	16.84
Container + Wet Sample, M_{cms}, (g)	70.86	74.82	100.21	159.29	87.45	90.81
Container + Dry Sample, M_{cds}, (g)	69.37	73.33	98.42	157.82	86.58	89.85
Moisture content w (%)	2.84	2.89	2.62	1.15	1.25	1.31
Average Moisture Content (%):	2.01					

Moisture content for specific gravity test calculations

Unweathered Sandstone – Atterberg Limit Data – Test 1

Liquid Limit Test			
Test Number	1	5	3
Empty Container (g)	18.80	30.28	16.90
Container + Wet Sample (g)	32.55	45.46	35.71
Container + Dry Sample (g)	30.25	43.01	33.00
Moisture content, w (%)	**20.09**	**19.25**	**16.83**
Weight of Water (g)	2.30	2.45	2.71
Number of Blows:	16	26	39

Liquid Limit Results

Plastic Limit Test			
Test Number	2	4	6
Empty Container (g)	17.4	30.46	16.9
Container + Wet Sample (g)	20.1	36.29	20.3
Container + Dry Sample (g)	19.71	35.51	19.82
Moisture content, w (%)	**16.88**	**15.45**	**16.44**
Weight of Water (g)	0.39	0.78	0.48

Plastic Limit Results

Unweathered Sandstone – Atterberg Limit Data – Test 2

Liquid Limit Test				
Test Number	1	3	5	7
Empty Container (g)	18.8	16.9	30.28	17.45
Container + Wet Sample (g)	30.65	32.69	39.02	32.05
Container + Dry Sample (g)	28.66	30.16	37.66	29.53
Moisture content w (%)	**20.18**	**19.08**	**18.43**	**20.86**
Weight of Water (g)	1.99	2.53	1.36	2.52
Number of Blows:	17	25	32	15

Liquid Limit Results

Plastic Limit Test				
Test Number	2	4	6	8
Empty Container (g)	17.4	30.46	16.9	16.87
Container + Wet Sample (g)	18.82	35.48	18.44	19.61
Container + Dry Sample (g)	18.62	34.74	18.22	19.24
Moisture content w (%)	**16.39**	**17.29**	**16.67**	**15.61**
Weight of Water (g)	0.2	0.74	0.22	0.37

Plastic Limit Results

Appendix V – Direct Shear Data

Unweathered Sandstone – Direct Shear Standard Proctor Compaction Data

Test Number	DS Specimen
Assumed moisture content (%)	10.75
Mold Weight (g), M_{md}	2042.22
Specimen+Mold Weight (g), M_t	3965.00
Volume of Mold (cm^3), V	940.00
Specific Gravity of Soil, G_s	2.69
Unit Weight of Water @ 20°C (KN/m^3), γ_w	9.79
Unit Weight of Water @ 20°C (lb/ft^3), γ_w	62.34
Moist Unit Weight of Compacted Specimen (g/cm^3), γ_m	2.05
Dry Unit Weight of Compacted Specimen (g/cm^3), γ_d	1.88
Dry Unit Weight of Compacted Specimen (KN/m^3), γ_d	**18.39**
Dry Unit Weight of Compacted Specimen (lb/ft^3), γ_d	117.11
Dry Unit Weight at S=1.0 (KN/m^3),γ_d	21.18
Dry Unit Weight at S=0.9 (KN/m^3),γ_d	20.73
Dry Unit Weight at S=1.0 (lb/ft^3), γ_d	134.88
Dry Unit Weight at S=0.9 (lb/ft^3), γ_d	132.01
Void Ratio, $e=((Gs*\gamma_w)/ \gamma_d)-1$	0.43
Degree of Saturation (%), $S=G_s*w/e$	0.56
Saturated Water Content, w_{sat} (%)	16.06
Compaction Energy kJ/m^3 ($ft\text{-}lb/ft^3$)	592.5 (12375)
Assumed moisture content (%)	10.75
Container Mass (g), Mc	209.89
Container+Moist Specimen Mass (g), Mcms	572.58
Intial Container+Oven Dry Specimen Mass (g), Mcds	542.50
Mass of Water (g), Mw= Mcms-Mcds	30.08
Mass of Solids (g), Ms= Mcds-Mc	332.61
Water Content, (%) W= (Mw/Ms)x100	9.04

Unweathered Sandstone – Direct Shear 34% Proctor Compaction Data

Test Number	34% Proctor Energy: DS
Assumed moisture content (%)	14.5
Mold Weight (g), M_{md}	1985.84
Specimen Weight (g)	1625.31
Specimen+Mold Weight (g), M_t	4000
Volume of Mold (cm^3), V	940
Specific Gravity of Soil, G_s	2.69
Unit Weight of Water @ 20°C (KN/m^3), γ_w	9.79
Unit Weight of Water @ 20°C (lb/ft^3), γ_w	62.34
Moist Unit Weight of Compacted Specimen (g/cm^3), γ_m	2.14
Dry Unit Weight of Compacted Specimen (g/cm^3), γ_d	1.89
Dry Unit Weight of Compacted Specimen (KN/m^3), γ_d	**18.56**
Dry Unit Weight of Compacted Specimen (lb/ft^3), γ_d	118.21
Dry Unit Weight at S=1.0 (KN/m^3),γ_d	19.45
Dry Unit Weight at S=0.9 (KN/m^3),γ_d	18.9
Dry Unit Weight at S=1.0 (lb/ft^3), γ_d	123.85
Dry Unit Weight at S=0.9 (lb/ft^3), γ_d	120.35
Void Ratio, $e=((G_s*\gamma_w)/\gamma_d)-1$	0.42
Degree of Saturation (%), $S=G_s*w/e$	0.85
Saturated Water Content, w_{sat} (%)	15.56
Compaction Energy kJ/m^3 ($ft\text{-}lb/ft^3$)	203.6 (4252)
Assumed moisture content (%)	14.5
Container Mass(g), Mc	17.43
Container+Moist Specimen Mass(g), Mcms	77.61
Intial Container+Oven Dry Specimen Mass(g), Mcds	70.61
Mass of Water(g), Mw= Mcms-Mcds	7
Mass of Solids(g), Ms= Mcds-Mc	53.18
Water Content, % W= (Mw/Ms)x100	13.16

Unweathered Sandstone – Direct Shear 11% Proctor Compaction Data

Test Number	11% Proctor DS
Assumed moisture content (%)	10.50
Mold Weight (g), M_{md}	1988.11
Specimen Weight (g)	1611.89
Specimen+Mold Weight (g), M_t	3600.00
Volume of Mold (cm^3), V	940.00
Specific Gravity of Soil, G_s	2.69
Unit Weight of Water @ 20°C (KN/m^3), γ_w	9.79
Unit Weight of Water @ 20°C (lb/ft^3), γ_w	62.34
Moist Unit Weight of Compacted Specimen (g/cm^3), γ_m	1.71
Dry Unit Weight of Compacted Specimen (g/cm^3), γ_d	1.71
Dry Unit Weight of Compacted Specimen (KN/m^3), γ_d	**16.81**
Dry Unit Weight of Compacted Specimen (lb/ft^3), γ_d	107.05
Dry Unit Weight at S=1.0 (KN/m^3),γ_d	26.34
Dry Unit Weight at S=0.9 (KN/m^3),γ_d	26.34
Dry Unit Weight at S=1.0 (lb/ft^3), γ_d	167.70
Dry Unit Weight at S=0.9 (lb/ft^3), γ_d	167.70
Void Ratio, $e=((G_s*\gamma_w)/\gamma_d)-1$	0.57
Degree of Saturation (%), $S=G_s*w/e$	0.00
Saturated Water Content, w_{sat} (%)	21.06
Compaction Energy kJ/m^3 ($ft\text{-}lb/ft^3$)	67.85 (1417)
Assumed moisture content (%)	10.50
Container Mass(g), Mc	30.44
Container+Moist Specimen Mass(g), Mcms	127.07
Intial Container+Oven Dry Specimen Mass(g), Mcds	118.27
Mass of Water(g), Mw= Mcms-Mcds	8.80
Mass of Solids(g), Ms= Mcds-Mc	87.83
Water Content, % W= (Mw/Ms)x100	10.02